Consequences of 11β-hydroxysteroid dehydrogenase deficiency during inflammatory responses

Agnes Elizabeth Coutinho

Doctor of Philosophy

University of Edinburgh

2009

Abstract

Glucocorticoids profoundly influence the immune system and pharmacological doses exert potent anti-inflammatory actions. During inflammation, glucocorticoids limit oedema and influence cell trafficking, differentiation programmes and gene transcription in glucocorticoid-sensitive leukocytes. Within cells, glucocorticoid action is modulated by a pre-receptor mechanism; glucocorticoid metabolism by the enzyme 11β-hydroxysteroid dehydrogenase (11β-HSD). Two 11β-HSD isozymes exist: 11β-HSD1, which catalyses amplification of glucocorticoid levels in intact cells by oxo-reduction of intrinsically inert cortisone (11-dehydrocorticosterone in rodents) into active cortisol (corticosterone in rodents) and 11β-HSD2, which performs the opposite reaction. Thus, amplification of intracellular glucocorticoid levels by 11β-HSD1 may represent an endogenous anti-inflammatory mechanism. This hypothesis has been tested in *Hsd11b1*$^{-/-}$ mice (homozygous for a targeted disruption in the *Hsd11b1* gene, encoding 11β-HSD1), using carageenan-induced pleurisy and experimental model of arthritis induced by injection of arthritogenic antibodies. In both models, *Hsd11b1*$^{-/-}$ mice showed more severe acute inflammation than control mice. During carrageenan-induced pleurisy, *Hsd11b1*$^{-/-}$ mice recruited more inflammatory cells to the pleural cavity than congenic controls, with a greater proportion of viable cells, at the onset and peak of pleurisy, suggesting a worse inflammatory response. Histological examination suggested impaired resolution of inflammation in *Hsd11b1*$^{-/-}$ mice with persistence of inflammation in the visceral pleura, activation of lymphoid aggregates, and uniquely in *Hsd11b1*$^{-/-}$ mice, formation of fibrous adhesions between lung lobes 48h after initiation of pleurisy. During experimental arthritis induced by injection of serum from arthritic

K/BxN mice, clinical signs of inflammation occurred earlier in *Hsd11b1*$^{-/-}$ mice and were slower to resolve than in control mice. Histological assessment of the acute phase (2d) of arthritis showed no difference in joint pathology between genotypes, despite greater oedema and higher clinical scores in the *Hsd11b1*$^{-/-}$ mice. However, when the inflammation had resolved (21d following injection of serum), compared to control mice, *Hsd11b1*$^{-/-}$ mice showed more severe exostosis, intense periarticular inflammation, more collagen deposition and uniquely, ganglion cyst formation. At 21d, whereas basal (morning) plasma corticosterone levels were normal in control mice, they remained elevated in *Hsd11b1*$^{-/-}$ mice, suggesting ongoing inflammation and persistent activation of the hypothalamic-pituitary-adrenal axis. Mast cells are critical in the initiation of an inflammatory response and are essential in this model of arthritis. Mast cells expressed 11β-HSD1 (but not 11β-HSD2) mRNA and activity. Although mast cell number did not differ in joints or peritoneum of *Hsd11b1*$^{-/-}$ mice, 11β-HSD1-deficient mast cells had a lower threshold for degranulation induced by K/BxN arthritogenic serum. As well as implicating a role for mast cell 11β-HSD1 in limiting initial inflammation in arthritis, these findings also have implications for infection, allergy and tolerance. Collectively, these data suggest that 11β-HSD1 deficiency worsens acute inflammation and results in slower resolution. Therefore, amplification of intracellular glucocorticoids levels, by 11β-HSD1, may represent an important mechanism to limit the acute inflammatory response and programme its subsequent resolution. Increasing leukocyte 11β-HSD1 or local delivery of substrate affords a novel approach for anti-inflammatory therapy.

To my husband Martinho,
Who has traveled half way around the world,
for me.

Acknowledgements

First and foremost I would like to thank my husband Martinho. I would not have been able to move to Edinburgh had he not had the inclination to come with me and leave everything behind while I completed the work presented in this thesis.

Likewise, I would not have had the opportunity to come to Edinburgh in the first place if Prof Karen Chapman had not invited me to visit the Endocrinology lab while completing my MSc studies in Toronto. I thank her for being a truly *fantastic* supervisor and mentor and especially for her patience and unfailing support over the years.

Thank you to my supervisors Prof Jonathan Seckl and Prof John Savill, for providing me with enthusiastic guidance and motivation. I am grateful to include Dr Mohini Gray in this section; she has played a key supervisory role in guiding my project. I thank all of my supervisors for sharing with me their knowledge and providing me with this amazing research opportunity.

I would like to express my gratitude and appreciation to my colleagues, who have helped me along the way and enriched my experience with their colourful personalities, particularly; Ms Katherine Miles, who has skillfully taught me very useful laboratory techniques. Mr Spike Clay who has shared his expert technical advice with me and performed difficult experimental procedures that contributed to this thesis. Dr Tiina Kipari and Mrs Shonna Johnston for their tremendous help with flow cytometry and also for their friendship. Ms Kay Samuel for her expert advice technical guidance and help with the bone marrow transfer experiment and flow cytometry analysis. And Ms Janet (Tak Yung) Man for her friendship and help in the lab throughout the years.

Thanks also to the rest of the staff of the Endocrinology Unit and the CIR, past and present, I would like to highlight the following people, who in their own way have helped along the way: Mrs Val Kelly, for teaching me how to extract RNA and for the lovely chats in the mornings. Ms Lynne Ramage for teaching me how to measure 11β-HSD1 acitivity. Mrs Aili Zhang and Ms Anne Grant for invaluable technical advice. Mr Fu Yang for help with tissue collections. Dr Jeremy Brown for technical and intellectual advice about mast cells. Dr David Brownstein and Prof Donald Salter for their expert interpretation of pathology. Dr Julie Nixon for teaching me how to set up real time PCRs. Dr Debbie Sawatzky for collaborating on the pleurisy experiments. Dr Ruth Andrew for help with HPLC analysis. Dr Rob van `t Hof for performing the μCT-scan analysis. Mrs Susan Harvey and Mr Bob Morris for histology assistance. Mr William Mungal and Larraine for looking after my mice. And although outside of the lab, Dr Sara Cay for being an amazing doctor.

Special thanks are due to Dr Cristina Esteves, Dr Sophie Rajaonah-Turban, Dr Jacqui Horn, Dr Sabrina Semprini and Dr Joyce Yau, for enlightening discussions regarding science and life, both in and outside of the lab, as well as their enthusiasm and encouragement.

And finally, I would like to thank my family and friends "back home" for being a constant source of motivation and for cheering me on all the way from "across the pond". I thank my parents, Elizabeth and Richard, as well as my sister Ilona, for believing that I could accomplish anything I set my mind to.

Declaration

I, Agnes Elizabeth Coutinho, declare that this thesis and the data presented in it are the result of my own efforts with technical help from the following individuals; Mr Spike Clay and Dr Deborah Sawatzky who performed the intra-pleural injections and pleural lavages in carrageenan-induced pleurisy experiments; Dr Mohini Gray who performed immunization with CIA-CFA and initiated the first K/BxN arthritis experiment; and Ms Kay Samuel who performed the irradiation and tail vain injections, as well as set up flow cytometric analysis, for the bone marrow transfer experiment. This work has not been submitted for any other professional qualification or degree, except as specified.

_____

Agnes E. Coutinho

Edinburgh, 2009

Table of Contents

Abstract ii

Dedication iv

Acknowledgements v

Declaration vii

Table of Contents viii

Index of Figures xiv

Index of Tables xviii

List of Abbreviations xix

Chapter One: Introduction and Review of Literature 1

1.1. Introduction 2

1.2. Inflammation 5

1.2.1. Mast Cells 7

1.3. The Immune and Neuroendocrine Connection 12

1.4. HPA Axis and GC Biosynthesis 14

1.4.1. Regulation of the HPA Axis 15

1.5. Glucocorticoids 15

1.5.1. GC receptor 16

1.5.2. GC function 19

1.5.2.1. The Immune System and GC 20

1.5.2.2. Metabolism and GC 26

1.6. 11β-Hydroxysteroid dehydrogenase 27

1.6.1. 11β-HSD2 27

1.6.2. 11β-HSD1 28

1.6.3. Mice Deficient in 11β-HSD1 30

1.6.4. 11β-HSD1 and the Immune System 31

1.6.5. Regulation of 11β-HSD1 33

1.7. 11β-HSD-deficiency and Inflammation 37

1.8. Hypothesis and Aims of the Thesis 38

1.8.1. Hypothesis 38

1.8.2. Aims 39

Chapter Two: Materials and Methods 40

2.1. Materials 41

2.2. Animals 43

2.3. Methods 43

2.3.1. Thioglycollate-induced sterile peritonitis 43

2.3.2. Cell culture 44

2.3.3. Enrichment of peritoneal mast cells 45

2.3.4. Bone marrow derived macrophages (BMD-Mϕ) 45

2.3.5. Bone marrow derived mast cells (BMD-MC) 46

2.3.6. Measurement of 11β-HSD1 activity 46

2.3.6.1. Preparation of [^{3}H] 11-dehydrocorticosterone 46

2.3.6.2. 11β-reductase/dehydrogenase assay 47

2.3.6.3. Thin Layer Chromatography (TLC) 48
2.3.7. Models of experimental arthritis 48
2.3.7.1. Collagen-Induced Arthritis (CIA) 48
2.3.7.2. KxB/N serum transfer model 49
2.3.7.2.1. The K/BxN model of inflammatory arthritis 49
2.3.7.2.2. Assessment of inflammatory arthritis 50
2.3.7.2.3. Histological assessment 51
2.3.8. Tail nick blood collection 52
2.3.9. Corticosterone radioimmunoassay 52
2.3.10. Carrageenan-induced pleurisy 53
2.3.10.1. Induction of pleurisy 53
2.3.10.2. Assessment of pleural inflammation 54
2.3.10.3. Cytokine measurements (ELISA and CBA kit) 54
2.3.10.4. Histological assessment 56
2.3.11. RNA Extraction and Analysis 56
2.3.11.1. RNA extraction 56
2.3.11.2. Reverse transcription 57
2.3.11.3. Polymerase Chain Reaction (PCR) 58
2.3.12. Centrifugation of cells 60
2.3.13. Immunohistochemistry (IHC) 60
2.3.13.1. In-house 11β-HSD1 antibody 62
2.3.13.2. Western Blot 64
2.3.14. Toluidine blue staining 65

2.3.15. Bone marrow transplantation (BMT) 65

2.3.16. Flow cytometry 66

2.3.17. Assessment of vascular permeability with Evan's Blue Dye 67

2.3.18. Mast cell degranulation 68

2.3.19. Statistics 69

Chapter Three: 11β-HSD1-deficiency worsens the inflammatory response during Carrageenan-induced pleurisy 70

3.1. Introduction 71

3.2. Results 72

3.2.1. More inflammatory cells are recruited in *Hsd11b1*$^{-/-}$ mice than in *Hsd11b1*$^{+/+}$ mice during carrageenan-induced pleurisy 72

3.2.2. Assessment of phenotype of intra-pleural inflammatory cells 76

3.2.3. Altered viability of intra-pleural inflammatory cells from *Hsd11b1*$^{-/-}$ mice 79

3.2.4. Resolution of lung inflammation is altered in *Hsd11b1*$^{-/-}$ mice 83

3.2.5. Lung cytokine profiles during carrageenan-induced pleurisy 91

3.3. Discussion 93

Chapter Four: Effects of 11β-HSD1-deficiency on experimental arthritis 98

4.1. Introduction 99

4.2. Results 100

4.2.1. C57BL/6 mice are resistant to arthritis in the CIA-CFA model 100

4.2.2. Earlier onset of arthritis and delayed resolution following K/BxN serum transfer in *Hsd11b1*$^{-/-}$ mice: Experiment 1, standard dose of K/BxN serum 102

4.2.2.1. Pathology analysis after 21d of K/BxN arthritis 105

4.2.2.2. Effects of K/BxN arthritis on anthropometric measurements 107

4.2.3. Earlier onset of arthritis and delayed resolution in *Hsd11b1*$^{-/-}$ mice: Experiment 2, reduced dose of K/BxN serum 109

4.2.3.1. Pathology analysis after 21d of K/BxN arthritis 112

4.2.3.2. Plasma corticosterone levels remained elevated in *Hsd11b1*$^{-/-}$ mice during the resolution stage of arthritis 112

4.2.3.3. Effects of K/BxN arthritis on anthropometric measurements 113

4.2.4. K/BxN arthritis: acute phase 117

4.2.5. Micro-CT scanning reveals altered bone micro-architecture in *Hsd11b1*$^{-/-}$ mice following K/BxN arthritis 119

4.3 Discussion 123

Chapter Five: 11β-HSD1 in Mast Cells 128

5.1. Introduction 129

5.2. Results 130

5.2.1. Immunohistochemical staining of 11β-HSD1 in peritoneal cells 130

5.2.2. 11β-HSD1 activity in BMD-MC 132

5.2.3. 11β-HSD1 mRNA is expressed in BMD-MC 135

5.2.4. MC number is not altered in peritoneum or joints of *Hsd11b1*$^{-/-}$ mice 138

5.2.5. Enhanced MC degranulation in *Hsd11b1*$^{-/-}$ mice 140

5.2.6. *Hsd11b1*$^{-/-}$ mice have an altered MC phenotype 144

5.2.7. Assessment of vascular leakage in skin 148

5.2.8. Assessment of vascular leakage in the peritoneum 150

5.3. Discussion 152

Chapter Six: Assessment of the immune system and its contribution to the inflammatory response in *Hsd11b1*$^{-/-}$ mice **156**

6.1 Introduction **157**

6.2 Results **158**

6.2.1 Effects of 11β-HSD1-deficiency on number of immune cells 158

6.2.2 Flow cytometric analysis of immune cells from *Hsd11b1*$^{-/-}$ and *Hsd11b1*$^{+/+}$ mice 158

6.2.3 Effects of 11β-HSD1-deficiency on immune cell populations 162

6.2.4 Bone marrow cell transfer between *Hsd11b1*$^{-/-}$and *Hsd11b1*$^{+/+}$ mice 168

6.2.5 Induction of K/BxN serum transfer arthritis following BMT 168

6.2.6 Assessment of immune cells following BMT and K/BxN arthritis 174

6.3 Discussion **178**

Chapter Seven: Summary and Discussion **181**

7.1 Summary **182**

7.2 Discussion **183**

References **190**

Appendix I: Summary of flow cytometric assessment of immune cells following BMT and K/BxN arthritis

Appendix II: Awards, Presentations and Publications

Index of Figures

Figure 1.1 Intracellular regulation of GC action by 11β-HSD 4

Figure 1.2 Activation of MC leads to release of inflammatory mediators which generate a wide array of biological effects 10

Figure 1.3 The immune system and neuroendocrine cross-talk 13

Figure 1.4 Schematic representation of GC action 17

Figure 1.5 Concentration of GC determines the degree of protective immune response 21

Figure 1.6 Increasing number of publications on 11β-HSD1 expression, function and regulation during inflammation 32

Figure 2.1 In-house 11β-HSD1 antibody detects 11β-HSD1 protein in control mice 63

Figure 3.1 *Hsd11b1*$^{-/-}$ mice show a more severe inflammatory response during the acute and peak stages of carrageenan-induced pleurisy 74

Figure 3.2 *Hsd11b1*$^{-/-}$ mice show a more severe inflammatory response at 72h following injection of carrageenan 75

Figure 3.3 Similar inflammatory cell types were recruited in *Hsd11b1*$^{-/-}$ and *Hsd11b1*$^{+/+}$ mice at 4h after carrageenan injection 77

Figure 3.4 Greater Gr-1^{+} F4/80^{+} sub-population of intra-pleural cells extracted from *Hsd11b1*$^{-/-}$ than *Hsd11b1*$^{+/+}$ mice at 4h and 24h 78

Figure 3.5 In study 1, more viable inflammatory cells were recovered from intra-pleural lavages of *Hsd11b1*$^{-/-}$ mice than of *Hsd11b1*$^{+/+}$ mice at 4h and 24h 80

Figure 3.6 PI and Annexin V staining of pleural inflammatory cells 81

Figure 3.7 In study 2, more viable Gr-1^{+} F4/80^{+} cells were present in lavages from *Hsd11b1*$^{-/-}$ mice than from *Hsd11b1*$^{+/+}$ mice at all time points during pleurisy 82

Figure 3.8 4h following injection of carrageenan inflammation is noticeable in both genotypes with thickened visceral pleura and enlarged mesothelial cells 85

Figure 3.9 Lymphoid aggregates in lung sections at 24h following injection of carrageenan in mice from both genotypes 86

Figure 3.10 Ongoing inflammation in *Hsd11b1*$^{-/-}$ mice at 48h following carrageenan injection 87

Figure 3.11 Greater peri-oesophageal mediastinum thickening with worse inflammation in *Hsd11b1*$^{-/-}$ mice 88

Figure 3.12 Persistent thickening in visceral pleura in *Hsd11b1*$^{-/-}$ mice 89

Figure 3.13 Adhesion of lung lobes 48h following intra-pleural injection of carrageenan in *Hsd11b1*$^{-/-}$ mice 90

Figure 3.14 Study 1, altered cytokine levels in *Hsd11b1*$^{-/-}$ versus *Hsd11b1*$^{+/+}$ mice following intra-pleural injection of carrageenan 92

Figure 4.1 A greater proportion of *Hsd11b1*$^{-/-}$ mice developed dermal ulcers following CIA-CFA immunization than *Hsd11b1*$^{+/+}$ mice 101

Figure 4.2 I.p. injection of K/BxN serum results in joint swelling 103

Figure 4.3 Earlier onset of arthritis and delayed resolution following K/BxN serum transfer in *Hsd11b1*$^{-/-}$ mice 104

Figure 4.4 Pathology does not differ between the genotypes after 21d of standard dose K/BxN serum transfer arthritis 106

Figure 4.5 Anthropometric differences between *Hsd11b1*$^{-/-}$ and *Hsd11b1*$^{+/+}$ mice in response to K/BxN serum transfer arthritis 108

Figure 4.6 Earlier onset and delayed resolution of arthritis in *Hsd11b1*$^{-/-}$ mice with reduced dose of K/BxN serum 110

Figure 4.7 The total number of joints, with more severe clinical scores, was higher in *Hsd11b1*$^{-/-}$ than in the *Hsd11b1*$^{+/+}$ mice 111

Figure 4.8 Histological assessment showed a more reactive bone phenotype and intense periarticular inflammation with severe exostosis and ganglion cyst formation in *Hsd11b1*$^{-/-}$ mice 114

Figure 4.9 High circulating corticosterone levels in *Hsd11b1*$^{-/-}$ mice at 21d after K/BxN serum injection 115

Figure 4.10 Anthropometric effects of 11β-HSD1 deficiency following K/BxN arthritis 116

Figure 4.11 More aggressive onset of inflammation in *Hsd11b1*$^{-/-}$ mice 2d after of K/BxN serum injection 118

Figure 4.12 Weaker and less connected trabecular bone in femurs of *Hsd11b1*$^{-/-}$ than *Hsd11b1*$^{+/+}$ mice following 21d of K/BxN arthritis 122

Figure 5.1 Immunofluorescent detection of 11β-HSD1 in tryptase-positive peritoneal MC 131

Figure 5.2 11β-HSD1 staining of resident peritoneal MC from *Hsd11b1*$^{+/+}$ mice 133

Figure 5.3 11β-HSD1 activity in BMD-MC 134

Figure 5.4 *Hsd11b1* mRNA in BMD-MC and other immune cells 136

Figure 5.5 BMD-MC transcribe *Hsd11b1* from the P1 promoter 137

Figure 5.6 Toluidine blue staining of MC in joints showed MC number did not differ between *Hsd11b1*$^{-/-}$ and *Hsd11b1*$^{+/+}$ mice, 2d following 7.5µl/g injection of K/BxN serum 139

Figure 5.7 Effect of ionomycin, CRH and K/BxN serum on MC degranulation measured by β-hexosaminidase release 142

Figure 5.8 Compared to control MC, 11β-HSD1-deficient peritoneal MC show greater degranulation induced by K/BxN serum 143

Figure 5.9 Comparable histochemical staining of peritoneal MC from *Hsd11b1*$^{-/-}$ and *Hsd11b1*$^{+/+}$ mice 145

Figure 5.10 A greater proportion of CD117^{+} peritoneal cells from *Hsd11b1*$^{-/-}$ mice express CD11b and F4/80 than in *Hsd11b1*$^{+/+}$ mice 146

Figure 5.11 Flow cytometric analysis of size and granularity of CD117^{+} peritoneal cells shows altered phenotype in *Hsd11b1*$^{-/-}$ mice 147

Figure 5.12 Assessment of vascular leakage in skin using MC secretagogues and Evan's Blue dye 149

Figure 5.13 Vascular leakage was not different between genotypes 4h following induction of TG-peritonitis and was highly variable within each genotype group 151

Figure 6.1 Total cell number in immune organs and leukocyte number in peripheral blood did not differ between *Hsd11b1*$^{-/-}$ and *Hsd11b1*$^{+/+}$ mice 159

Figure 6.2 Representative dot plots and histograms used for flow cytometric analysis of immune cells from naïve *Hsd11b1*$^{-/-}$ and *Hsd11b1*$^{+/+}$ mice 161

Figure 6.3 *Hsd11b1*$^{-/-}$ mice have more T cells but fewer granulocytes in the peritoneum than *Hsd11b1*$^{+/+}$ mice 163

Figure 6.4 Altered distributions of B cells and granulocytes in the BM of untreated *Hsd11b1*$^{-/-}$ mice 164

Figure 6.5 Experimental design for BMT-arthritis 170

Figure 6.6 Time course of arthritis in non-BMT mice is similar to that observed previously 171

Figure 6.7 High variability in clinical scoring following injection of K/BxN serum in individual BMT-mice 172

Figure 6.8 Similar clinical scores for WT(KO) and KO(WT) mice following injection of K/BxN serum 173

Figure 6.9 Following arthritis, *Hsd11b1*$^{-/-}$ mice had fewer spleenocytes and BM cells but a similar number of peritoneal cells and thymocytes as *Hsd11b1*$^{+/+}$ mice 175

Figure 6.10 Similar number of immune cells in WT(KO) and KO(WT) mice with or without arthritis 176

Figure 6.11 Severity of arthritis was positively associated with BM cells, irrespective of genotype 177

Appendix I, Figure 1.1 Altered cell markers in cells from BM in BMT-arthritis mice

Index of Tables

Table 1.1 Examples of immune-related genes regulated by GC 25

Table 1.2 Regulation of 11β-HSD1 levels by inflammatory mediators 36

Table 4.1 Histomorphometric parameters for trabecular bone from Micro-CT scanning of femur bones 2d after injection of K/BxN serum 120

Table 4.2 Histomorphometric parameters for trabecular bone from Micro-CT scanning of femur bones 21d after injection of K/BxN serum 121

Table 4.3 Histomorphometric parameters for cortical bone from Micro-CT scanning of femur bones 21d after injection of K/BxN serum 121

Table 6.1 Overview of antibodies used for the flow cytometric assessment of inflammatory cell phenotype in *Hsd11b1*$^{-/-}$ mice 160

Table 6.2 Flow cytometric comparison of peripheral blood cells from untreated *Hsd11b1*$^{-/-}$ and *Hsd11b1*$^{+/+}$ mice 165

Table 6.3 Flow cytometric comparison of thymocytes from untreated *Hsd11b1*$^{-/-}$ and *Hsd11b1*$^{+/+}$ mice 166

Table 6.4 Flow cytometric comparison of spleenocytes from untreated *Hsd11b1*$^{-/-}$ and *Hsd11b1*$^{+/+}$ mice 167

Appendix I, Table 1. Flow cytometry analysis of $CD4^+$ and $CD8^+$ cells in the thymus from all BMT/arthritis experimental groups

Appendix I, Table 2. Flow cytometry analysis of spleenocytes and BM cells from normal *Hsd11b1*$^{-/-}$ and control mice subjected to 21d of K/BxN arthritis

Appendix I, Table 3. Flow cytometry comparison of BM cells, peritoneal cells and spleenocytes from WT(KO) and KO(WT) mice following BMT-arthritis

List of Abbreviations

11β-HSD	11beta-Hydroxysteroid dehydrogenase
11-DHC	11-Dehydrocorticosterone
ACTH	Adrenocorticotrophic hormone
ANOVA	Analysis of variance
AP-1	Activator protein-1
APC	Allophycocyanin
BMD	Bone marrow derived
BMT	Bone marrow transfer
bp	Base pairs
BSA	Bovine serum albumin
C48/80	Compound 48/80
CBA	Cytometric bead assay
CBG	Corticosterone binding globulin
CD	Cluster of differentiation
CNS	Central nervous system
COX-2	Cyclo-oxygenase 2
CRH	Corticotrophin releasing hormone
DAB	Diaminobenzidine
DC	Dendritic cell
DEPC	Diethylpyrocardbonate
DMEM	Dulbeco's modified Eagle's medium
DNA	Deoxyribo-nucleic acid
DTT	Dithiothriotol
EDTA	Ethylene diamine tetraacetic acid
EtOH	Ethanol
FCS	Foetal calf serum
FITC	Fluorescein isothiocyanate
GM-CSF	Granulocyte/Mϕ colony stimulating factor
GC	Glucocorticoids
GR	Glucocorticoid receptor
GRE	Glucocorticoid response element
H6PDH	Hexose-6-phosphate dehydrogenase
HPA-axis	Hypothalamic-pituitary gland-adrenal gland-axis
HPLC	High pressure liquid chromatography
hps	Heat shock protein
HRP	Horse radish peroxidase
IFN-γ	Inteferon gamma
Ig	Immunoglobulin
IL	Interleukin
i.p.	Intra-peritoneal
i.v.	Intra-venous
LPS	Lipopolysaccharide

Mϕ	Macrophage
MC	Mast cell
MCP-1	Monocyte chemoattractant protein l
MIP-1	Mϕ-inflammatory protein 1 alpha
mMCP	Mouse mast cell protease
MR	Mineralocorticoid receptor
mRNA	Messenger RNA
NAD	Nicotinamide adenine dinucleotide
NADP	Nicotinamide adenine dinucleotide phosphate
NFκB	Nuclear factor-kappa B
NT	Neurotensin
PBS	Phosphate buffered saline
PCR	Polymerase chain reaction
PE	Phycoerythrin
RBC	Red blood cells
RNA	Ribo-nucleic acid
RT	Room temperature
SP	Substance P
TAE	Tris EDTA acetate
TG	Thioglycollate
TGF-β	Transforming growth factor beta
TLC	Thin Layer Chromatography
TNF-α	Tumor necrosis factor alpha
VEGF	Vascular endothelial growth factor
VIP	Vasoactive intestinal peptide

Chapter One

Introduction and Review of Literature

1.1 Introduction

Inflammation, comprising altered blood flow, recruitment and activation of immune cells, is an essential part of the response to injury, characterized by a rise in temperature, redness, swelling, and pain at the injured site. Glucocorticoids (GC) are potent regulators of the immune system and have been widely used to treat inflammatory and auto-immune diseases for over 50 years. Today, synthetic GC, as well as natural GC (cortisone and cortisol), are commonly prescribed for a variety of inflammatory conditions and immune disorders (eg. eczema, asthma and auto-immune diseases) as well as the management of the immune response in organ transplantation. Philip S. Hench was the first to recognize the potent anti-inflammatory properties of the endogenous adrenal hormone cortisone (Hench et al., 1949), first discovered by Edward Calvin Kendall. In 1950, together with Kendall and Tadeus Reichstein, Hench was awarded a Nobel Prize, initiating the beginning of GC therapy for the treatment of inflammatory and autoimmune diseases. Since then, research into the protective 'anti-inflammatory' mechanisms of adrenal hormones has revealed that GC levels during physiological stress and at pharmacological doses exert powerful immuno-suppressive effects, whereas normal circulating GC levels have modulatory effects on the immune system (Munck et al., 1984). Overall, it is commonly accepted that GC serve to limit an immune response, preventing its overshoot. Moreover, during the onset of inflammation they attenuate oedema and regulate leukocyte trafficking, haematopoietic differentiation programs and gene transcription within GC sensitive cells (Munck et al., 1984; McEwen et al., 1997; Ashwell et al., 2000). The mechanism(s) by which GC prevent and/or suppress inflammation resulting from infectious, mechanical, chemical, and

immunological stimuli is still unclear. Better knowledge of the regulation of endogenous GC action during an inflammatory response will improve our understanding of susceptibility to and development of diseases as well as possibly leading to improved treatment and/or disease prevention. Regulation of GC action is multi-level and is dependent on the concentration of steroid in the circulation as well as the distribution and concentration of receptors. The last decade has produced a wealth of information on the importance of pre-receptor GC metabolism by an intracellular enzyme, 11β-hydroxysteroid dehydrogenase (11β-HSD), which modulates the amount of GC that reaches the receptors. 11β-HSD interconverts active GC (cortisol in humans, corticosterone in rodents) and intrinsically inert 11-keto metabolites (cortisone in humans, 11-dehydrocorticosterone or 11-DHC in rodents). Whereas 11β-HSD Type 2 (11β-HSD2), predominantly inactivates GC, *in vivo* 11β-HSD1 predominantly reactivates GC (Figure 1.1). Therefore, 11β-HSD1 orchestrates a further and important level of regulation over GC action, influencing cellular GC action by increasing GC concentration within target cells. Thus, orally administered cortisone is first converted by 11β-HSD1 to the active GC, cortisol, in order to be effective. This chapter will review the current knowledge of GC metabolism and GC physiology, emphasizing the role of 11β-HSD1 and its effect on inflammation. The chapter concludes with the hypotheses and aims of the thesis.

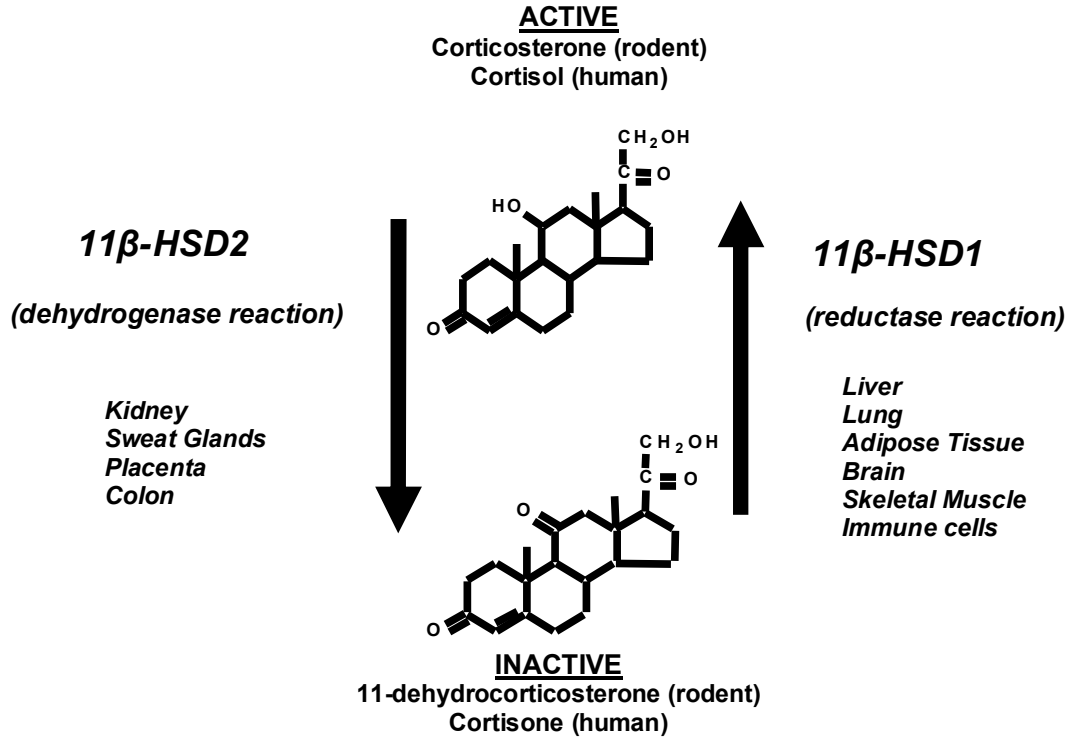

Figure 1.1 Intracellular regulation of GC levels by 11β-HSD.
11β-HSD enzyme modulates the amount of GC that reaches the receptors by interconverting active GC (cortisol in humans, corticosterone in rodents) and intrinsically inert 11-keto metabolites (cortisone in humans, 11-dehydrocorticosterone or 11-DHC in rodents). Two isozymes exist; 11β-HSD2 inactivates GC (Albiston et al., 1994; Brown et al., 1996), whilst within intact cells 11β-HSD1 is predominantly a GC reactivating enzyme (Low et al., 1994a; Jamieson et al., 1995; Brem et al., 1995; Rajan et al., 1996; Jamieson et al., 2000). 11β-HSD2 expression is mainly restricted to kidney and sweat glands, whereas 11β-HSD1 is more widespread with highest expression in liver and more modest expression in adipose tissue, kidney, brain, lung, etc.

1.2 Inflammation

Inflammation is a central feature of the host's defense system and although specific characteristics depend on the immune exposure (irritant versus pathogen), the recruitment process and activation of inflammatory cells are common. For the most part, inflammation is an essential part of a response to injury and is necessary to return the body to homeostasis by successful elimination of the irritant (eg. bacteria) ultimately leading to resolution and tissue repair (Savill et al., 2002; Hanson et al., 2005). Although categorically distinct, the innate (mainly myeloid cells) and adaptive (T and B lymphocytes) immune systems interact and often overlap during an inflammatory response. However, this thesis concentrates on the role played by the innate system in the inflammatory response and the early induced responses that do not generate immunological memory. Thus, the following section focuses specifically on myeloid cells.

In general, an inflammatory response consists of 3 separate phases; onset, expansion and effector/resolution. The **onset** or 'induction' phase begins when a regional or systemic insult is detected. Resident innate immune cells such as macrophages (Mϕ) and mast cells (MC) play key roles in the induction phase (Metcalfe et al., 1997; He & Walls, 1998), providing important sources of the inflammatory mediators that cause oedema and recruit leukocytes and instruct the adaptive immune system. Circulating leukocytes migrate toward the location of the initiating stimulus in response to a concentration gradient of inflammatory mediators; chemokines and cytokines. The inflammatory

mediators secreted by resident Mϕ and MC include prostaglandins, histamine, leukotrienes, complement derived peptides and cytokines particularly cytokines interleukin (IL)-1, IL-6 and tumour necrosis factor alpha (TNF-α) and the chemoattractants, IL-8 and monocyte chemotactic protein (MCP)-1 (Lewis & Holmes, 1991; Topley et al., 1993; Topley et al., 1994; Bauermeister et al., 1998; Kolaczkowska et al., 2001; Kolaczkowska et al., 2002). These mediators regulate and shape the subsequent inflammatory response, influencing growth, differentiation and activation of immune cells (Borish & Steinke, 2003). Pro-inflammatory cytokines activate cells through binding to surface receptors and trigger signal transduction pathways including receptor tyrosine kinases, mitogen-activated protein kinases (MAPK), and janus kinases. Chemokine gradients attract and guide leukocytes to the source of injury leading to the second stage of an inflammatory response.

The **expansion** phase is characterized by an influx of neutrophils (which dominate the early response), followed by inflammatory monocytes that will subsequently differentiate into inflammatory Mϕ (Serhan & Savill, 2005). Extravasation of leukocytes into the tissue is accommodated by increased vascular diameter, blood flow, expression of adhesion molecules on endothelial cells and vascular (local) permeability. It is important to note that non-immune cells, such as fibroblasts that line the serosal cavities (eg. peritoneal and pleural), also participate in an inflammatory response by manipulating the local environment through the production of cytokines and chemokines (Witowski et al., 2001; Loghmani et al., 2002).

The third stage of the inflammatory response is the '**effector**' or resolution phase, when the initiating stimulus is neutralized and inflammation is resolved. Resolution requires neutrophils to undergo apoptosis (Jonsson et al., 2005) followed by their successful removal, primarily by phagocytic leukocytes (Savill et al., 2002). "Professional" phagocytes (such as neutrophils and Mϕ) ingest microbial pathogens and debris from apoptotic and necrotic cells (reviewed in (Greenberg & Grinstein, 2002)). Phagocytosis is an essential process for innate immunity and, because phagocytosis by Mϕ and dendritic cells (DC) leads to presentation of antigen on the cell surface, also serves as a bridge between innate (eg. DC) and acquired (lymphocyte) immune responses. Adequate removal of apoptotic leukocytes and cell debris prevents release of cytotoxic granules and pro-inflammatory mediators from the dying cells. Failure to resolve acute inflammation leads to a chronic inflammatory state that can progress to irreversible organ damage (Savill et al., 1989; Stern et al., 1992; Meagher et al., 1992; Heasman et al., 2003).

1.2.1 Mast Cells

The work in this thesis places strong emphasis on MC and therefore the following section grants more attention to these cells. Although discovered over 130 years ago, until relatively recently, most research on MC focused on allergic and hypersensitivity reactions. This view has now changed so that MC are recognized as "effector" immune cells with a direct impact on many other cells, shaping and regulating immune

responses. MC are critical in host defense mechanisms against certain microbes and parasites, and they participate in tissue remodeling processes such as wound healing, angiogenesis, and fibrogenesis following chronic inflammation (reviewed in (Marshall & Jawdat, 2004)).

Mature MC exist exclusively in tissues as resident cells and are not present in the circulation. MC accumulate in chronically inflamed tissue in humans and in mice, and have consistently been observed in high numbers in human rheumatoid arthritis (reviewed by (Woolley, 2003), in Crohn's disease (Gelbmann et al., 1999) and in the bronchus of asthmatic patients (reviewed in (Kassel & Cato, 2002)). Whilst MC act as potent effector cells releasing various molecules that collectively enhance the inflammatory response (see below), in turn, inflammatory mediators released by MC and other leukocytes modulate the course of MC proliferation and differentiation.

In vitro, MC development from bone marrow (BM) progenitors is dependent on IL-3 (Razin et al., 1984) and SCF (Stem cell factor, also known as kit ligand). SCF is also required for MC survival; its removal from human or mouse MC culture (and IL-3 from the latter) leads to MC apoptosis (Mekori et al., 1993; Iemura et al., 1994). IL-3 is produced mainly by T cells, but also by monocytes, endothelial cells, natural killer (NK) cells, keratinocytes and MC themselves (reviewed by (Frendl, 1992)). SCF is a stromal cell derived cytokine released by fibroblasts (Furitsu et al., 1989) which not only regulates MC growth but also regulates the function of mature MC (Hogaboam et al., 1998). In addition to IL-3 and SCF, numerous cytokines (such as IL-4, 9, 10, 13) and TGF-β, also contribute to MC development, however, these are not essential for their

survival (reviewed (Hu et al., 2007)). MC are heterogeneous and, like Mϕ, have been subtyped; in the case of MC into 'mucosal' and 'connective tissue' types, based on histochemical staining that differs according to the type of heparin proteoglycan present in the secretory granules (Reynolds et al., 1990; Stevens et al., 1994).

Mature MC contain cytoplasmic granules loaded with preformed inflammatory mediators, while the cell surface contains numerous receptors which, upon activation, can trigger exocytosis of granules. Following stimulation, MC release various preformed inflammatory mediators (Figure 1.2) and continue to synthesize additional molecules by new gene transcription and translation (Gordon & Galli, 1990; Sylvestre & Ravetch, 1996). These mediators act to recruit a variety of inflammatory cells (monocytes, neutrophils, DC, lymphocytes and eosinophils), stimulating them to produce their own inflammatory mediators. MC degranulation can be stimulated by cross-linking of immunoglobulin E (IgE) with high affinity cell surface Fcε-RI-receptors, as happens in allergy (reviewed in (Turner & Kinet, 1999)). MC can also be activated by IgG-dependent signaling through Fcγ-RII and Fcγ-RIII-receptor, as well as directly or indirectly by pathogens (bacteria, viruses and parasites) via Toll-like receptors (TLRs) (reviewed in (Marshall & Jawdat, 2004; Galli et al., 2005)). Non-immunological stimulatory pathways have also been described, such as physical stress (cold, trauma, ischemia/reperfusion-induced oxidant production) (Kanwar & Kubes, 1994) and various secretagogues (eg. neuropeptide substance P (SP) and polypeptide analogue compound 48/80) (Gibbs et al., 2001).

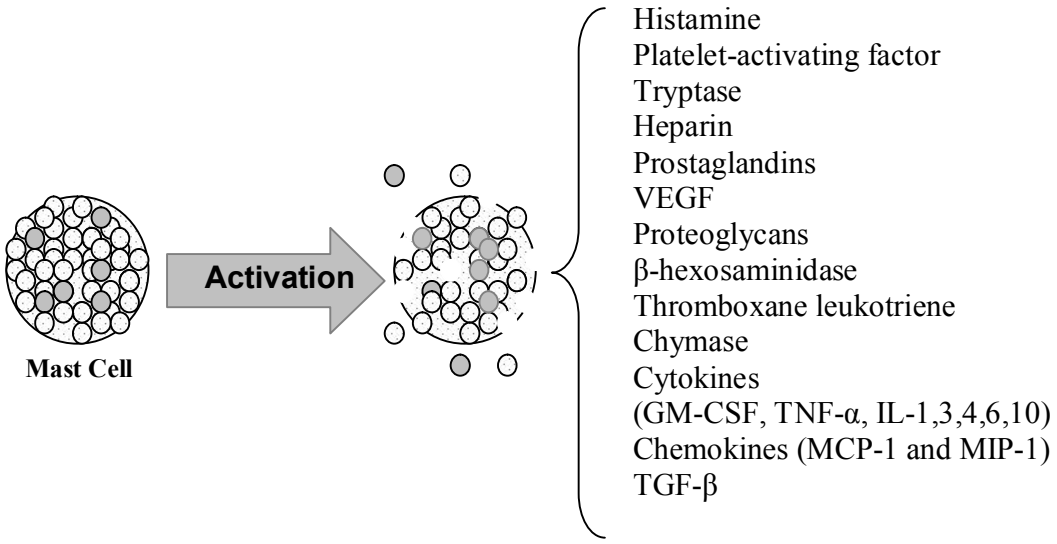

Figure 1.2 Activation of MC leads to release of inflammatory mediators which generate a wide array of biological effects.
These mediators (and others not listed) act to enhance vasopermeability, induce endothelial expression of adhesion molecules, recruit circulating leukocytes, and activate infiltrating, as well as resident, immune cells (reviewed in (Gordon & Galli, 1990; Marshall & Jawdat, 2004)). VEGF, Vascular endothelial growth factor; GM-CSF, Granulocyte/Mϕ colony. stimulating factor; TNF-α, Tumor necrosis factor alpha; IL, Interleukin; MCP-1, Monocyte chemoattractant protein l; MIP-1α, Mϕ-inflammatory protein 1 alpha; TGF-β, transforming growth factor beta.

Finally, MC have been implicated in arthritis (Woolley, 2003). In human inflamed synovium, MC together with neutrophils and TNF-α and IL-1 significantly contribute to the pathogenesis of rheumatoid arthritis (Kiener et al., 1998; Olsson et al., 2001). In mice, MC have been implicated in the K/BxN arthritis model as one of the key and early regulators of pathogenic mechanisms (Lee et al., 2002; Binstadt et al., 2006). Following K/BxN serum transfer, there is a rapid (within minutes) degranulation of MC leading to tissue oedema and infiltration of leukocytes (Binstadt et al., 2006). MC degranulation has also been detected during the chronic phase of K/BxN serum transfer-mediated arthritis, suggesting their ongoing participation (Lee et al., 2002). Indeed, $Kit^{W/W\text{-}v}$ mice which are deficient in MC, are resistant to the development of arthritis following transfer of K/BxN serum (Nagle et al., 1995). Synovial MC show a "connective tissue" phenotype, yet adoptive transfer of MC into $Kit^{W/W\text{-}v}$ mice confers susceptibility to the disease with a similar disease course to normal control mice (Lee et al., 2002). MC have also been implicated in sterile peritonitis, being required for changes in vascular permeability and maximal leukocyte recruitment following injection of zymosan (Ajuebor et al., 1999; Kolaczkowska et al., 2001) or thioglycollate (TG) (Qureshi & Jakschik, 1988).

Although MC are widely portrayed as "promoters" of inflammation, in specific biological responses these cells can have anti-inflammatory properties, albeit perhaps at different stages of the inflammatory response. For example, both IL-10 and transforming growth factor beta (TGF-β), often considered "anti-inflammatory", are stored and released by MC (Gordon & Galli, 1990; Grimbaldeston et al., 2007). Recently, MC

derived IL-10 has been shown to limit ear swelling associated with certain types of contact hypersensitivity (Grimbaldeston et al., 2007)). Thus, the precise role of MC during inflammation, particularly with reference to the different stages of inflammation and type of stimulus, remains to be clarified.

1.3 The Immune and Neuroendocrine Connection

The neuroendocrine system plays an important role in the control of systemic and local immune function through neurons and endocrine cells. For example, neuropeptides such as SP, corticotrophin-releasing hormone (CRH), and vasoactive intestinal peptide (VIP), exert double-edged effects (both pro- and anti-inflammatory) on the immune system (Delgado et al., 2004; Guhl et al., 2005). In turn, the immune system communicates with the neuroendocrine system through a complex network of cytokines, chemokines and other inflammatory messengers resulting in bi-directional signaling between the systems (Figure 1.3 and reviewed in (Sternberg, 2006)). Importantly, the central nervous system (CNS) has direct control over the endocrine system, including corticosteroid synthesis and GC release through the hypothalamic-pituitary-adrenal (HPA) axis (discussed below). Overall, this forms a vast and complex network of reciprocally regulated mechanisms that are aimed at the appropriate initiation of an inflammatory response, neutralization of threat and effective down-regulation of the response in order to prevent unnecessary tissue damage. GC regulation of the immune system is discussed in more detail in Section 1.5.2.1.

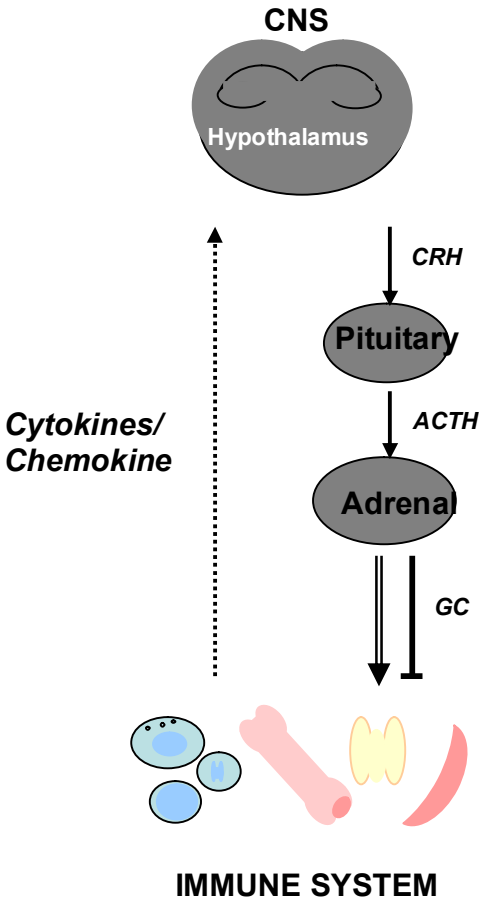

Figure 1.3 The immune system and neuroendocrine cross-talk.
Through the HPA axis, GC orchestrate control over both systemic and local immune function. As well as directly mediating the inflammatory response, cytokines produced at the site of inflammation enter the circulation, cross the blood-brain barrier and stimulate the HPA axis increasing GC secretion (reviewed in (Chesnokova & Melmed, 2002)). CNS, central nervous system; CRH, corticotrophin-releasing hormone; ACTH, adrenocorticotrophic hormone; GC, glucocorticoid.

1.4 HPA Axis and GC Biosynthesis

Classically activated by stress, the HPA axis controls adrenal cortical function partly through the synthesis and release of adrenocorticotrophic hormone (ACTH) from the anterior pituitary. ACTH is the principal hormone stimulating adrenal GC biosynthesis, and is itself regulated by two neuropeptides; CRH (Vale et al., 1981) and arginine vasopressin (AVP) (Salata et al., 1988). These neuropeptides are secreted from the paraventricular nucleus (PVN) of the hypothalamus in response to various stressors. CRH and AVP travel through the portal hypophyseal circulation to the corticotroph cells of the anterior pituitary where they stimulate the synthesis and processing of pro-opiomelanocortin (POMC), a precursor of ACTH (Horrocks et al., 1990; Mountjoy & Wong, 1997). After ACTH binds to its cognate receptor a biochemical pathway is activated leading to an increase in intracellular cyclic adenosine monophosphate (cAMP). Increased cAMP levels induce the expression of steroidogenic acute regulatory protein (StAR), a rate-limiting step in GC steroidogenesis in the zona fasciculata and, to a lesser extent, the zona reticularis of the adrenal cortex. StAR mediates the entry of cholesterol (the precursor to steroids), through the inner membrane of the mitochondria, leading to increased GC synthesis and secretion through a series of enzymatic steps. However, GC are not stored in the adrenal gland, but are synthesised *de novo* and released when required.

1.4.1 Regulation of the HPA Axis

HPA activity is regulated in a circadian rhythm manner (in humans GC plasma levels are highest just prior to waking and reaching a nadir in the evening) and by physiological stress. GC production itself is autoregulated via a negative feedback control loop at the level of both the hypothalamus and the pituitary (De Kloet et al., 1991). An increase in plasma GC levels reduces CRH and AVP production in the hypothalamus and inhibits ACTH production in the pituitary. Inflammatory stimuli activate the HPA axis by promoting production of ACTH and other inflammatory mediators; noradrenaline, pituitary adenylate cyclase-activating polypeptide, vasopressin and other cytokines, released both within the CNS and in the periphery (Chesnokova & Melmed, 2002). Dysregulation of the HPA axis at any level, is associated with autoimmunity and inflammatory and allergic diseases in humans and animal models (Neeck et al., 1990; Lechner et al., 1996; Cutolo et al., 1999).

1.5 Glucocorticoids

GC directly or indirectly regulate multiple processes within the CNS, cardiovascular, immune and reproductive systems, as well as intermediary metabolism, homeostatic processes, growth and development. The bioactivity of GC is associated with the hydroxyl group at carbon 11 (Figure 1.1), such that C11-keto-GC do not bind to GC receptor (GR), whereas C11-hydroxy-GC bind to GR and are therefore active. Circulating cortisol/corticosterone is ~95% bound to carrier proteins; chiefly corticosteroid binding globulin (CBG) (Dunn et al., 1981), but also albumin. In contrast

to active GC, cortisone/11-DHC remains unbound and apparently crosses cell membranes freely (Figure 1.4). The binding of the steroid to CBG prohibits the combined molecules from crossing cell membranes of the target tissues, thus CBG is an important regulator of circulating GC availability. CBG becomes saturated at high physiological GC levels, as seen following stress, allowing for greater availability of free steroids, which may play a role in GC delivery during inflammation (Hammond et al., 1990).

1.5.1 GC Receptor

GC bind to 2 nuclear receptor subtypes; the mineralocorticoid receptor (MR), and the GR. GC exert most of their physiological effects through the 94 kDa GR protein which is a member of the superfamily of nuclear receptors, designated as nuclear receptor subfamily 3, group C, member 1 (NR3C1). MR have a high affinity for physiological GC, ~10-fold greater than that of GR (eg. MR Kd is ~0.5nM, while GR Kd is ~5nM for corticosterone), and they are anatomically restricted to specific tissues including the kidneys, sweat glands, colon and brain (reviewed in (Funder, 1997; Odermatt & Atanasov, 2009)). In contrast, GR is distributed throughout the periphery and brain (Reul & de Kloet, 1985; Reul et al., 1989). GR expression levels vary between and within tissues contributing to tissue-specific sensitivity to GC.

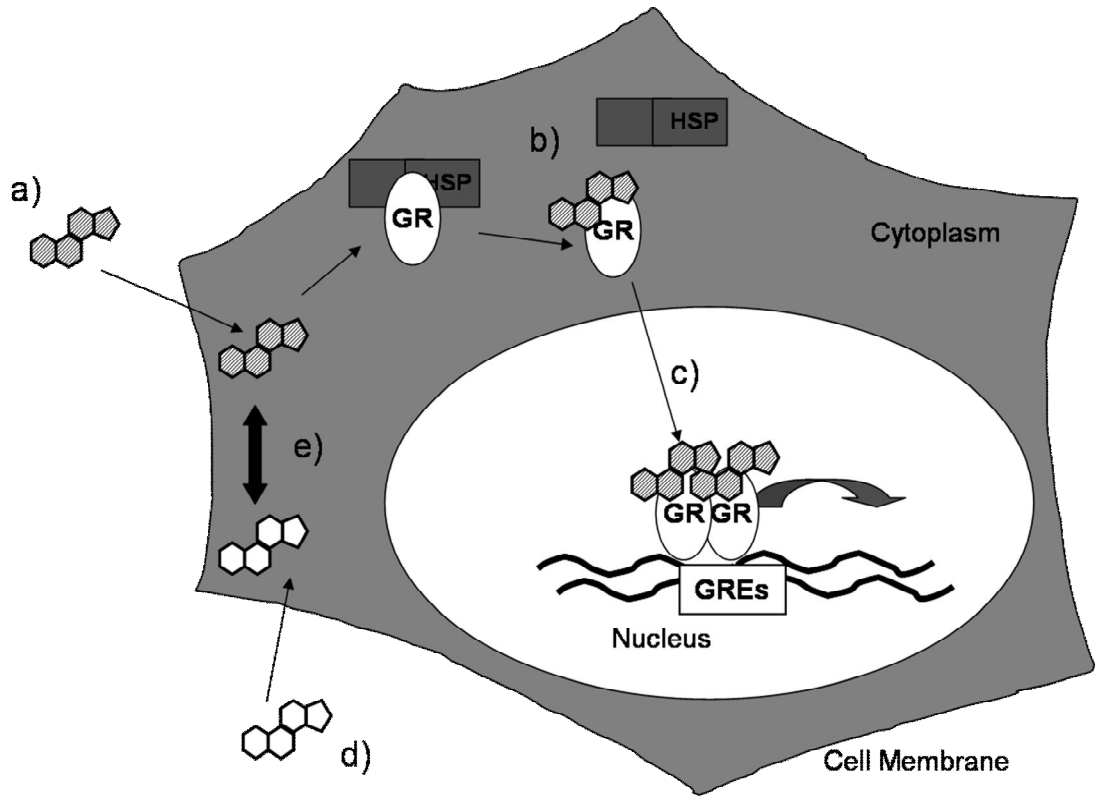

Figure 1.4 Schematic representation of GC action.
Showing a) extracellular ligand (active GC), b) intracellular active GC binding to GR, dissociation of HSP, c) import of GC-GR complex into the nucleus, and binding to GRE. d) inactive GC cross cell membranes freely and e) are subjected to reversible inter-conversion between active and inactive GC by 11β-HSD. The role of 11β-HSD in modulating GC function is discussed in detail in Section 1.6. GR, glucocorticoid receptor; GREs, glucocorticoid-response elements; HSP, heat shock proteins.

In the absence of ligand, GR resides predominantly in the cytoplasm as part of a multi-protein complex comprising several heat shock proteins (hsp), notably hsp90, but also hsp70, and several other proteins, which keep the receptor in an inactive state and prevent GR from entering the nucleus (reviewed in (Grad & Picard, 2007)). The molecular chaperone hsp90 regulates receptor folding, trafficking and transcriptional activation (reviewed in (Pratt & Toft, 1997). Upon ligand binding, the GR-ligand complex dissociates from these proteins, forms homodimers and shifts to the nucleus. Once in the nucleus, together with other transcription factors, GR homodimers induce gene transcription by binding to specific DNA sequences (i.e. GC response elements or GRE) in the regulatory regions of target genes, leading to chromatin remodeling and recruitment of RNA polymerase II to sites of local DNA unwinding (Ito et al., 2000). At some genes, the GR-GC complex binds to DNA and acts as a transcription repressor. Repression by GR may also be effected by non-DNA binding mechanisms, for example by binding to activator protein-1 (AP-1) or nuclear factor κB (NFκB) (Auphan et al., 1995) to inhibit transactivation by these transcription factors. This mechanism, however, remains controversial and more recent data suggest that many of the "repressive" actions of GC are actually mediated by mechanisms involving gene activation (reviewed in (Necela & Cidlowski, 2004)).

Moreover, although most of the literature shows that GC exert their effects by regulating genomic activity, there is some evidence which suggests that GC can also exert non-genomic actions through membrane-bound GR (Bartholome et al., 2004) or by

cytosolic GR (Croxtall et al., 2002). The effects of GC are apparent within minutes of addition of GC, too rapid for changes in gene transcription to occur. Two possible explanations might be that signaling at the membrane occurs via classical GR which localizes in the vicinity of the cell surface or by another (distinct) membrane receptor. Alternatively, dissociation of GR from chaperone proteins results in the release of other proteins (eg. FKBP51/52) which may also signal.

1.5.2 GC Function

A significant amount of the literature describing the effects of GC, particularly those relating to the immune system, is based on *in vitro* or *in vivo* experiments using very high doses of GC (in excess of 1μM), or synthetic GC such as dexamethasone (DEX; 9α-fluoro-16α-methyl-11β, 17α, 21-hydroxypregn-1, 4-diene-3, 20-dione). Dexamethasone is 10-30x more potent than endogenous GC due to its higher affinity for GR (Kd ~0.5nM) and also its higher $t_{1/2}$ in the circulation (Tailor et al., 1999; Almawi & Tamim, 2001; Schramm et al., 2002). At supra-physiological concentrations, the immune-suppressive effects of GC are likely to predominate, and thus findings may not reflect the true physiological relevance of GC action. Caution must be therefore applied when interpreting the GC literature.

1.5.2.1 The Immune System and GC

At pharmacological concentrations, GC have profound inhibitory effects on inflammation and the immune system in general (Sapolsky et al., 2000), which account for their most common therapeutic application. Suppression of inflammation is commonly regarded as the prevalent, clinically relevant function of GC. Much of the research focuses on the anti-inflammatory properties of GC, overshadowing the critical point that GC are a necessary component of a coordinated inflammatory response. In fact, GC are essential for survival following administration of endotoxin or cytokine challenge with pro-inflammatory cytokines, such as IL-1 and TNF-α (Bertini et al., 1988). Mice lacking GR in Mϕ exhibit high mortality following lipopolysaccharide (LPS) administration and fail to suppress Mϕ p38 MAPK and its downstream targets, cyclo-oxygenase 2 (COX-2), IL-6 and TNF-α (Bhattacharyya et al., 2007). In contrast, mice with 2 additional copies of the GR gene show reduced mortality after LPS challenge (Reichardt et al., 2000).

It is important to stress, that despite an overwhelming amount of evidence in the literature highlighting the immunosuppressive functions of GC, there is parallel evidence that they are not exclusively anti-inflammatory, and endogenous levels exert both suppressive and stimulatory effects during an inflammatory response (Figure 1.5) (Sapolsky et al., 2000). Thus, perhaps the physiological function of GC is best termed as *immunomodulatory* rather than immunosuppressive (Munck et al., 1984; Sapolsky et al., 2000; Yeager et al., 2004).

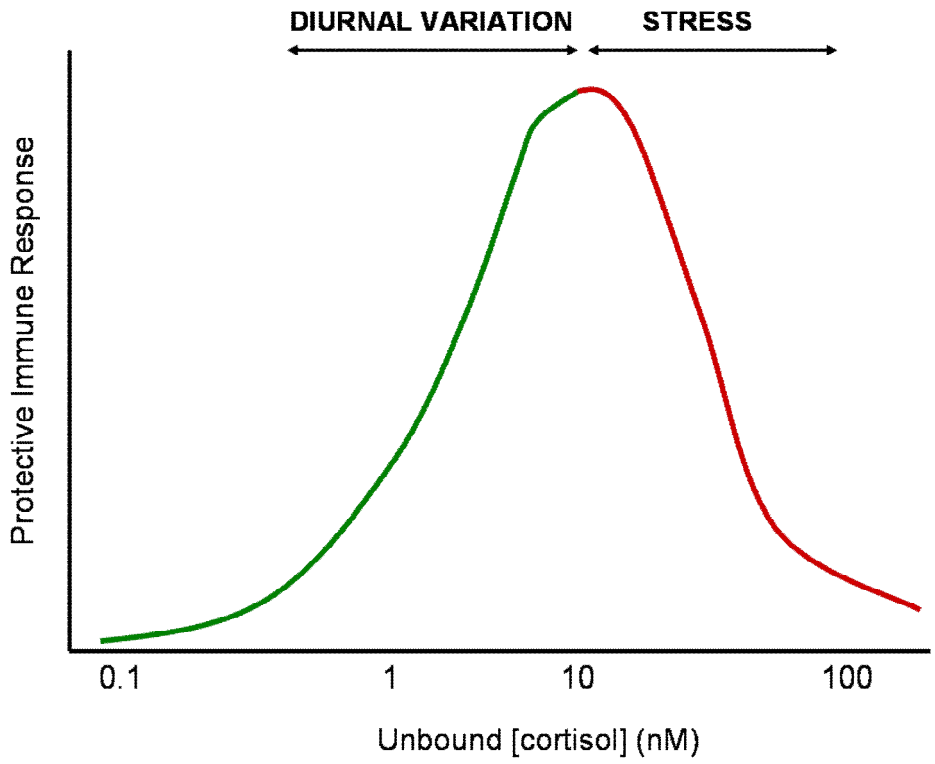

Figure 1.5 Concentration of GC determines the degree of protective immune response.
Bell-shaped curve representing the degree of protection of immune function by GC over a range of endogenous (unbound) cortisol levels. The permissive, or stimulatory, effects (green line) occur under low concentrations of GC that occur during normal diurnal variation, whilst the high concentrations (red line), such as seen during stress response, result in suppressive effects (adapted from (Yeager et al., 2004)).

GC regulate both the adaptive and innate immune systems (Miller et al., 1998). They inhibit maturation of various immune cells, such as DC (Matyszak et al., 2000), programme the maturation of monocytes into highly phagocytic Mϕ (Giles et al. 2001), and induce apoptosis in other cells, such as lymphocytes. GC have direct actions on both T and B lymphocytes by inhibition of immunoglobulin synthesis, thus altering T-cell function and B-cell proliferation (Cupps et al., 1985). Furthermore, GC modulate the cellular function of the immune system by altering the distribution and trafficking of immune cells (Asai et al., 1993; Poon et al., 2001). They decrease circulating lymphocyte, monocyte and eosinophil numbers by reducing the availability of chemoattractants and suppressing adhesion molecules (eg. ICAM-1 and E-selectin) (Schneider et al., 1997). GC also alter granulocyte apoptosis (Meagher et al. 1996). Most circulating leukocytes decrease in number after GC treatment, however, neutrophil numbers in blood increase in response to GC (Nakagawa et al., 1998), possibly due to longer survival (delay in apoptosis (Zhang et al., 2001)) and/or increased mobilization from BM. Moreover, GC promote the resolution of inflammation, for example by inducing Mϕ phagocytosis of apoptotic leukocytes (Liu et al., 1999; Heasman et al., 2003) and increasing the expression of anti-inflammatory mediators such as IL-10 and IL-1ra (Barnes 1998).

The benefits of GC are a result of multiple and complex mechanisms; including the regulation of differentiation programs and gene transcription, and whilst some are known, the exact pathways remain uncertain. GC are commonly accredited with down-

regulating gene transcription of pro-inflammatory molecules (Schobitz et al., 1993) while up-regulating transcription of anti-inflammatory mediators (Eisen et al., 1988; Tonko et al., 2001; Erlandsson et al., 2002) (Table 1.1 lists some but not all of the genes).

However, GR binding sites are absent from many pro-inflammatory genes, such as those regulated NFκB and AP-1 (Demoly et al., 1992), and suppression occurs through GR interference with the action of these transcription factors. For example, activation of the NFκB pathway by inflammatory stimuli (eg. TNF-α) leads to separation of NFκB from its inhibitor IκB, allowing it to move freely into the nucleus and influence gene transcription. GC inhibit the effects of NFκB, which is a potent pro-inflammatory mediator that up-regulates genes promoting inflammation (eg. IL-1), cell adhesion and angiogenesis. However, there is no clear consensus as to which pathway is responsible for this and the exact mechanism by which GR antagonizes NFκB and AP-1 function remains the subject of debate.

Briefly, several mechanisms by which GR interferes with NFκB and AP-1 function have been described including; (a) GR directly interferes with action of transcription factors in a manner independent of DNA binding. This was supported by generation of mice which do not dimerize GR and therefore cannot bind to the palindromic GREs (Reichardt et al., 2000). However, this interpretation was called into question with the demonstration that the mutant GR can bind to alternative arrangement of GRE binding sites (as occurs in the PNMT gene) to activate transcription (Adams et al., 2003). (b) GR

induces expression of IκB (Auphan et al., 1995; Scheinman et al., 1995). (c) More recently, an alternative mechanism has been suggested where GR induces expression of DUSP-1 (through gene activation) which controls MAPK signaling cascade ((Abraham et al., 2006) and reviewed in (Clark, 2007)).

Table 1.1 Examples of immune-related genes regulated by GC

Increased transcription	Decreased transcription
Annexin-1	IL-1,2,3,4,5,6,8,9,11,12,13,16,17,18
β_2-adrenoreceptor	TNF-α
	Granulocyte Mϕ stimulating factor (GM-SCF)
I-κBα	
Secretory leukocyte inhibitory protein (SLPI)	Stem cell factor (SCF)
Phospholipase A_2 inhibitor (CC10)	RANTES
	Monocyte chemoattractant protein (MCP)-1, 3, 4
IL-1 receptor antagonist	Eotaxin
MAPK phosphatase (MKP-1)	Mϕ inflammatory protein (MIP)-1α
Cluster differentiation (CD)163	Inducible cyclo-oxygenase (COX-2)
	Endothelin-1
	Adhesion molecules (ICAM-1, E-selectin)
	Neurokinin receptors (1 and 2)
	Inducible nitric oxide synthase (iNOS)

RANTES, regulated upon activation normal T-cell expressed and secreted;
ICAM-1, intercellular adhesion molecule I;
Adapted from (Adcock & Lane, 2003)

1.5.2.2 Metabolism and GC

Although not the focus of the work in this thesis, it is important to note that GC play a important role in the regulation of daily energy flow and mobilization of energy (glucose and free fatty acids) during a stress response (Munck et al., 1984). GC promote hepatic glucose output (increased gluconeogenesis), mobilizing stored glycogen and decreasing glucose uptake into peripheral tissues (eg. muscle). They also promote lipolysis of stored triglycerides from adipose tissue. Moreover, GC play a key role in differentiation of pre-adipocytes into adipocytes and in the overall regulation of fat metabolism (Gaillard et al., 1991), as well as determination of fat distribution in favour of preferential storage of central fat (Andrews & Walker, 1999; Stewart & Tomlinson, 2002). Intriguingly, GC excess (e.g. in Cushing's syndrome, (Lindholm, 2000)) is characterized by central obesity, insulin resistance, hyperglycemia and hypertension. On the other hand, GC insufficiency (as for example in Addison's disease) results in weight loss and hypoglycemia, amongst other symptoms.

1.6 11β-Hydroxysteroid dehydrogenase

1.6.1 11β-HSD2

11β-HSD2 is a 40kDa, NAD dependent enzyme, with high substrate affinity (K_M values for corticosterone and cortisol of 5.1nM and 47nM, respectively) and predominant dehydrogenase reaction direction *in vivo* and *in vitro* (Albiston et al., 1994; Brown et al., 1996). Its expression is largely restricted to classical mineralocorticoid target tissues (kidneys, colon, sweat and salivary glands, etc.) and the placenta (Brown et al., 1996; Sun et al., 1997; Stewart & Krozowski, 1999). This isozyme is absent from the pituitary and most regions of the adult CNS (Roland et al., 1995; Robson et al., 1998). In the kidney 11β-HSD2 inactivates GC, preventing inappropriate binding to MR (Edwards et al., 1988; Funder et al., 1988). Inhibition or congenital deficiency of 11β-HSD2 in kidney leads to the GC-dependent 'syndrome of apparent mineralocorticoid excess' characterized by hypertension, hypokalemia and hypernatremia (Mune et al., 1995; Kotelevtsev et al., 1999). In contrast, in the fetus and placenta 11β-HSD2 prevents GC binding to GR and lack of this inhibition due to decreased levels of 11β-HSD2 may "programme" decreased birth weight in the offspring and alter their behaviour in adulthood (Holmes et al., 2006).

1.6.2 11β-HSD1

11β-HSD1 uses NADP(H) as co-substrate and has a lower affinity for GC (apparent K_M in intact cells is ~200nM for cortisol and 2μM for corticosterone), than 11β-HSD2, with which it shares less than 30% identity. Although 11β-HSD1 is bi-directional *in vitro* (Lakshmi & Monder, 1988) (and is frequently assayed in the dehydrogenase direction in homogenates), within intact cells it is predominantly a GC reactivating enzyme (including in hepatocytes and in liver (Jamieson et al. 1995; Jamieson et al. 2000) and vascular smooth muscle cells (Brem et al. 1995)). Mice which lack 11β-HSD1 (discussed in detail below) cannot convert 11-DHC to corticosterone *in vivo*, proving this is the only 11β-reductase enzyme in mice (Kotelevtsev et al., 1997). The predominant reductase direction of 11β-HSD1 *in vivo* results from its colocalisation with hexose-6-phosphate dehydrogenase (H6PDH) within the endoplasmic reticulum (Atanasov et al. 2004; Bujalska et al. 2005; and reviewed in (Hewitt et al. 2005)).

It is now accepted that 11β-HSD1 provides an important intracellular amplification of GC action by activating inert 11-ketosteroids derived from blood to yield active GC (Seckl & Walker 2001). The enzyme is widely distributed throughout the body; with the highest levels in the liver, and more modest levels elsewhere, including adipose tissue, skeletal muscle, vasculature, kidney (proximal tubules), lung, brain, anterior pituitary, and the ovaries (reviewed in (Stewart & Krozowski 1999; Seckl and Walker 2001; Tomlinson et al. 2004)). Although not the focus of this thesis, it is important to note that 11β-HSD1 is expressed in the brain (Moisan et al., 1990; Rajan et al., 1996) and contributes to the feedback regulation of HPA activity (Harris et al., 2001).

Importantly, in obese humans and in some rodent genetic models of obesity, 11β-HSD1 is increased in adipose tissue, with levels unchanged or even decreased in the liver (Livingstone et al., 2000; Rask et al., 2001). These findings have led to the proposal that increased 11β-HSD1 in adipose tissue, contributing to elevated GC actions in this tissue, is causal in the pathogenesis of the metabolic syndrome (Bujalska et al., 1997; Seckl et al., 2004). In line with this hypothesis, transgenic mice over-expressing 11β-HSD1 in adipose tissue exhibit essential features (such as visceral obesity, insulin resistance, dyslipidaemia) of the metabolic syndrome (Masuzaki et al., 2001; Masuzaki et al., 2003). In contrast, mice that are deficient in 11β-HSD1 (described below in Section 2.5.3) have a protective metabolic phenotype (Morton et al., 2001), especially on a high fat diet (Morton et al., 2004). Studies in mice using specific 11β-HSD1 inhibitors have shown decreased blood glucose levels, improved hepatic insulin sensitivity in hyperglycaemic mice and inhibition of atherosclerotic plaque formation (Alberts et al., 2003; Hermanowski-Vosatka et al., 2005; Wang et al., 2006). Taken together, these data suggest that excess GC contribute to pathogenesis of cardio-metabolic disease and highlight 11β-HSD1 as a promising drug target for treatment with over 100 patents (for 11β-HSD1 inhibitor) to date.

1.6.3 Mice Deficient in 11β-HSD1

A line of mice homozygous for a targeted disruption in the *Hsd11b1* gene encoding 11β-HSD1 (*Hsd11b*$^{-/-}$ mice) was generated by replacing a genomic fragment including exons 3 and 4 with a neomycin-resistance cassette, through specific recombination in mouse ES cells, resulting in disruption of the *Hsd11b1* gene (Kotelevtsev et al., 1997). The *Hsd11b*$^{-/-}$ mice do not regenerate corticosterone from inert 11-DHC confirming that 11β-HSD1 is the predominant or sole 11β-reductase in the body (Kotelevtsev et al., 1997). These mice have been extremely valuable in elucidating the various roles of 11β-HSD1 (Seckl, 2004). *Hsd11b1*$^{-/-}$ mice are viable, fertile and have a phenotype consistent with cellular GC deficiency, despite normal (on the C57BL6/J strain background), or mildly elevated (on the 129/MF1 background) circulating GC levels (Kotelevtsev et al., 1997; Harris et al., 2001; Morton et al., 2004; Yau et al., 2007). *Hsd11b1*$^{-/-}$ mice show defective induction of hepatic PEPCK, the rate-determining enzyme in gluconeogenesis, upon fasting (Kotelevtsev et al., 1997) and are protected against metabolic disease when fed a high fat diet (reviewed in (Seckl et al., 2004)). They resist cognitive decline as they age (Yau et al., 2001; Yau et al., 2007). In addition, *Hsd11b1*$^{-/-}$ mice show increased angiogenesis following injury suggesting that endogenous GC, amplified by 11β-HSD1, regulate angiogenesis in a GC-mediated manner (Small et al. 2005). Recently the phenotype of these mice during an inflammatory response has been examined and is discussed below.

1.6.4 11β-HSD1 and the Immune System

Although the anti-inflammatory effects of GC in the onset and resolution (reviewed in (Heasman et al., 2003)) of inflammation are well recognized, the available literature on 11β-HSD1 expression, function and regulation in the immune system (Figure 1.6) remains limited, especially in comparison to the volume of research on the metabolic function of 11β-HSD1 and the consequences of its inhibition. Past studies using an 11β-HSD inhibitor, glycyrrhetinic acid, suggested a role for 11β-HSD in the immune response (Finney & Somers, 1958; Pompei et al., 1979; Teelucksingh et al., 1990). However, glycerrhetinic acid inhibits both of the 11β-HSD isozymes and therefore, these effects are likely to be a result of increased GC in response to inhibition of 11β-HSD2. More recently, expression of 11β-HSD1 has been reported in immune cells, including Mϕ (Thieringer et al., 2001; Gilmour et al., 2006), $CD4^+$, $CD8^+$, and $B220^+$ lymphocytes (Zhang et al., 2005), as well as DC (Freeman et al., 2005). Interestingly, although 11β-HSD1 is not expressed in human monocytes (Thieringer et al., 2001; Freeman et al., 2005), it is induced upon differentiation to Mϕ (Thieringer et al., 2001) or DC (Freeman et al., 2005), suggesting tissue-specific and maturation-dependent regulation (regulation of 11β-HSD1 is discussed below, Section 2.7). Nonetheless, the relatively small amount of research available to date points to a protective, anti-inflammatory role for 11β-HSD1 during an acute inflammatory response (reviewed in (Chapman et al., 2006; Chapman & Seckl, 2008)).

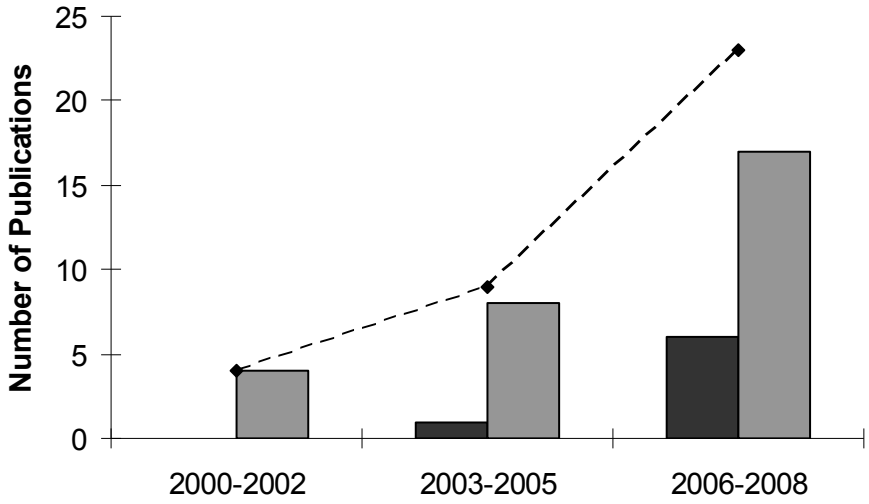

Figure 1.6 Increasing number of publications on 11β-HSD1 expression, function and regulation during inflammation.
Figure represents the increasing trend of publications (line) including research papers (light bars) and reviews (dark bars). Publication list obtained from Pubmed search (*www.pubmed.gov*) using key words; '11beta HSD1' and 'inflammation' on 27th of November 2008. Key word '11beta HSD1' alone generated 597 results, whilst key word 'inflammation' alone generated 289,278 publications.

In support of a role in inflammation, 11β-HSD1 activity and/or expression increases at sites of inflammation (Gilmour et al., 2006; Vagnerova et al., 2006). Rapid up-regulation of 11β-HSD1 occurs in peritoneal cells during sterile peritonitis (Gilmour et al., 2006) and in colitis (Bryndova et al., 2004; Zbankova et al., 2007). Increased activity of 11β-HSD1 (in fibroblasts) occurs in human rheumatoid arthritis (Hardy et al., 2008) and synovial inflammation (assessed by increased cellularity) correlates with cortisone reactivation, suggesting elevated local 11β-HSD1 activity within the synovium (Schmidt et al., 2005). 11β-HSD1 is expressed in leukocytes and synovial fibroblasts within the rheumatoid joint (Schmidt et al., 2005).

1.6.5 Regulation of 11β-HSD1

There are 3 promoters that drive transcription of the *Hsd11b1* gene; the distal promoter (P1) (Bruley et al., 2006) mainly used in lung and kidney, the proximal promoter (P2) (Bruley et al., 2006) used in liver, adipose tissue and brain, and promoter P3 used in kidney (Moisan et al., 1992) (personal communication with Prof Karen Chapman). Transcription factors of the CAAT/enhancer-binding protein (C/EBP) family play a key role in regulation of 11β-HSD1 both *in vivo* and *in vitro* (Williams et al., 2000; Bruley et al., 2006; Gout et al., 2006; Sai et al., 2008; Payne et al., 2007). The P2 promoter is activated by C/EBP, with C/EBPα having a greater effect than C/EBPβ in hepatocytes (Williams et al., 2000), whilst in pre-adipocytes, C/EBPβ appears the major regulator (Gout et al., 2006). During adipocyte differentiation of 3T3-L1 cells, 11β-HSD1 mRNA increases with C/EBPα expression (Payne et al., 2007). Interestingly, whilst the P2

promoter is dependent on C/EBPα, the P1 promoter is C/EBPα-independent (Bruley et al., 2006). In support of this, C/EBPα knockout mice exhibit a severe deficit in 11β-HSD1 mRNA in liver (which uses the P2 promoter), whilst they have normal levels of 11β-HSD1 mRNA in lung, which uses the P1 promoter (Williams et al., 2000; Bruley et al., 2006). Since 11β-HSD1 plays a diverse role in the control of GC action, understanding of its regulation is critical. Although there is a report of cortisol-induced GR binding to a GRE in the P2 promoter region of 11β-HSD1 in placental cells (Yang et al., 2007), in a different system (A549 lung epithelial cells), it appears that 11β-HSD1 induction by GC is dependent on transcriptional regulation by C/EBPβ (Sai et al., 2008).

Another recognized transcription factor involved in the modulation of 11β-HSD1 is the peroxisome proliferator activator receptor (PPAR) which regulates several pathways involved in insulin activity (Bahr et al., 2002). Briefly, 11β-HSD1 expression and activity is down-regulated by PPARα agonists in liver (Hermanowski-Vosatka et al., 2000) and by PPARγ in adipocytes (Berger et al., 2001). PPARγ and C/EBPα co-operate in their promotion of adipocyte differentiation (Wu et al., 1999), during which time 11β-HSD1 is switched on (Payne et al., 2007). However, to date there are no reports on regulation of 11β-HSD1 through C/EBP and/or PPAR in the immune system, although both have been shown to have anti-inflammatory effects (Poli, 1998; Zhang et al., 2007).

The regulation of both the expression and activity of 11β-HSD1 is largely tissue specific, and unsurprisingly, the HPA axis and its own modulators are also involved in this regulation. Regulation of 11β-HSD1 activity and gene expression involves

numerous hormones and growth factors. GC themselves have been shown to up-regulate 11β-HSD1 in human pre-adipocytes and adipocytes (Bujalska et al., 1999; Engeli et al., 2004), myoblasts (Whorwood et al., 2001), fibroblasts (Hammami & Siiteri, 1991) and rat hepatoma cells (Voice et al., 1996). GC also induce 11β-HSD1 mRNA *in vivo* in a tissue specific manner (Jellinck et al., 1997; Jamieson et al., 1999). In contrast, 11β-HSD1 activity is inhibited by insulin and expression is reduced by thyroid hormone, growth hormone (GH), insulin-like growth factor-1 (IGF-1) and sex steroids (Low et al., 1994b; Arcuri et al., 1996; Whorwood et al., 1993; Stewart & Tomlinson, 2002). Additionally, chronic stress up-regulates 11β-HSD1 (Low et al., 1994a), while the sympathetic nervous system both increases (through β-adrenergic stimulation) and decreases (through α-adrenergic stimulation) 11β-HSD1 activity (Hochberg et al., 2004).

Although there is increasing evidence that interleukins (especially IL-1) and other inflammatory agents (including TNF-α) increase 11β-HSD1 activity and gene expression (summarized in Table 1.2), the exact molecular mechanisms governing inflammation associated induction of 11β-HSD1 are yet to be determined. Other inflammatory mediators, such as prostaglandins, may also be important regulators of 11β-HSD1 expression (Alfaidy et al., 2001). Despite the significant gaps in the understanding of the mechanisms which govern 11β-HSD1 during inflammation, the possibility of its anti-inflammatory role (Chapman et al., 2006; Chapman & Seckl, 2008) has stimulated much interest in uncovering the regulatory mechanisms and has set the precedents for future research.

Table 1.2 Regulation of 11β-HSD1 levels by inflammatory mediators

Cytokine	Cell Type	11β-HSD1 mRNA	11β-HSD1 activity	Reference
IL-1α	Ovarian epithelial cells	↑	n/a	Rae et al., 2004
	Ovarian epithelial cells	↑/↔	n/a	Gubbay et al., 2005
IL-1β	Glomerular mesangial cells	↑	↑	Escher et al., 1997
	Granulosa cells	↑	n/a	Tetsuka et al., 1999
	Amnion fibroblasts	n/a	↑	Sun and Myatt, 2003
	Adipose stromal cells	n/a	↑	Tomlinson et al., 2001
	Aortic smooth muscle cells	↑	↑	Cai et al., 2001
	Osteoblasts	↑	↑	Cooper et al., 2001
	Monocytes	↔	↔	Thieringer et al., 2001
	Ovarian epithelial cells	↑	↑	Yong et al., 2002
	Adipocytes	n/a	↑	Friedberg et al., 2003
	BM fibroblasts	↑	↔	Hardy et al. 2006
	Dermal fibroblasts	↑	↑	Hardy et al. 2006
	Synovial fibroblasts	↑	↑	Hardy et al. 2006
IL-4	Granulosa-lutein cells	n/a	↑	Evagelatou et al. 1996
	Monocytes	n/a	↑	Thieringer et al., 2001
IL-5	Granulosa-lutein cells	n/a	↑	Evagelatou et al. 1997
IL-6	Granulosa-lutein cells	n/a	↑	Evagelatou et al. 1997
IL-13	Monocytes	n/a	↑	Thieringer et al., 2001
IL-6	Adipose stromal cells	↑/↔	n/a	Tomlinson et al., 2001
TNF-α	Glomerular mesangial cells	↑	↑	Escher et al., 1997
	Adipose stromal cells	↑	↑	Handoko et al., 2000
	Amnion fibroblasts	n/a	↔	Sun and Myatt, 2003
	Adipose stromal cells	↔	↑	Tomlinson et al., 2001
	Aortic smooth muscle cells	↑	↑	Cai et al., 2001
	Osteoblasts	↑	↑	Cooper et al., 2001
	Monocytes	↔	↔	Thieringer et al., 2001
	Adipocytes	n/a	↑	Friedberg et al., 2003
IFN-γ	Granulosa-lutein cells	n/a	↑	Evagelatou et al. 1997

↔ represents no change, n/a represents information not available

1.7 11β-HSD-deficiency and Inflammation

Although *Hsd11b1*$^{-/-}$ mice have been used extensively for metabolic studies, they have only recently been used to investigate the effect of 11β-HSD1-deficiency on the immune system. During sterile peritonitis, *Hsd11b1*$^{-/-}$ mice show delayed acquisition of Mϕ phagocytic competence *in vivo* with increased numbers of free apoptotic neutrophils two days following injection with TG (Gilmour et al., 2006). *In vitro* phagocytosis of apoptotic neutrophils by Mϕ from wild-type mice is stimulated equally by corticosterone and 11-dehydrocorticosterone (the substrate for 11β-HSD1), with the effect of the latter prevented with carbenoxolone (CBX), an inhibitor for 11β-HSD, confirming the effect is due to 11β-HSD1-mediated GC reactivation. Further, whilst corticosterone treatment increases the ability of *Hsd11b1*$^{-/-}$ Mϕ to phagacytose apoptotic neutrophils, indicating that the mechanism of GC response is intact in these cells, 11-dehydrocorticosterone is without effect (Gilmour et al., 2006).

Furthermore, TG-elicited peritoneal Mϕ from *Hsd11b1*$^{-/-}$ mice produce more IL-6 (a GC repressed cytokine (Almawi & Tamim, 2001; Schobitz et al., 1993)) following stimulation with LPS *ex vivo* (Gilmour et al., 2006), consistent with impaired GC action. The greater cytokine response to LPS by Mϕ from *Hsd11b1*$^{-/-}$ mice (Gilmour et al., 2006; Zhang & Daynes, 2007) shows that exposure to 11β-HSD1 substrate (*in vivo*) affects the differentiation and/or activation state of Mϕ. In addition, after administration of LPS, *Hsd11b1*$^{-/-}$ mice exhibit greater weight loss and higher serum levels of TNF-α, IL-6 and IL-12p40 compared to control mice (Zhang & Daynes, 2007). In contrast, *in vivo*

inhibition of 11β-HSD1 in the *apoe*$^{-/-}$ mouse model, with a specific 11β-HSD1 inhibitor, resulted in lower levels of circulating MCP-1, a cytokine that plays a role in the recruitment of monocytes to sites of injury (Hermanowski-Vosatka et al., 2005). Therefore, it remains to be clarified what effect 11β-HSD1 inhibition has on both the immune system and its modulators. Since 11β-HSD1 has been viewed as a therapeutic target for the treatment of the metabolic syndrome (discussed above, Section 1.6.2.), with 11β-HSD1 inhibitors in clinical trials for type 2 diabetes, it is important to establish and clearly define the role of 11β-HSD1 in limiting and resolving inflammation, to ensure that metabolically beneficial drugs are not complicated by pro-inflammatory side-effects.

1.8 Hypothesis and Aims of the Thesis

1.8.1 Hypothesis

Amplification of intracellular GC levels by 11β-HSD1 represents an important mechanism to limit the acute inflammatory response and programme its subsequent resolution.

1.8.2 Aims

This thesis aimed to test the above hypothesis, by determining the contribution of 11β-HSD1 to an acute inflammatory response, using *Hsd11b1*$^{-/-}$ mice subjected to experimental models of inflammation. Furthermore, to provide insights into its role in the inflammatory response, the expression and regulation of 11β-HSD1 was investigated in *Hsd11b1*$^{+/+}$ control mice. In particular the specific aims were:

FIRSTLY, to identify experimental models of inflammation in which to characterize the role of 11β-HSD1 using *Hsd11b1*$^{-/-}$ mice.

SECONDLY, having identified a suitable model and shown that *Hsd11b1*$^{-/-}$ mice exhibit worse inflammation in this model, to investigate the mechanisms underlying the altered inflammatory response in *Hsd11b1*$^{-/-}$ mice, including identifying the inflammatory cells that express 11β-HSD1.

THIRDLY, to test whether MC 11β-HSD1 plays an important role in limiting acute inflammation and to use *in vitro* systems to identify the mechanisms which may contribute to the consequences of 11β-HSD1-deficiency in these cells during an inflammatory response.

Chapter Two

Materials and Methods

2.1. Materials

Unless otherwise stated all chemicals and reagents were purchased from Sigma-Aldrich Company Ltd, (Poole, UK) or from Invitrogen Life Technologies (Paisley, UK). Double deionized water (H_20) was used to prepare buffers and solutions.

Buffers and Solutions

Borate buffer: 8.25g Boric acid, 2.7g NaOH, and 3.5ml HCl (33M) was made up to 1L with H_20 (pH 7.4), then 0.5% BSA (0.5g/100ml) was added and stored at -20°C

C buffer: 63g glycerol, 8.77g NaCl, 186mg EDTA and 3.03g Tris was made up to 500ml with H_20, (pH 7.7) and stored at 4°C

DEPC-treated H_20: H_20 was mixed with diethylpyrocarbonate (DEPC; 1 drop/100 ml), mixed and left overnight prior to autoclaving

Evans Blue Dye: 25mg Evans blue was dissolved in 5ml H_20 (0.5% w/v)

Homogenization buffer: 100g glycerol, 300mg Tris and 186mg EDTA was made to 500ml in H_20, (pH 7.5), stored at 4°C and supplemented with 7.7mg dithiothreitol (DTT) per 50ml immediately prior to use (buffer was kindly prepared by Ms Lynne Ramage, CCVS)

Ketamine/Metatomedine: 0.38ml of ketamine and 0.50ml of metatomedine in 5ml PBS

Lipopolysaccharide (LPS): 10mg LPS (derived from *Escherichia coli* serotype 0111:B4) was solubilised in 5ml sterile 0.9% NaCl and stored in 200µl aliquots at -20°C. For a working concentration of 0.5mg/ml, aliquots were diluted further in sterile 0.9% NaCl

Nicotinamide Adenine Dinucleotide (NAD): 17.1mg made up to 1ml in C buffer (for final concentration of 25mM)

Phosphate buffered Saline (PBS): 1 x PBS tablet (Oxoid Limited, Hampshire, UK) (containing 8g/L sodium chloride, 0.2g/L potassium chloride, 1.15g/L Di-sodium hydrogen phosphate and 0.2g/L potassium dihydrogen phosphate) dissolved in 100ml H_20

Placental Homogenate: Kindly prepared by Ms Lynne Ramage (CCVS), 2 Wistar rat placentas were mechanically homogenised in 1ml homogenisation buffer and stored in 300µl aliquots at -80°C

10x TBE buffer: 56g Tris, 57.5g boric acid, 20ml 0.5M EDTA was made up to 500ml with H_20 and autoclaved before use

Thioglycollate solution (10%): 10g of Brewer's thioglycollate powder (DIFCO, Detroit, MI, USA) was dissolved in 0.1L PBS and autoclaved

Toluidine Blue Working Solution: 5ml Toluidine Blue stock solution (1g Toluidine blue O in 100ml 70% ethanol) was mixed with 45ml 1% NaCl (pH 2.3), solution was always made fresh and discarded after use

Wash buffer (ELISA/Immunohistochemistry): PBS with 0.05% Tween20 (pH 7.5)

Steroids and Radiolabeled Steroids

Dexamethasone (DEX): (FW=392g) was dissolved in 100% ethanol to a stock concentration of 10mM and stored at –20°C

Corticosterone (B): (FW=346.5g) was dissolved in 100% ethanol to a stock concentration of 10mM and stored at –20°C

11-Dehydrocorticosterone (A): (FW=344.4g) was dissolved in 100% ethanol to a stock concentration of 10mM and stored at –20°C

[^{3}H]-Corticosterone: Commercial stock solutions of [$^3H_4$]-Corticosterone (specific activity ~80 Ci/mmol; Amersham Pharmacia Biotech, Buckingham, UK) in ethanol (with concentrations of 13.7nmol/ml) were stored at -20°C

[^{3}H]-11-Dehydrocorticosterone: [$^3H_4$]-11-Dehydrocorticosterone was synthesized in-house (preparation described in detail in Section 2.3.6.1), re-suspended in ethanol (for final concentrations of ~10-15nmol/ml) and stored at -20°C

2.2. Animals

All experimentation was conducted in strict accord with accepted standards of humane animal care under the auspices of the Animal (Scientific Procedures) Act UK 1986 following prior approval by the local ethical committee. Unless stated otherwise, male mice, homozygous for a targeted disruption of the *Hsd11b1* gene (*Hsd11b1*$^{-/-}$) on a C57BL/6J background (>8 backcrosses) (Kotelevtsev et al., 1997, Morton et al., 2004) were bred in-house at the Biomedical Research Facility, Little France, Edinburgh, UK and were used with age-matched C57BL/6J wild type controls (*Hsd11b1*$^{+/+}$) which were either bred in-house or purchased from Harlan (Orlac, Bicester, UK). All mice were housed individually or in groups of 2 to 5 mice per cage and kept under controlled conditions (7:30am to 7:30pm light/dark cycle, 21˚C) with *ad libitum* access to H_20 and standard rodent chow (Special Diet Services, U.K.). Unless stated otherwise, mice were killed between 8:00am and 11:00am by cervical dislocation or by intra-peritoneal (i.p.) injection of 200µl ketamine/metatomedine solution.

2.3. Methods

2.3.1. Thioglycollate-induced sterile peritonitis

Thioglycollate (TG)-induced sterile peritonitis is a mild and self-resolving (by 5d) model of systemic inflammation (Gallily et al., 1964). Intra-peritoneal (i.p.) injection of TG causes a rapid influx of activated neutrophils (peaking at 6-12h) (Baron & Proctor, 1982) and monocytes (by 24h) (Melnicoff et al., 1989) into the peritoneum. This model was previously used for characterization of the course of inflammation and its resolution

in *Hsd11b1*$^{-/-}$ mice (Gilmour, 2002; Gilmour et al., 2006). The exact stimulus of the inflammatory response in this model is not completely known and may be non-specific (Li et al., 1997; Ajuebor et al., 1999). TG injection into the peritoneum is also widely used to obtain relatively pure populations of Mϕ (at 4d). It also allows for Mϕ to be isolated and manipulated *in vivo* and analyzed at the onset, peak and resolution stage of inflammation.

Peritonitis was induced in mice by i.p. injection of 0.5ml of 10% thioglycollate (TG) solution. At various times following injection, mice were killed by cervical dislocation and underwent peritoneal lavage. The body was sprayed with 75% ethanol prior to blunt dissection of peritoneum skin and a 19G needle was used to lavage the peritoneum with 5ml sterile PBS. Generally, ~4ml lavage fluid was recovered per mouse. Cells were recovered by centrifugation of lavage fluid at 300g (Labofuge 400R Centrifuge, Heraeus, Essex, UK) for 5min at 4ºC, washed in 5ml PBS, re-suspended in 1ml PBS and counted using a haemocytometer (Neubauer).

2.3.2. Cell culture

Unless otherwise stated, basic culture medium used was Dulbeco's modified Eagle's medium (DMEM) with 10% v/v heat inactivated fetal calf serum (FCS), 1% penicillin/streptomycin. Cells were counted using a haemocytometer.

2.3.3. Enrichment of peritoneal mast cells

Following peritoneal lavage (with 5ml sterile PBS), cells were washed once with PBS and re-suspended in 80µl medium (as above but containing 2% FCS) per 10^7 cells. In order to magnetically label cells for enrichment of mast cells (MC), 20µl of CD117 (c-kit) beads (Miltenyi Biotec, Surrey, UK) were added per 10^7 cells and incubated for 15min at 4ºC. Cells were then washed with 1ml medium (containing 2% FCS) and re-suspended in 500µl of the same medium. A MACS magnet and LS columns (Miltenyi Biotec) were used to recover labeled cells (according to manufacturer's instructions). First, the unlabelled cells were allowed to pass through the magnetic column (while the labeled cells attached to the magnet), then once the column was removed from the magnet the magnetically labeled cells were flushed through and collected. Purification was tested microscopically on cytospins or by flow cytometry.

2.3.4. Bone marrow derived macrophages (BMD-Mϕ)

Following Schedule 1 killing, the femur bone was carefully extracted from the body and remaining muscle and connective tissue were removed. In a sterile hood, both epiphyses were cut away with a scalpel. By inserting a 23G needle into the diaphysis compartment and forcing fluid through it, cells were flushed with 5ml medium supplemented with L929 conditioned supernatant, which contains Mϕ colony stimulating factor (M-CSF), into a sterile Teflon pot (Roland Vetter Laborbedarf, Ammerbuch, Germany) (1 femur per pot). The process was repeated with the other end of the femur. The total cell suspension was gently aspirated 10 times through a 19G needle to disrupt cell clumps.

Teflon pots were incubated at 37ºC, in CO_2 (5%). On alternate days 25% of the medium was replenished. Cells were harvested on 7d.

2.3.5. Bone marrow derived mast cells (BMD-MC)

BM was retrieved from mouse femurs as described above (2.3.4). The volume of the total cell suspension was made up to 50ml in a Falcon tube with warm basic culture medium, and 10µl was used to count cells. Cells were then centrifuged at 230g for 7min and the supernatant was discarded. The cell pellet was re-suspended in basic culture medium supplemented with recombinant mouse IL-3 and SCF (both from PeproTech EC, Ltd. 20µg/ml IL-3 stock and 1mg/ml SCF stock, using 10µl of each per 200ml of medium). Cells were placed in 162cm^2 culture flasks at 5x10^{5}cells/ml and incubated at 37ºC, 5% CO_2. Cells were checked daily for contamination and allowed to mature for 3 weeks. Half the medium was replaced on Mondays, Wednesdays and Fridays with fresh MC-differentiating medium.

2.3.6. Measurement of 11β-HSD1 activity

2.3.6.1. Preparation of [^{3}H] 11-dehydrocorticosterone

[^{3}H]-11-Dehydrocorticosterone was prepared as previously described (Low et al., 1994). Briefly, 120µl (5nM) of [^{3}H]-corticosterone was added to 200µl of 25mM NAD^+, 300µl of rat placental homogenate (gift from Ms Lynne Ramage) and 4.45ml of C buffer, and

gently shaken at 37°C for at least 3h. Next, 4ml of ethyl acetate was added; the solution was then vortexed and centrifuged (Labofuge 400R Centrifuge) at 2,000rpm for 5min. The organic (upper) layer containing the steroid was transferred into a clean tube and re-centrifuged. The organic layer was then dried under air, approximately 800µl at a time in HPLC tube. Once dry, the steroid was reconstituted in 200µl of 100% ethanol. Recovery, purity and specific activity were assessed in a 1µl aliquot by thin layer chromatography (TLC) (Methods 2.3.6.3.) and counted in scintillation fluid (Pico-fluor 40, Canberra Packard, Berkshire, UK) in a β-counter (Wallac 1450 Microbeta Plus liquid scintillation counter, Milton Keynes, UK). The prepared [^{3}H]-11-dehydrocorticosterone was stored at -20°C for future use.

2.3.6.2. 11β-reductase/dehydrogenase assay

11β-HSD1 activity was measured in intact cells as previously reported (Low et al., 1994). Conversion of [^{3}H]-corticosterone to [^{3}H]-11-dehydrocorticosterone (11β-dehydrogenase activity) or [^{3}H]-11-dehydrocorticosterone to [^{3}H]-corticosterone (11β-reductase activity) was measured in intact primary cells. Normally, 10^6 cells were seeded per well of a 24-well plate in 1ml of medium and incubated at 37ºC for the duration of the experiment (1h to 24h). A trace amount of tritiated steroid (normally 5nM) was diluted with unlabelled steroid and added to the cell medium to give a final concentration of 200nM steroid. Aliquots of medium (200µl) were collected at various times after addition of [^{3}H]-11-dehydrocorticosterone or [^{3}H]-corticosterone. Steroids were extracted with >4x vol ethyl acetate and dried in HPLC tubes as above. [^{3}H]-Cortisone conversion to cortisol was measured in experiments with human neutrophils.

2.3.6.3. Thin Layer Chromatography (TLC)

Dried steroids were re-suspended in 40µl of 100% ethanol containing unlabelled corticosterone and 11-dehydrocorticosterone (each at 5mg/ml) to aid visualization under UV light on the developed TLC plate (aluminium sheets, 20x20cm, silica gel, VWR). Samples were spotted onto the plates at 8µl at a time. Chromatography was carried out in 100ml methanol:chloroform (92:8, v/v), until the solvent almost reached the top of the plate. TLC plates were exposed to ^{3}H phosphorimager screens (Fuji; Raytek, Sheffield, UK) for 3-5d. ^{3}H-steroids were visualised using a phosphorimager (Fuji FLA-2000) and quantitated using Aida software (Raytek; Sheffield, UK). Results are expressed as % conversion of substrate ([^{3}H]-11-dehydrocorticosterone) into product ([^{3}H]-corticosterone). Alternatively, steroids from 11β-HSD1 activity assay were measured by high-performance liquid chromatography (HPLC), which was carried out by Dr Ruth Andrews.

2.3.7. Models of experimental arthritis

2.3.7.1. Collagen-Induced Arthritis (CIA)

Responsiveness to CIA is linked to the major histocompatibility complex (MHC) class II H-2 haplotype, with H-2^{q} haplotype having the highest response rate and H-2^{b}, the lowest (Wooley et al., 1981). C57BL/6 mice bear H-2^{b} and thus, tend to be resistant to CIA, unlike other strains, such as DBA/1 mice, where arthritis symptoms generally develop between 28d to 40d after initial immunization (personal communication, Dr Mohini Gray). A modified immunization protocol, where the collagen is mixed with

complete Freund's adjuvant (CFA), and in which 60-70% of C57BL/6 mice developed arthritis, has been previously described (Campbell et al., 2000). Briefly, to induce arthritis using collagen type II in complete Freund's adjuvant (CII-CFA), a solution of 2mg/ml of chicken sternal collagen type II (Sigma) in 10mM sterile acetic acid was emulsified in an equal volume of complete Freund's adjuvant (Incomplete Freund's Adjuvant (Sigma) mixed with 5mg/ml of Mycobacterium tuberculosi (Difco Laboratories)). Using a 100µl Hamilton glass syringe, *Hsd11b1*$^{-/-}$ or *Hsd11b1*$^{+/+}$ male mice (n=10/group) were immunized (between 8am and 10am) intradermally at the base of the tail with 100µl of freshly prepared CII-CFA solution on d0 and again, 21d later. In this model, arthritis usually develops ~51d after the first immunization (Campbell et al., 2000).

2.3.7.2. KxB/N serum transfer model

2.3.7.2.1 The K/BxN model of inflammatory arthritis

The K/BxN serum transfer model of arthritis, applicable to most strains of mice (Ji et al., 2001), has proved to be a useful experimental model in examining the mechanisms that underlie inflammatory arthritis (Matsumoto et al., 1999). K/BxN TCR transgenic mice spontaneously develop auto-antibodies to glucose-6-phosphate isomerase (G-6-PI), resulting in onset of severe arthritis by ~3 weeks of age (Kouskoff et al., 1996). Injection of serum or purified G-6-PI antibodies from arthritic K/BxN mice into healthy recipient mice rapidly (by 24-48h) and reproducibly induces an inflammatory arthritis which is

progressive, symmetric and is characterized by synovitis, periarticular inflammation, pannus formation, and destruction of cartilage and bone (Matsumoto et al., 1999; Matsumoto et al., 2002). The arthritis is self-resolving by 21d (as the G-6-PI antibody is cleared from the system), although it can be perpetuated with repeated injections of K/BxN serum. Myeloid cells, and particularily MC (Lee et al., 2002), are implicated in K/BxN arthritis (Ji et al., 2002). Lymphocytes are not required (Korganow et al., 1999) since arthritis progression is normal in RAG-1 knockout mice, which lack mature T and B cells (Mombaerts et al., 1992; Shultz et al., 2000). Thus, by injecting K/BxN arthritogenic serum, the lymphocyte-dependent induction phase of arthritis is bypassed, allowing examination of the inflammatory 'effector' stage of disease (Ji et al., 2001).

KxB/N arthritis was induced in *Hsd11b1*$^{-/-}$ and *Hsd11b1*$^{+/+}$ male mice by either a single i.p. injection of K/BxN serum (5.6µl/g body weight) (gift from Dr Mohini Gray) on d0 or 2 injections of 7.5µl/g body weight on d0 and d2. All injections occurred between 8am and 10am.

2.3.7.2.2 Assessment of inflammatory arthritis

Daily monitoring of disease development and progression included visual examination of carpal and hock joints for redness/swelling. Clinical scoring was carried out according to a clinical index based on redness and swelling of the affected joints. Two methods of clinical scoring were used. For Method 1, each paw was given a score of 0-3 (maximum score of 12) depending on severity of inflammation; 0 indicated no evidence of

inflammation, 1 indicated subtle inflammation (metatarsal phalanges joints, individual phalanx, or localized oedema), 2 indicated more obvious swelling localized to dorsal or ventral surface of paw, and 3 involved swelling of the entire paw (Lee et al., 2002). For Method 2, each red paw was assigned 0.5 point and for each swollen paw 1 point was assigned, resulting in a maximum score of 4 per mouse (Ji et al., 2002). During the maximal dose experiment, ankle thickness was measured using a calliper (Kroeplin POCO-2T, Wessex Metrology, UK). Right tarsal joint swelling was defined as the difference in width (mm) from that measured at d0.

2.3.7.2.3 Histological assessment

Arthritic joints (carpal and hock) from acute and chronic experiments were dissected and fixed in 10% formalin, followed by decalcification in 10% EDTA in neutral buffered formalin at room temperature (RT). The decalcification lasted at least 4 weeks. Sections were stained with haematoxylin and eosin (H&E) to assess pathology, while remaining sections were used for immunohistochemistry (IHC) (Section 2.3.13). Sectioning was carried out by the core Pathology Service, Edinburgh University. The H&E sections were examined by Dr David Brownstein and by Dr Donald Salter. The objective was to determine whether there were differences in inflammation within and around the arthritic joint cavity between *Hsd11b1*$^{-/-}$ and control mice at the onset of inflammation or whether the degree of bone and cartilage erosion and destruction differed between genotypes following resolution.

2.3.8. Tail nick blood collection

For measurement of basal plasma corticosterone levels, peripheral blood was collected under non-stressed conditions via tail nick between 0730h and 0830h. Briefly, one mouse at a time was quickly lifted from its cage and a small cut was made at the base of tail with a sterile scalpel. Approximately 25µl of blood was then collected into EDTA coated microvettes (Sarstedt Inc., UK) and placed on ice. Samples were centrifuged at 4˚C for 10min at 12,000rpm and plasma stored at -20ºC until further analysis.

2.3.9. Corticosterone radioimmunoassay

Plasma corticosterone levels were measured by radioimmunoassay. Plasma samples were diluted 1:10 in borate buffer, heated for 30min at 75˚C then centrifuged (Labofuge 400R Centrifuge) for 2min at 13,000rpm at RT. In a 96-well plate, 20µl of each sample was added to 50µl borate buffer containing [^{3}H]-corticosterone (10,000cpm per sample) and corticosterone antibody was added. The rabbit-anti-rat corticosterone antiserum (kindly provided by Dr Chris Kenyon) was added at 1:10,000 dilution in borate buffer. This mix was incubated at RT for 1h. Next, 50µl of anti-rabbit scintillation proximity assay (SPA) beads were added to each well and incubated for 24h at RT before using a β-scintillation counter. The corticosterone concentration in each sample was determined from a standard curve and calculated using Multicalc software (Wallac, Milton Keynes, UK).

2.3.10. Carrageenan-induced pleurisy

Carrageenan-induced pleurisy is a well-established model of acute inflammation. (Cuzzocrea et al., 1999; Frode-Saleh & Calixto, 2000; Salvemini et al., 2001) Carrageenan is an Irish sea-moss and injection of it into the pleural cavity induces neutrophilia at the injection site and development of biphasic sub-pleural inflammation (Vinegar et al., 1976). The mechanism leading to influx of neutrophils into the pleural cavity is uncertain. This cavity model of inflammation is self limiting and usually resolves within 48h. It is a similar model to sterile peritonitis, allowing straightforward extraction of inflammatory cells from the pleural cavity by lavage. The model is characterized by recruitment of phagocytic cells to the intra-pleural cavity, commencing with a rapid influx of neutrophils (initiated at 1h after injection of carrageenan (Vinegar et al., 1976), followed by monophasic monocyte mobilization.

2.3.10.1. Induction of pleurisy

Carrageenan-induced pleurisy was induced as previously described (Vinegar et al., 1976; Vinegar et al., 1982; Gilroy et al., 1999) by Dr Deborah Sawatzky or Mr Michael (Spike) Clay (both from MRC Centre for Inflammation Research). Briefly, male mice were anesthetized with i.p injection of isoflurane and a small incision was made between the 6^{th} and 8^{th} intercostal muscles, 100µl of 0.1% λ-carrageenan (Marine Colloids Inc, USA) in PBS was injected using a blunted needle and the wound was closed using the autoclip system. All injections occurred between 8am and 10am. Mice were killed and cells and tissues were collected at various time points (4h, 24h, 48h and 72h following intra-pleural injection) by lavaging the intra-pleural cavity using 1ml of PBS. Entire

thorax, or lung tissue only, was dissected and fixed in 10% formalin for subsequent histology. The process of pleural lavage is invasive and occasionally results in samples contaminated with blood. Red blood cell contamination affects the measurement of the recruited leukocyte number. Accordingly, bloody pleural lavages were excluded from cell counts for this reason.

2.3.10.2. Assessment of pleural inflammation

Comparative assessment of inflammation between *Hsd11b1*$^{-/-}$ and *Hsd11b1*$^{+/+}$ mice was achieved by measuring exudate volume, and total cell number (by haemocytometer). Greater infiltration of cells was used to infer greater inflammation. Flow cytometry was used to quantify percent of apoptotic and necrotic cells as well as cell types (using inflammatory cell markers described in Section 2.3.16.). In addition, cytospins (Section 2.3.12.) were prepared to confirm cell identification and ratio. Histological assessment of lungs was performed by Dr David Brownstein to identify the degree of tissue damage at various stages of disease (Section 2.3.10.3.).

2.3.10.3. Cytokine measurements (ELISA and CBA kit)

Cytokine levels were determined using a cytometric bead assay (CBA) mouse inflammation kit (BD Biosciences, Oxford, UK) which simultaneously measures IL-6, IL-10, IL-12p70, MCP-1, IFN-γ and TNF-α. Samples were diluted in assay diluent (supplied with the kit), mixed thoroughly and transferred into assay tubes containing 50µl mixed capture beads and 50µl of the Mouse Inflammation PE Detection Reagent

(supplied with the kit). Samples were then incubated in the dark for 2h at RT, washed with wash buffer (supplied with the kit) and the supernatant discarded. The bead pellet was re-suspended in 300µl of wash buffer and samples were analyzed by flow cytometry (BD FACArray Bioanalyser) and analysis was performed using BD FACSComp Software. Using the provided standards, the concentration of each cytokine was calculated from a standard curve for each protein, this covered a defined set of concentrations from 20 – 5000pg/ml).

A general protocol for DuoSet ELISA kit (R&D Systems, Abingdon, UK) was used to measure cytokines individually. Briefly, a 96-well plate was coated overnight with capture antibody (diluted according to manufacturer's instructions), washed and incubated with 300µl block solution (PBS with 1% BSA and 5% sucrose) for a minimum of 1h at RT. 100µl of provided standards or samples were added to wells and incubated at RT for 2h. Plates were then washed with PBS (containing 0.05% Tween20) and the detection antibody (diluted according to manufacturer's instructions) was added and incubation carried out at RT for a further 2h. The plates were washed again and incubated with 100µl of streptavidin horseradish peroxidase (HRP) (diluted according to manufacturer's instructions) for 20min at RT in the dark. After a final wash, 100µl of peroxidase substrate solution (SureBlue Reserve, KPL, Gaithersburg, MD, USA) was added to each well and incubated for another 20min in the dark. The reaction was stopped by adding 100µl of stop solution (0.6M H_2SO_4) to each well and absorbance at 450nm was determined using a microplate reader.

2.3.10.4. Histological assessment

For lung histology, previously fixed thorax (in 10% formalin) from each mouse was washed in 15ml 5% nitric acid for 3h at RT to decalcify the ribs. Each sample was then placed with the dorsal side of the thorax face down in cryostat cassettes and embedded in hot wax. 3-5µm sections were cut from embedded samples using a microtome and mounted on glass slides. Alternatively, isolated lungs fixed in 10% formalin were paraffin-embedded and sectioned without the process of decalcification. Sections were subjected to IHC (2.3.13.) or were stained with H&E to assess pathology (by Dr David Brownstein).

2.3.11. RNA Extraction and Analysis

2.3.11.1. RNA extraction

Only autoclaved glassware and tubes were used and all equipment was treated with RNaseZap to protect RNA samples from contamination and degradation by nucleases. Solutions were made with DEPC H_2O or were used from previously unopened nuclease-free stocks. To isolate RNA from cells in suspension, the cells were centrifuged (300g at 4°C, 5min) (Labofuge 400R Centrifuge) and the pellet re-suspended in TRIzol (Invitrogen) at $5x10^6$ cells/ml. TRIzol reagent allows one-step isolation of RNA based on a modified Chomczynski and Sacchi method of RNA extraction using guanidium thiocyanate (Chomczynski & Sacchi, 1987). 200µl of chloroform was added per 1ml of TRIZOL and vortexed. Following centrifugation (7,500g at 4°C, 5min) to separate the

phases, the aqueous phase was carefully removed so as not to disturb the DNA-containing interface or the lower protein-containing phenol-choloform phase and transferred to a fresh tube. 500µl of isopropanol was added and left for 10min at RT. RNA was recovered by centrifugation and the RNA pellet was washed in 80% ethanol by vortexing and centrifugation (7,500g at 4°C, 5min). After heating at 70ºC for 2-3min the pellet was dissolved in 30µl DEPC H_2O. 1µl was removed for quantification and the remaining sample was stored at 80°C until required. 1µl RNA solution diluted in 99µl DEPC H_2O was used to assess RNA purity and concentration by UV absorbance at wavelengths of 260nM and 280nM using the GeneQuant RNA/DNA calculator (Pharmacia Biotech, UK). A ratio of >1.8 indicated RNA free of protein and not de-purinated.

2.3.11.2. Reverse transcription

Reverse transcriptase was used to produce single-stranded cDNA from total RNA. Using Invitrogen's Superscript III reverse transcriptase system (Invitrogen), 20µl reactions were prepared containing 0.5µg total RNA, 1µl 10mM dNTPs, 1µl Random Primers (Promega Corporation, Wisconsin, USA). Using a thermal cycler (Genius, Techne) reactions were incubated for 5min at 65°C then immediately placed on ice for ≥1min. The contents were collected by brief centrifugation and 4µl of 5x First-Strand Buffer (supplied with the kit), 1µl 0.1M DTT, 1µl 1U/µl RNasin (ribonuclease inhibitor) and 1µl 200U/µl SuperScript III reverse transcriptase were added before the samples were incubated at 25°C for 5min then 50°C for 1h. Finally, the reaction was heated at 70°C

for 15min to inactivate the reverse transcriptase and then rapidly cooled to 4°C. Negative controls contained DEPC H_2O instead of either reverse transcriptase or total RNA and were performed in parallel.

2.3.11.3. Polymerase Chain Reaction (PCR)

GoTaq DNA Polymerase kit (Promega Corporation) was used to amplify cDNA by PCR. The following components were combined in a 0.5ml PCR reaction tube in H_2O for a total vol of 50µl per single reaction; 1µl cDNA (product of reverse transcription reaction obtained as described above), 5µl 5X DNA polymerase reaction buffer (supplied with the kit) containing 1.5mM $MgCl_2$, 0.5µl of 10mM dNTP and 1µl of each primer (see bellow). Finally, 0.25µl of GoTaq DNA polymerase (supplied with the kit) enzyme was added. Negative controls contained H_2O instead of cDNA.

The PCR conditions were: 95°C for 5min for an initial denaturation, then 95°C for 30s, 60°C for 30s, 72°C for 1.5min for a total of 35 cycles. The cycles were followed by 7min extension at 72°C and then were held at 4°C until retrieval. The products were mixed with 1µl of loading buffer and electrophoresis was carried out on a standard 1% Agarose/TBE gel containing 0.005% ethidium bromide (EtBr) at 100-150V for 30-45min. DNA size markers were included to confirm the size of amplified products. The gel was viewed on a transilluminator at 260nm.

Primer sequences:

11β-HSD1 PCR reactions used a common reverse primer complementary to exon 6, **868P** 5'-AGGATCCAG/AAGCAAACTTGCTTGCA-3' (Rajan et al., 1995), and one of the following forward primers:

869P in exon 3 (Rajan et al., 1995), common to all 11β-HSD1 transcripts:

869P 5'-AAAGCTTGTCACA/TGGGGCCAGCAAA-3' (469bp)

OR one of the 3 forward primers for one of the 3 promoters:

P1, 5'-GGAGCCGCACTTATCTGAA-3' (627bp)

P2, 5'-GGAGGTTGTAGAAAGCTCTG-3' (647bp)

P3, 5'-GTATGGAAAGCAAGACAAGG-3' (542bp)

11β-HSD2 forward 5'-CTGAAGCTGCTGCAGATTGGAT- 3'
reverse 5'-GAGCAGCCAGGCTTGATAATG-3' (400bp)

2.3.12. Centrifugation of cells

Samples of freshly isolated primary cells or cultured cells ($2x10^5$) were suspended in 120µl PBS containing 10% FCS, then centrifuged for 3min at 300rpm onto SuperFrost plus slides (VWR International) using a Cytocentrifuge (Shandon 3, UK). Slides were then allowed to air dry and were fixed in freshly prepared 90% acetone/10% methanol (v/v) for 10min at RT. Alternatively, dried slides were stained in a 3-stage process; 1) slides were dipped in methanol for 2min, then 2) slides were placed in Dade Diff-Quick Red (Dade Diagnostica, Siemens Healthcare Diagnostics, New York, USA) for 1min, and lastly 3) slides were dipped for 30s in Reastain Diff-Quick Blue (Dade Diagnostica) then rinsed in H_2O.

2.3.13. Immunohistochemistry (IHC)

All IHC procedures were carried out at RT and PBS supplemented with 0.05% Tween20 was used as wash buffer unless otherwise stated. Sections of tissues embedded in paraffin were de-waxed prior to staining by double immersion in xylene for 1min and 5min, then in ethanol (100%, 95%, 85% and 75% for 1min each), and finally in H_2O. Generally, for HRP staining, slides were soaked first in peroxidase block (2% H_2O_2 in 100% methanol) for 10min then briefly washed in a bath of PBS. Slides were then loaded into a Sequenza unit in PBS, and each slide was incubated with 3 drops of Vector Avidin/Biotin block (Vector, Burlingame, CA, USA) for 10min each and washed with PBS (2x 5min). 125µl protein block (Dako Cytomation, Cambridgeshire, UK) was added for 10min, followed by primary antibody diluted in Dako diluent (Dako

Cytomation) (125µl total volume) for 1h at RT or overnight at 4ºC. Slides were then washed twice with PBS and secondary antibody, appropriately diluted in Dako diluent (125µl total volume), was applied for 30min at RT. Slides were again washed twice with PBS and incubated with 3 drops of Vector ABC RTU (Vector, Burlingame, CA, USA) for 30min, washed again and incubated with 125µl diaminobenzidine (DAB) colour reagent (Dako Cytomation) for 5min in the dark. Finally, slides were washed, transfered to a staining rack, counterstained in haematoxylin (10s to 30s, then washed in Scots H_2O) and mounted with cover slip (Chance Propper Ltd., Warley, UK).

For 11β-HSD1 HRP staining the primary antibodies used were: a) polyclonal rabbit-anti-11β-HSD1 (Cayman Chemical Company, Ann Arbor, MI, USA) (used at 1:100) or b) polyclonal sheep-anti-11β-HSD1 (gift from Dr Scott Webster) (1:1000). Secondary antibodies were: a) polyclonal goat-anti-rabbit (Dako) (1:400) and b) rabbit-anti-sheep (Upstate Cell Signaling Solutions, New York, USA) (1:1000). Sheep IgG and rabbit IgG isotype controls (gift from Dr Jeremy Brown) were used at 1:1000.

For immunofluorescent staining, slides were soaked first in PBS for 5min and then loaded into a Sequenza unit and blocked with PBS (containing 0.05% Tween and 10% mouse serum) for 15-30min at RT. 125µl primary antibody, at the dilution given above for 11β-HSD1 or with MC markers antibodies (mMCP-2, 1:500; or mMCP-6/7, 1:100) (gift from Dr Jeremy Brown) for 1h at RT or overnight at 4ºC. Sheep-anti-mouse IgG and rabbit-anti-mouse IgG isotype controls were used at 1:1000. Slides were washed twice with PBS and 125µl secondary antibody was added: fluorescein isothiocyanate

(FITC) conjugated donkey-anti-sheep (1:100) or rhodamine red-x conjugated donkey-anti-rabbit (1:200) (both from Jackson Immuno Research Laboratories, Inc., USA). Tissue sections were dehydrated following staining by brief soaking in 95% then 100% ethanol, cleared in xylene and mounted with a cover slip using resinous mounting medium.

2.3.13.1. In-house 11β-HSD1 antibody

Total protein from liver, lung and kidney from *Hsd11b1*$^{-/-}$ and *Hsd11b1*$^{+/+}$ mice was used in western blot analysis (Section 2.3.13.2.) of 11β-HSD1 expression. Using the in-house, sheep derived antibody (generated by Dr Scot Webster and purified by Dr Sophie Turban and Mr Fu Yang) a band of the size expected for 11β-HSD1 (34kDa) was clearly detected in samples from the *Hsd11b1*$^{+/+}$ mice. However, only a faint band was seen for the *Hsd11b1*$^{-/-}$ mice, in lung only (Figure 2.1.). The intensity of the 11β-HSD1 band (in liver samples from *Hsd11b1*$^{+/+}$ mice) was reduced when the antibody was pre-incubated overnight with the mouse recombinant protein against which the antibody was raised (Figure 2.1. A1 and A2).

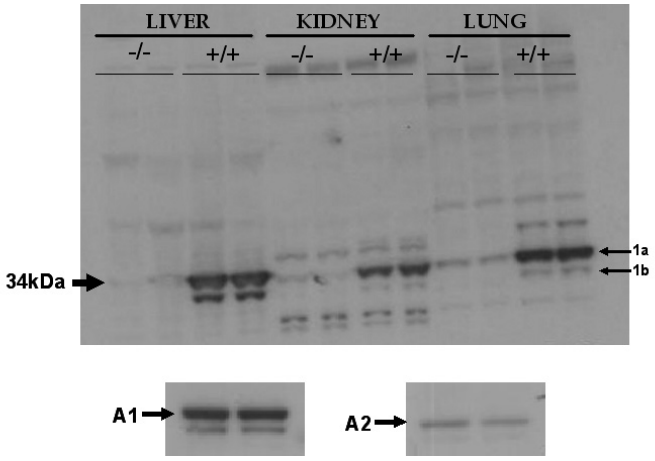

Figure 2.1 In-house 11β-HSD1 antibody detects 11β-HSD1 protein in control mice. Western blot technique was used to detect 11β-HSD1 protein expression in liver, lung and kidney tissue from untreated *Hsd11b1*$^{-/-}$(-/-) and *Hsd11b1*$^{+/+}$ (+/+) mice using sheep-anti-mouse 11β-HSD1 antibody (primary antibody used at 1:1000 dilution, HRP conjugated secondary anti-sheep antibody used at 1:2000 dilution). 24μg of total protein was loaded per well. 1a shows the 34kDa protein band, which is likely to be a doubly-glycosylated protein, whilst 1b is likely to be mono-glycosylated protein, which is most visible in the *Hsd11b1*$^{+/+}$ liver samples. Samples were prepared by homogenization of tissues from two separate *Hsd11b1*$^{-/-}$ and *Hsd11b1*$^{+/+}$ mice (shown side by side for each genotype, per tissue). Overnight pre-incubation with the 11β-HSD1 recombinant protein, against which the antibody was raised, significantly reduced the antibody signal (A2) in liver samples from two *Hsd11b1*$^{+/+}$ mice in comparison to the same liver samples incubated with only the 11β-HSD1 antibody (A1).

2.3.13.2. Western Blot

Frozen tissues were homogenized on ice using cold buffer (100g glycerol, 300mg Tris, 186mg EDTA, and 7.7mg DTT made up to 500ml in H_20, pH to 7.5). Total protein concentration was determined using BioRad protein assay (BioRad Laboratories, UK) and 24µg of total protein was loaded per well. SeeBlue Plus2 pre-stained standards (Invitrogen) were used as size markers. Invitrogen's XCell II Blot Module was used to separate and transfer the proteins using NuPAGE Novex Bis-Tris gel according to manufacturer's instructions. Briefly, the gel was run at 200V for ~45min in NuPAGE MES running buffer and transferred in NuPAGE transfer buffer on to a nitrocellulose membrane (Invitrogen) at 30V for ~1h. Immediately after protein transfer, the membrane was placed in 20 ml of blocking solution (5% non-fat dry milk in PBS) and incubated with gentle shaking for 1-2h at RT. Incubation with primary antibody was performed overnight at 4°C. Following incubation with the primary antibody, the membrane was washed 3 times at RT with wash buffer (PBS + 0.1% Tween-20) for 15min per wash. The membrane was incubated with the secondary antibody in blocking solution with gentle shaking for 1-2h at RT. Following incubation with the secondary antibody, the membrane was washed 4 times at RT with wash buffer (same as above) for 15min per wash. The membrane was developed using chemiluminescence detection kit (Invitrogen) according to manufacturer's instructions.

2.3.14. Toluidine blue staining

Toluidine blue (which stains sulfated polysacharides purple) results in metachromatic staining of MC, while staining the remaining background (orthochromatic staining) light blue. Deparaffinized, re-hydrated sections (Section 2.3.13.) were stained in toluidine blue working solution (listed in materials) for 2-3min at RT, then washed three times in H_2O. Stained slides were dehydrated by briefly dipping slides in 95% and 100% ethanol, then in xylene before mounting with a cover slip using resinous mounting medium.

2.3.15. Bone marrow transplantation (BMT)

BMT experiment was carried out by Ms Kay Samuel. 7d prior to irradiation, the H_2O supply of recipient mice was supplemented with antibiotics (Baytril and Borgal 24% (trimethoprim-sulpha), provided by BRF, WGH). Mice were lethally irradiated using a γ-Cell 40 irradiator (MDS Nordian GammaCell 40E, ^{137}Cs source) using a dose of 1050R (10.50Gy) for 10min. A single cell suspension of donor BM (10^7 cells in 200µl PBS) was prepared for intra-venus (i.v.) injection into recipient mice in a 1ml syringe fitted with a 25G needle (collection of BM was the same as in Section 2.3.4.). Following the irradiation, recipient mice were warmed in a 'hot box' (37ºC) for 10-15min to dilate the tail vein prior to injection. A physical restraint (plastic tube) was required to hold the mouse still during injection. Antibiotics were discontinued 28d later and mice were used for arthritis experiments after 56d, when the reconstitution of recipient mice should be complete.

2.3.16. Flow cytometry

Prior to flow cytometric analysis, cells in polystyrene tubes were incubated on ice for 30min in PBS with 10% mouse serum (to block non-specific binding). In general, conjugated antibodies were added to the cells at concentrations suggested by the supplier and incubated on ice for 30min in the dark. The cells were washed in 2ml PBS and recovered by centrifugation at 300g for 5min with 400µl PBS prior to analysis. Specific and non-specific fluorescence was determined by processing ≥5000 cells/sample through a FACScan or FACScalibur (Becton Dickinson, Oxford, UK) machine, using Cellquest software (Becton Dickinson). The following antibodies were used at 1:100 dilution (eBiosciences, UK unless otherwise stated): CD11b conjugated to FITC, GR-1 phycoerythrin (PE), c-kit PE, B220 (mouse CD45R) PE, F4/80 allophycocyanin (APC) and F4/80 PE (Caltag, UK). Data analysis was performed using CellQuest (Becton Dickinson, UK) as well as FlowJo software (Treestar, Oregon, USA). Antibody specificity and reactivity can vary and the assessment of cell number is dependent upon the positioning of the gates. For this reason, the same gates were used for each sample in order to minimize variation due to this potentially confounding issue (shown in Chapter 6, Figure 6.2).

2.3.17. Assessment of vascular permeability with Evan's Blue Dye

A preliminary experiment was conducted using C57BL/6 mice in order to determine whether an i.v. injection of 200µl of 1% Evan's Blue was measurable in peritoneal lavages, and whether the concentration of dye in the peritoneum changed over the course of peritonitis. A sample of blood was also collected (via cardiac puncture following Schedule 1 cull) in order to measure Evan's Blue concentration in the circulation. Circulating Evan's Blue levels were used as a marker of total Evan's Blue injected per animal to standardize all data. Based on results from 4 mice (n=1 per time point) Evan's Blue was detectable (absorbance of 620nm) following i.p. injection of PBS only (optical density (OD) 0.022) and increased in concentration at 4h (OD 0.048), 1d (OD 0.049) and 2d (OD 0.037) following TG injection (corrected for concentration of Evan's Blue in blood).

2.3.18. Mast cell degranulation

Total peritoneal cells were obtained by peritoneal lavage (as described above, Section 2.3.1.) from *Hsd11b1*$^{-/-}$ and *Hsd11b1*$^{+/+}$ male and female mice. Cell pellets (containing 2x10^6 cells per sample) were re-suspend in 50µl of Tyrode's buffer (10 mM Hepes buffer (pH 7.4), 130mM NaCl, 5mM KCl, 1.4mM CaCl2, 1mM MgCl2, 5.6mM glucose, 0.1% BSA) alone or with K/BxN serum or other secretagory peptides, and incubated for 15min at 37°C. The release of the granule enzyme β-hexosaminidase was measured as previously described (Razin et al 1984). Briefly, following incubation the samples were centrifuged at 5000rpm for 3min and 5µl aliquots of the supernatant were transferred to wells (96-well plate) in triplicate. The remaining supernatant was carefully removed and the cell pellets were solubilized with 50µl Tyrode's buffer + 0.5% Triton X-100. Following solubilization of the pellet 5µl aliquots were transferred into wells in triplicate. Next, 50µl of substrate solution (1.3 mg ml-1 *p*-nitrophenyl-*N* -acetyl-b-D-glucosamine (Sigma) in 0.1M sodium citrate, pH 4.5.) was added to each well and incubated for 40min at 37°C. To stop the reaction 50µl of stop solution (0.2M glycine, pH 10.7) was added to each well and the calorimetric readout was measured at 405 nm absorbance.

Calculation:

$$\% \text{ degranulation} = \frac{\text{OD supernatant}}{\text{OD supernatant} + \text{OD pellet}} \times 100$$

2.3.19. Statistics

Statistical analysis was performed using GraphPad Prism 4.00 software with $P \leq 0.05$ as the criterion for statistical significance. All data are expressed as mean ± standard error of mean (SEM). Data were analysed by Student's t-tests, Analysis of Variance (ANOVA) or Two-way repeated ANOVA followed by post-hoc tests where appropriate.

Chapter Three

11β-HSD1-deficiency worsens the inflammatory response during carrageenan-induced pleurisy.

3.1. Introduction

Previous experiments using a model of sterile peritonitis suggested a more severe inflammatory response in *Hsd11b1*$^{-/-}$ mice, with greater recruitment of inflammatory cells than in control (*Hsd11b1*$^{+/+}$) mice (Gilmour, 2002). However, inflammation resolved at a similar time in both *Hsd11b1*$^{-/-}$ and *Hsd11b1*$^{+/+}$ mice. Carrageenan-induced pleurisy represents an alternative, and perhaps more physiologically relevant experimental model of inflammation than thioglycollate-induced peritonitis (Chapter 2, Section 2.3.1.). As in peritonitis, this model allows for isolation and analysis of recruited inflammatory cells at the onset, peak and resolution stages of inflammation. However, unlike the peritonitis model, the pleurisy model also allows histological analysis of lung tissue following induction of inflammation. Injection of carrageenan induces a single, monophasic mobilization of neutrophils and monocytes during the acute phase of inflammation which normally resolves, or at least starts to clear, by 48h. The experiments described in this chapter were carried out in collaboration with Dr Deborah Sawatzky, who helped with the methods and analysis of the first experiment (Study 1) and Mr Michael (Spike) Clay, who performed the intra-pleural injections and assisted with pleural lavages in the second experiment (Study 2).

3.2. Results

3.2.1. More inflammatory cells are recruited in Hsd11b1$^{-/-}$ mice than in Hsd11b1$^{+/+}$ mice during carrageenan-induced pleurisy

Study 1

Intra-pleural lavages (with 1ml sterile PBS) were carried out on *Hsd11b1*$^{-/-}$ and *Hsd11b1*$^{+/+}$ mice at 4h, 24h and 48h following injection of carrageenan. Significantly more inflammatory cells were recruited in *Hsd11b1*$^{-/-}$ mice than in *Hsd11b1*$^{+/+}$ mice both at the early stage (4h) and peak stage (24h) of inflammation (Figure 3.1). No difference was seen at 48h between genotypes. Oedema was assessed by weighing the collected lavages. There was no difference in lavage volume between *Hsd11b1*$^{-/-}$ and control mice at any time point: 4h (*Hsd11b1*$^{-/-}$; 1.06±0.04ml versus *Hsd11b1*$^{+/+}$; 0.97±0.07ml, $p>0.05$), 24h (*Hsd11b1*$^{-/-}$; 1.01±0.02ml versus *Hsd11b1*$^{+/+}$; 0.93±0.05ml, $p>0.05$) or 48h (*Hsd11b1*$^{-/-}$; 1.0±0.03ml versus *Hsd11b1*$^{+/+}$; 1.0±0.06ml, $p>0.05$).

Because inflammation had failed to resolve as expected at 48h (in both genotypes), a subsequent time point (72h) was examined in a separate experiment. However, at 72h more cells were recovered from both *Hsd11b1*$^{-/-}$ and control mice than were recovered at any time point in the initial experiment, and similar to the earlier time points, there were significantly more cells present in lavages from *Hsd11b1*$^{-/-}$ than those from *Hsd11b1*$^{+/+}$ mice (Figure 3.2). The lavage volume was similar between the genotypes (*Hsd11b1*$^{-/-}$; 0.8±0.06ml versus *Hsd11b1*$^{+/+}$; 0.83±0.06ml). A subsequent health report revealed the presence of *Pasteurella pneumotropica* in the animal facility (Western General Hospital,

Edinburgh) at this time, providing a likely explanation for the exaggerated inflammatory response at 72h in both genotypes of mice (see Discussion below). Accordingly, no further analysis was carried out on the 72h time point.

Study 2

To address whether the differences seen between genotypes at 4h and 24h, and the lack of signs of resolution at 48h were confounded by an underlying sub-clinical lung infection, a second study was carried out at a later date in a separate animal facility (New Royal Infirmary, Edinburgh). Unfortunately, lavages from 4h and 48h following carrageenan injection contained too many red blood cells (RBC) to properly assess cell numbers microscopically, and it was only possible to count cells from the 24h time point, confirmed greater cell recruitment in *Hsd11b1*$^{-/-}$ than in *Hsd11b1*$^{+/+}$ mice (*Hsd11b1*$^{-/-}$; $3.0\pm0.4\text{x}10^7$ versus *Hsd11b1*$^{+/+}$;$1.9\pm0.3\text{x}10^7$, $p<0.05$). Nonetheless, the cells from all three time points in the second experiment were used for flow cytometry assessment and the results are described in this Chapter.

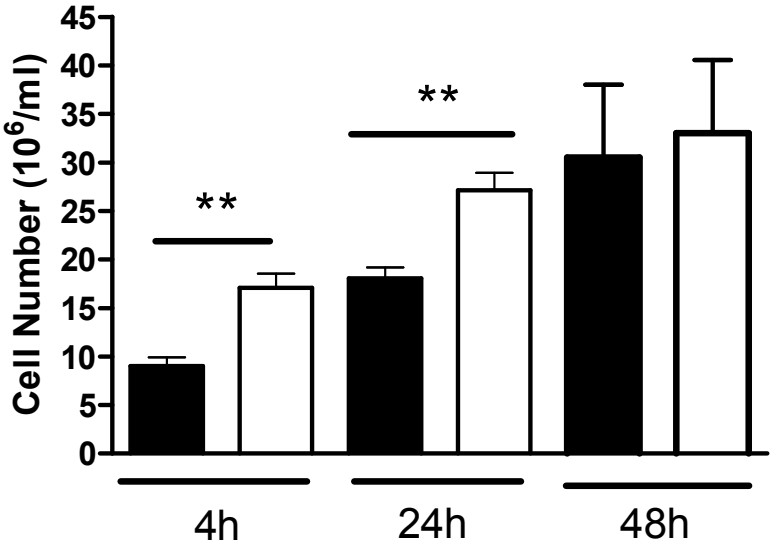

Figure 3.1 *Hsd11b1*$^{-/-}$ mice show a more severe inflammatory response during the acute and peak stages of carrageenan-induced pleurisy.
In Study 1, following intra-pleural injection of carrageenan (100µl of 0.1% carrageenan), significantly more inflammatory cells (expressed per ml) were recovered from *Hsd11b1*$^{-/-}$ (white bars) than *Hsd11b1*$^{+/+}$ mice (black bars) at 4h, and 24h (n=7/genotype). Similar numbers of cells were recruited in both genotypes at 48h (n=7/genotype). Values shown are mean ± SEM. ** $p<0.01$, compared by Two-way ANOVA.

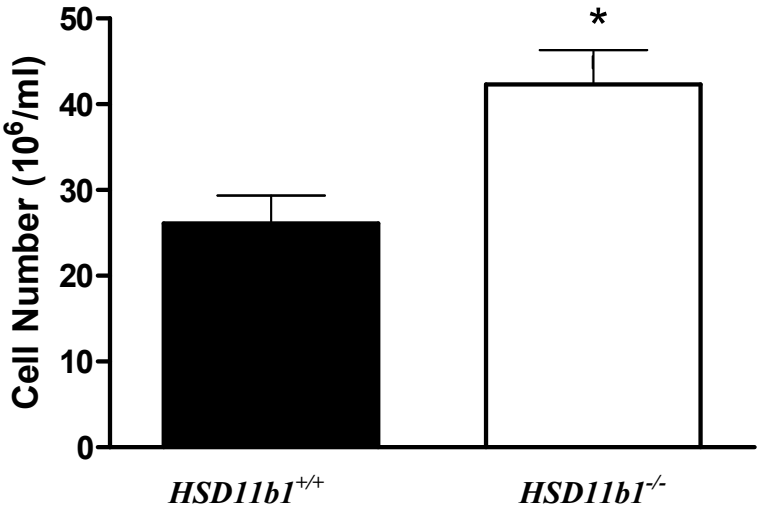

Figure 3.2 *Hsd11b1*$^{-/-}$ mice show a more severe inflammatory response at 72h following injection of carrageenan.
In Study 1, 72h following intra-pleural injection of carrageenan (100µl of 0.1% carrageenan) mice of both genotypes had elevated numbers of inflammatory cells (expressed per ml), with significantly more cells in *Hsd11b1*$^{-/-}$ (white bar) than *Hsd11b1*$^{+/+}$ mice (black bar) (n=6/group). Values shown are mean ± SEM. * $p<0.05$, compared by unpaired Student's t-test.

3.2.2. Assessment of phenotype of intra-pleural inflammatory cells

Study 1

Differential cell counts were carried out on cells recovered from lavage fluid. Based on microscopic observation of Quick-Diff stained cytocentrifuged cells, there was no difference between genotypes in the proportion of cell types (neutrophils, monocytes and Mϕ) elicited into the intra-pleural cavity 4h following carrageenan injection (Figure 3.3). Cytocentrifuged cells from later time points (24h and 48h) contained clumps making distinction of individual cells, and counting, extremely difficult and inaccurate (data not shown).

Study 2

In the second carrageenan experiment, flow cytometry (Chapter 2, Section 2.3.16.) was used to quantitate and characterize recruited cells using antibodies (anti-F4/80 and anti-Gr-1) which should label the vast majority of these cells (neutrophils, monocytes and Mϕ). This additionally had the advantage of obtaining specific counts despite a large number of RBC being present. At 4h and 24h, *Hsd11b1*$^{-/-}$ mice had more Gr-1^{+}/F4/80^{+} cells than *Hsd11b1*$^{+/+}$ mice (Figure 3.4.A). Whilst no difference between genotypes was found in the Gr-1^{+}/F4/80^{+} subpopulation at 48h, *Hsd11b1*$^{-/-}$ mice showed a higher number of Gr-1^{+}/F4/80^{-} cells than the controls at this time point (Figure 3.4.B).

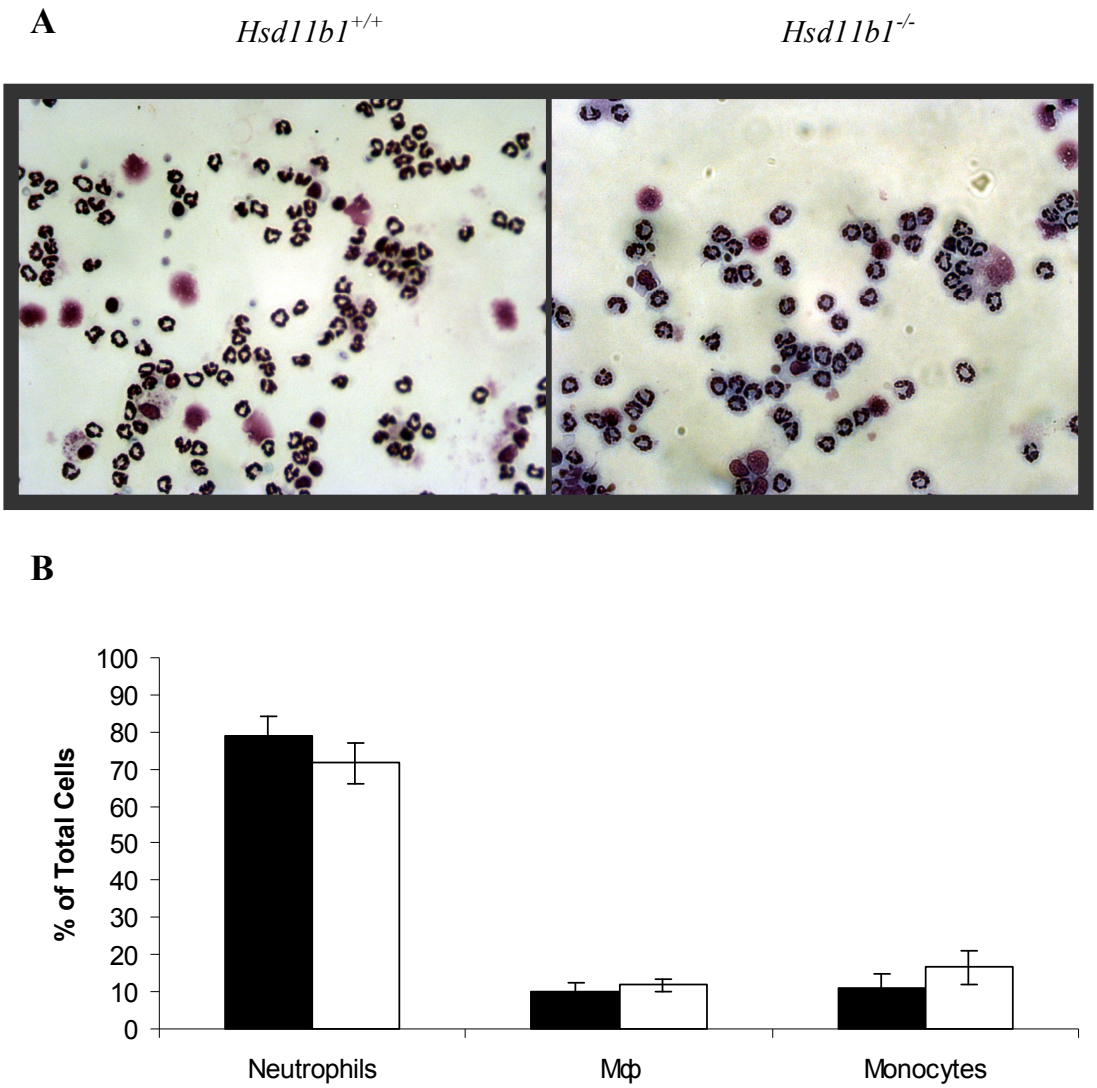

Figure 3.3 Similar inflammatory cell types were recruited in *Hsd11b1*$^{-/-}$ and *Hsd11b1*$^{+/+}$ mice at 4h after carrageenan injection.
(A) Relative numbers of cell types were assessed microscopically (blind to genotype), by counting Diff-Quick stained cytocentrifuged cells prepared from *Hsd11b1*$^{+/+}$ and *Hsd11b1*$^{-/-}$ mice from Study 1. (B) Two-way ANOVA did not reveal differences in cell types recruited between *Hsd11b1*$^{-/-}$ (white bars) and *Hsd11b1*$^{+/+}$ (black bars) mice. Values shown are mean ± SEM.

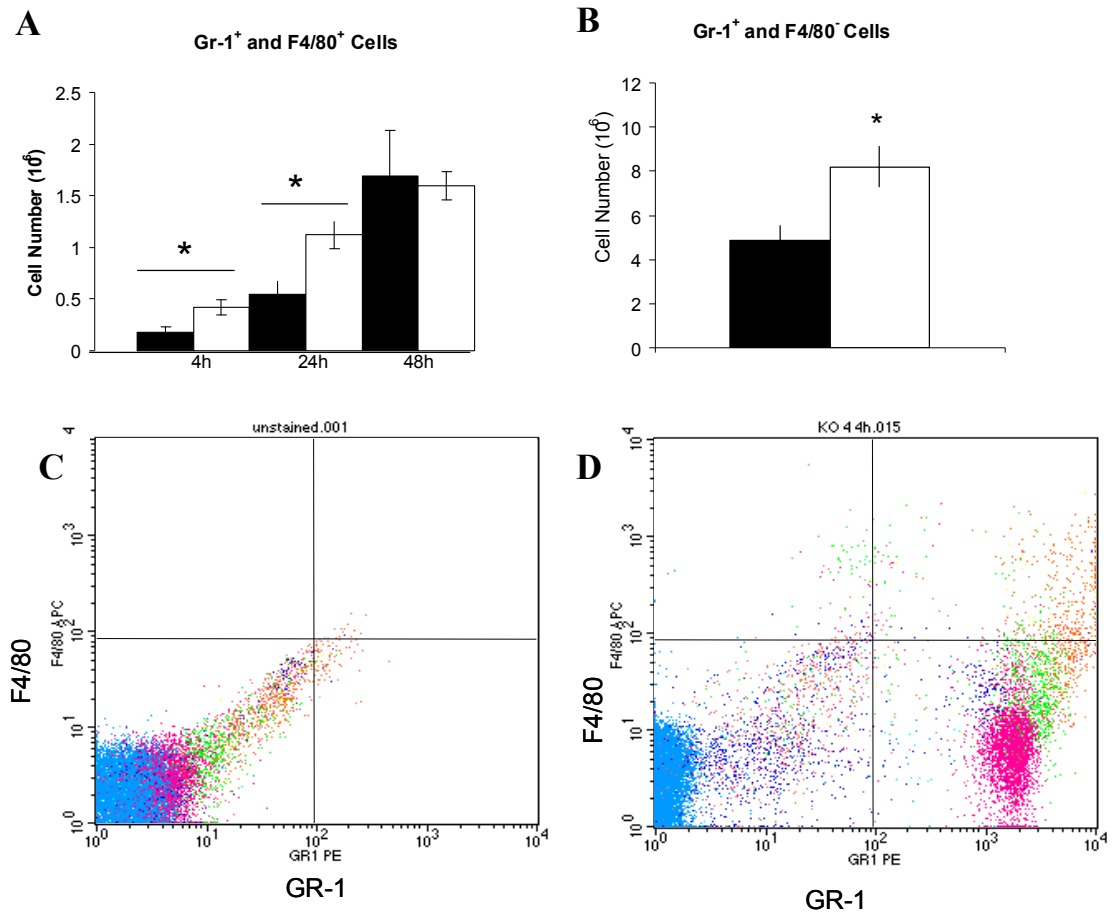

Figure 3.4 Greater Gr-1$^+$ F4/80$^+$ sub-population of intra-pleural cells extracted from *Hsd11b1*$^{-/-}$ than *Hsd11b1*$^{+/+}$ mice at 4h and 24h.
(A) In Study 2, flow cytometry revealed more Gr-1$^+$/F4/80$^+$ cells in intra-pleural lavages from *Hsd11b1*$^{-/-}$ (white bars) than *Hsd11b1*$^{+/+}$ mice (black bars) at 4h and 24h after carrageenan injection. At 48h, *Hsd11b1*$^{-/-}$ mice had more Gr-1$^+$ F4/80$^-$ cells than *Hsd11b1*$^{+/+}$ mice (B), but no difference was seen in the Gr-1$^+$ F4/80$^+$ population at this time. Values shown are mean ± SEM. * $p<0.05$ when compared by Two-way ANOVA (A) or unpaired Student's t-test (B). Analysis was based on gating using unstained cell samples (C). (D) Representative image of dot plot from 4h lavage from *Hsd11b1*$^{-/-}$ stained with Gr-1 and F4/80 antibodies.

3.2.3. Altered viability of intra-pleural inflammatory cells from Hsd11b1$^{-/-}$ mice

Study 1

Viability of intra-pleural inflammatory cells was assessed by flow cytometry. Following recovery from lavages, cells were labeled with annexin V to detect apoptotic cells and propidium iodide (PI) which stains necrotic cells. The proportion of cells undergoing apoptosis 4h and 48h after injection of carrageenan was lower in *Hsd11b1*$^{-/-}$ mice compared to *Hsd11b1*$^{+/+}$ mice (Figure 3.5.A). The proportion of cells which were apoptotic did not differ between genotypes at 24h. *Hsd11b1*$^{-/-}$ mice also had a lower proportion of cells that were necrotic at 4h (Figure 3.5.B). As a result the proportion of viable cells was greater in *Hsd11b1*$^{-/-}$ mice at 4h and 48h (Figure 3.4.C). Because the total number of cells was greater in *Hsd11b1*$^{-/-}$ mice at 4h and 24h, the number of *viable* cells was actually greater in *Hsd11b1*$^{-/-}$ mice than in *Hsd11b1*$^{+/+}$ mice (Figure 3.5.D).

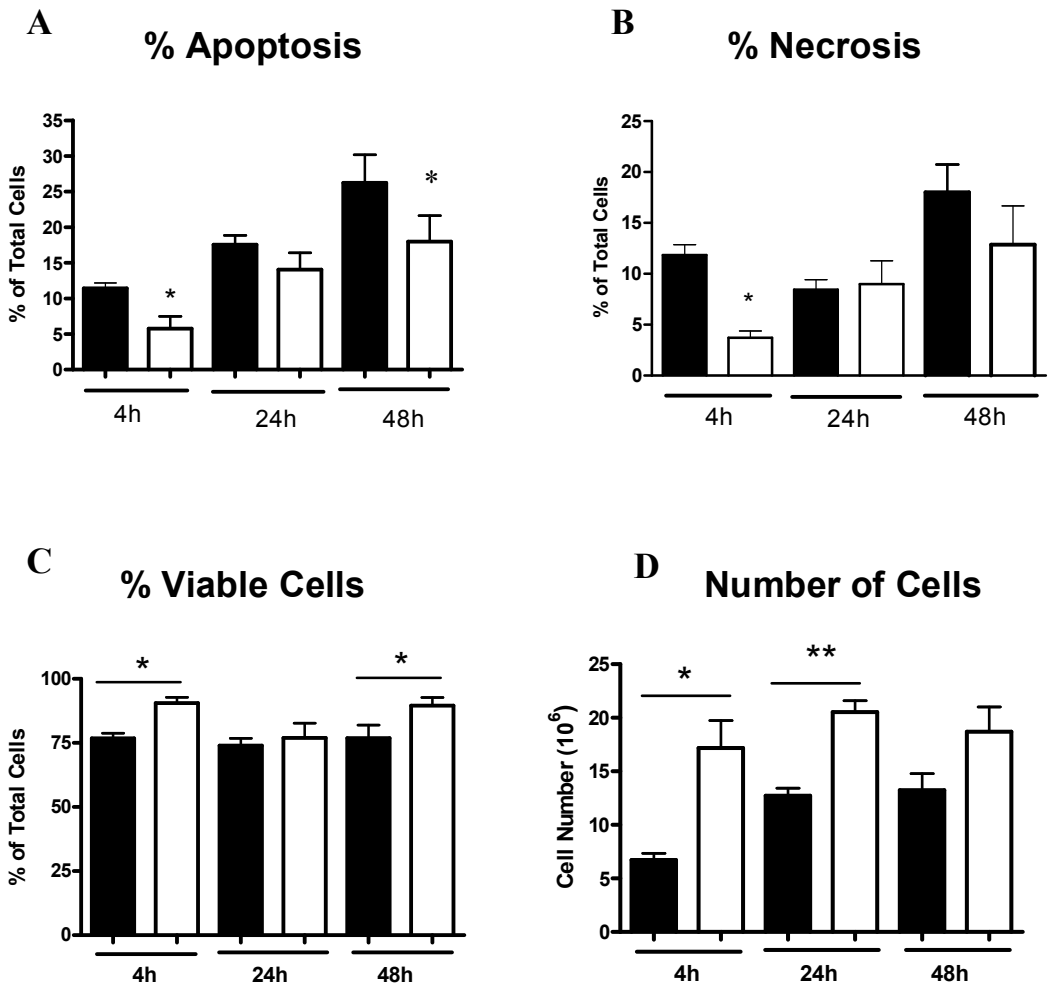

Figure 3.5 In study 1, more viable inflammatory cells were recovered from intra-pleural lavages of *Hsd11b1*$^{-/-}$ mice than of *Hsd11b1*$^{+/+}$ mice at 4h and 24h.
Proportion of apoptotic (A) and necrotic (B) cells recovered at 4h, 24h, and 48h after injection of carrageenan, resulting in greater percent of viable cells (C) (at 4h and 48h), contributing to an overall greater number of cells (D) in lavages collected from *Hsd11b1*$^{-/-}$ (white bars) than *Hsd11b1*$^{+/+}$ mice (black bars) (n=7/genotype/time point). Values shown are mean ± SEM. *p<0.05 and ** p<0.01 when compared by Two-way ANOVA.

Study 2

Cell viability was measured in sub-populations of cells which were determined by flow cytometry using Gr-1 and F4/80 cell markers. Thus, PI and Annexin V were analyzed in individually gated sub-populations (Figure 3.6). At 4h and 48h there was no difference in cell viability between the genotypes when comparing the total cell population (gating around all cells in sample), and only at 24h were there more viable cells (actual number) in *Hsd11b1*$^{-/-}$ than in *Hsd11b1*$^{+/+}$ mice (*Hsd11b1*$^{-/-}$; $2.7x10^7 \pm 0.4$ vs *Hsd11b1*$^{+/+}$; $1.7x10^7 \pm 0.3$). However, for all time points there was a significantly higher proportion (Figure 3.7.A) and number (Figure 3.7.B) of viable cells in the Gr-1$^+$ F4/80$^+$ sub-population of intra-pleural cells in *Hsd11b1*$^{-/-}$ than in *Hsd11b1*$^{+/+}$ mice. No differences in cell viability between genotypes were noted at any time point in the Gr-1$^-$ F4/80$^-$ sub-population (data not shown). Taken together, results from both pleurisy studies suggest a higher number of viable inflammatory cells, present in the lavages from *Hsd11b1*$^{-/-}$ mice during carrageenan-induced lung inflammation.

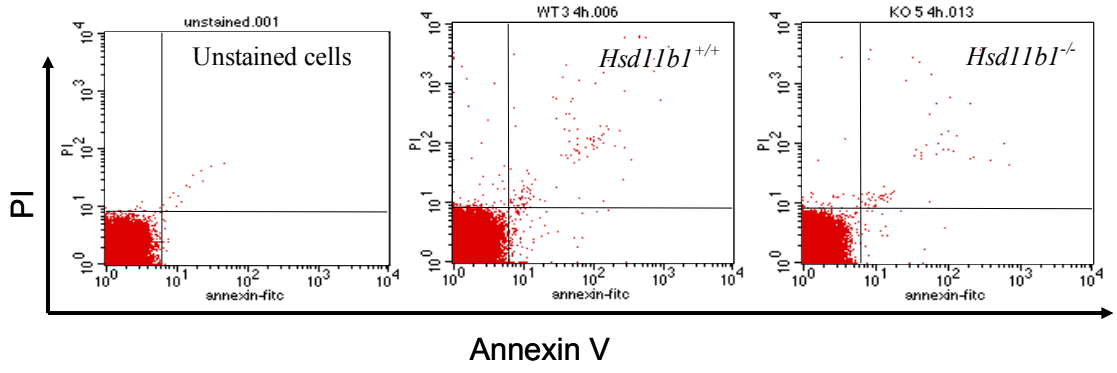

Figure 3.6 PI and Annexin V staining of pleural inflammatory cells.
Representative flow cytometry plots showing PI (y axis) and Annexin V (x axis) analysis of unstained cells (left), *Hsd11b1*$^{+/+}$ mice (middle) and *Hsd11b1*$^{-/-}$ mice (right).

A

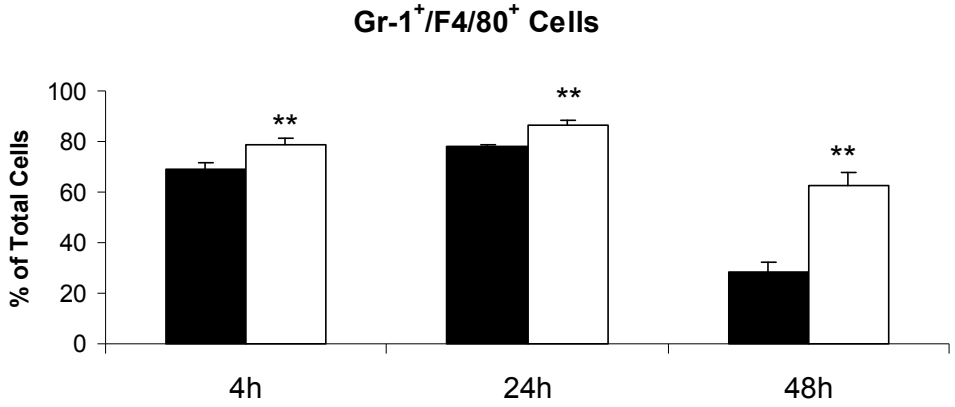

B

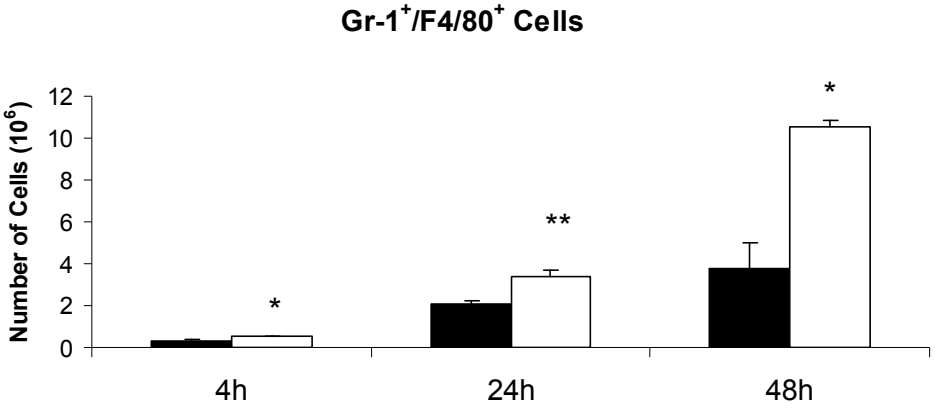

Figure 3.7 In study 2, more viable Gr-1$^+$ F4/80$^+$ cells were present in lavages from *Hsd11b1*$^{-/-}$ mice than from *Hsd11b1*$^{+/+}$ mice at all time points during pleurisy.
Hsd11b1$^{-/-}$ mice (white bars) had higher percent (A) and total number (B) of viable Gr-1$^+$ F4/80$^+$ cells than *Hsd11b1*$^{+/+}$ mice (black bars) at 4h, 24h, and 48h following injection of carrageenan. (n=7/genotype/time point). Values shown are mean ± SEM. *$p<0.05$ and ** $p<0.01$ when compared by Two-way ANOVA.

3.2.4. Resolution of lung inflammation is altered in Hsd11b1$^{-/-}$ mice

Histological assessment of lungs from untreated mice or mice sacrificed 4h, 24h, or 48h following intra-pleural injection of carrageenan (Study 1 and 2) was performed blind to genotype by an expert rodent pathologist, Dr David Brownstein. There were no differences in lung histology between untreated *Hsd11b1*$^{+/+}$ and *Hsd11b1*$^{-/-}$ mice (data not shown). At 4h following injection of carrageenan, there was noticeable inflammation in both genotypes with thickened visceral pleura (due to enlarged and/or activated mesothelial cells) and infiltration of inflammatory cells (dominated by neutrophils) (Figure 3.8). There was substantial histological variability within groups at 4h, and accordingly it was not possible to ascertain any difference in severity of inflammation between the genotypes. Although by 24h inflammation had worsened compared to 4h, in both genotypes, there was variability within groups with no clear qualitative or quantitative difference between genotypes. The visceral pleura were thicker and lymphoid aggregates (comprised of plasma cells, lymphocytes, neutrophils and Mϕ) were apparent within the mediastinum to a similar extent in both genotypes (Figure 3.9). Interestingly, while at 24h the lymphoid aggregates appeared similar between both genotypes (Figure 3.10, A and B), inflammation began to resolve in *Hsd11b1*$^{+/+}$ mice 48h after injection of carrageenan, yet was still in progress in *Hsd11b1*$^{-/-}$ mice (Figure 3.10, C and D). The ongoing inflammation in *Hsd11b1*$^{-/-}$ mice was not only evident by the continued presence of lymphoid aggregates (Figure 3.10) which had largely disappeared in *Hsd11b1*$^{+/+}$ mice, but also by continued thickened peri-oesophageal mediastinum (Figure 3.11) and visceral pleura (Figure 3.12). Importantly, adhesion of

lung lobes was observed only in *Hsd11b1*$^{-/-}$ mice at 48h, a qualitative difference between genotypes (Figure 3.13).

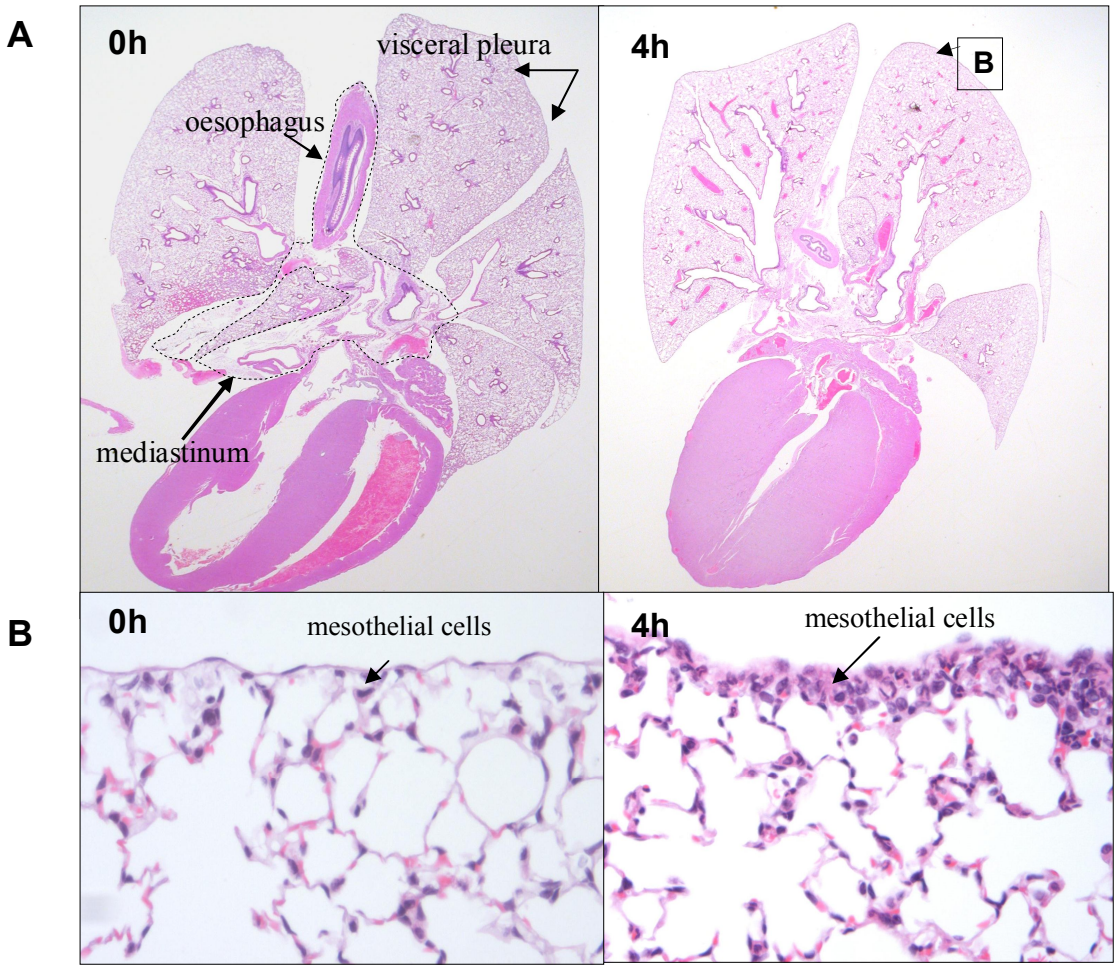

Figure 3.8 4h following injection of carrageenan inflammation is noticeable in both genotypes with thickened visceral pleura and enlarged mesothelial cells.
Representative histology images showing lungs from a control *Hsd11b1*$^{+/+}$ mouse (A, 5x original magnification) and mesothelial cells (B, 100x original magnification) at 0h and 4h following intra-pleural injection of carrageenan (100µl of 0.1% carrageenan). Lung sections from 0h were similar in both genotypes. At 4h, both genotypes exhibited similar thickened pleura, reactive mesothelium, and inflammatory infiltrate dominated by neutrophils.

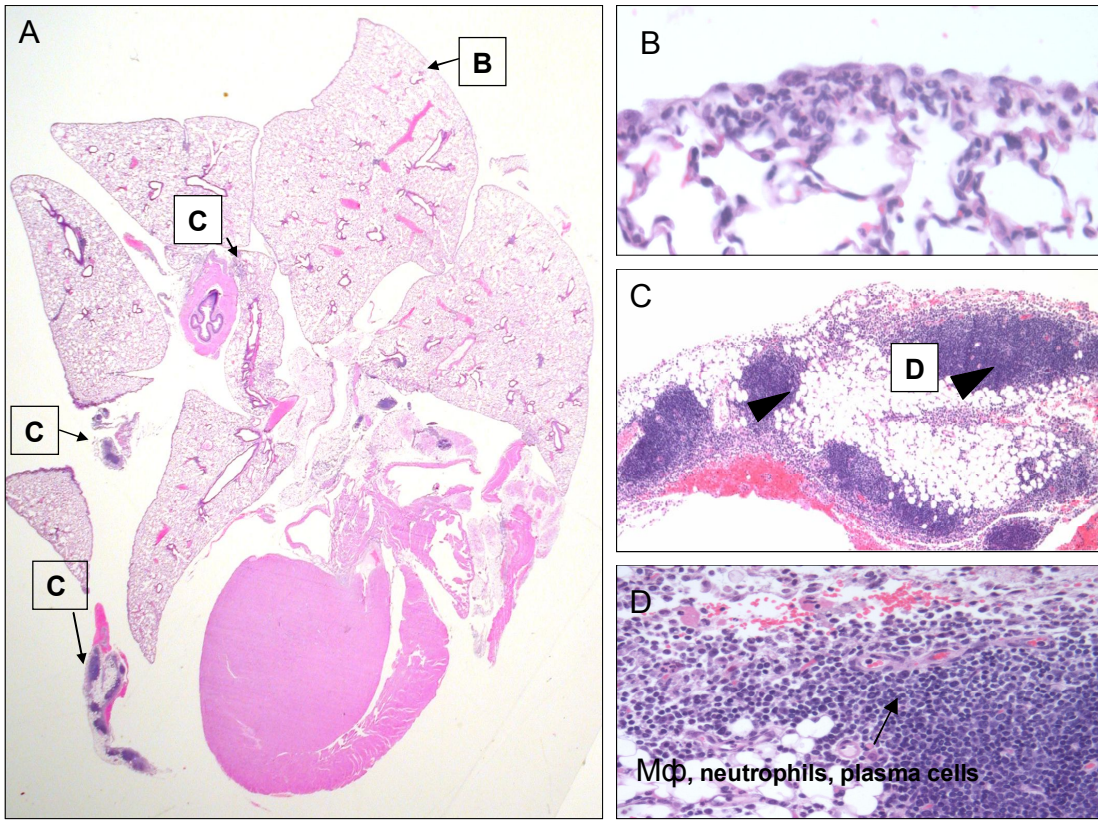

Figure 3.9 Lymphoid aggregates in lung sections at 24h following injection of carrageenan in mice from both genotypes.
Representative image of lung section from a *Hsd11b1*$^{+/+}$ mouse at 24h (A, 5x original magnification) following intra-pleural injection of carrageenan (100µl of 0.1% carrageenan). The thickening of visceral pleura (B, 100x original magnification) and formation of lymphoid aggregates (C; arrows indicate lymphoid aggregates, 50x original magnification) in the mediastinum was similar in the two genotypes. The lymphoid aggregates (D, 100x original magnification) were composed of Mϕ, neutrophils and plasma cells.

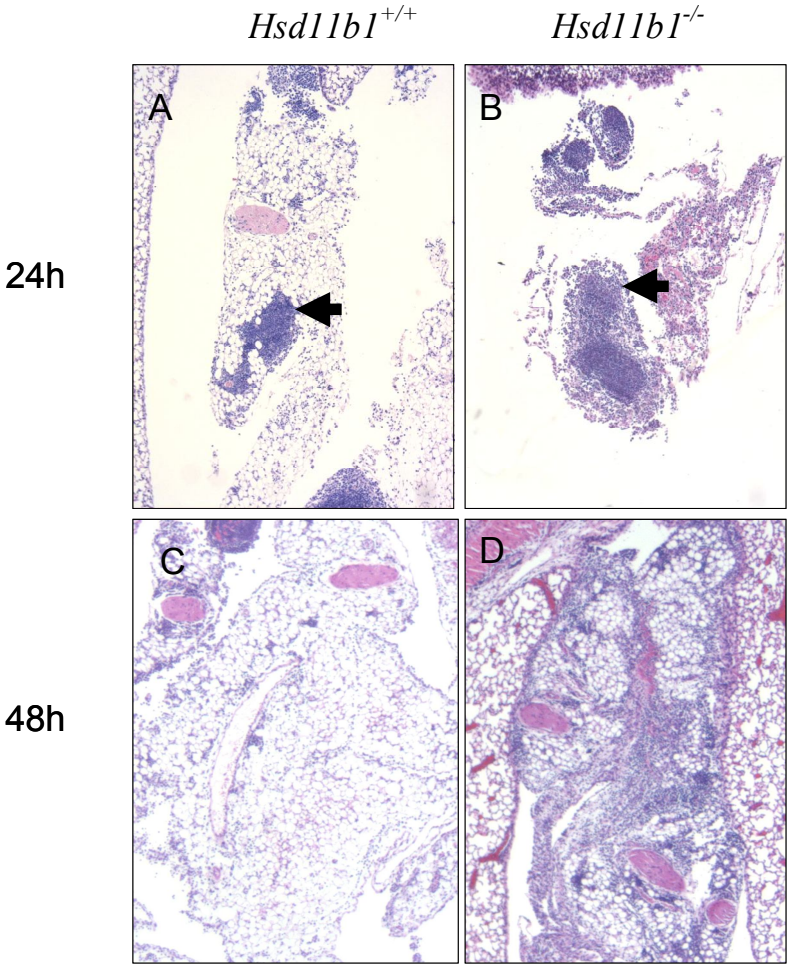

Figure 3.10 Ongoing inflammation in *Hsd11b1*$^{-/-}$ mice at 48h following carrageenan injection.
Intensity of lymphoid aggregates is similar in *Hsd11b1*$^{+/+}$ mice (A) and *Hsd11b1*$^{-/-}$ mice (B), 24h following intra-pleural injection of carrageenan (upper panels). At 48h (lower panels), more evidence of resolution of inflammation is seen in the *Hsd11b1*$^{+/+}$ mice (C) than in *Hsd11b1*$^{-/-}$ mice (D). Arrows indicate lymphoid aggregates. Images are 50x original magnification.

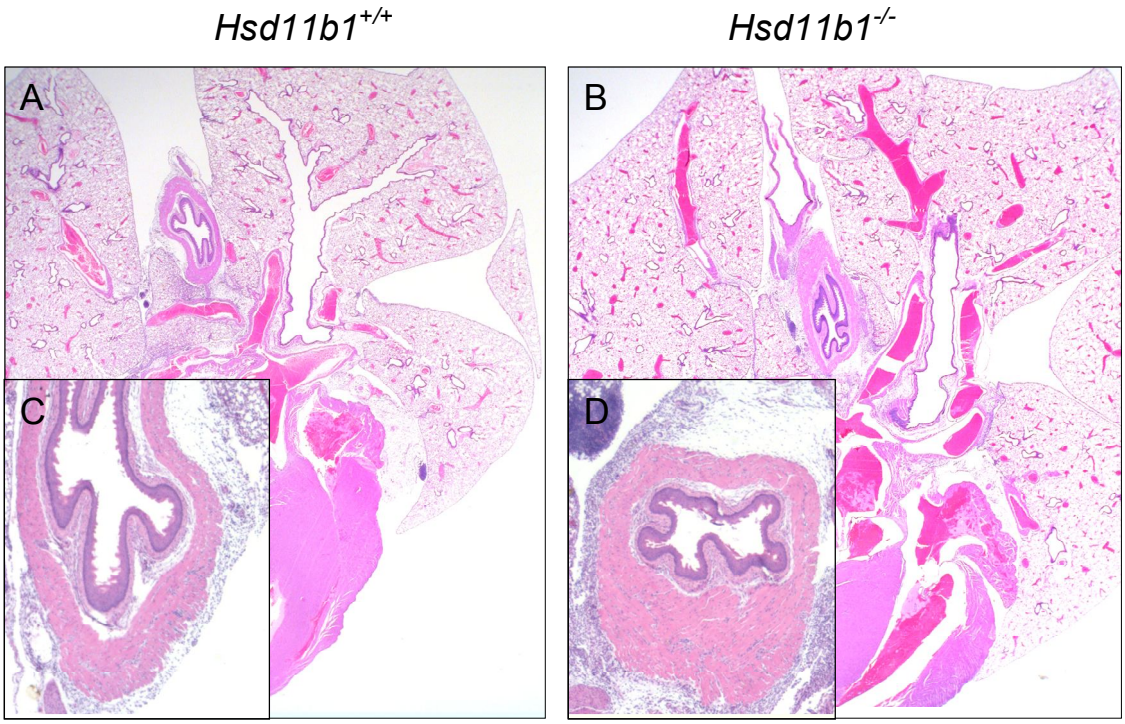

Figure 3.11 Greater peri-oesophageal mediastinum thickening with worse inflammation in *Hsd11b1*$^{-/-}$ mice.
Representative histology image of lungs from *Hsd11b1*$^{+/+}$ (A and C,) and *Hsd11b1*$^{-/-}$ (B and D) mice 48h following intra-pleural injection of carrageenan. There is persistence of peri-oesophageal mediastinum thickening with worse inflammation in *Hsd11b1*$^{-/-}$ (D) than in *Hsd11b1*$^{+/+}$ mice (C). A and B are 5x original magnification. C and D are 50x original magnification.

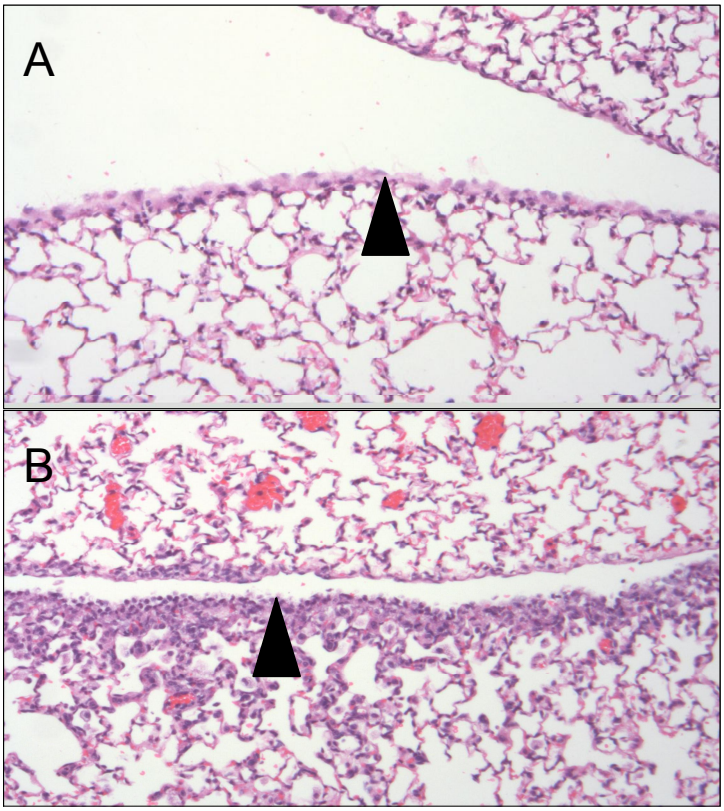

Figure 3.12 Persistent thickening in visceral pleura in *Hsd11b1*$^{-/-}$ mice.
Representative images of visceral pleura at 48h following intra-pleural injection of carrageenan. There is persistent thickening in visceral pleura in *Hsd11b1*$^{-/-}$ mice (B) that is not seen in the controls (A). Images are 50x original magnification. Arrow heads indicate mesothelial cells that line the pleura.

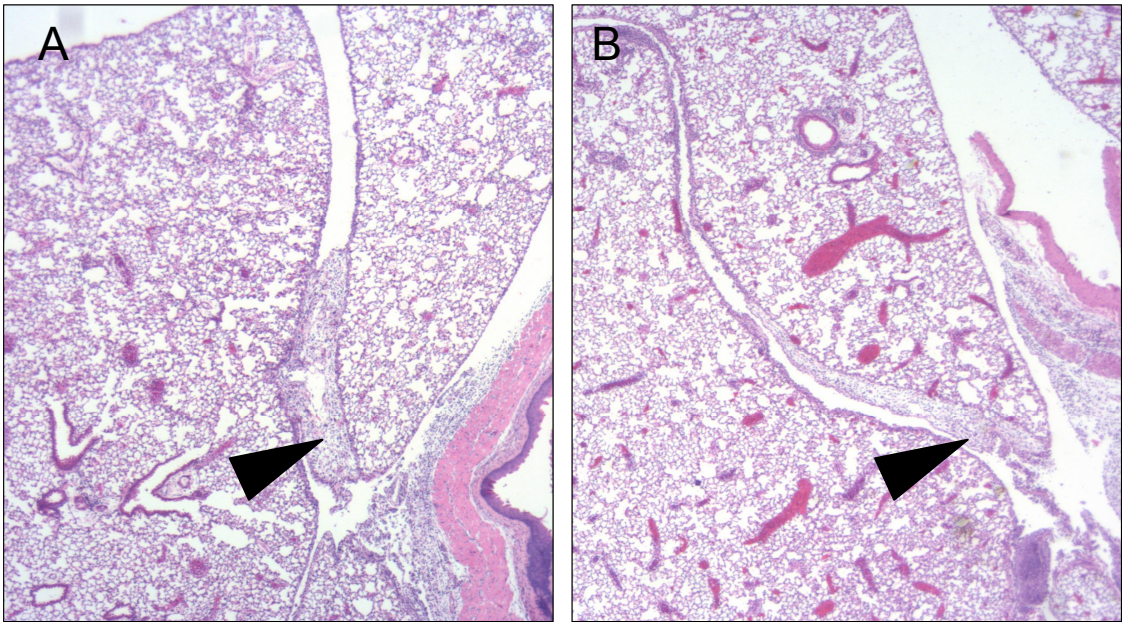

Figure 3.13 Adhesion of lung lobes 48h following intra-pleural injection of carrageenan in *Hsd11b1*$^{-/-}$ mice.
Representative images of lung section from *Hsd11b1*$^{-/-}$ mice (images from sections taken from 2 separate *Hsd11b1*$^{-/-}$ mice) showing adhesion of lung lobes 48h following intra-pleural injection of carrageenan. Adhesion of lung lobes was seen uniquely in *Hsd11b1*$^{-/-}$ mice (A and B) and not in the controls (not shown). Images are 50x original magnification. Arrow heads indicate adhesion between lung lobes.

3.2.5. Lung cytokine profiles during carrageenan-induced pleurisy

Previously, differences in cytokine release have been shown between *Hsd11b1*$^{-/-}$ and *Hsd11b1*$^{+/+}$ mice (Gilmour et al., 2006; Zhang & Daynes, 2007). Therefore, to determine whether cytokine responses to carrageenan-induced pleurisy differed between *Hsd11b1*$^{+/+}$ and *Hsd11b1*$^{-/-}$ mice, IL-6, IL-10, IL-12p70, MCP-1, IFN-γ and TNF-α cytokine levels were measured in pleural exudates from Study 1 using a cytometric bead assay (CBA) mouse inflammation kit. In both genotypes, TNF-α levels were highest at 4h and although there was a trend for TNF-α to be higher in *Hsd11b1*$^{-/-}$ mice, it did not reach statistical significance (Figure 3.14). Similarly, IL-6 levels were highest at 4h, with much lower levels at 24h and undetectable levels at 48h and 72h and did not differ between genotypes at any time point (Figure 3.14). INFγ, IL-12p70 and IL-10 all peaked at 24h, and whilst INFγ and IL-10 did not differ between genotypes, peak levels of IL-12p70 at 24h after carrageenan injection, were lower in *Hsd11b1*$^{-/-}$ than in *Hsd11b1*$^{+/+}$ mice (Figure 3.14). Levels of MCP-1 were high for the first 48h following carrageenan injection and were similar in both genotypes at 4h and 24h (although at both time points MCP-1 reached the maximum limit detection of the assay in many of the samples) (Figure 3.14).

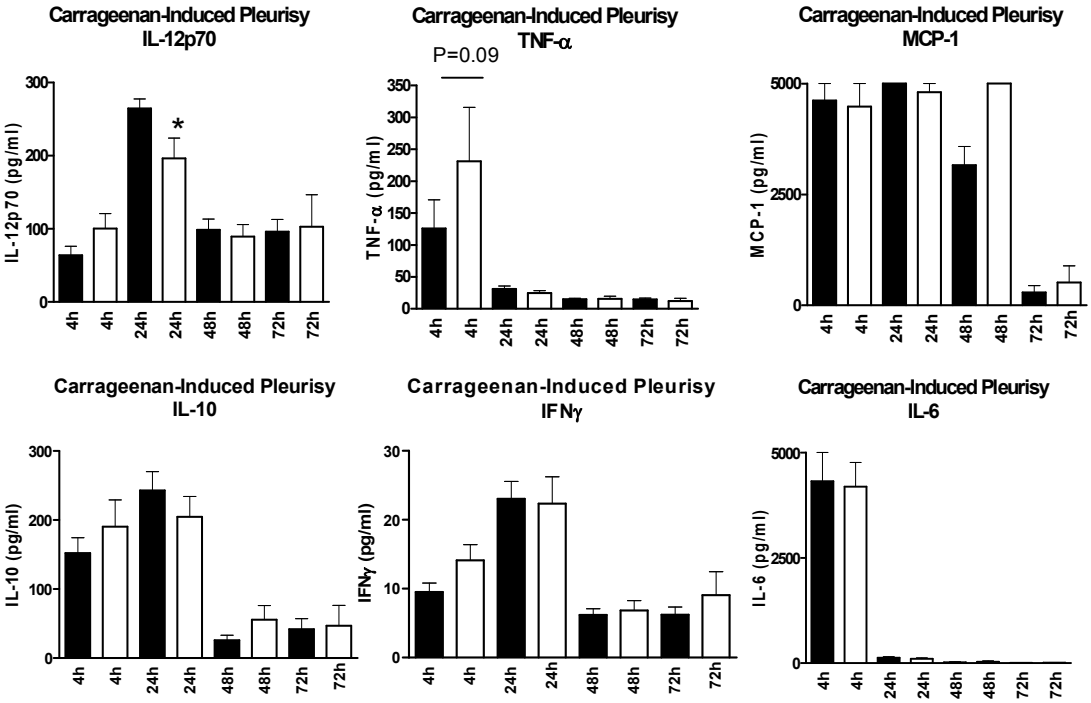

Figure 3.14 Study 1, altered cytokine levels in *Hsd11b1*$^{-/-}$ versus *Hsd11b1*$^{+/+}$ mice following intra-pleural injection of carrageenan.
Results based on CBA mouse inflammation kit which was used to simultaneously measure IL-6, IL-10, IL-12p70, MCP-1, IFN-γ and TNF-α levels in pleural exudates at the indicated times following injection of carrageenan. Peak levels (24h) of IL-12p70 (top left panel) were lower in lavages from *Hsd11b1*$^{-/-}$ mice (white bars) than in lavages from *Hsd11b1*$^{+/+}$ mice (black bars). There was a trend (p=0.09) for higher peak levels (at 4h) of TNF-α in *Hsd11b1*$^{-/-}$ mice. Values shown are mean ± SEM. * $p<0.05$ represents a significant difference between genotypes (n=6-7/genotype/time) when compared by Two-way ANOVA followed by Benferroni post-hoc analysis.

3.3. Discussion

The comparative assessment of carrageenan-induced lung inflammation described in this Chapter is consistent with a role for 11β-HSD1 in limiting acute inflammation. These results suggest that, compared to control mice, *Hsd11b1*$^{-/-}$ mice show an exaggerated inflammatory response to carrageenan injection and possibly impaired resolution. Despite similar lavage volumes, more cells were recovered from the pleural cavity of *Hsd11b1*$^{-/-}$ mice than from controls following intra-pleural injection of carrageenan. The recruitment of more inflammatory cells in *Hsd11b1*$^{-/-}$ mice is indicative of a greater inflammatory response.

Based on previous characterization of this model, the increased number of recovered cells seen in *Hsd11b1*$^{-/-}$ mice at 4h following injection of carrageenan is likely to be due to an influx of neutrophils with the increase at 24h likely to be due to increased numbers of monocytes (Vinegar et al., 1982a). Microscopic examination of cytocentrifuged cells was consistent with this conclusion, and is consistent with previous data showing increased numbers of recruited inflammatory cells in TG-induced peritonitis but no difference in the population recruited (Gilmour, 2002; Gilmour et al., 2006). However, further assessment by flow cytometry revealed that a sub-population of cells expressing F4/80 and Gr-1 cell markers differed between the two genotypes, suggesting that the recruited cells may differ in phenotype. In addition, the level of cell death in recruited inflammatory cells was lower at the onset of inflammation in *Hsd11b1*$^{-/-}$ than in *Hsd11b1*$^{+/+}$ mice. Resolution of inflammation is dependent on the successful removal of

inflammatory cells (by migration or phagocytosis) and pro-inflammatory stimuli they produce, as well as cessation of recruitment of viable cells. Thus, ongoing influx of *viable* cells, such as neutrophils, and their continued release of pro-inflammatory mediators, will prolong the inflammatory response.

Measurement of cytokine concentrations in exudates suggested differences in levels of inflammatory mediators between the two genotypes. Unfortunately, the CBA assay was not sufficiently sensitive for all the cytokines measured and levels in some samples were outside the range of the assay. Nonetheless, peak levels of IL-12p70, which plays a major role in driving the T cell response towards a Th1 pattern of cytokine secretion (Trinchieri et al., 2003; Trinchieri, 2003), was lower in lavage fluid from *Hsd11b1*$^{-/-}$ than in *Hsd11b1*$^{+/+}$ mice, 24h following intra-pleural injection of carrageenan. Pro-inflammatory functions of IL-12 include induction of IFN-γ (Trinchieri et al., 2003). However, IFN-γ levels were similar between genotypes at all times following injection. In addition, although not significant, levels of TNF-α, an early pro-inflammatory cytokine, were increased in *Hsd11b1*$^{-/-}$ mice at 4h after injection. Level of MCP-1, a chemoattractant for monocytes, was increased in *Hsd11b1*$^{-/-}$ mice at 48h after injection (although all *Hsd11b1*$^{-/-}$ samples were above assay detection limit and therefore statistical analysis was not possible for these samples). This is intriguing as MCP-1 may be of key importance in the recruitment of monocytes in pulmonary infections, whilst 11β-HSD1 inhibitor decreases MCP-1 levels in aorta of *apoe*$^{-/-}$ mice (Hermanowski-Vosatka et al., 2005).

Normally, carrageenan-induced pleurisy involves a monophasic mobilization of neutrophils followed by monocytes (Vinegar et al., 1982b). Resolution in this model is usually observed by 48h. However, this was not seen. Although a direct comparison between the 72h experiment and the other time points (4h, 24h and 48h) in Study 1 is not possible since the experiments were completed separately, the elevated levels of recruited inflammatory cells at 72h (above levels at 24h and 48h) were surprising and difficult to explain. During routine health monitoring at the animal facility (Western General Hospital, Edinburgh), where all the carrageenan-induced pleurisy experiments were carried out, *Pasteurella pneumotropica* infections were found in sentinel animals (January 2005 report) at the time of the experiments. This opportunistic organism is found in many research colonies of rodents and in the presence of primary pathogens can potentiate the severity of disease (Brennan et al., 1965). Therefore, although the groups of mice were well matched between the experiments it is possible that infection with *Pasteurella pneumotropica* confounded some or all of these experiments, accounting for the failure to fully resolve inflammation at 48h and for the unexpectedly high cellularity in the separate experiment at 72h. Indeed, although the cellularity was greatly increased at 72h, cytokine levels had returned to basal at this time, suggesting cessation of pro-inflammatory mediators.

Histological assessment did not reveal any differences between lungs of untreated *Hsd11b1*$^{-/-}$ and *Hsd11b1*$^{+/+}$ mice, suggesting that any differences observed following inflammation are not due to an underlying pathology, but are due to the inflammatory stimulus itself. During the onset and peak of inflammation, both genotypes showed

progressively worse inflammation. At 48h, control mice showed signs of resolution with less inflamed pleura and fewer aggregates, whereas most *Hsd11b1*$^{-/-}$ mice had ongoing inflammation. Uniquely, *Hsd11b1*$^{-/-}$ mice exhibited adhesions on lung lobes suggesting possible fibrosis development if left for longer duration. This raises the possibility that worse tissue damage (scarring) will ultimately occur in *Hsd11b1*$^{-/-}$ mice. The fibrous adhesions might be a direct reaction to the greater influx of inflammatory cells in *Hsd11b1*$^{-/-}$ mice. However, given the qualitative nature of the differences between genotypes it is perhaps likely due to a greater reaction of the non-leukocyte cells (eg. resident fibroblast and mesothelial cells) to the pro-inflammatory environment. During pleural inflammation, mesothelial cells secrete chemokines (including IL-8, MIP-1α and MCP-1) to recruit neutrophils and monocytes (Antony et al., 1995; Mohammed et al., 1998; Mohammed et al., 1999). Fibroblasts exist in the interstitial stroma beneath mesothelial cells and also contribute to leukocyte recruitment during serosal inflammation (Faull, 2000; Witowski et al., 2001; Loghmani et al., 2002).

In summary, this Chapter corroborates previous findings in TG-peritonitis experiments (Gilmour, 2002), suggesting that *Hsd11b1*$^{-/-}$ mice exhibit an altered course of acute inflammation. Importantly, this model demonstrated that the worse acute inflammatory response seen in *Hsd11b1*$^{-/-}$ mice is not limited to sterile peritonitis. The findings in the carrageenan-induced pleurisy model are novel but remain preliminary. However, they provide a basis for further investigation. Future experiments using this model should focus on identifying exactly which cells in lung (both resident and inflammatory)

express 11β-HSD1 and how the levels of expression are altered by inflammation during the onset, peak and resolution phases. Histology data implies that *Hsd11b1*$^{-/-}$ mice are not only slower to resolve inflammation but also that they might be at higher risk for fibrotic disease. Finally, corticosterone levels are high (350-400ng/ml) in pleural exudates at the acute phase, but return to normal 24h after carrageenan injection (Gilroy et al., 2004). In future experiments, it will be important to measure corticosterone levels in both plasma and pleural exudate (not completed in these experiments) to determine if the HPA response and tissue corticosterone penetration during caraggeenan-induced inflammation is altered in *Hsd11b1*$^{-/-}$ mice.

Chapter Four

Effects of 11β-HSD1-deficiency on experimental arthritis.

4.1. Introduction

Since GC are commonly and successfully used to treat inflammatory arthritis in humans a model of experimental arthritis was also used to further investigate whether and how 11β-HSD1 deficiency confers an inflammatory phenotype. There are many experimental models of arthritis, but none fully address the complexity of human rheumatoid arthritis. In addition, considerable heterogeneity exists between mouse strains in susceptibility to different models of experimental arthritis. Hence, the initial aim was to select a model suited for C57BL/6 mice and which allowed for assessment of inflammation during onset, peak and resolution of disease, providing opportunity for histological assessment. Two separate and previously established models were tested. Type II collagen-induced arthritis with complete Freund's adjuvant (CIA-CFA) (reviewed in Chapter 2, Section 2.3.7.1.) is widely used and well characterized in rodents. However, not all mouse strains respond to this model of arthritis. The second model was the more recently described K/BxN serum transfer model (Kouskoff et al., 1996). Injection of serum or purified G-6-PI antibodies from arthritic K/BxN mice into healthy recipient mice rapidly and reproducibly induces an inflammatory arthritis which is self-resolving (as the antibody is cleared), bypassing the lymphocyte-dependent induction phase of arthritis (reviewed in Chapter 2, Section 2.3.7.2.).

4.2. Results

4.2.1. C57BL/6 mice are resistant to arthritis in the CIA-CFA model

Despite previous reports of successful induction of arthritis using the CIA-CFA model in C57BL/6 mice (Campbell et al, 2000), inoculation with CIA-CFA failed to produce arthritis in C57BL/6 (control) mice. Clinical assessment of redness and swelling of limbs (as described in Chapter 2, Section 2.3.7.2.3) was carried out to determine disease onset and severity. Only intermittent symptoms (eg. redness of skin around carpal joints without swelling) were observed and only in 1 (of 10) *Hsd11b1*$^{-/-}$ mice after 60d of observation (data not shown). No signs were observed in the control mice.

Accordingly, this model was not used further to investigate the course of arthritis in *Hsd11b1*$^{-/-}$ mice. During the course of this experiment, it was noted that following sub-dermal injection of emulsion containing collagen with CFA, mice developed temporary, self-resolving ulcers at the site of injection, at the base of the tail. Ulceration was more severe, with more bleeding in *Hsd11b1*$^{-/-}$ mice than the control mice (Figure 4.1). In addition, there was delayed healing of the wounds in *Hsd11b1*$^{-/-}$ mice compared to controls, such that at 60d there were significantly more *Hsd11b1*$^{-/-}$ mice with ulcers than controls.

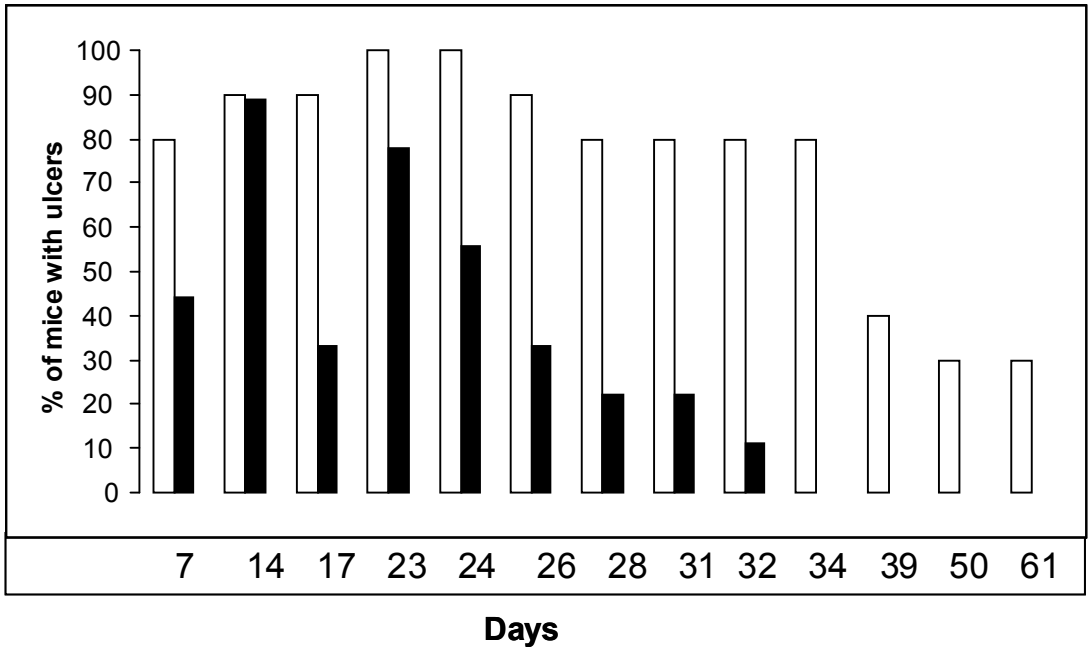

Figure 4.1 A greater proportion of *Hsd11b1*$^{-/-}$ mice developed dermal ulcers following CIA-CFA immunization than *Hsd11b1*$^{+/+}$ mice.
Hsd11b1$^{-/-}$ (white bars; n=10) and *Hsd11b1*$^{+/+}$ mice (black bars; n=9) received sub-dermal injection of 100µl CIA-CFA on d0 and d21. Mice were observed for 61d following initial injection, and ulcer formation was recorded. Values represent % of mice with ulcers in each group. Two-way ANOVA showed significant interaction ($p<0.001$).

4.2.2. Earlier onset of arthritis and delayed resolution following K/BxN serum transfer in Hsd11b1$^{-/-}$ mice: Experiment 1, standard dose of K/BxN serum

The standard dose (i.p. injections of 7.5µl K/BxN serum/g body weight administered on 0d and 2d) previously reported in the literature was initially chosen as it has been shown to cause arthritis in C57BL/6 mice (Ji et al., 2002). Administration of K/BxN serum produced symmetrical (in all 4 limbs) arthritis in both *Hsd11b1*$^{-/-}$ and *Hsd11b1*$^{+/+}$ control mice (Figure 4.2). Clinical score was monitored until the arthritis had resolved in the control mice (at 21d). Inoculation with the standard dose of serum resulted in an earlier onset of symptoms in *Hsd11b1*$^{-/-}$ mice, with significantly higher clinical scores than the controls until 4d (Figure 4.3.A.). However, by 5d, the clinical score for both groups reached maximum, and remained high until approximately 12d. Although the peak score was similar between the 2 genotypes, the area under the curve (AUC), based on 21d observation, was significantly greater in the *Hsd11b1*$^{-/-}$ than the *Hsd11b1*$^{+/+}$ mice (Figure 4.3.B.). Consistent with worse clinical score, the AUC for caliper measurement of ankle (right tarsal joint) diameter was significantly greater in *Hsd11b1*$^{-/-}$ compared to *Hsd11b1*$^{+/+}$ mice (Figure 4.3.C). Inflammation in both groups started to resolve by 16d (Figure 4.3.A.). However, the improvement in clinical score for *Hsd11b1*$^{-/-}$ mice lagged ~1d behind the controls.

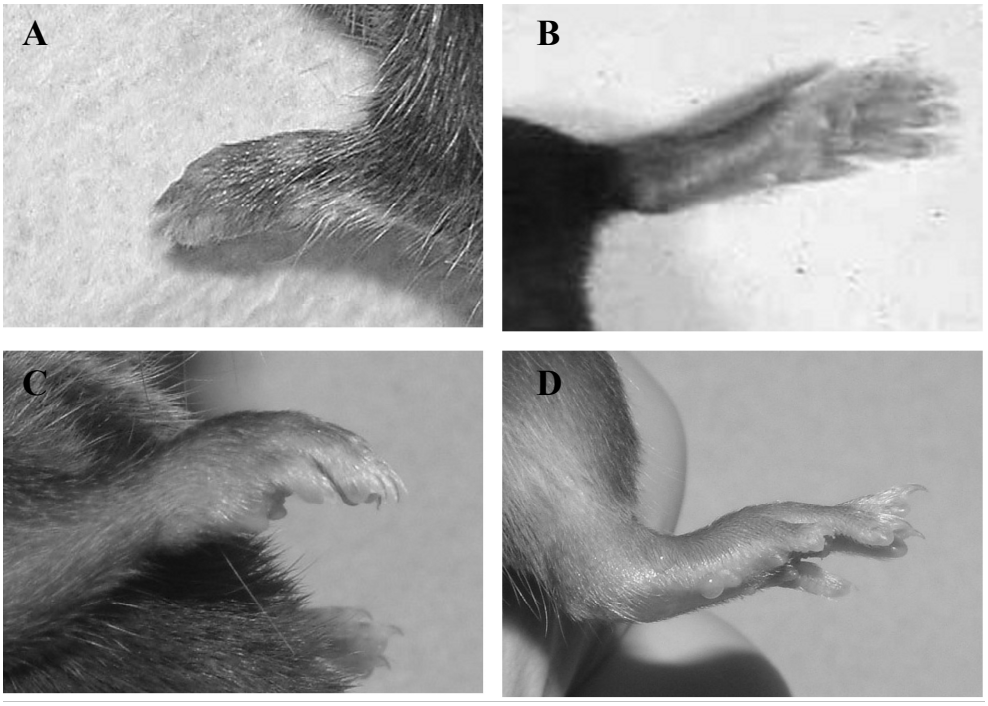

Figure 4.2 I.p. injection of K/BxN serum results in joint swelling.
The appearance of a normal hind limb of a C57BL/6 *Hsd11b1*$^{+/+}$ mouse (A and B), in contrast to the appearance (C and D) 10d following injection of the standard dose (2 i.p. injections of 7.5µl/g body weight on 0d and 2d) of K/BxN serum. In all K/BxN arthritis experiments mice were injected with serum between 8am and 10am. The representative arthritic paws shown were assigned the maximal clinical score of 3 (Clinical scoring further explained in Chapter 2, Section 2.3.7.2.3).

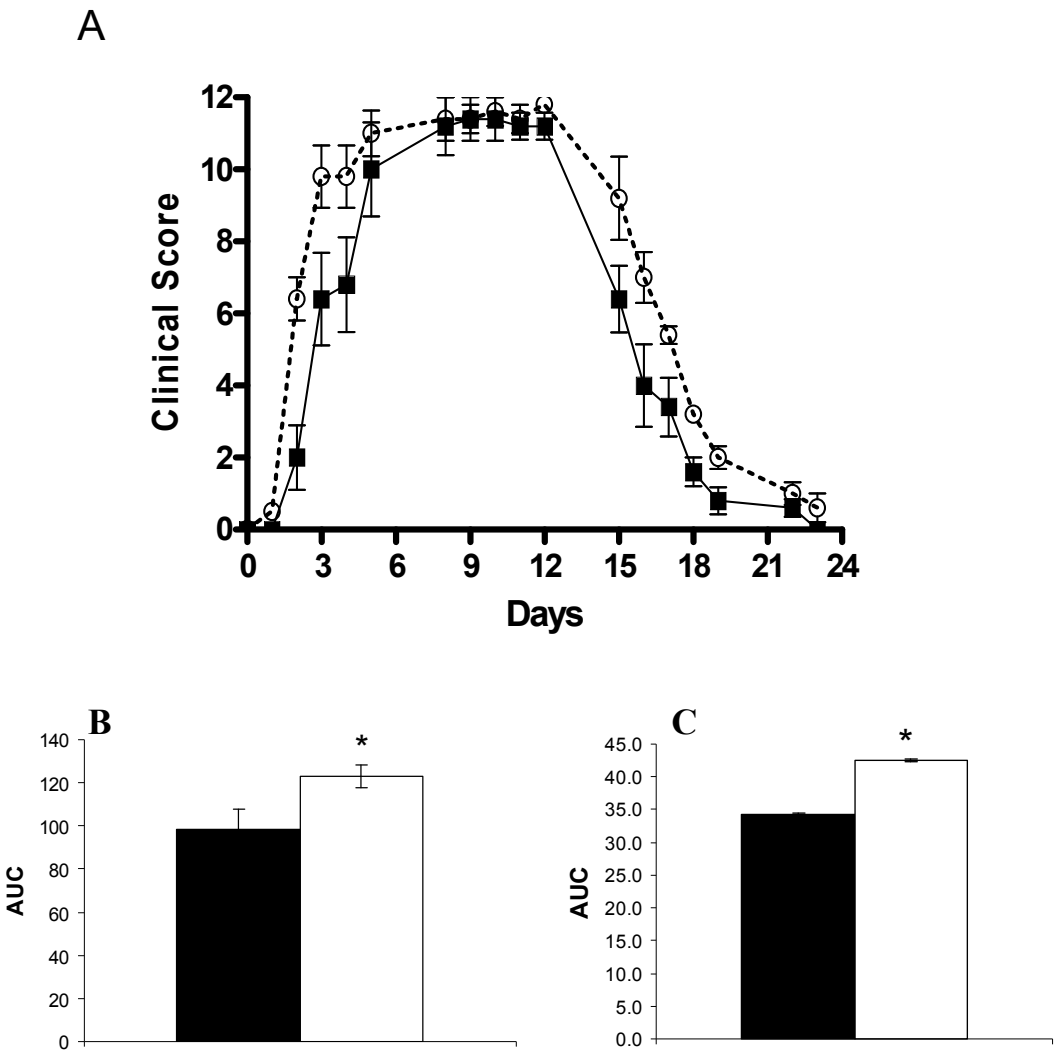

Figure 4.3 Earlier onset of arthritis and delayed resolution following K/BxN serum transfer in *Hsd11b1*$^{-/-}$ mice.

(A) Standard dose (i.p. injections of 7.5µl/g body weight on 0d and 2d) of K/BxN serum showing daily clinical scores (characterized by oedema and redness of carpal and hock joints) over 21d. Two-way mixed ANOVA showed significant interaction between genotype ($p<0.01$). (B) AUC for *Hsd11b1*$^{-/-}$ mice (white bar) compared to *Hsd11b1*$^{+/+}$ mice (black bar) (n=5/group), and (C) AUC for caliper measurement of ankle (right tarsal joint) diameter was also greater in *Hsd11b1*$^{-/-}$ compared to *Hsd11b1*$^{+/+}$ mice. Clinical scoring in this experiment was performed together with Dr Mohini Gray. * $p<0.05$ when compared by unpaired Student's t-test. Values shown represent mean ± SEM.

4.2.2.1. Pathology analysis after 21d of K/BxN arthritis

Histological analysis (carried out by Dr D. Brownstein, CCVS) of H&E sections of joints after 21d of arthritis showed periarticular inflammation in the bones and tendons leading towards the joint for both genotypes (Figure 4.4). However, no qualitative differences were found between the two genotypes. In addition, both genotypes showed little evidence of exudate volume, panus (none in carpal, possibly some in tarsal joints) or erosion at 21d, and any intra-articular inflammation had resolved by this time. Fibroblast proliferation around the joint, new cartilage and bone, and thickening of tendon sheath was found in both genotypes, but no striking observable difference between genotypes was noted. Additionally, there was strong evidence of periarticular disease, involving the tendons and tendon sheaths in both groups.

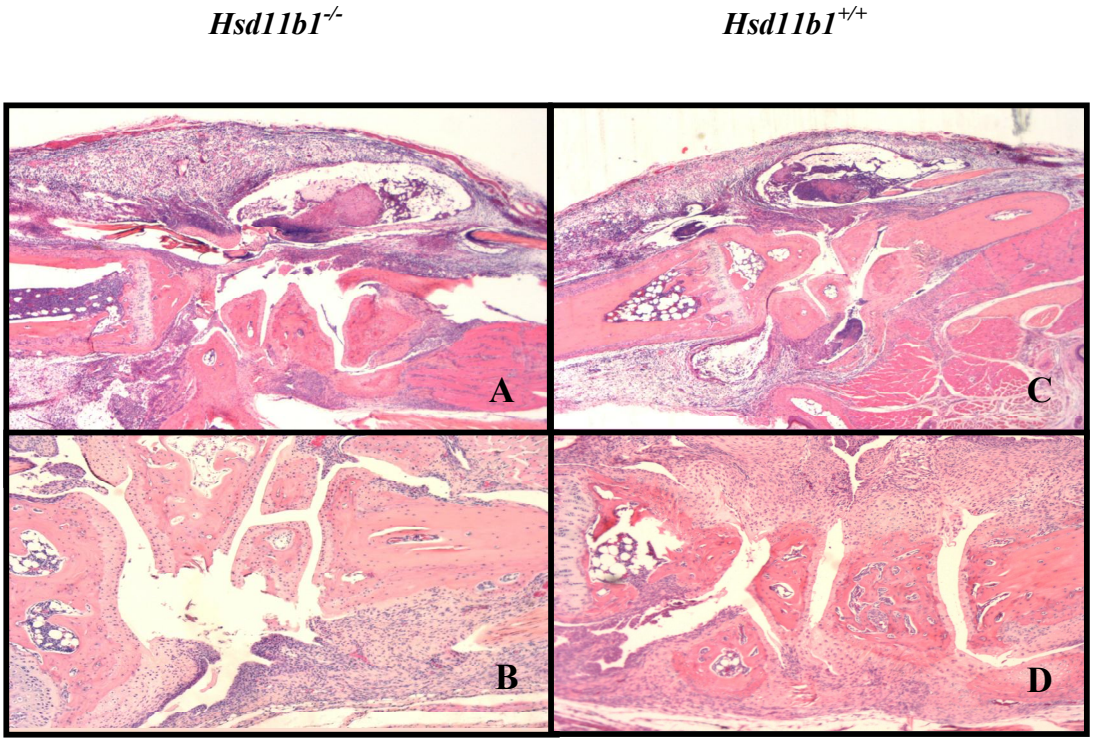

Figure 4.4 Pathology does not differ between the genotypes after 21d of standard dose K/BxN serum transfer arthritis.
Joints were collected 21d following experimental arthritis (i.p. injections of 7.5µl K/BxN serum/g body weight on d0 and d2) (n=5/group). Representative images of H&E sections, showing carpal joints, from *Hsd11b1*$^{-/-}$ (A and B) and *Hsd11b1*$^{+/+}$ mice (C and D). Images are 50x original magnification.

4.2.2.2. Effects of K/BxN arthritis on anthropometric measurements

Anthropometric differences were observed between the genotypes in response to K/BxN arthritis. The body weight of the *Hsd11b1*$^{-/-}$ mice was significantly greater at both the start (*Hsd11b1*$^{+/+}$; 29.0±0.7g versus *Hsd11b1*$^{-/-}$; 32.0±0.5g, $p<0.01$**)**, despite *Hsd11b1*$^{+/+}$ control mice being age matched, and end of the experiment (*Hsd11b1*$^{+/+}$; 29.2±0.8g versus *Hsd11b1*$^{-/-}$; 33.8±0.5g, $p<0.01$**)**. Thymus weight, expressed as percent of body mass, was significantly lower in *Hsd11b1*$^{-/-}$ than in *Hsd11b1*$^{+/+}$ mice (Figure 4.5.A). Although the right adrenal was significantly heavier in *Hsd11b1*$^{-/-}$ than in *Hsd11b1*$^{+/+}$ mice (with a trend for larger left adrenal), this did not reach significance when expressed as percent body weight (data not shown). Overall, *Hsd11b1*$^{-/-}$ mice had a significantly lower thymus:adrenal ratio (corrected for body weight) than *Hsd11b1*$^{+/+}$ mice (Figure 4.5.B). These changes were not observed in *Hsd11b1*$^{-/-}$ mice following arthritis induced by a *lower* dose of K/BxN serum (Experiment 2, discussed below), indicating that the altered thymus:adrenal ratio is likely to result from this arthritis challenge.

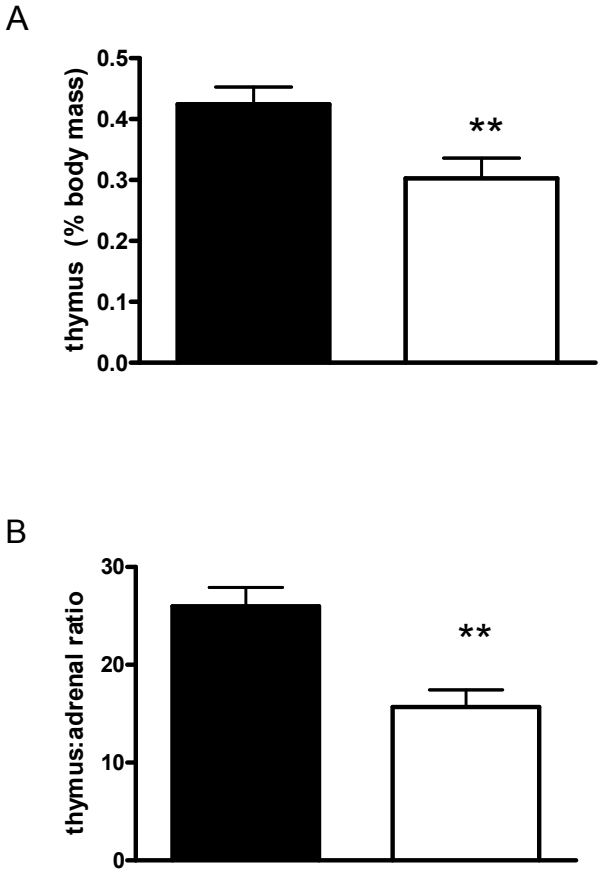

Figure 4.5 Anthropometric differences between *Hsd11b1*$^{-/-}$ and *Hsd11b1*$^{+/+}$ mice in response to K/BxN serum transfer arthritis.
Thymus weight, expressed as % body mass, and thymus:adrenal ratio were significantly lower in *Hsd11b1*$^{-/-}$ (white bar) than in *Hsd11b1*$^{+/+}$ mice (black bar) 21d following injection of K/BxN serum (n=5/genotype). ** $p<0.01$ when compared by unpaired Student's t-test.

4.2.3. Earlier onset of arthritis and delayed resolution in Hsd11b1$^{-/-}$ mice: Experiment 2, reduced dose of K/BxN serum

The standard dose of K/BxN serum (described above) produced severe arthritis with maximum clinical scores (maximum score=12) in *Hsd11b1*$^{+/+}$ as well as *Hsd11b1*$^{-/-}$ mice. In order to detect greater severity of inflammation in *Hsd11b1*$^{-/-}$ than in *Hsd11b1*$^{+/+}$ mice (the predicted hypothesis), it was therefore necessary to cause a sub-maximal arthritis in *Hsd11b1*$^{+/+}$ mice. Accordingly, the inoculum of K/BxN serum was reduced to a single injection of 5.6µl/g body weight on 0d. Administration of the reduced dose resulted in the development of a milder arthritis in both genotypes (Figure 4.6).

Similar to the standard dose experiment, inoculation with the reduced dose of K/BxN serum resulted in an earlier onset of symptoms in *Hsd11b1*$^{-/-}$ mice with clinical scores remaining above those of *Hsd11b1*$^{+/+}$ mice for the duration of the experiment (Figure 4.6.A). The reduced inoculum resulted in a significantly higher AUC in *Hsd11b1*$^{-/-}$ mice than in *Hsd11b1*$^{+/+}$ mice (Figure 4.6.B). As with the standard dose, resolution of clinical symptoms in *Hsd11b1*$^{-/-}$ mice was delayed ~1d compared to *Hsd11b1*$^{+/+}$ mice (Figure 4.6.A), with ~50% reduction in clinical scoring at ~16d in *Hsd11b1*$^{-/-}$ compared to ~11d in *Hsd11b1*$^{+/+}$ mice (Figure 4.6.A). Furthermore, the more aggressive onset of inflammation was reflected in the greater number of joints with higher clinical scores in *Hsd11b1*$^{-/-}$ than in *Hsd11b1*$^{+/+}$ mice (Figure 4.7).

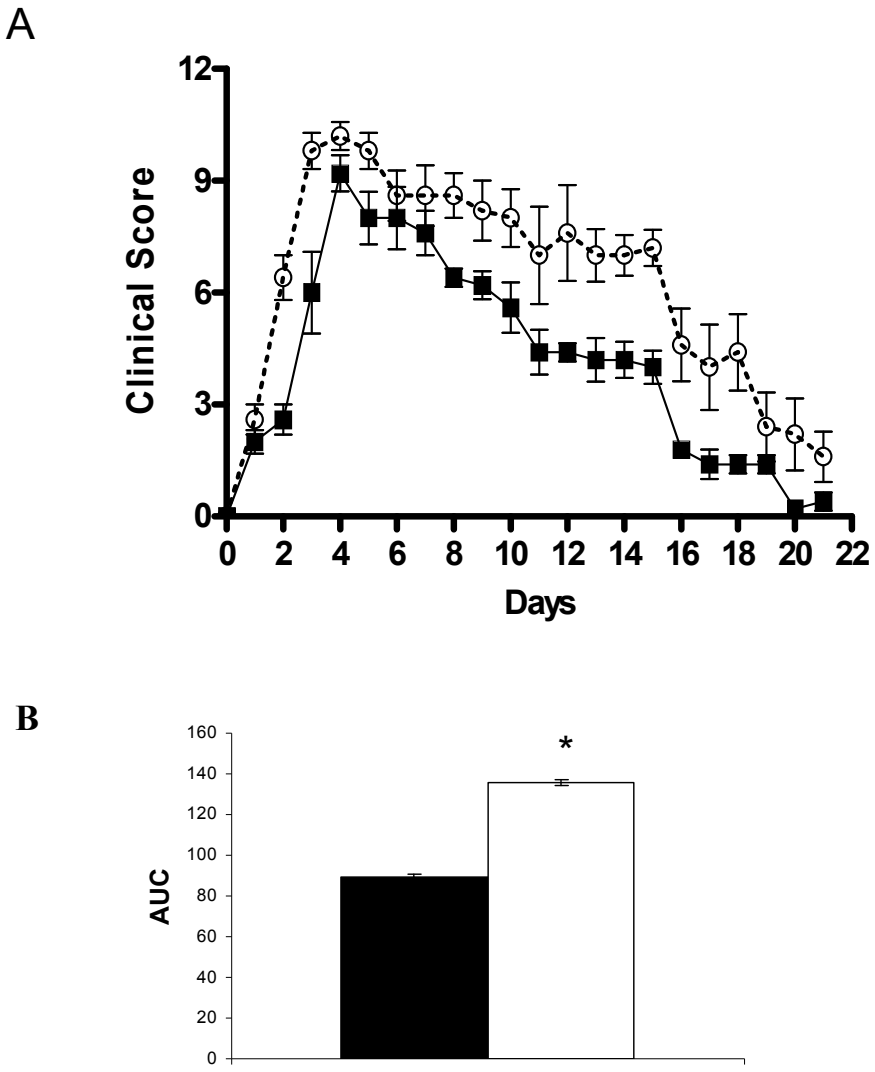

Figure 4.6 Earlier onset and delayed resolution of arthritis in *Hsd11b1*$^{-/-}$ mice with reduced dose of K/BxN serum.
Higher clinical scores (A) over 21d of arthritis, and greater AUC (B) following reduced dose (single injection of 5.6µl/g body weight on d0) of K/BxN serum transfer in *Hsd11b1*$^{-/-}$ mice (white) compared to *Hsd11b1*$^{+/+}$ mice (black) (n=5/genotype). Clinical scoring was performed blind to genotype. Values shown are mean ± SEM. Two-way ANOVA showed significant interaction ($p<0.01$). For AUC, * $p<0.05$ when compared by unpaired Student's t-test.

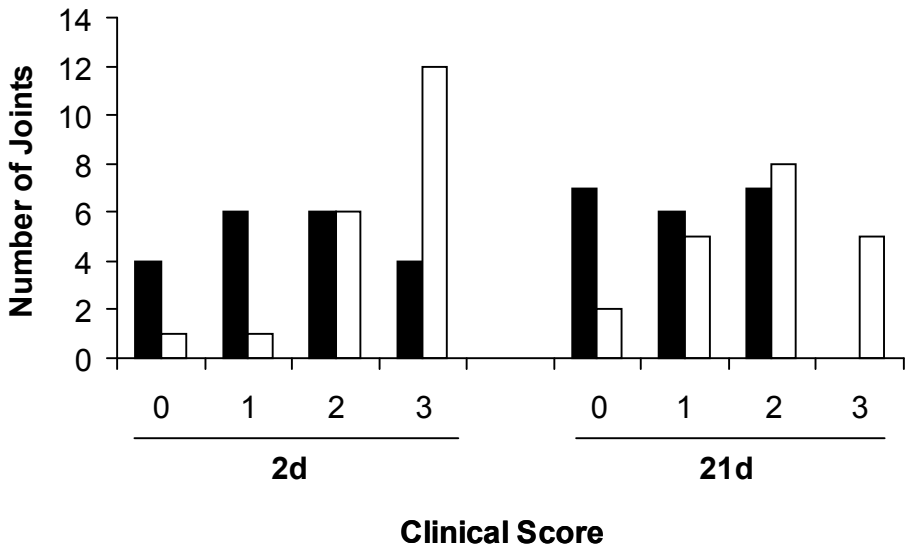

Figure 4.7 The total number of joints, with more severe clinical scores, was higher in *Hsd11b1*$^{-/-}$ than in the *Hsd11b1*$^{+/+}$ mice.
More aggressive onset of inflammation, reflected by higher number of paws with higher clinical score in the *Hsd11b1*$^{-/-}$ (white bars) than in the *Hsd11b1*$^{+/+}$ mice (black bars) following reduced dose (single injection of 5.6µl/g body weight on d0) of K/BxN serum transfer. Chi Square analysis showed a significant difference ($p<0.05$) between genotypes (n=5/genotype).

Inoculation with a reduced dose resulted in a less symmetric arthritis with high variability in both genotypes. The asymmetrical pattern of arthritis made it difficult to obtain reproducible measurements of paw swelling with the caliper. As a result, significant differences could not be detected between genotypes with caliper measurements of the ankle (right tarsal joint) diameter (data not shown).

4.2.3.1. Pathology analysis after 21d of K/BxN arthritis

Histological assessment of joint sections (21d post injection) from the reduced dose experiment revealed that *Hsd11b1*$^{-/-}$ mice had a more reactive bone phenotype and intense periarticular inflammation with more severe exostosis and collagen deposition. Uniquely, ganglion cyst formation was observed in *Hsd11b1*$^{-/-}$ mice but not in *Hsd11b1*$^{+/+}$ mice (Figure 4.8).

4.2.3.2. Plasma corticosterone levels remained elevated in Hsd11b1$^{-/-}$ mice during the resolution stage of arthritis

Plasma was collected at the nadir of corticosterone secretion (0800h) under stress-free conditions for measurement of corticosterone levels at d2 and d21. At d2, the acute stage of disease, both genotypes had elevated plasma corticosterone levels (Figure 4.9). However, at d21, a time point at which mice of both genotypes showed significant levels of recovery (based on clinical scoring), corticosterone remained elevated in *Hsd11b1*$^{-/-}$ mice (Figure 4.9), consistent with an ongoing stress response. In contrast, corticosterone

levels in *Hsd11b1*$^{+/+}$ mice were significantly lower at d21 in comparison to d2 (Figure 4.9).

4.2.3.1.Effects of K/BxN arthritis on anthropometric measurements

Following the reduced dose of K/BxN serum, all mice lost body weight by 21d (Figure 4.10.A). At the end of the experiment there was no difference in thymus weight (expressed as % body mass) between the 2 genotypes (Figure 4.10.B). Although the right adrenal mass (% body mass) was larger in *Hsd11b1*$^{-/-}$ compared to *Hsd11b1*$^{+/+}$ mice (Figure 4.10.C), there was no difference in the left adrenal as well as total adrenal weight (% body mass), and the thymus:adrenal ratio was similar between the genotypes (Figure 4.10.D).

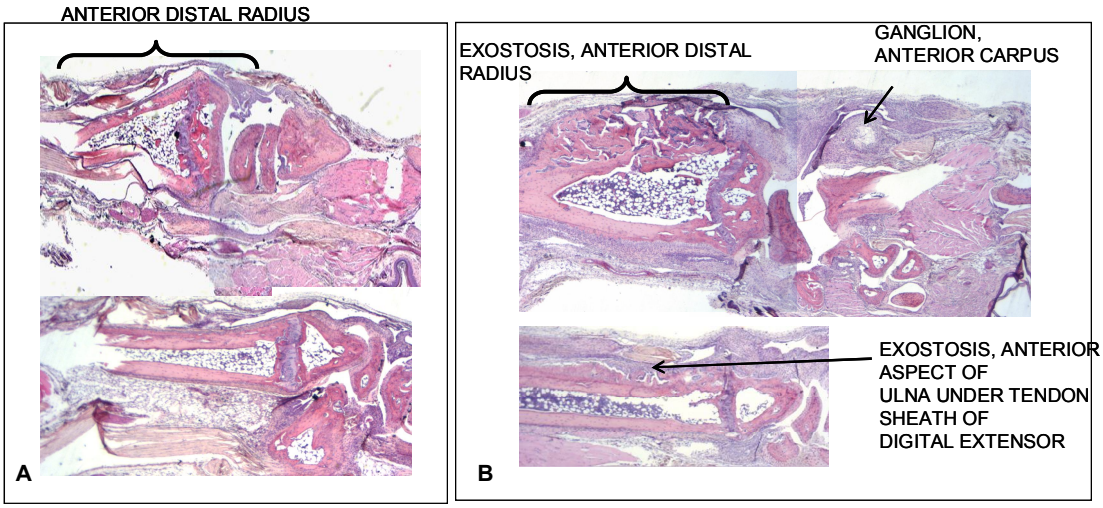

Figure 4.8 Histological assessment showed a more reactive bone phenotype and intense periarticular inflammation with severe exostosis and ganglion cyst formation in *Hsd11b1*$^{-/-}$ mice.
Joints were collected 21d following induction of experimental arthritis with K/BxN serum (single injection of 5.6µl/g body weight on d0) (n=5/genotype). Representative images of H&E sections, showing left carpus, from *Hsd11b1*$^{+/+}$ (A) and *Hsd11b1*$^{-/-}$ mice (B). Images are 50x original magnification.

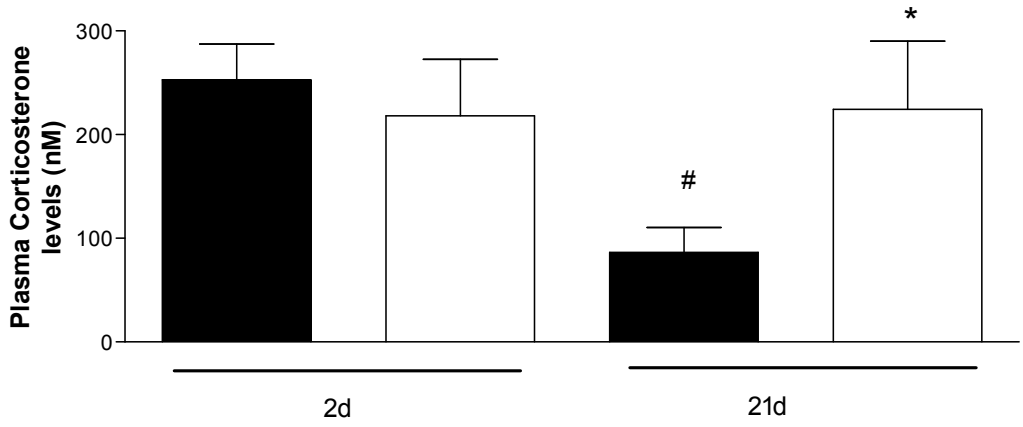

Figure 4.9 High circulating corticosterone levels in *Hsd11b1*$^{-/-}$ mice at 21d after K/BxN serum injection.
Morning circulating corticosterone levels 2d and 21d post arthritis challenge (single injection of 5.6µl/g body weight on d0) in *Hsd11b1*$^{-/-}$ (white) and *Hsd11b1*$^{+/+}$ mice (black) (n=5/group). Values shown are mean ± SEM. Two-way ANOVA showed a significant interaction ($p<0.05$). * $p<0.05$ indicates significant difference between genotypes at 21d, # $p<0.05$ indicates significant difference between d2 and d21 in *Hsd11b1*$^{+/+}$ mice.

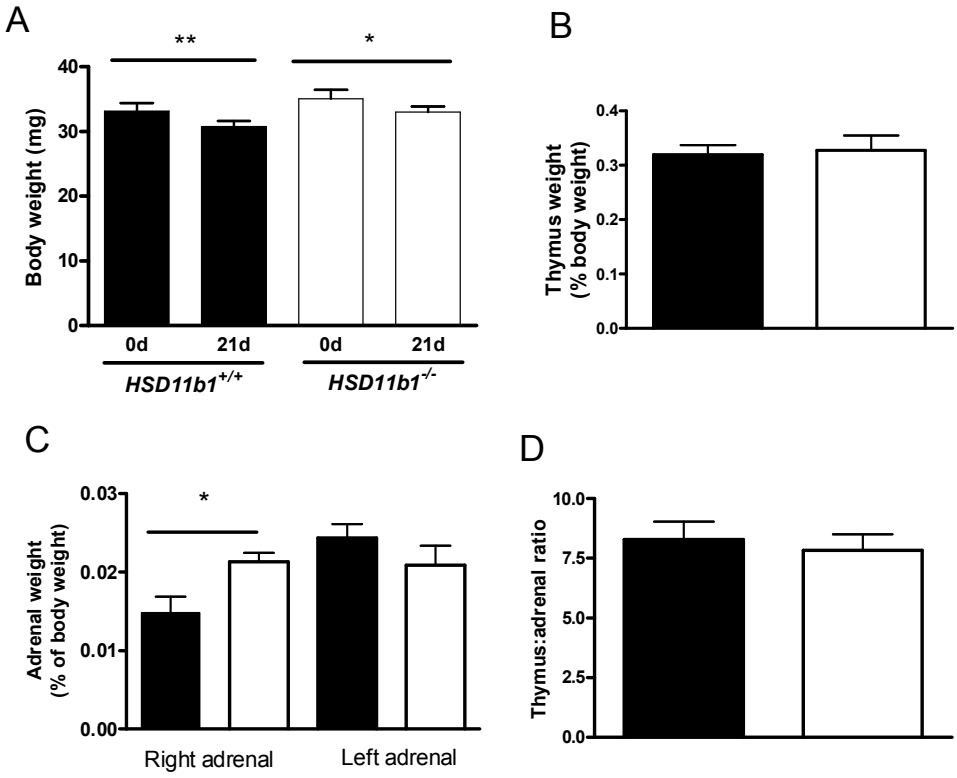

Figure 4.10 Anthropometric effects of 11β-HSD1 deficiency following K/BxN arthritis.

Body weight (A) was measured on d0 and d21 during K/BxN arthritis with reduced dose (single injection of 5.6µl/g body weight on d0) in *Hsd11b1*$^{-/-}$ (white) and *Hsd11b1*$^{+/+}$ mice (black) (n=5/group). Thymus (B) and adrenals (C) were collected and weighed on d21, from which thymus:adrenal ratio was determined (D). All tissue weights are expressed as % body weight. Values shown are mean ± SEM. * $p<0.05$ and ** $p<0.01$ indicate significant difference between genotypes at 21d when compared by unpaired Student's t-test.

4.2.4. K/BxN arthritis: acute phase

The most pronounced difference in clinical symptoms between the genotypes occurred at the acute phase of arthritis, with a more rapid onset of inflammation in the *Hsd11b1*$^{-/-}$ mice (Figure 4.3 and 4.6). As a result, an acute experiment was carried out using 5.6µl K/BxN serum/g body weight in order to observe histological differences, with mice killed 2d following injection of serum. Similarly to the previous experiments, *Hsd11b1*$^{-/-}$ mice showed a more rapid onset of inflammation with higher clinical scores, reflecting greater redness and swelling of the joints, than *Hsd11b1*$^{+/+}$ mice, 2d following injection of serum (Figure 4.11).

Histological examination (Prof Donald Salter) of 2d arthritic joint sections showed a severe inflammatory response in mice from both genotypes (data not shown). However, no qualitative differences were detected between genotypes, despite the earlier onset of inflammation in *Hsd11b1*$^{-/-}$ mice. Exudate within the joint space and inflammation (based on influx of acute inflammatory cells into the joint synovium) was apparent throughout the proximal third of the limb, particularly in the tendon sheath, of all mice.

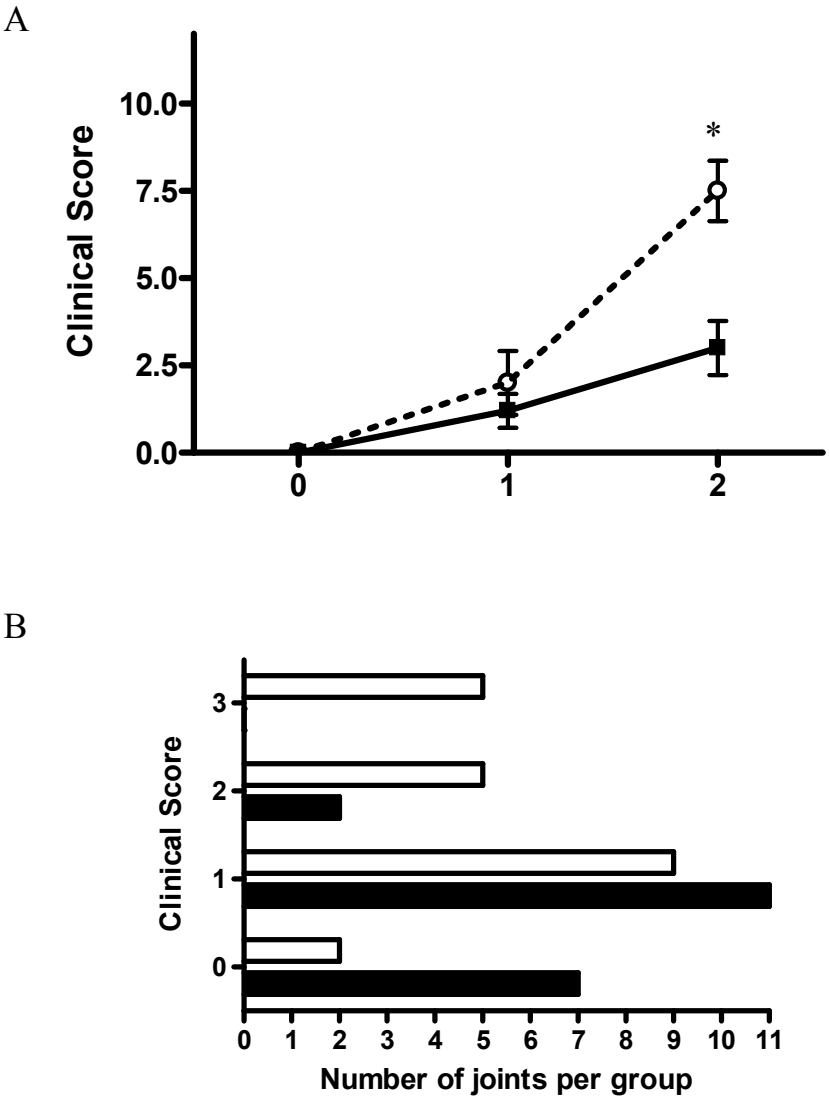

Figure 4.11 More aggressive onset of inflammation in *Hsd11b1*$^{-/-}$ mice 2d after of K/BxN serum injection.
(A) Higher clinical scores following a single injection of 5.6µl of K/BxN serum/g body weight on d0 in *Hsd11b1*$^{-/-}$ mice (white circles) compared to controls (black squares). Two-way ANOVA showed a significant interaction ($p<0.01$). (B) More joints with higher clinical score in *Hsd11b1*$^{-/-}$ mice (white bars) compared to *Hsd11b1*$^{+/+}$ (black bars). Chi square analysis showed a significant difference ($p<0.05$) between genotypes. Clinical scoring was performed blind to genotype (n=5/genotype).Values shown are mean ± SEM.

4.2.5. Micro-CT scanning reveals altered bone micro-architecture in Hsd11b1$^{-/-}$ mice following K/BxN arthritis

Femurs, taken from mice 2d or 21d following a single injection of 5.6µl K/BxN serum/g body weight on d0, were subjected to micro-CT scanning (this was carried out by Dr Rob van 't Hof). The scans suggested that bone micro-architecture in *Hsd11b1*$^{-/-}$ mice differed from that in *Hsd11b1*$^{+/+}$ mice following 21d (discussed below), but not 2d of arthritis (Table 4.1). Lack of differences at the early stages of arthritis suggests that any differences seen at the later time point cannot be attributed to innate differences between the genotypes. This is in accordance with a previously published observation that under normal conditions (untreated) *Hsd11b1*$^{-/-}$ mice maintain normal bone formation (Justesen et al., 2004).

Trabecular bone (cancellous or spongy bone) differed between *Hsd11b1*$^{-/-}$ and *Hsd11b1*$^{+/+}$ mice following 21d of K/BxN arthritis (Table 4.2). Although trabecular bone volume did not significantly differ between the genotypes, trabecular separation and thickness were greater in *Hsd11b1*$^{-/-}$ mice, and the trabecular number was lower, in comparison to the *Hsd11b1*$^{+/+}$ mice. Structure Model Index (SMI), measuring level of weakness, and Trabecular Pattern Factor (TPF), a measure of connectedness, were both higher in the *Hsd11b1*$^{-/-}$ than the *Hsd11b1*$^{+/+}$ mice (Figure 4.12.). Cortical bone measurements showed that, overall, after arthritis *Hsd11b1*$^{-/-}$ mice had smaller femur bones, based mainly on smaller tissue volume, while cortical thickness remained similar between the two groups (Table 4.3).

Table 4.1 Histomorphometric parameters for trabecular bone from Micro-CT scanning of femur bones 2d after injection of K/BxN serum

Parameter	*Hsd11b1*$^{+/+}$	*Hsd11b1*$^{-/-}$	T-test
Tissue volume	2.11	1.92	*p>0.05*
Bone volume	0.36	0.34	*p>0.05*
Percent bone volume	16.8	17.3	*p>0.05*
Trabecular thickness	0.045	0.054	*p>0.05*
Trabecular separation	0.17	0.18	*p>0.05*
Trabecular number	3.72	3.21	*p>0.05*
Trabecular pattern factor	17.23	17.21	*p>0.05*
Structure model index	1.40	1.58	*p>0.05*

Table 4.2 Histomorphometric parameters for trabecular bone from Micro-CT scanning of femur bones 21d after injection of K/BxN serum

Parameter	*Hsd11b1*$^{+/+}$	*Hsd11b1*$^{-/-}$	T-test
Tissue volume	$2.7x10^{9}$	$2.6x10^{9}$	*p>0.05*
Bone volume	$5x10^{8}$	$4.1x10^{8}$	***p<0.01***
Percent bone volume	$1.9x10^{1}$	$1.6x10^{1}$	*p>0.05*
Tissue surface	$1.4x10^{7}$	$1.3x10^{7}$	*p>0.05*
Bone surface	$3.5x10^{7}$	$2.6x10^{7}$	***p<0.01***
Bone surface / volume ratio	$7.1x10^{-2}$	$6.3x10^{-2}$	***p<0.01***
Bone surface density	$1.3x10^{-2}$	$1x10^{-2}$	***p<0.01***
Trabecular thickness	$5x10^{1}$	$5.3x10^{1}$	***p<0.01***
Trabecular separation	$2x10^{2}$	$2.3x10^{2}$	***p<0.01***
Trabecular number	$3.7x10^{-3}$	$2.9x10^{-3}$	***p<0.01***

Table 4.3 Histomorphometric parameters for cortical bone from Micro-CT scanning of femur bones 21d after injection of K/BxN serum

Parameter	*Hsd11b1*$^{+/+}$	*Hsd11b1*$^{-/-}$	T-test
Tissue volume	$1.7x10^{9}$	$1.5x10^{9}$	***p<0.01***
Bone volume	$5.4x10^{8}$	$5x10^{8}$	***p<0.01***
Percent bone volume	$3.2x10^{1}$	$3.4x10^{1}$	*p>0.05*
Tissue surface	$1.3x10^{7}$	$1x10^{7}$	*p>0.05*
Bone surface	$1.1x10^{7}$	$9.6x10^{6}$	***p<0.01***
Bone surface / volume ratio	$2x10^{-2}$	$1.9x10^{-2}$	*p>0.05*
Bone surface density	$6.3x10^{-3}$	$6.5x10^{-3}$	*p>0.05*
Cortical thickness:	$1.6x10^{2}$	$1.6x10^{2}$	*p>0.05*
major axis	$2.8x10^{3}$	$2.6x10^{3}$	***p<0.05***
minor axis	$1.4x10^{3}$	$1.3x10^{3}$	***p<0.05***
axis ratio	2	2.1	*p>0.05*

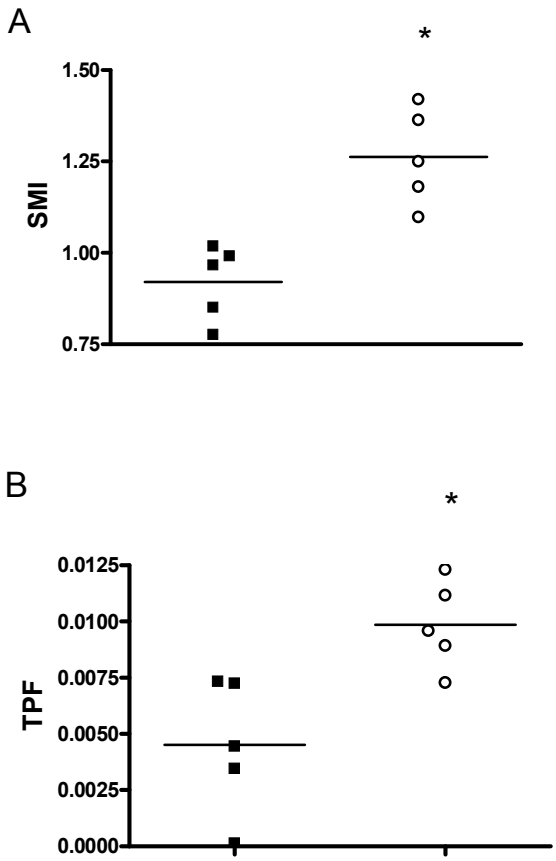

Figure 4.12 Weaker and less connected trabecular bone in femurs of *Hsd11b1*$^{-/-}$ mice than *Hsd11b1*$^{+/+}$ mice following 21d of K/BxN arthritis.
Higher Structure Model Index (SMI), measuring level of "weakness", and Trabecular Pattern Factor (TPF), measuring bone connectedness, in *Hsd11b1*$^{-/-}$ mice (open circles) and *Hsd11b1*$^{+/+}$ mice (black squares) 21d following a single injection of 5.6µl of K/BxN serum/g body weight on d0. Values represent individual mice. * $p<0.05$ indicates significant difference between genotypes compared by unpaired Student's t-test.

4.3. Discussion

The aim of the experiments described in this Chapter was to establish a suitable model of arthritis to evaluate disease course in *Hsd11b1*$^{-/-}$ mice for comparison to *Hsd11b1*$^{+/+}$ mice. The CIA-CFA arthritis model was tried first. C57BL/6 mice are resistant to CIA (see Chapter 2, Section 2.3.7.1.). However, Campbell et al. (2000) have described a modified immunization protocol (used here), where the collagen is mixed with complete Feund's adjuvant (CFA), and in which 60-70% of C57BL/6 mice developed arthritis. Unfortunately, this model failed to produce arthritis in either genotype, with none of the control mice showing any signs of arthritis and only one *Hsd11b1*$^{-/-}$ mouse showing intermittent symptoms. Since the CIA-CFA did not produce arthritis in any of the mice, this model was not pursued. However, an interesting observation was made suggesting an altered immune reaction to CFA in *Hsd11b1*$^{-/-}$ mice. During the experiment most mice developed ulcers, following the injection, but with greater frequency and prolonged bleeding in *Hsd11b1*$^{-/-}$ mice.

The alternative model tried, K/BxN serum transfer, produced arthritis in all mice. Importantly, there was a highly reproducible earlier onset of symptoms in *Hsd11b1*$^{-/-}$ mice irrespective of the dose of K/BxN serum used to initiate arthritis. In all experiments, the peak clinical score of inflammation did not differ. The shape of the curves for clinical scoring within each experiment was similar for both genotypes. However, scores for *Hsd11b1*$^{-/-}$ mice always remained above the controls for the duration of the experiments (except in the standard dose experiment where both

genotypes peaked at the same level). Unlike the standard protocol, in the reduced serum protocol the joints of the recipient mice were not uniformly affected. With reduced dose the disease progressed at a variable rate and other limbs could become involved at later intervals. Whilst an asymmetrical pattern of arthritis is more representative of human rheumatoid arthritis, it made it difficult to obtain reproducible measurements of paw swelling with caliper. Resolution occurred at approximately the same time in both 21d experiments, which probably reflects the half life of antibody (stable arthritis being the "plateau" and resolution occurring rapidly as the antibody is cleared), but interestingly, *Hsd11b1*$^{-/-}$ mice were slower to recover. The slower resolution may be related to the earlier onset; however, it may reflect a separate mechanism.

Consistent with more severe inflammation, *Hsd11b1*$^{-/-}$ mice had a more reactive bone phenotype and greater periarticular inflammation than the controls, characterized by exostosis and ganglion cyst formation. In humans, ganglion cysts (previously undescribed in rodents) may be early signs of arthritis and are suggestive of worse inflammation (personal communication with Dr David Brownstein), whilst exostosis is a reaction of bone to inflammation in the overlying tendon sheath. It remains unexplained however, why no pathological differences between genotypes were detected at the onset of arthritis (2d after injection of K/BxN serum), when differences in oedema were obvious. One possible explanation is that vasopermeability and/ or vasodilation in response to the K/BxN serum differs between the genotypes. A possible mechanism for increased blood vessel leakiness is addressed more fully in Chapter 5. Excessive angiogenesis contributes to the pathology of rheumatoid arthritis and GC have been

shown to inhibit angiogenesis (Folkman *et al.* 1983). Moreover, a role for endogenous GC by 11β-HSD1 in repair angiogenesis has been demonstrated, and not surprisingly, *Hsd11b1*$^{-/-}$ mice show increased angiogenesis (Small *et al.* 2005) suggesting an alteration in blood vessels of *Hsd11b1*$^{-/-}$ mice. It will be interesting to determine if the vascular bed within the joints differs between genotypes before and after arthritis. To date, there is no suggestion that developmental angiogenesis differs in *Hsd11b1*$^{-/-}$ mice.

Bone deformation and severe exostosis may occur in cyclical episodes of bone necrosis and repair, as is the case with chronic inflammation. The literature suggests a cyclic response during inflammation involving necrosis, resorption, inflammation, and proliferation of bone tissue. Arthritis-induced persistent inflammation caused bone remodeling that was more severe in *Hsd11b1*$^{-/-}$ mice than in the controls. In addition to greater exostosis in carpal bones around the affected joints (local response) in *Hsd11b1*$^{-/-}$ mice, micro-CT scanning of femur bones revealed that following K/BxN arthritis, the micro-architecture of the femur bone, away from the joint (therefore a systemic response), was also altered. By indicating that the injection of K/BxN serum also has a systemic effect, affecting bone away from the joints, the micro CT scanning data provides additional information on the K/BxN model of arthritis which, unlike its effects within the synovial joint, is not discussed broadly in the literature.

The micro-architecture determines stability of bone and can be described more specifically by histomorphometric parameters; TPF, which provides assessment of the connectedness of bone tissue, and SMI which reflects the level of weakness (personal

communication with Dr Rob van 't Hof). Higher levels of TPF and SMI were measured in bones from *Hsd11b1*$^{-/-}$ mice, indicating thinner and less well connected bones than the in controls following arthritis. GC have profound effects on bone (Chiodini et al., 1998; Dalle et al., 2001) and the presence of functional 11β-HSD1 in bone (Justesen et al., 2004) suggests that it too plays a role in bone metabolism. Previous *in vitro* data showed that over-expression of 11β-HSD1 in osteoblasts reduced cellular proliferation and increased cellular differentiation (Eyre et al., 2001). Interestingly, differences between genotypes were only seen following 21d of arthritis and not at the early stages (2d). This suggests normal structure of bones in untreated *Hsd11b1*$^{-/-}$ mice. This would be in accordance with previous reports on bone assessment of *Hsd11b1*$^{-/-}$ mice showing that deficiency of 11β-HSD1 did not affect bone mass or bone turnover (Justesen et al., 2004). However, to better explain the bone related findings of this chapter, in the future bone histomorphometry and assessment of osteoclast and osteoblast numbers should be made in both genotypes prior to and following inflammatory arthritis.

Finally, under normal conditions *Hsd11b1*$^{-/-}$ mice, on their original MF1/129 genetic background, have elevated plasma GC levels, both basally and following acute stress (10 min restraint stress) (Harris et al., 2001). However, *Hsd11b1*$^{-/-}$ mice on C57BL/6 background show normal plasma corticosterone levels (Yau et al., 2007). Plasma corticosterone levels were elevated to a similar extent in *Hsd11b1*$^{-/-}$ and control mice 2d following a single injection of K/BxN serum, indicating that differential HPA axis activation between the genotypes does not underlie this acute inflammatory phenotype. Interestingly, plasma corticosterone levels failed to return to normal in *Hsd11b1*$^{-/-}$ mice

during the resolution stage (d21) indicating a greater and prolonged stress in these mice in response to arthritis. Taken together, these data suggest that any differences in HPA response to stress between genotypes are influenced by the type of stimulus and its duration. It will be important to further investigate this in the future.

In summary, mice deficient in 11β-HSD1 exhibit an exaggerated response in the K/BxN serum transfer model of arthritis. These experiments are consistent with the original observations by Gilmour (2002), demonstrating worse acute inflammation in *Hsd11b1*$^{-/-}$ mice, with greater recruitment of inflammatory cells following TG-induced sterile peritonitis. However, in contrast to the TG-induced peritonitis model, where resolution occurred simultaneously in both genotypes, here, the resolution of arthritis (judged by clinical scoring of inflamed joints and supported by histology at 21d) was delayed in *Hsd11b1*$^{-/-}$ mice. This finding is in agreement with the data from carrageenan-induced pleurisy described in Chapter 4, where resolution of pleural inflammation was altered in *Hsd11b1*$^{-/-}$ mice. These findings strongly support a role for 11β-HSD1 as an endogenous modulator of inflammation. Future experiments using the K/BxN model should be aimed at the onset and resolution phases specifically to determine if they are regulated by a single mechanism or two separate factors. Also, it will be of critical importance to establish which cells (resident and inflammatory immune cells or non-immune cells) are responsible for the worse inflammation seen in *Hsd11b1*$^{-/-}$ mice in this model.

Chapter Five

11β-HSD1 in Mast Cells

5.1. Introduction

Compared to the metabolically protective aspects of 11β-HSD1-deficiency, much less is known regarding inflammatory/immune consequences, and only relatively recently has interest in the role of 11β-HSD1 in immune cells arisen. Although some older studies examined the 11β-HSD 'shuttle' in immune cells and organs (Hennebold et al., 1996), they predated the realization that 11β-HSD comprises two distinct enzymes and it is only relatively recently that this has been re-examined in the context of two separate isozymes (reviewed in Chapman et al., 2006, 2008). MC play an early role during the inflammatory response and are essential for K/BxN arthritis (Lee et al., 2002). The results in this chapter focus on characterisation of 11β-HSD1 in MC, as well as the consequences of 11β-HSD1-deficiency in these cells. MC function was assessed in *Hsd11b1*$^{-/-}$ mice to investigate a possible mechanism for the altered inflammatory response, with earlier onset of oedema, during arthritis challenge in these mice (Chapter 4). In addition to assessment of MC number and morphology in *Hsd11b1*$^{-/-}$ mice, *in vitro* MC degranulation experiments, using peritoneal MC retrieved from both genotypes, were used to examine the functional consequences of 11β-HSD1-deficiency in these cells.

5.2. Results

5.2.1. *Immunohistochemical staining of 11β-HSD1 in peritoneal cells*

Peritoneal cells exhibit 11β-reductase activity, which increases rapidly and markedly following TG injection (Gilmour et al., 2006). To determine whether peritoneal MC express 11β-HSD1, cytocentrifuge preparations of resident peritoneal cells from *Hsd11b1*$^{+/+}$ mice were first stained with a commercially available rabbit-anti-mouse 11β-HSD1 antibody (from Cayman) and a sheep-anti-mouse tryptase (mMCP-6/7) antibody (gift from Dr Jeremy Brown), specific for mouse MC. Strong staining for 11β-HSD1 was seen in a subset of peritoneal cells, all of which also stained with mMCP-6/7 antibody, suggesting high 11β-HSD1 expression in peritoneal MC (Figure 5.1.A). Staining of other peritoneal cells was much lower, with background level in resident Mϕ. Unfortunately, this antibody proved to be non-specific as even greater staining was detected in resident peritoneal cells from *Hsd11b1*$^{-/-}$ mice (Figure 5.1.B). Therefore, the Cayman antibody must recognize an epitope other than 11β-HSD1, and was not used in further experiments.

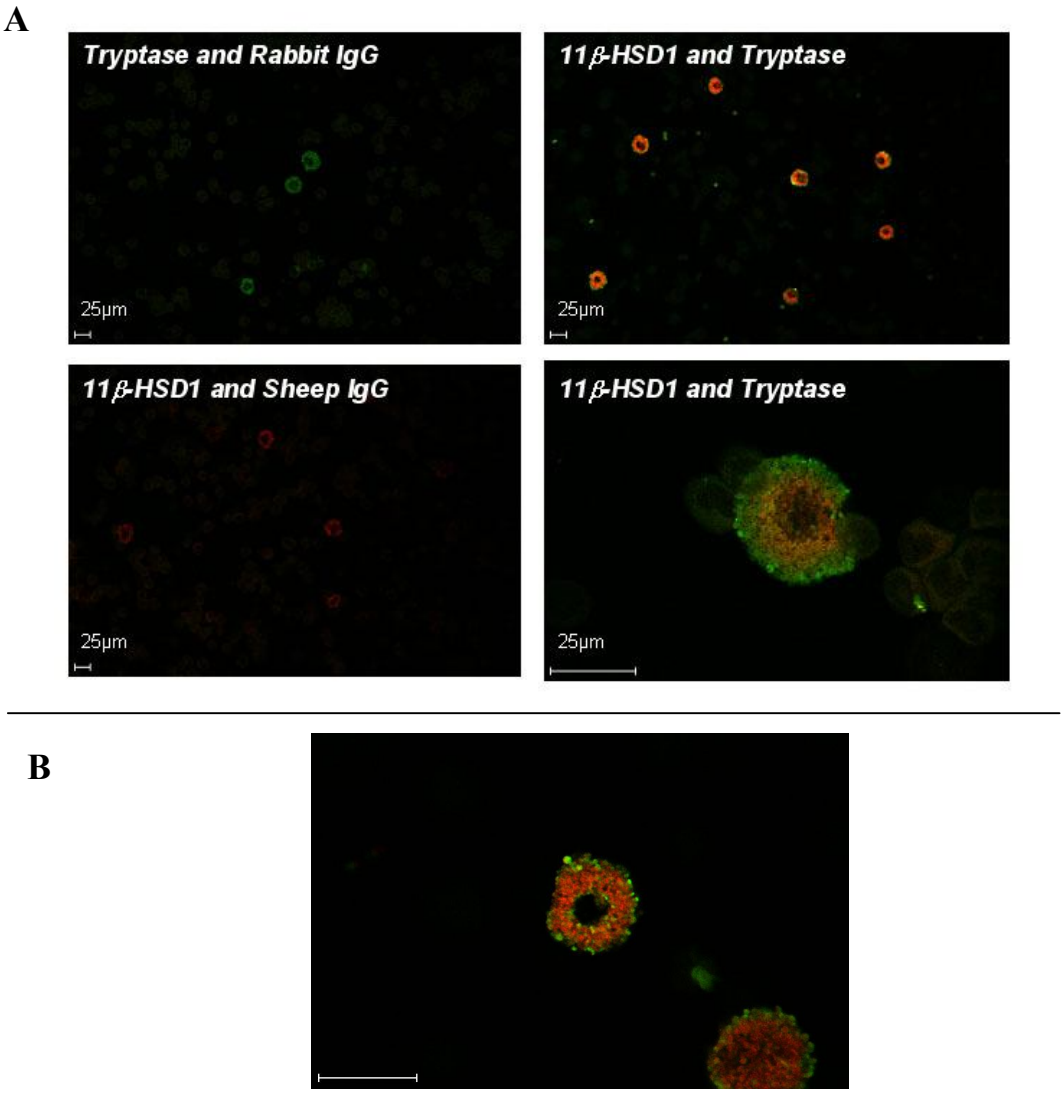

Figure 5.1 Immunofluorescent detection of 11β-HSD1 in tryptase-positive peritoneal MC.
Co-staining of peritoneal MC with a commercially available rabbit-anti-mouse 11β-HSD1 antibody (Cayman) (1:100) and sheep-anti-mouse tryptase (mMCP-6/7) antibody (1:100) carried out on cytospins of resident peritoneal cells from *Hsd11b1*$^{+/+}$ mice (A), or *Hsd11b1*$^{-/-}$ mice (B). Sheep-anti-mouse IgG and rabbit-anti-mouse IgG isotype controls were used at 1:1000. Secondary antibodies were FITC conjugated rat-anti-sheep (green) (1:100) and Rhodamine red-conjugated rat-anti-rabbit (red) (1:200). Scale bar indicates 25μm in (A) and (B).

Accordingly, HRP IHC was repeated using a purified in-house sheep-anti-mouse 11β-HSD1 antibody (raised against recombinant mouse 11β-HSD1 protein), which was confirmed to be specific for 11β-HSD1 (see Chapter 2, Section 2.3.13.1.). IHC on cytocentrifuge preparations from resident peritoneal cells with the in-house 11β-HSD1 antibody and a tryptase (mMCP-6/7) antibody showed 11β-HSD1 was localized in cells with the characteristic morphology of MC (Figure 5.2.). However, co-staining with both antibodies was not possible due to the identical origin of both antibodies (both raised in sheep). Nonetheless, the distinct morphology of MC allows for relatively easy identification of MC on cytospins.

5.2.2. *11β-HSD1 activity in BMD-MC*

To measure 11β-HSD activity in MC, highly pure population of BMD-MC (Chapter 2, Section 2.3.5.) from *Hsd11b1*$^{+/+}$ mice was assayed for dehydrogenase and reductase activity over 2h, 5h, and 24h. Only 11β-reductase activity was detected, with no dehydrogenase activity, suggesting the presence of 11β-HSD1 and not 11β-HSD2 in BMD-MC (Figure 5.3.). Cultured BMD-MC were used due to the difficulty of obtaining sufficient numbers of pure, un-stimulated peritoneal MC. 11β-HSD activity was also measured in BMD-Mϕ cultured from the same BM cells (data not shown). As previously reported (Gilmour, 2002; Gilmour et al., 2006), BMD-Mϕ showed only 11β-reductase activity (12pmol corticosterone/h/10^6 cells), with levels comparable to activity measured in BMD-MC (Figure 5.3.).

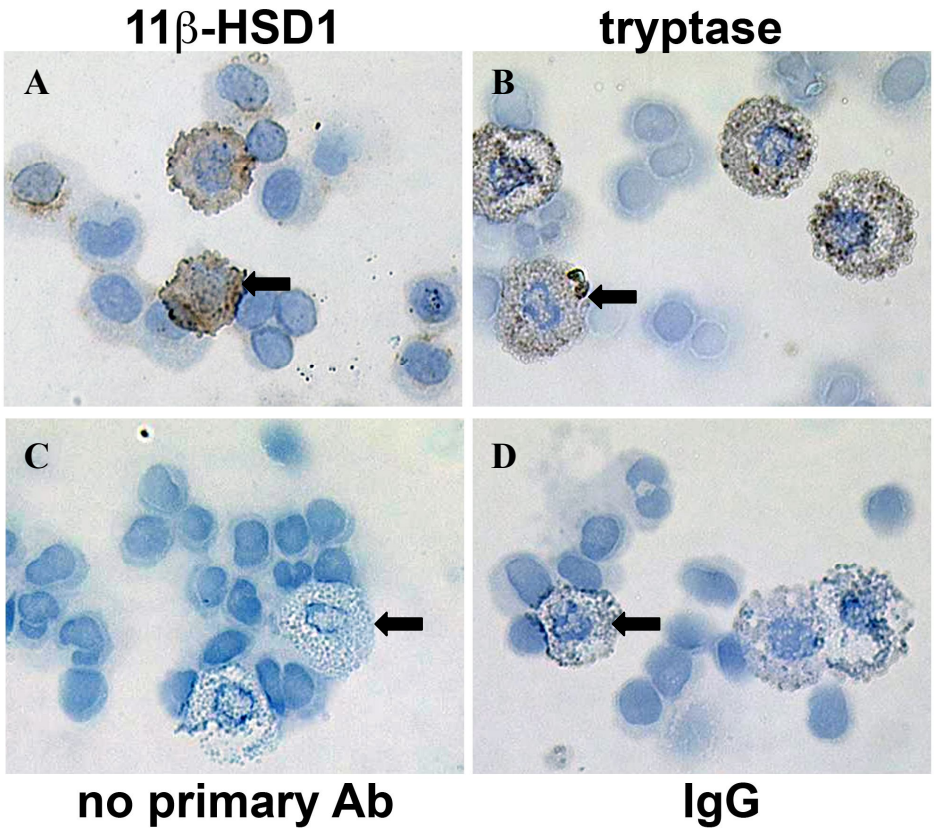

Figure 5.2 11β-HSD1 staining of resident peritoneal MC from *Hsd11b1*$^{+/+}$ mice.
HRP IHC was performed on cytocentrifuge preparations of peritoneal cells from untreated *Hsd11b1*$^{+/+}$ mice by incubation of slides with primary antibodies; sheep-anti-mouse 11β-HSD1 (A), tryptase antibody (B) or sheep IgG control (D), followed by incubation with secondary HPR conjugated anti-sheep antibody (1:1000). No primary antibody control (C) was incubated with secondary antibody only. Colour was developed using DAB without nickel as the chromogen. Original images were taken at 400x magnification. Arrows indicate MC.

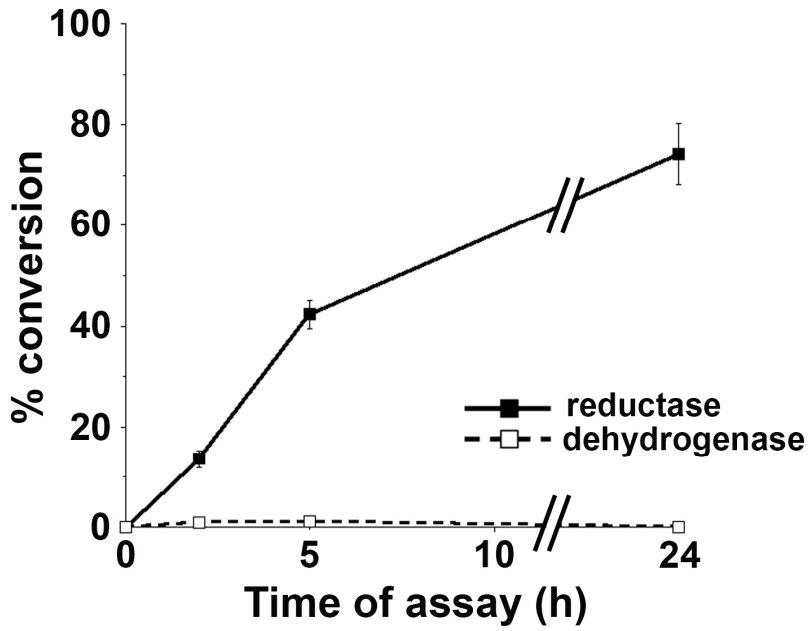

Figure 5.3 11β-HSD1 activity in BMD-MC.
11β-HSD1 reductase and dehydrogenase activities in BMD-MC were measured by adding ^{3}H-substrate to the medium, removing aliquots at various times up to 24h and calculating conversion of substrate to product. Data are expressed as % conversion of 200nM substrate by $2x10^{6}$ cells, over time. Solid lines/square symbols, reductase activity (conversion of 11-dehydrocorticosterone to corticosterone); dashed lines/open symbols, dehydrogenase activity (conversion of corticosterone to 11-dehydrocorticosterone). The level of 11β-reductase activity was 16.9±1.1pmol corticosterone/h/10^{6} cells. Values are mean ± SEM of 3 independent assays carried out on pooled BMD-MC.

5.2.3. *11β-HSD1 mRNA is expressed in BMD-MC*

11β-HSD1 mRNA expression was demonstrated in BMD-MC by reverse transcription-PCR (Figure 5.4). Similar to other immune cells (mouse thymocytes, spleen B and T cells, and T cells isolated from lymph nodes, as well as BMD-Mϕ), no PCR product was observed using primers specific for 11β-HSD2 (Figure 5.4). To determine which promoter of *Hsd11b1* was utilized in MC, total BMD-MC mRNA was subject to reverse transcription-PCR using primers specific for each of the 3 different promoters of *Hsd11b1*; P1 used in lung and kidney; P2 widely used including in liver and adipose tissue and P3, used in kidney (for details see Chapter 1, Section 1.6.5. and Chapter 2, Section 2.3.11.3.). Control reverse transcription-PCR reactions from liver and kidney mRNA served as positive controls for the transcription of *Hsd11b1* from the P2 and P3 promoters, respectively. BMD-MC utilized only the P1 promoter of the *Hsd11b1* gene (Figure 5.5). No PCR product was produced with the P2 or P3 primers (Figure 5.5). As an additional control, mRNA from BMD-MC prepared in a separate laboratory (supplied by Dr Pamela Knight) was also used to confirm these findings (Figure 5.5).

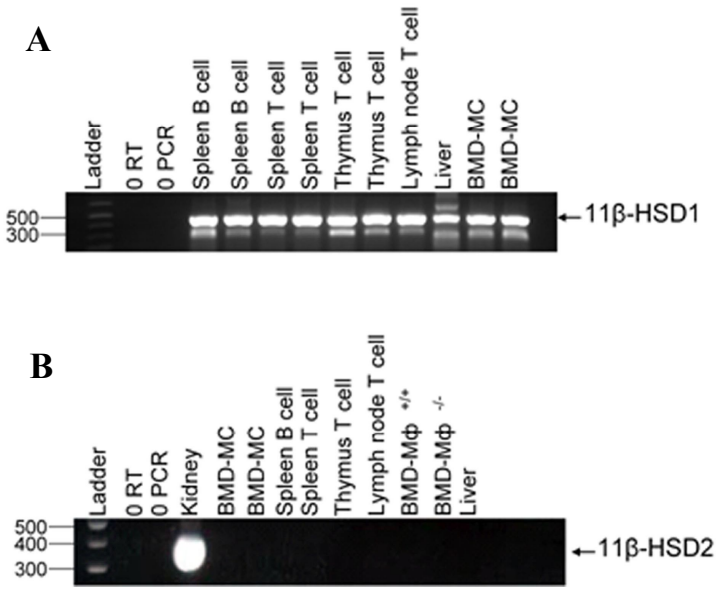

Figure 5.4 *Hsd11b1* mRNA in BMD-MC and other immune cells.
(A) BMD-MC express 11β-HSD1 mRNA (469bp reverse transcription-PCR product with primers 868P and 869P) but not 11β-HSD2 mRNA (B) (400bp reverse transcription-PCR product). Positive controls were liver mRNA (positive control for 11β-HSD1) and kidney mRNA (positive control for 11β-HSD2). Reverse transcription-PCR products for BMD-MC are from 2 independent BMD-MC RNA samples. 0 RT lane contains a reaction without reverse transcriptase (but with BMD-MC RNA) and 0 PCR reaction contains water instead of cDNA. Lane 1 contains a 100bp ladder. BMD-M$\phi^{-/-}$ refers to *Hsd11b1*$^{-/-}$ BMD-Mϕ, whilst BMD-M$\phi^{+/+}$ refers to *Hsd11b1*$^{+/+}$ BMD-Mϕ.

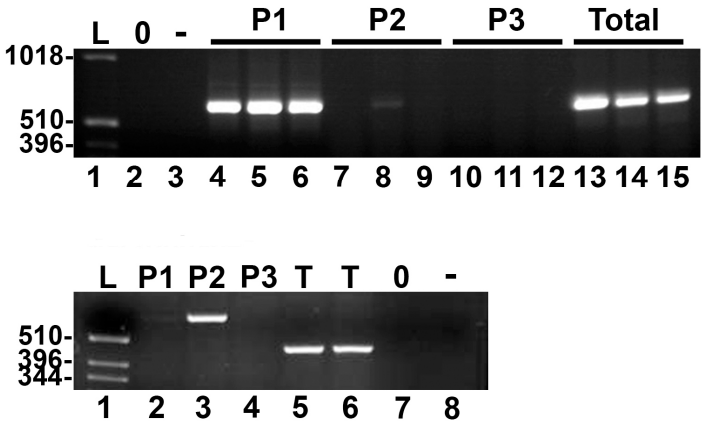

Figure 5.5 BMD-MC transcribe *Hsd11b1* from the P1 promoter.
MC transcribe *Hsd11b1* from the P1 promoter (upper panel), whereas Mϕ use the P2 promoter (lower panel, image provided by Mr Fu Yang). Upper panel; reverse transcription-PCR products from 3 independent BMD-MC RNA samples showing the 627bp reverse transcription-PCR product from transcripts initiated at the P1 promoter (lanes 4-6), but not the P2 (predicted product of 647bp, lanes 7-9) or P3 promoters (predicted product of 542bp, lanes 10-12) of 11β-HSD1. Total 11β-HSD1 mRNA was detected using primers common to all transcripts (lanes 13-15, 587bp product with primers ex2 and 868P). Lower panel; reverse transcription-PCR products from BMD-Mϕ RNA showing the 647bp reverse transcription-PCR product arising from transcription initiated at the P2 promoter (lane 3), but not the P1 (lane 2) or P3 promoters (lane 4) of 11β-HSD1. Total 11β-HSD1 mRNA (T) was detected using 868P and 869P primers, common to all transcripts (lanes 5, 6; 469bp product). Lane 1 in both panels contains a 1kb ladder. Lanes marked (0) contain water instead of cDNA and lanes marked (-) show reverse transcription-PCR reactions from which the reverse transcriptase was omitted from the RT reaction.

5.2.4. *MC number is not altered in peritoneum or joints of Hsd11b1$^{-/-}$ mice*

Since MC are known to accumulate in tissues during inflammation, play a key role in K/BxN arthritis, and *Hsd11b1*$^{-/-}$ mice exhibit worse onset of inflammation using this model (Chapter 4), MC number was quantified in carpal joints collected 2d following injection of the arthritic serum (5.6µl/g of body weight). Paraffin embedded joint sections were stained with Toluidine blue (Figure 5.6.A) and MC were counted microscopically in randomly chosen fields. The number of Toluidine blue stained MC was similar in *Hsd11b1*$^{-/-}$ and *Hsd11b1*$^{+/+}$ mice (Figure 5.6.B).

Peritoneal MC number also did not differ between genotypes. Flow cytometry analysis showed no difference in the total number or proportion of c-kit^{+} cells within the peritoneum (range between 2% and 3% of total peritoneal cells in both *Hsd11b1*$^{-/-}$ and *Hsd11b1*$^{+/+}$ mice in multiple comparisons between genotypes) or bone marrow (*Hsd11b1*$^{-/-}$ $3.6x10^{7}$±0.6 versus *Hsd11b1*$^{+/+}$ $4.8x10^{7}$±0.7 cells). Similarly, there was no difference in peritoneal MC number based on differential cell counts from Diff-Quick stained cytocentrifuge preparations of peritoneal cells (Figure 5.9).

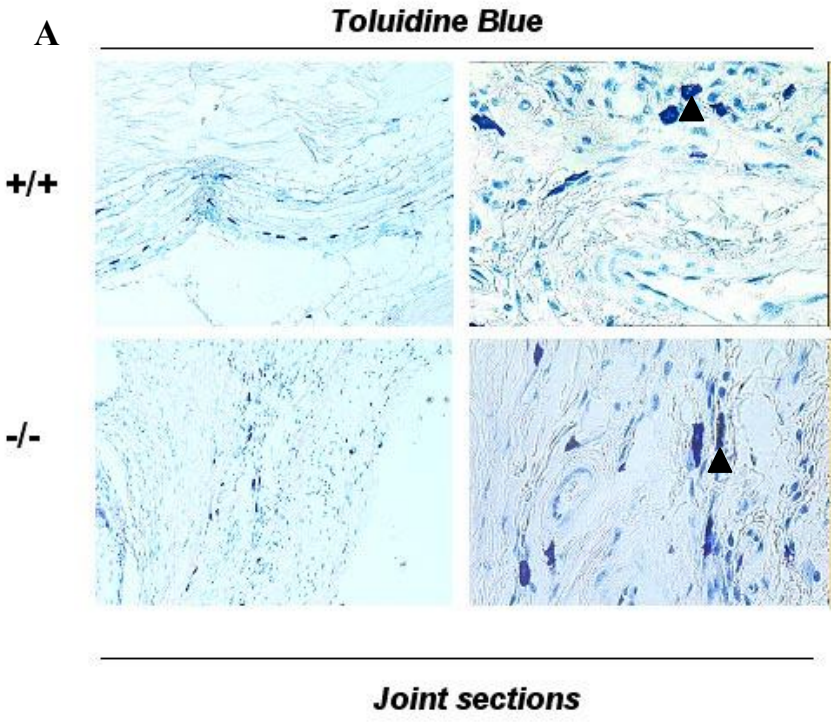

Figure 5.6 Toluidine blue staining of MC in joints showed MC number did not differ between *Hsd11b1*$^{-/-}$ and *Hsd11b1*$^{+/+}$ mice, 2d following 5.6µl/g injection of K/BxN serum.

(A) Representative images of deparaffinized and hydrated joint sections from *Hsd11b1*$^{+/+}$ (+/+) and *Hsd11b1*$^{-/-}$ (-/-) mice stained with Toluidine blue (arrow heads indicate stained MC). Original images were taken at 100x (left panels) and 400x (right panels) magnification. (B) MC were counted using a 100µm^2 reticule. Fields were chosen at random for counting (n=5/genotype). Data are expressed as mean ± SEM.

5.2.5. *Enhanced MC degranulation in Hsd11b1$^{-/-}$ mice*

To investigate whether 11β-HSD1-deficiency alters MC degranulation following stimulus, cell degranulation was measured in total peritoneal cells from naïve *Hsd11b1*$^{-/-}$ and *Hsd11b1*$^{+/+}$ mice using an *in vitro* assay of β-hexosaminidase, released from MC granules. Initial experiments using peritoneal cells from control mice were performed to establish the appropriate concentration of cells and stimulus, as well as the timing of assay. Ionomycin causes MC degranulation in a dose dependent manner, and therefore was used as a positive control in MC degranulation assays (Figure 5.7.A). CRH is a known stimulus of MC degranulation (Theoharides et al., 1998; Donelan et al., 2006). However, it did not result in degranulation above background levels (Figure 5.7.A), and thus was not used in further experiments. K/BxN serum has been shown to cause MC degranulation both *in vivo* (Lee et al., 2002; Binstadt et al., 2006) and *in vitro* (Binstadt et al., 2006). Diluted 1:2 in Tyrode's buffer, K/BxN serum caused maximal degranulation, comparable to the response of MC to 10μM ionomycin (Figure 5.7.A). When peritoneal cells from *Hsd11b1*$^{-/-}$ and control mice were compared, there was no difference between genotypes in β-hexosaminidase release in response to increasing concentrations of ionomycin (0.5μM, 2μM and 10μM), (Figure 5.7.B), and no difference in un-stimulated cells (not shown), suggesting that degranulation in response to Ca^{2+} ionophore is normal in *Hsd11b1*$^{-/-}$ MC cells.

Crucially, when a sub-maximal dilution of K/BxN serum was added to peritoneal cells, degranulation was significantly higher in *Hsd11b1*$^{-/-}$ cells than in cells from *Hsd11b1*$^{+/+}$ mice after 15min incubation with 1:8 dilution of K/BxN serum (Figure 5.8.A). In

contrast, a 1:2 dilution of serum caused similar degranulation in cells of both genotypes (Figure 5.8.A). Cytokine measurements using ELISA kits (VEGF and TNF-α) were attempted on the remaining supernatant from the degranulation assay experiments. However, cytokine levels were below the detection limits of the assays. Degranulation in response to K/BxN serum was also observed microscopically using an enriched population of $CD117^{+}$ peritoneal cells (50-70% MC purified with MACS columns, Chapter 2, Section 2.3.3.), incubated with or without 1:8 dilution of K/BxN serum. After 21h, cells were photographed. Control cells from *Hsd11b1*$^{+/+}$ mice showed little effect of incubation with K/BxN serum, whereas *Hsd11b1*$^{-/-}$ cells showed significant degranulation (Figure 5.8.B).

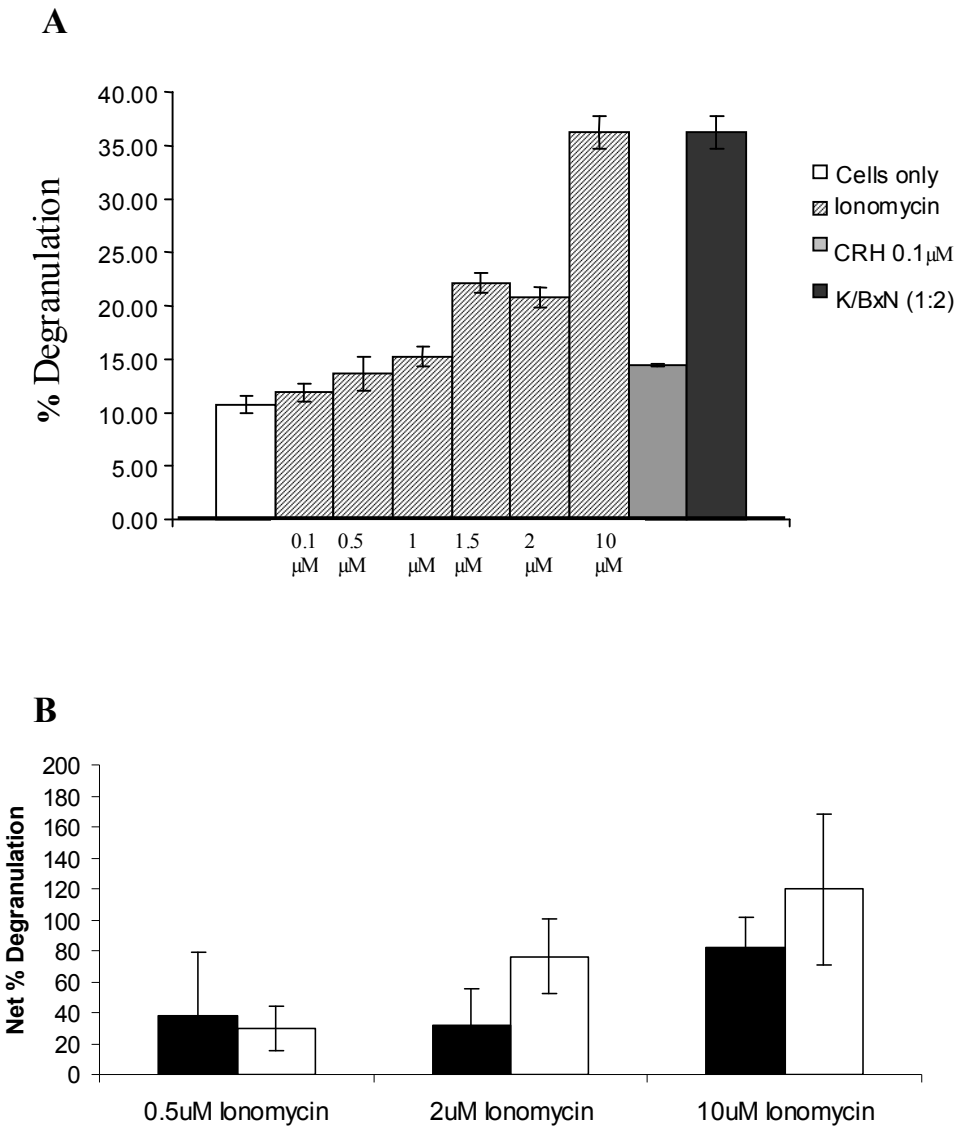

Figure 5.7 Effect of ionomycin, CRH and K/BxN serum on MC degranulation measured by β-hexosaminidase release.
(A) Release of β-hexosaminidase from total peritoneal cells ($2x10^6$) from control mice in response to 15min incubation with Tyrode's buffer alone (0), ionomycin (0.1-10 µM), 0.1µM CRH, or K/BxN serum (diluted 1:2 in Tyrode's buffer). (B) Net release of β-hexosaminidase from peritoneal cells ($2x10^6$) from *Hsd11b1*$^{+/+}$ (black bars) and *Hsd11b1*$^{-/-}$ mice (white bars) was measured following 15min incubation with ionomycin (0.5µM, 2µM, or 10µM in Tyrode's buffer). Data are expressed as mean % degranulation ± SEM; assay completed in triplicate (n=4/genotype). CRH, corticotrophin releasing hormone.

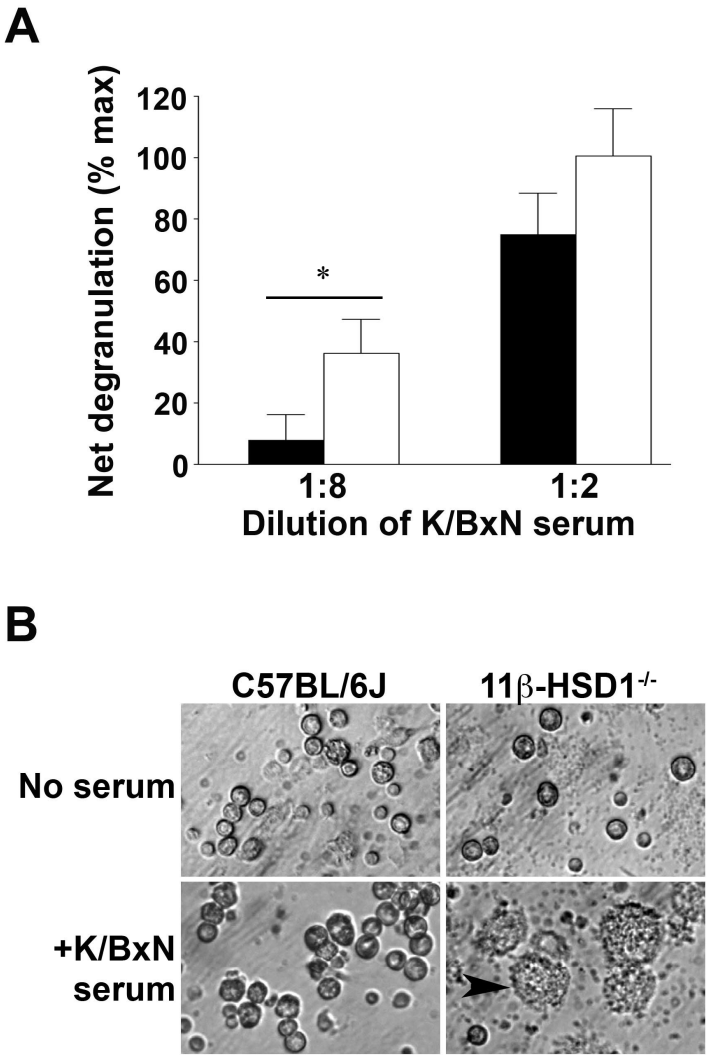

Figure 5.8 Compared to control MC, 11β-HSD1-deficient peritoneal MC show greater degranulation induced by K/BxN serum.
(A) Net degranulation was measured by release of β-hexosaminidase from peritoneal cells ($2x10^6$) from *Hsd11b1*$^{-/-}$ (white bars) or *Hsd11b1*$^{+/+}$ (black bars) mice following 15 min incubation with K/BxN serum (diluted 1:8 or 1:2 in Tyrode's buffer). Data are expressed as mean ± SEM; n=12-13, *$p<0.05$ when compared by Two-way ANOVA. (B) Representative micrographs of enriched peritoneal CD117$^+$ cells from *Hsd11b1*$^{+/+}$ (left panels) or *Hsd11b1*$^{-/-}$ mice (right panels) following 21h incubation with buffer (top panels) or K/BxN serum (1:8 dilution) (lower panels). Arrow indicates degranulated MC. Original images were taken at 400x magnification.

5.2.6. *Hsd11b1*$^{-/-}$ *mice have an altered MC phenotype*

Histochemical staining and flow cytometry analysis were performed to investigate if *Hsd11b1*$^{-/-}$ MC showed an altered cell phenotype. Staining of cytocentrifuge preparations of naïve peritoneal cells with Alcian blue or Safranin O, did not reveal any obvious histochemical differences between MC from the two genotypes (Figure 5.9). In contrast, flow cytometry analysis of peritoneal cells revealed a greater proportion of CD117^{+} (or c-kit^{+}) cells which also expressed CD11b and F4/80 cell markers in *Hsd11b1*$^{-/-}$ mice compared to *Hsd11b1*$^{+/+}$ mice (Figure 5.9). In addition, comparison of SSC (side scatter, measurement of cell granularity) histogram patterns from both genotypes, showing distribution of cells according to granularity, indicated that CD117^{+} cell distribution was altered in the *Hsd11b1*$^{-/-}$ mice (Figure 5.10.A and B). Analysis of side scatter histograms revealed that CD117^{+} peritoneal cells from *Hsd11b1*$^{-/-}$ mice were more granular than cells from the controls (*Hsd11b1*$^{-/-}$ mice, 45.3±5.1% vs *Hsd11b1*$^{+/+}$ mice, 28.2±6.8%). Finally, there was no difference in cell size between the two genotypes based on indirect assessment of FSC (forward scatter, measurement of cell size) histogram of CD117^{+} cells (Figure 5.10.C).

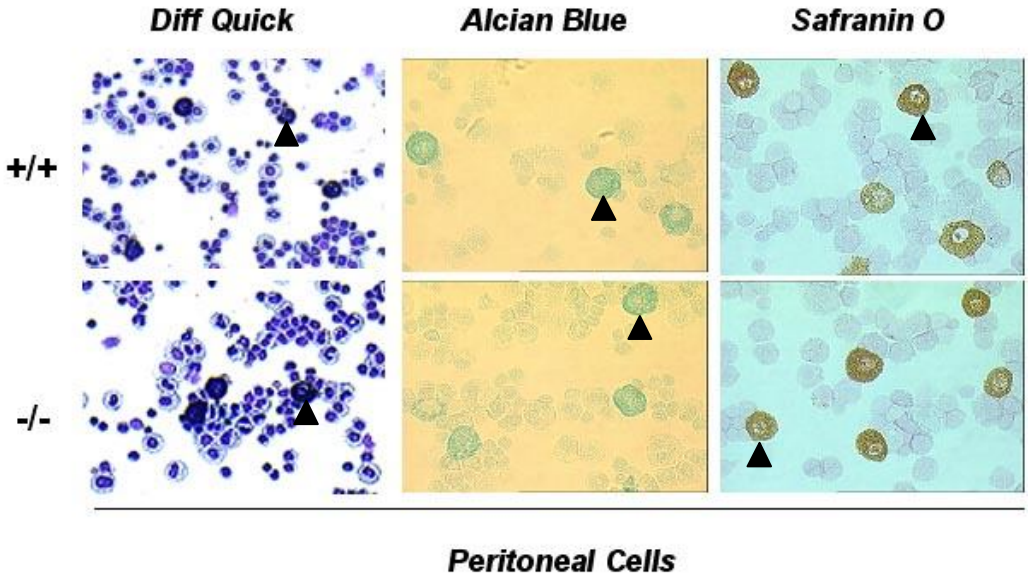

Figure 5.9 Comparable histochemical staining of peritoneal MC from *Hsd11b1*$^{-/-}$ and *Hsd11b1*$^{+/+}$ mice.
Representative images of Diff-Quick, Alcian blue and Safranin O staining of freshly prepared cytocentrifuge preparations of cells from peritoneal lavages showing similar histochemical characteristics of MC from both *Hsd11b1*$^{-/-}$ (-/-) and *Hsd11b1*$^{+/+}$ (+/+) mice (cells from 5 mice per genotype were examined). Arrow heads indicate MC. Original images were taken at 400x magnification.

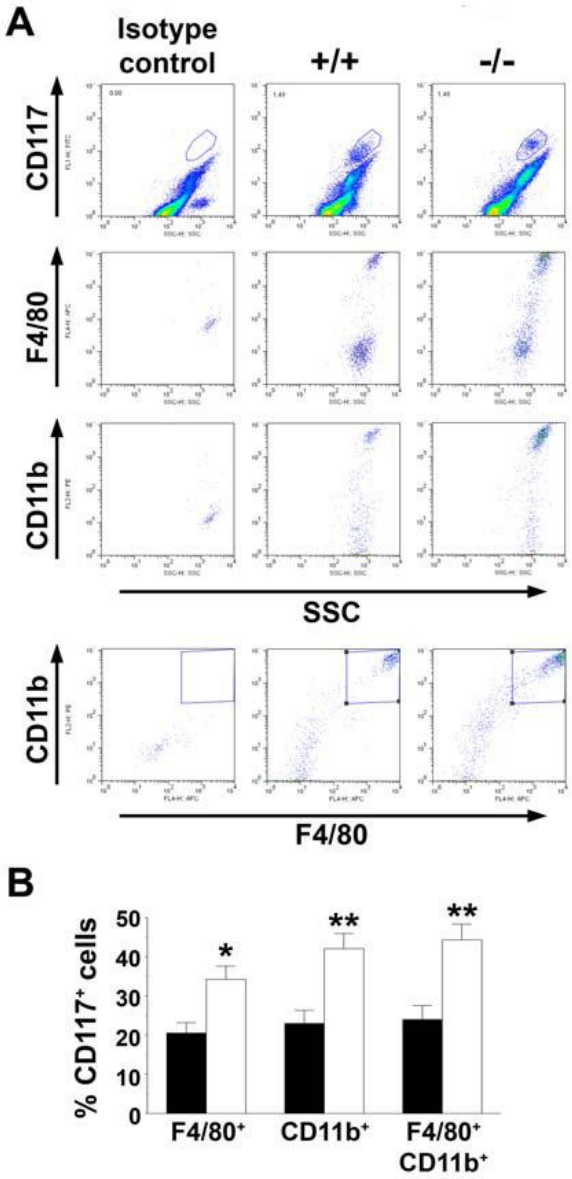

Figure 5.10 A greater proportion of CD117$^+$ peritoneal cells from *Hsd11b1*$^{-/-}$ mice express CD11b and F4/80 than in *Hsd11b1*$^{+/+}$ mice.
Staining was performed in freshly isolated peritoneal cells ($5x10^5$) incubated with CD117, CD11b and F4/80 antibodies or the appropriate isotype controls. (A) Representative flow cytometry dot plot of CD11b and F4/80 staining of CD117$^+$ cells from *Hsd11b1*$^{-/-}$ mice (-/-) and CD117$^+$ cells from *Hsd11b1*$^{+/+}$ (+/+) mice. (B) Gating on CD117$^+$ peritoneal cells, *Hsd11b1*$^{-/-}$ mice (white bars) contained a significantly greater proportion of CD11b and F4/80 positive cells then *Hsd11b1*$^{+/+}$ mice (black bars). Data are expressed as mean ± SEM, n=6/genotype, *p<0.05, **p<0.01 when compared by Two-way ANOVA.

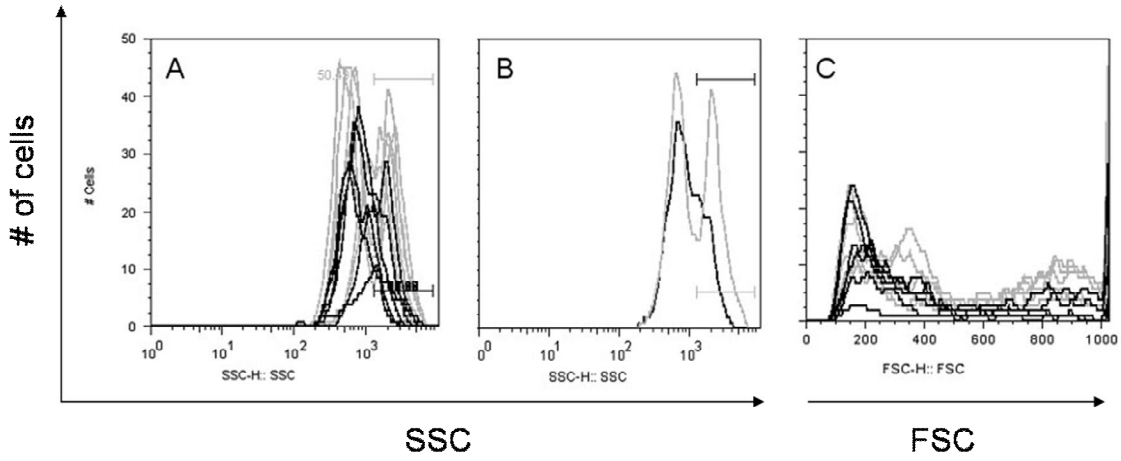

Figure 5.11 Flow cytometric analysis of size and granularity of CD117^{+} peritoneal cells shows altered phenotype in *Hsd11b1*$^{-/-}$ mice.
Freshly isolated peritoneal cells (5x10^{5}) from *Hsd11b1*$^{-/-}$ (grey) and *Hsd11b1*$^{+/+}$ (black) mice were analysed by flow cytometry. Representative histograms showing SSC (side scatter; representing cell granularity), in individual mice (A), or mean SSC for each genotype (B). Unlike SSC, FSC (forward scatter; representing cell size) did not differ between the genotypes (C), (n=6/genotype).

5.2.7. *Assessment of vascular leakage in skin*

To test the hypothesis that increased MC degranulation in response to K/BxN serum resulted in worse oedema and acute inflammation in *Hsd11b1*$^{-/-}$ mice, vascular leakage was measured in skin of *Hsd11b1*$^{-/-}$ and *Hsd11b1*$^{+/+}$ mice. An assay of MC-induced vascular leakage in skin has been previously described (Donelan et al., 2006). In this assay, Evan's Blue dye is injected into the tail vein 1h prior to intra-dermal injection of potent inducers of MC degranulation into the skin; 1μM SP, 1μM neurotensin (NT), 0.1μM CRH, and 1μM Compound 48/80 (C48/80, a synthetic MC secretagogue used as a positive control). K/BxN serum was also tested (Figure 5.12.A). Sterile PBS was used as a negative control. However, this method proved technically difficult to perform, and vascular leakage (visualized as blue patches on the inside of the skin) was extremely variable between mice of the same genotype and even within a single mouse (Figure 5.12.B and data not shown). In addition, other confounding factors, such as an irregular pattern of blood vessels (the location and the size of vessels) as well as skin blemishes and pigmentation present on the underside of the dermal layer, prevented accurate delivery and assessment of vascular leakage by this technique. Accordingly, an alternative assay of vascular leakage (described below) was tried.

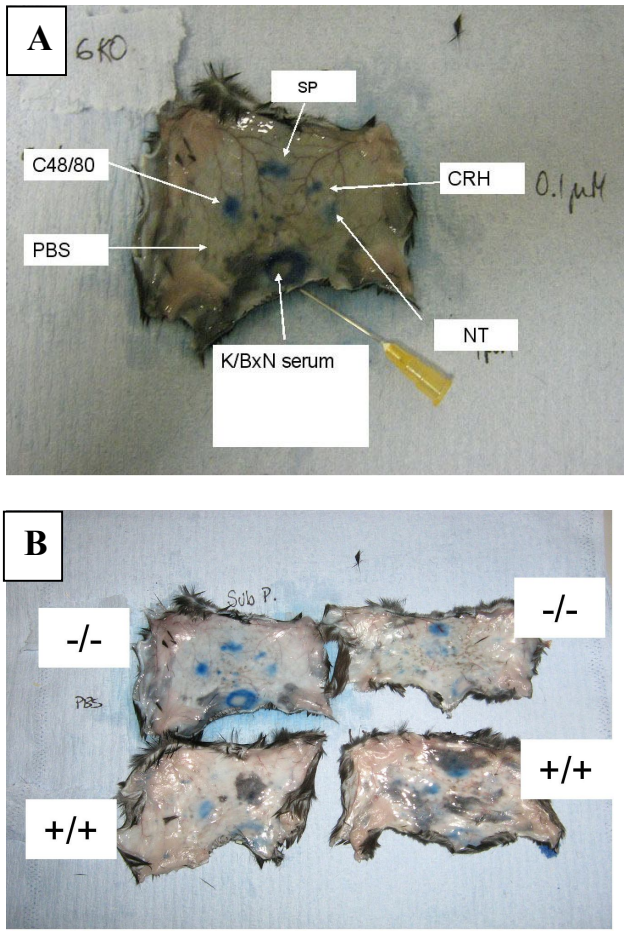

Figure 5.12 Assessment of vascular leakage in skin using MC secretagogues and Evan's Blue dye.
Anaesthetized mice received iv injection of 200µl Evan's Blue dye followed by 50µl intra-dermal injection of various MC degranulation triggers (clockwise starting from top: 1µM SP, 0.1µM CRH, 1µM NT, 1:2 dilution K/BxN serum, 1µg/ml C48/80 or PBS, as a negative control). After 30min mice were euthanized and skin was removed for examination. (A) Representative image from *Hsd11b1*$^{-/-}$ mouse. (B) Two representative skin samples from *Hsd11b1*$^{-/-}$ (-/-) and *Hsd11b1*$^{+/+}$ (+/+) mice. SP, substance P; CRH, corticotrophin releasing hormone; NT, neurotensin; C48/80, compound 48/80.

5.2.8. *Assessment of vascular leakage in the peritoneum*

A second assay was tried to measure vasopermeability in *Hsd11b1*$^{-/-}$ and *Hsd11b1*$^{+/+}$ mice during inflammation, this time in a model of sterile peritonitis (Chapter 2, Section 2.3.1.). Evan's Blue dye was injected i.v. 1h prior to i.p. injection of 10% TG (0.5ml). Vascular leakage was then measured by the appearance of blue dye in the peritoneum. Based on preliminary experiments in C57BL/6 mice, a time point of 4h after TG was chosen for quantification of Evan's blue dye in peritoneal lavage fluid (Chapter 2, Section 2.3.17.). Subsequent experiments included mice from both genotypes and vascular leakiness was assessed at 4h following TG injection. Using this assay, no differences were seen between *Hsd11b1*$^{-/-}$ and *Hsd11b1*$^{+/+}$ mice (Figure 5.13). However, during the course of the experiment, it was noted that the amount of dye in the lavage fluid was strongly dependent on the conditions in which it was collected (eg. the length of time the mouse was left on the warming pad), so this may not have been reliable.

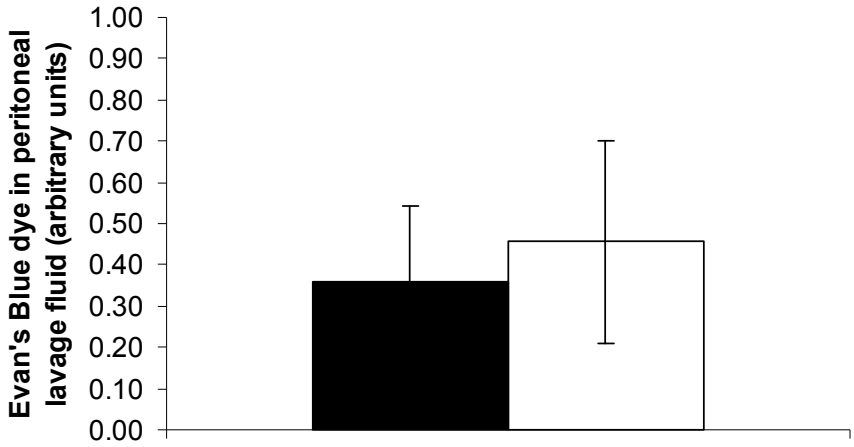

Figure 5.13 Vascular leakage was not different between genotypes 4h following induction of TG-peritonitis and was highly variable within each genotype group. Concentration of Evan's Blue dye in peritoneal lavages 4h following TG injection in *Hsd11b1*$^{-/-}$ (white bar) and *Hsd11b1*$^{+/+}$ mice (black bar) (n=8/genotype). Absorbance at 620nm was measured in peritoneal lavages (corrected for by levels of Evan's Blue in blood, representative of the volume of Evan's Blue injected).

5.3. Discussion

The data contained in this chapter show unequivocally that MC express functional 11β-HSD1 and suggest that, in its absence, MC function is altered. Initial observations were made with IHC staining of 11β-HSD1 in resident peritoneal MC from untreated *Hsd11b1*$^{+/+}$ mice which showed MC to have high 11β-HSD1 expression compared to the other resident cells. However, due to the difficulty of obtaining sufficient numbers of relatively pure and un-stimulated peritoneal MC. BMD-MC, previously shown to have 'connective' tissue-like properties when cultured under appropriate conditions, were used for RNA and enzyme activity measurements. Highly pure BMD-MC, differentiated *in vitro* expressed 11β-HSD1 mRNA and activity, but not 11β-HSD2 mRNA, a pattern which was also seen in other immune cells (discussed in Chapter 6). Reductase activity in BMD-MC was higher than in T lymphocytes (<0.1pmol/h/10^6 cells; (Zhang et al., 2005)) and BMD-DC (7pmol/h/10^6 cells; (Freeman et al., 2005)) and comparable with levels in BMD-Mϕ.

Interestingly, *Hsd11b1* gene transcription in BMD-MC initiates at the upstream P1 promoter (Bruley et al., 2006), with little or no transcription from the downstream P2 (Bruley et al., 2006) and P3 (Moisan et al., 1992) promoters. This contrasts with BMD-Mϕ in which the *Hsd11b1* gene is transcribed from the P2 promoter, and suggests a distinct regulation in MC compared with most other cell types (eg. liver, adipose tissue, and neurons) which utilize the P2 promoter. Intriguingly, expression of C/EBPα, a potent activator of the P2 promoter of the *Hsd11b1* gene transcription (Bruley et al.,

2006), is not compatible with MC differentiation (Arinobu et al., 2005) possibly explaining the use of P1 in this cell type.

The functional role of 11β-HSD1 in MC was addressed both *in vitro* and *in vivo*. MC accumulate at sites of chronic inflammation, including rheumatoid arthritis (Gelbmann et al., 1999; Kassel & Cato, 2002; Woolley, 2003). However, MC number was not altered in peritoneum or in joints of *Hsd11b1*$^{-/-}$ mice compared to the control mice (albeit 2d after the induction of arthritis) and therefore could not underlie the phenotypic difference. However, peritoneal MC from *Hsd11b1*$^{-/-}$ mice, showed a decreased threshold for degranulation induced by K/BxN serum immune complexes. This increased sensitivity, at least in part, is likely to contribute to the earlier onset of inflammation seen in *Hsd11b1*$^{-/-}$ mice.

Hsd11b1$^{-/-}$ mice had more CD117^{+} cells which were also positive for CD11b and F4/80, than *Hsd11b1*$^{+/+}$ mice, suggesting an increase in a subpopulation of MC in *Hsd11b1*$^{-/-}$ mice. CD11b is not normally considered a MC marker. It is preferentially expressed on neutrophils, monocytes, and Mϕ, while F4/80 is a classical Mϕ marker. However, CD11b and F4/80 have been described on MC, and their expression on MC is associated with monocyte-like morphology (Nishiyama et al., 2004), although the relevance of this is unclear at present. It has been suggested that CD11b is expressed on immature MC and is involved in emigration of MC precursors into tissues (Rosenkranz et al., 1998). Following diptheria toxin treatment of mice expressing the human diptheria toxin

receptor under the control of the CD11b promoter, MC were depleted >90% (although with a later time course than Mϕ) (Cailhier et al., 2006), consistent with expression of CD11b on MC as well as Mϕ. Moreover, over-expression of PU.1 (the master haematopoietic regulator) in MC progenitors induces CD11b, F4/80 and c-kit (Nishiyama et al., 2004). Interestingly, GC receptor and PU.1 exert mutually antagonistic effects in some haematopoietic cell precursors (Gauthier et al., 1993), yet in monocytes they functionally co-operate (Aittomaki et al., 2000). Thus, it is possible that GC regeneration via 11β-HSD1 regulates the differentiation, phenotype, or function of MC (and other leukocytes), depending upon the availability of enzyme substrate. It will of great interest to determine whether haematopoietic cell differentiation is affected in *Hsd11b1*$^{-/-}$ mice.

Injection of K/BxN arthritic serum into mice induces a rapid vascular leak localized to peripheral extremities (Binstadt et al., 2006). Attempts were made to measure vascular leakiness in *Hsd11b1*$^{-/-}$ mice. The methods used here have previously been used to show differences in vasodilation between C57BL/6 mice and W/W^{v} mice (which are completely deficient in MC) (Donelan et al., 2006). However, these experiments were unsuccessful largely due to technical difficulties. In the future it will be important to establish whether *Hsd11b1*$^{-/-}$ exhibit increased vascular leakage. Interestingly, *Hsd11b1*$^{-/-}$ mice show increased angiogenesis following injury (Small et al., 2005), indicating susceptibility of vascular regulation by 11β-HSD1, at least during tissue repair. Since MC occur in highly vascular tissues, where they are found next to blood

vessels, it will be of interest to establish whether MC play a role in this phenotype of *Hsd11b1*$^{-/-}$ mice.

Although 11β-HSD1-deficiency in MC provides an intriguing mechanism that may contribute to the worsened inflammatory response in *Hsd11b1*$^{-/-}$ mice, it remains unclear whether it is the 11β-HSD1-deficiency in resident cells or the recruited inflammatory cells that are responsible for the altered inflammatory response in *Hsd11b1*$^{-/-}$ mice.

Chapter 6

Assessment of the immune system and its contribution to the inflammatory response in *Hsd11b1*$^{-/-}$ mice.

6.1. Introduction

Expression of 11β-HSD1 has previously been reported in Mϕ (Thieringer et al., 2001, Gilmour et al., 2006), $CD4^+$, $CD8^+$, and $B220^+$ lymphocytes (Zhang et al., 2005), as well as DC (Freeman et al., 2005). It is important to note, however, that 11β-HSD1 is also expressed in various non-immune cells which play a role during an inflammatory response. Therefore, the inflammatory phenotype of *Hsd11b1*$^{-/-}$ mice may be due to 11β-HSD1-deficiency in recruited immune cells (eg. monocytes, neutrophils, eosinophils), resident immune cells (such as MC and Mϕ), local tissue microenvironment (eg. blood vessels), or a combination of these factors. A BM transfer (BMT) experiment (Chapter 2, Section 2.3.15.) was carried out in an attempt to determine the relative contributions of 11β-HSD1 in tissues versus recruited immune cells to the anti-inflammatory phenotype. However, it was also important to establish whether BM cells in *Hsd11b1*$^{-/-}$ were normal. Therefore, to determine whether 11β-HSD1-deficiency alters immune cell sub-populations, cells from BM, spleen, thymus, peritoneum, as well as peripheral blood were isolated from untreated *Hsd11b1*$^{-/-}$ mice and *Hsd11b1*$^{+/+}$ mice, for quantification of total cell numbers and cell types by flow cytometric measurement of standard cell markers. The BMT experiment described in this chapter was carried out in collaboration with Kay Samuel, who performed the irradiation and tail vain injections as well as providing help with flow cytometry organization and analysis.

6.2. Results

6.2.1. Effects of 11β-HSD1-deficiency on number of immune cells

The number of cells collected from BM, spleen, thymus, peritoneum, as well as peripheral blood cells, did not differ between genotypes (Figure 6.1). This finding was consistent with results from Chapter 5, where both *Hsd11b1*$^{-/-}$ and *Hsd11b1*$^{+/+}$ mice exhibited a similar number of MC in peritoneum and joints (Chapter 5, Section 5.2.5).

6.2.2. Flow cytometric analysis of immune cells from Hsd11b1$^{-/-}$ *and Hsd11b1*$^{+/+}$*mice*

Flow cytometric analysis (Chapter 2, Section 2.3.16.), using antibodies against c-kit, B220, Thy-1, Gr-1, CD45, Lin and Sca-1 (see Table 6.1 for details) was used to characterize cells obtained from both *Hsd11b1*$^{-/-}$ and *Hsd11b1*$^{+/+}$ mice. The ratio of CD4^{+}/CD8^{+} T-cells was measured only in the thymus. For analysis of peritoneal, spleen and BM cells, antibodies were combined as follows: CD45/Thy-1/B220 to stain T and B-cells, CD45/CD11b/Gr-1 to stain monocytes/granulocytes, CD45/LIN/c-kit and CD45/Sca-1/c-kit to stain MC. Data were analysed in dot plots and histograms (Figure 6.2), and a similar analysis template was used for all experiments described in this Chapter.

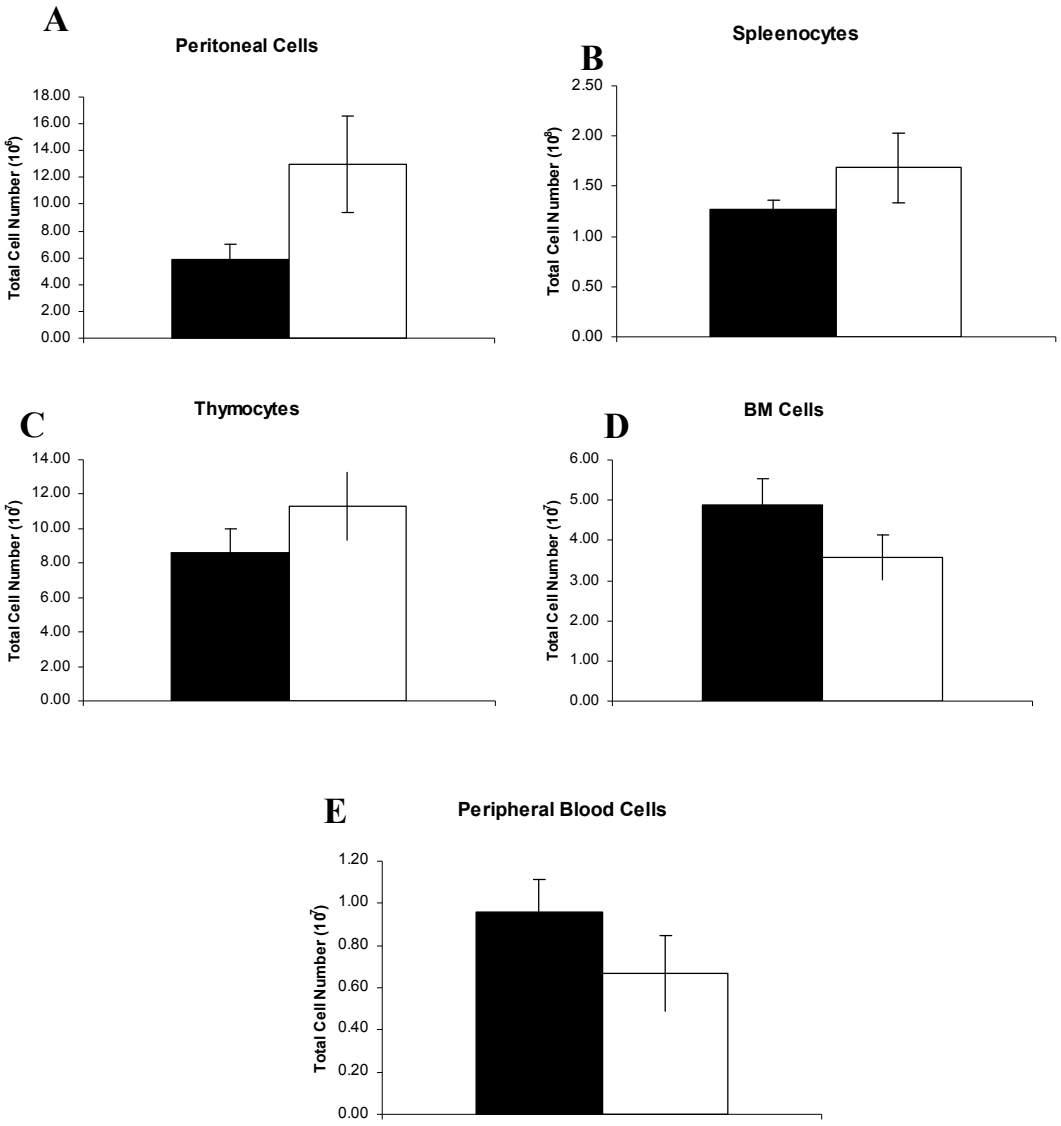

Figure 6.1 Total cell number in immune organs and leukocyte number in peripheral blood did not differ between *Hsd11b1*$^{-/-}$ and *Hsd11b1*$^{+/+}$ mice.
Cell counts (determined microscopically using haemocytometer) of peritoneal cells (A), spleenocytes (B), thymocytes (C), total BM cells from both femurs (D) and peripheral blood leukocytes (E) revealed no differences in cell numbers between *Hsd11b1*$^{+/+}$ (black bars) and *Hsd11b1*$^{-/-}$ mice (white bars). Data represent total number of cells per compartment per mouse and are expressed as mean ± SEM; n=5/genotype. No significant differences were detected between the genotypes when compared by unpaired Student's t-test.

Table 6.1 Overview of antibodies used for the flow cytometric assessment of inflammatory cell phenotype in *Hsd11b1*$^{-/-}$ mice.

Antibody	Main Target	Comments	Other names
B220	B lymphocytes	Also found on activated T cells, subset of DC and other antigen presenting cells	Ly-5, CD45R
CD11b	Monocytes, Mϕ and granulocytes, not lymphocytes	Also found on NK cells and activated lymphocytes	Mac-1 $Alpha_M$ integrin
CD4	T helper cells	Co-receptor in MHC II-restricted antigen induced T cell activation	Ly-4,L3T4
CD8	T cell suppressor / cytotoxic cells	MHC I-restricted receptor	Ly-2
CD45	All hematopoietic cells, except mature erythrocytes and platelets	Essential regulator of T and B cell antigen receptor-mediated activation	Leukocyte common antigen (LCA)
CD117	Hematopoietic stem cells and mature MC	Important for development and survival of MC	c-kit, Steel factor
Gr-1	Granulocytes	Also found on Mϕ and transiently expressed on differentiating monocytes	Ly6G, and includes Ly6C
Lin	Monoclonal antibody cocktail	Containing: CD2, CD3, CD4, CD5, CD8, NK1.1, B220, TER-119, Gr-1	Hematopoietic lineage markers
Sca-1	Immature hematopoietic	Found on early hematopoietic progenitor cells that can populate BM	Ly6A/E or Ly6D
CD90	T lymphocytes and thymocytes	Also found on neural cells, cells of granulocytic lineage, early hematopoietic progenitors, fibroblasts, neurons and Kupffer's cells	Thy-1

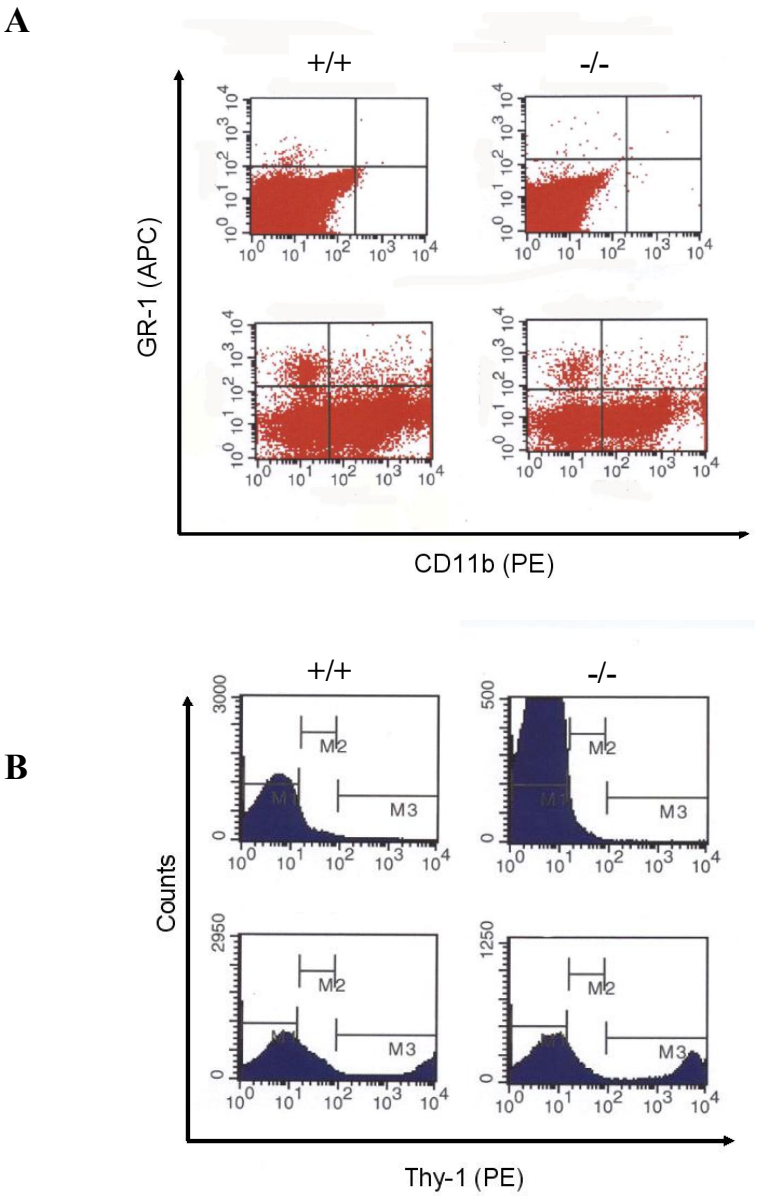

Figure 6.2 Representative dot plots and histograms used for flow cytometric analysis of immune cells from naïve *Hsd11b1*$^{-/-}$ and *Hsd11b1*$^{+/+}$ mice.
(A) Dot plots showing unstained cells (upper panel) and cells stained for CD11b (PE; x-axis) and Gr-1 (APC; y-axis) (lower panel) from *Hsd11b1*$^{-/-}$ (-/-) and *Hsd11b1*$^{+/+}$ (+/+) mice. (B) Histograms of unstained cells (upper panel) and Thy-1 positive cells (lower panel) showing 3 gates (M1; unstained cells, M2; Thy-1 low, and M3; Thy- high). The same templates (dot plots and histograms) were used for assessment of cells from whole blood, peritoneum, spleen, thymus and BM.

6.2.3. Effects of 11β-HSD1-deficiency on immune cell populations

Comparison of cells recovered from untreated *Hsd11b1*$^{-/-}$ and *Hsd11b1*$^{+/+}$ mice revealed differences in cell populations between genotypes, in peritoneum and BM (Figure 6.3, Figure 6.4 and Table 6.2). Peritoneal cells from *Hsd11b1*$^{-/-}$ mice contained a higher proportion of Thy-1^{+} cells, and a lower proportion of Gr-1^{-}/CD11b^{+} cells and Gr-1^{+}/CD11b^{+} cells than *Hsd11b1*$^{+/+}$ mice (Figure 6.3). In BM, compared to *Hsd11b1*$^{+/+}$ mice, *Hsd11b1*$^{-/-}$ mice had a greater proportion of B cells (B220^{+}) and lower proportion of Gr-1^{+} cells (Figure 6.4). No differences were seen between the genotypes in cell populations in peripheral blood (Table 6.2), thymus (Table 6.3) or spleen (Table 6.4).

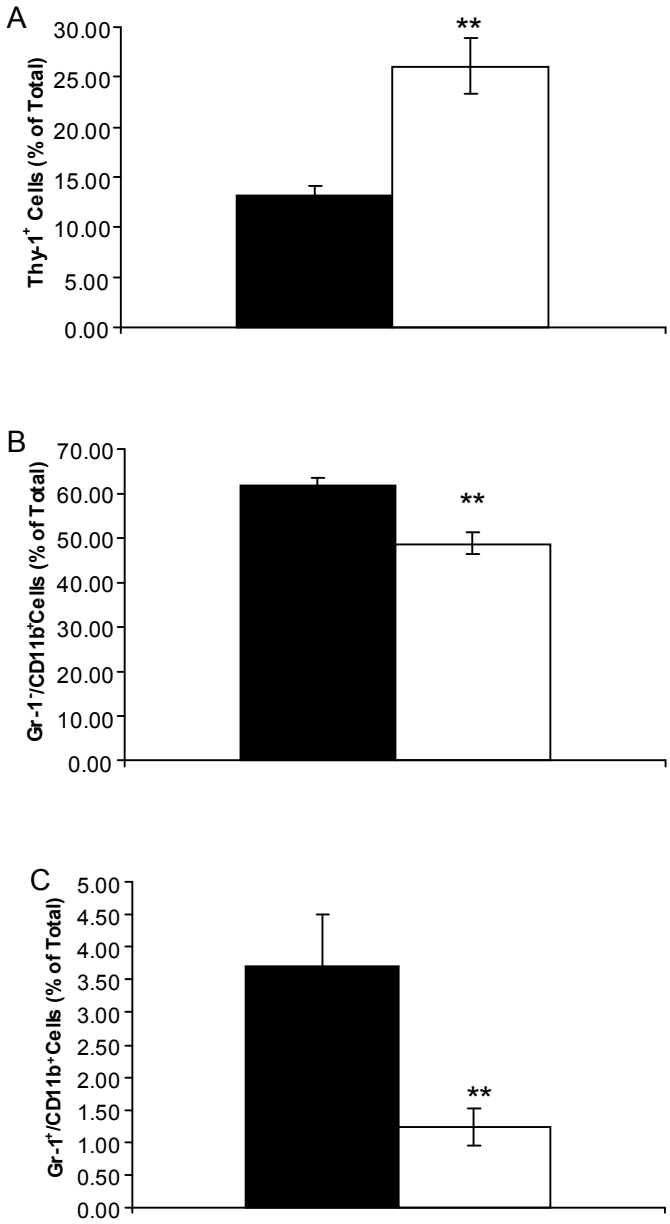

Figure 6.3 *Hsd11b1*$^{-/-}$ mice have more T cells but fewer granulocytes in the peritoneum than *Hsd11b1*$^{+/+}$ mice.
Flow cytometry analysis of peritoneal cells from *Hsd11b1*$^{+/+}$ (black bars) and *Hsd11b1*$^{-/-}$ mice (white bars) showed a greater proportion of Thy-1^{+} cells (A), and a lower proportion of Gr-1^{-}/CD11b^{+} (B) and Gr-1^{+}/CD11b^{+} cells (C) in the peritoneum of *Hsd11b1*$^{-/-}$ mice. Data are mean ± SEM; n=5/genotype. ** $p<0.01$ when compared by unpaired Student's t-test.

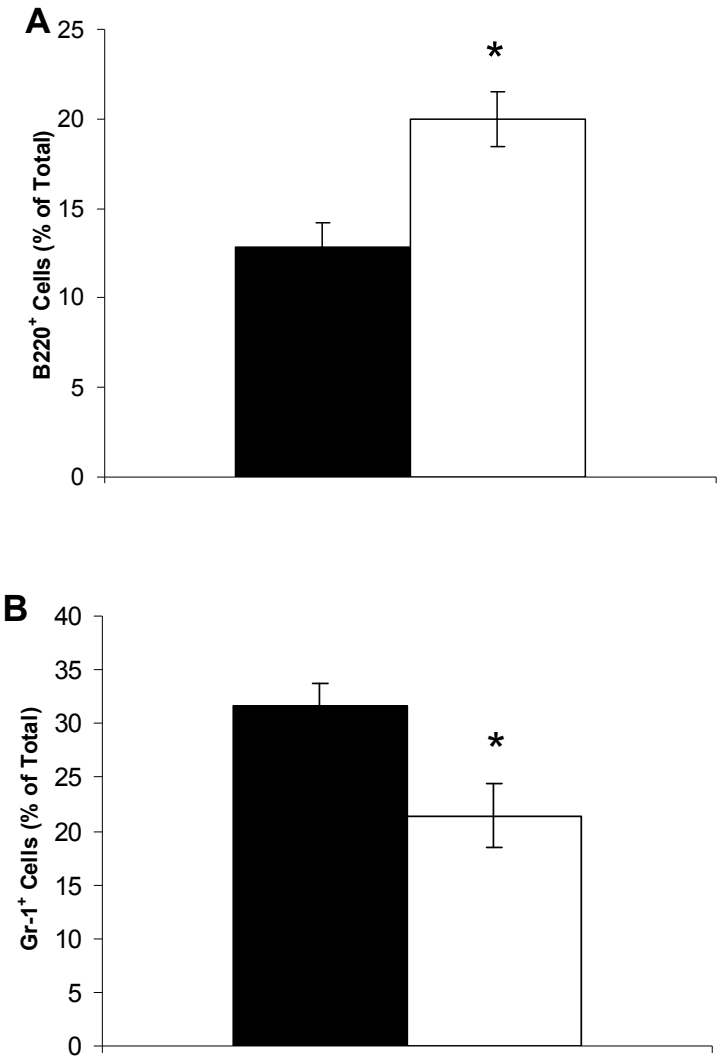

Figure 6.4 Altered distributions of B cells and granulocytes in the BM of untreated *Hsd11b1*$^{-/-}$ mice.
Flow cytometry analysis of BM cells revealed that in comparison to *Hsd11b1*$^{+/+}$ mice (black bars), *Hsd11b1*$^{-/-}$ mice (white bars) had a greater proportion of B220^{+} cells (A) and fewer Gr-1^{+} cells (B). Data represent mean ± SEM; n=5/genotype. * $p<0.05$ when compared by unpaired Student's t-test.

Table 6.2 Flow cytometric comparison of peripheral blood cells from untreated *Hsd11b1*$^{-/-}$ and *Hsd11b1*$^{+/+}$ mice.

Blood Cells	*Hsd11b1*$^{+/+}$ (n=5)	*Hsd11b1*$^{-/-}$ (n=5)	*T-test*
B220^{+}/Thy-1^{-}	25.7±5.1	21.2±3.7	*p>0.05*
B220^{+}/Thy-1^{+}	2.1±0.3	2.7±0.2	*p>0.05*
B220^{-}/Thy-1^{-}	49.3±3.4	44.5±3.7	*p>0.05*
B220^{-}/Thy-1^{+}	22.9±6.7	31.6±4.2	*p>0.05*
B220^{+}/Gr-1^{-}	26.7±5.4	21.1±3.7	*p>0.05*
B220^{+}/Gr-1^{+}	2.4±1.1	3.9±1.2	*p>0.05*
B220^{-}/Gr-1^{-}	54.5±7.6	49.5±1.6	*p>0.05*
B220^{-}/Gr-1^{+}	16.4±6.1	25.5±4.7	*p>0.05*

Table 6.3 Flow cytometric comparison of thymocytes from untreated *Hsd11b1*$^{-/-}$ and *Hsd11b1*$^{+/+}$ mice.

Thymocytes	*Hsd11b1*$^{+/+}$ (n=5)	*Hsd11b1*$^{-/-}$ (n=5)	*T-test*
B220^{+}/Thy-1^{-}	0±0	0±0	*p>0.05*
B220^{+}/Thy-1^{+}	0.022±0.01	0.014±0.01	*p>0.05*
B220^{-}/Thy-1^{-}	22.57±5.51	25.84±5.91	*p>0.05*
B220^{-}/Thy-1^{+}	76.324±5.15	74.234±5.94	*p>0.05*
B220^{+}/Gr-1^{-}	0±0	0±0	*p>0.05*
B220^{+}/Gr-1^{+}	0.022±0.02	0.022±0.02	*p>0.05*
B220^{-}/Gr-1^{-}	98.742±0.69	99.95±0.02	*p>0.05*
B220^{-}/Gr-1^{+}	0.064±0.02	0.048±0.02	*p>0.05*

Table 6.4 Flow cytometric comparison of spleenocytes from untreated *Hsd11b1*$^{-/-}$ and *Hsd11b1*$^{+/+}$ mice.

Spleenocytes	*Hsd11b1*$^{+/+}$ (n=5)	*Hsd11b1*$^{-/-}$ (n=5)	T-test
B220^{+}/Thy-1^{-}	56.4±1.5	55.8±2.6	*p>0.05*
B220^{+}/Thy-1^{+}	7.7±0.4	7.4±0.4	*p>0.05*
B220^{-}/Thy-1^{-}	15.4±1.4	12.7±5.5	*p>0.05*
B220^{-}/Thy-1^{+}	20.6±2.0	20.7±1.1	*p>0.05*
B220^{+}/Gr-1^{-}	63.21±1.0	62.5±2.3	*p>0.05*
B220^{+}/Gr-1^{+}	0.9±0.2	0.8±0	*p>0.05*
B220^{-}/Gr-1^{-}	34.6±1.4	35.7±2.4	*p>0.05*
B220^{-}/Gr-1^{+}	1.3±0.3	1.1±0.1	*p>0.05*
B220^{+}/c-kit^{-}	59.5±2.6	63.8±2.7	*p>0.05*
B220^{+}/c-kit^{+}	0.1±0	0.1±0.03	*p>0.05*
B220^{-}/c-kit^{-}	40.5±2.6	36.0±2.7	*p>0.05*
B220^{-}/c-kit^{+}	0.03±0.01	0.03±0	*p>0.05*
Gr-1^{+}/CD11b^{-}	1.0±0.1	1.0±0.2	*p>0.05*
Gr-1^{+}/CD11b^{+}	6.0±1.0	4.7±0.9	*p>0.05*
Gr-1^{-}/CD11b^{-}	78.8±2.1	80.7±1.9	*p>0.05*
Gr-1^{-}/CD11b^{+}	14.2±1.0	13.7±0.8	*p>0.05*

6.2.4. Bone marrow cell transfer between Hsd11b1$^{-/-}$ and Hsd11b1$^{+/+}$ mice

Following lethal gamma irradiation (described in Chapter 2, Section 2.3.15.), *Hsd11b1*$^{-/-}$ mice were reconstituted with 10^7 BM cells from *Hsd11b1*$^{+/+}$ mice via tail vein injection; designated KO(WT) mice. Conversely, irradiated *Hsd11b1*$^{+/+}$ mice were reconstituted with BM from *Hsd11b1*$^{-/-}$ mice; designated WT(KO) mice. Unfortunately, survival was low following irradiation and BMT, with ~half of the mice dying ~12d following the procedure. A second BMT procedure was performed in order to generate sufficient mice for an arthritis experiment. Due to a lag in time (~2 weeks) between the two BMT procedures, two separate BMT-arthritis experiments were carried out and data were pooled as presented below.

6.2.5. Induction of K/BxN serum transfer arthritis following BMT

After 56d of recovery, BMT recipient mice, as well as non-irradiated (non-BMT) *Hsd11b1*$^{-/-}$ and *Hsd11b1*$^{+/+}$ mice were subjected to K/BxN arthritis (Figure 6.5). The time course of arthritis onset in non-BMT *Hsd11b1*$^{-/-}$ and *Hsd11b1*$^{+/+}$ mice was similar to previous experiments (Figure 6.6, compare with Figure 4.6), demonstrating that the serum batch used for this experiment had a similar potency to previous batches. Following *in vivo* reconstitution of BM in lethally irradiated mice, recovery and the subsequent injection of K/BxN serum, all mice developed disease. However, unlike previous arthritis experiments using non-BMT mice, the disease course in BMT mice showed very large within-group variability (Figure 6.7), resulting in overlap of the group means (Figure 6.8). The area under the curve for clinical scores was not statistically different between groups (data not shown). Nonetheless, at all but 3 of the time points,

the mean clinical score was higher for KO(WT) than for WT(KO) mice, although this did not reach statistical significance.

A

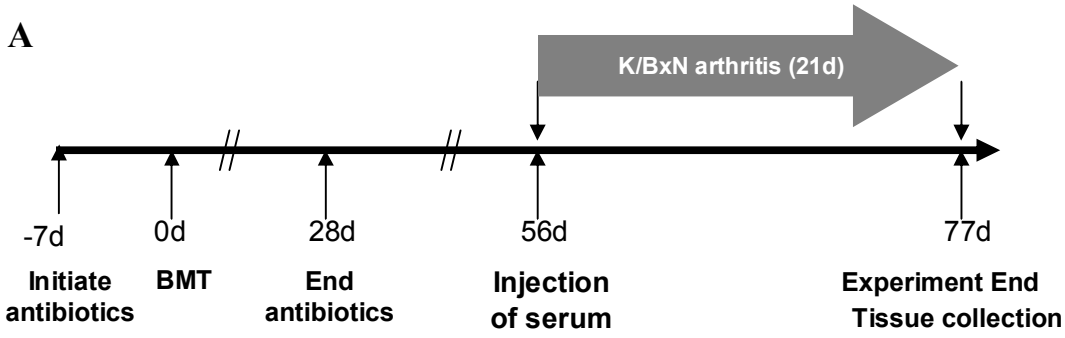

B

Groups	*BMT*	*arthritis*	*n*
WT(KO)	✓	✓	**7**
KO(WT)	✓	✓	**5**
***Hsd11b1*$^{-/-}$**		✓	**3**
***Hsd11b1*$^{+/+}$**		✓	**3**
WT(KO)	✓		**2**
KO(WT)	✓		**2**

Figure 6.5 Experimental design for BMT-arthritis.
(A) Antibiotics were initiated 7d prior to commencement of BMT-arthritis experiment. Irradiation of mice and reconstitution with 10^7 donor cells via tail vein injection occurred on d0. After 56d of recovery arthritis was induced with a single injection of K/BxN serum (5.6µl/g body weight). After 21d of arthritis (d77), mice from all experimental groups were culled and tissues were collected for analysis. (B) List of experimental groups; KO(WT) indicates *Hsd11b1*$^{-/-}$ mice which were reconstituted with BM cells from *Hsd11b1*$^{+/+}$ mice, whilst WT(KO) indicates *Hsd11b1*$^{+/+}$ mice which were reconstituted with BM cells from *Hsd11b1*$^{-/-}$ mice. Checkmark indicates whether BMT and/or arthritis were performed. n indicates number of mice in each group.

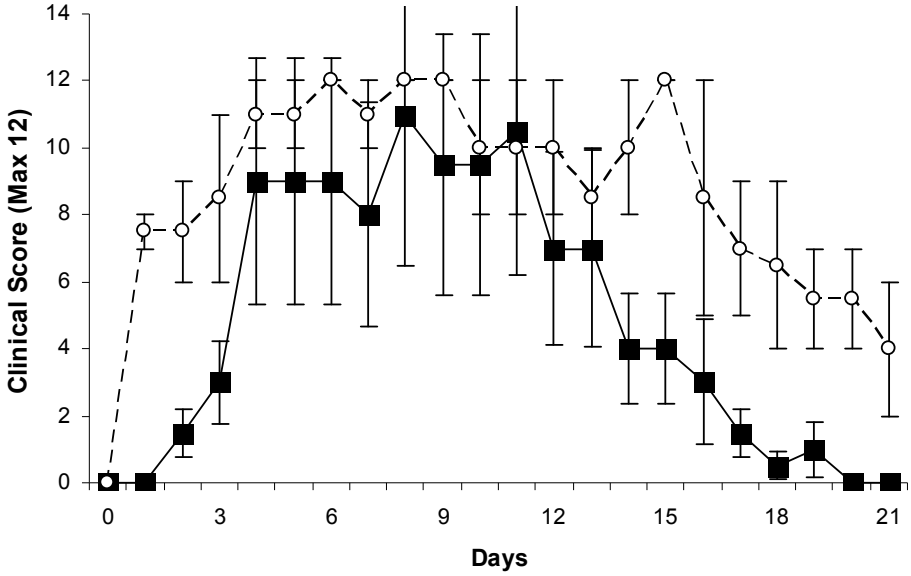

Figure 6.6 Time course of arthritis in non-BMT mice is similar to that observed previously.

Clinical score over 21d following a single injection of 5.6µl/g body weight of K/BxN serum on 0d. *Hsd11b1*$^{-/-}$ mice (white circles, dashed line) are compared to *Hsd11b1*$^{+/+}$ mice (black squares, solid line) (n=3/genotype). Clinical scoring was preformed blind to group/genotype. Values shown are mean ± SEM.

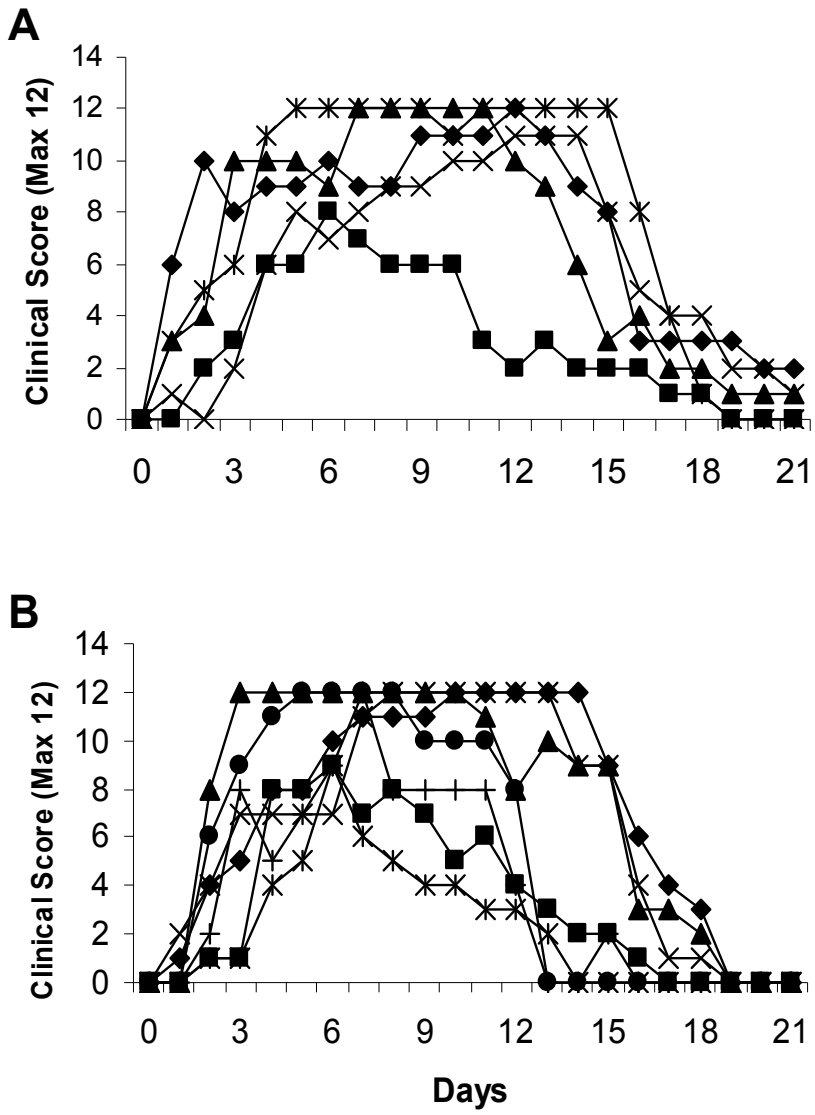

Figure 6.7 High variability in clinical scoring following injection of K/BxN serum in individual BMT-mice.

Clinical score following a single injection of K/BxN serum (5.6µl/g body weight) on d0 in KO(WT) (n=5) (A) and in WT(KO) (B) (n=7) mice. Values shown are for individual mice.

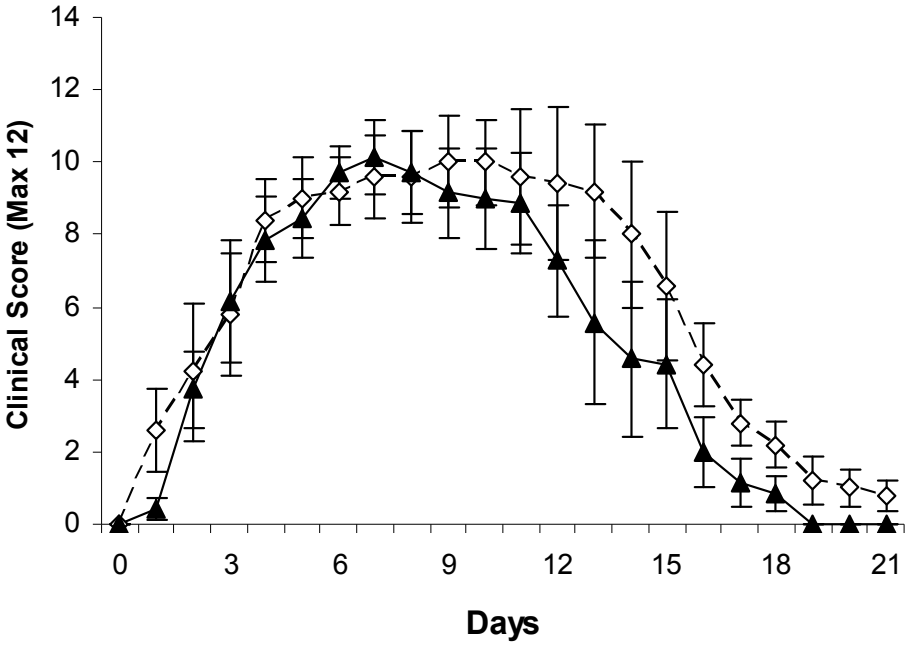

Figure 6.8 Similar clinical scores for WT(KO) and KO(WT) mice following injection of K/BxN serum.
Clinical scores (pooled data from both BMT-arthritis experiments) showing KO(WT) mice (white diamonds, dashed line) (n=5) compared to WT(KO) (black triangles, solid line) (n=7). Values shown are mean ± SEM. Two-way ANOVA did not show statistically significant differences between the two groups.

6.2.6. Assessment of immune cells following BMT and K/BxN arthritis

Following arthritis, cells were recovered from the peritoneum, thymus, spleen and BM (as described above for untreated mice, Section 6.2.1) for total cell counts (Figure 6.9 and Figure 6.10). In contrast to untreated mice, following arthritis, *Hsd11b1*$^{-/-}$ mice without BMT had higher number of total spleenocytes and BM cells than *Hsd11b1*$^{+/+}$ mice, without BMT (Figure 6.9, compared with Figure 6.1). The number of thymocytes and peritoneal cells remained similar in both genotypes (Figure 6.9).

Following both BMT and arthritis, there were no differences in cell counts between the KO(WT) and WT(KO) groups (Figure 6.10). However, BMT-mice, compared to non-BMT groups, lost the most weight, appeared sickly and failed to show symptoms of arthritis following injection of K/BxN serum (77d following BMT) (data not shown). This was similar in both the KO(WT) and WT(KO) mice. Interestingly, there was a positive correlation between the area under the curve of the clinical score (indicating the severity of arthritis) and the number of BM cells (including total cell number from both femurs/mouse) (Figure 6.11.A). In addition, there was a positive correlation between the number of BM cells and spleenocytes (Figure 6.11.B), as well as BM cells and thymocytes (Figure 6.11.C).

Finally, flow cytometric analysis was performed on cells following BMT and K/BxN arthritis. However, due to the high mortality rate following irradiation and sub-optimal health of surviving BMT mice it is difficult to draw reliable conclusions from these data. The results have been included in Appendix I.

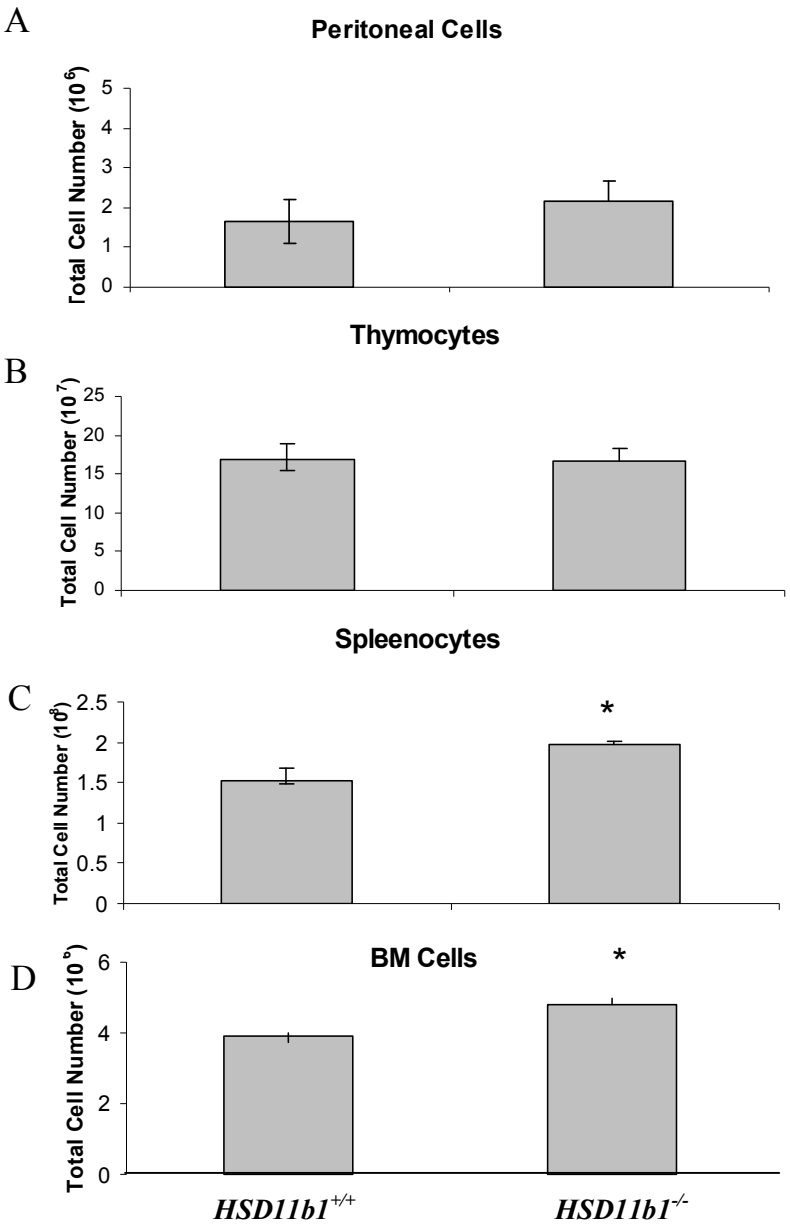

Figure 6.9 Following arthritis, *Hsd11b1*$^{-/-}$ mice had more spleenocytes and BM cells, but a similar number of peritoneal cells and thymocytes as *Hsd11b1*$^{+/+}$ mice.
Cell counts (determined microscopically using haemocytometer) of peritoneal cells (A), thymus (B), and spleen (C) and BM (D) from *Hsd11b1*$^{-/-}$ and *Hsd11b1*$^{+/+}$ mice with arthritis (n=3/group). Values shown are mean ± SEM. * $p<0.05$ when compared by unpaired Student's t-test.

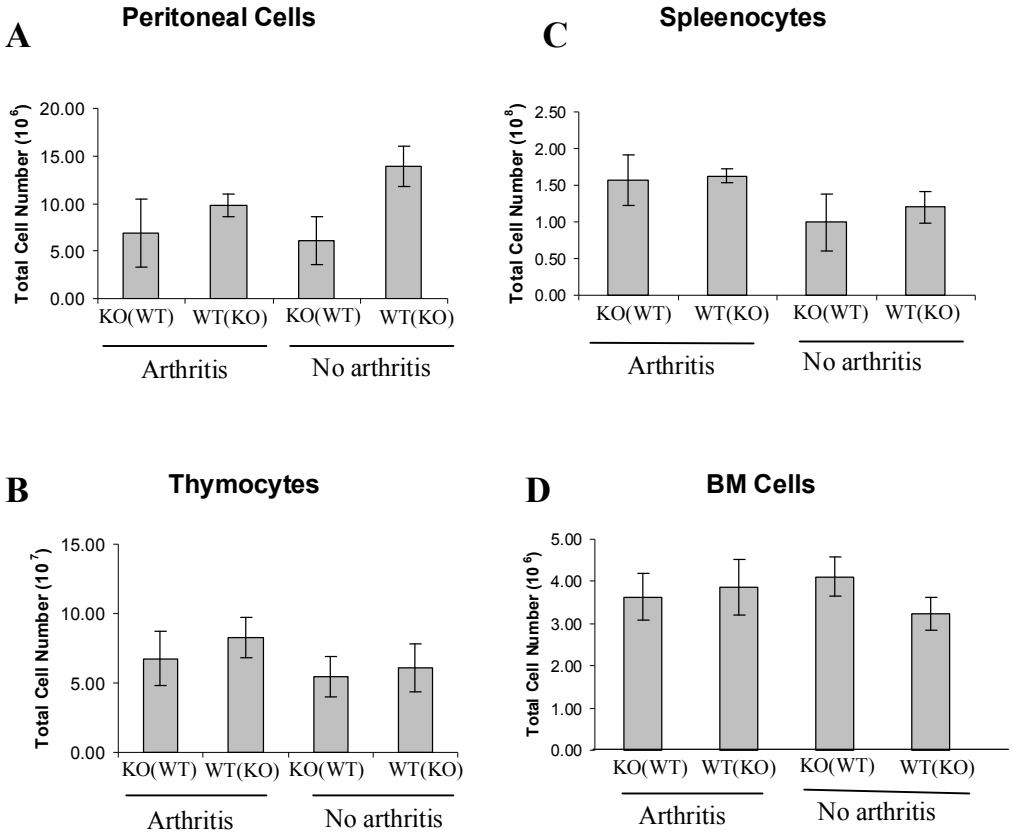

Figure 6.10 Similar number of immune cells in WT(KO) and KO(WT) mice with or without arthritis.

Cell counts (determined microscopically using haemocytometer) of cells from peritoneum (A), thymus (B), spleen (C) and BM (D) from KO(WT) with arthritis (n=5), WT(KO) with arthritis (n=7), KO(WT) without arthritis (n=2) and WT(KO) without arthritis (n=2). Values shown are mean ± SEM. No statistical differences were detected in groups with arthritis (unpaired Student's t-test). Statistical tests were not performed on groups without arthritis due to insufficient group sizes (n=2/group).

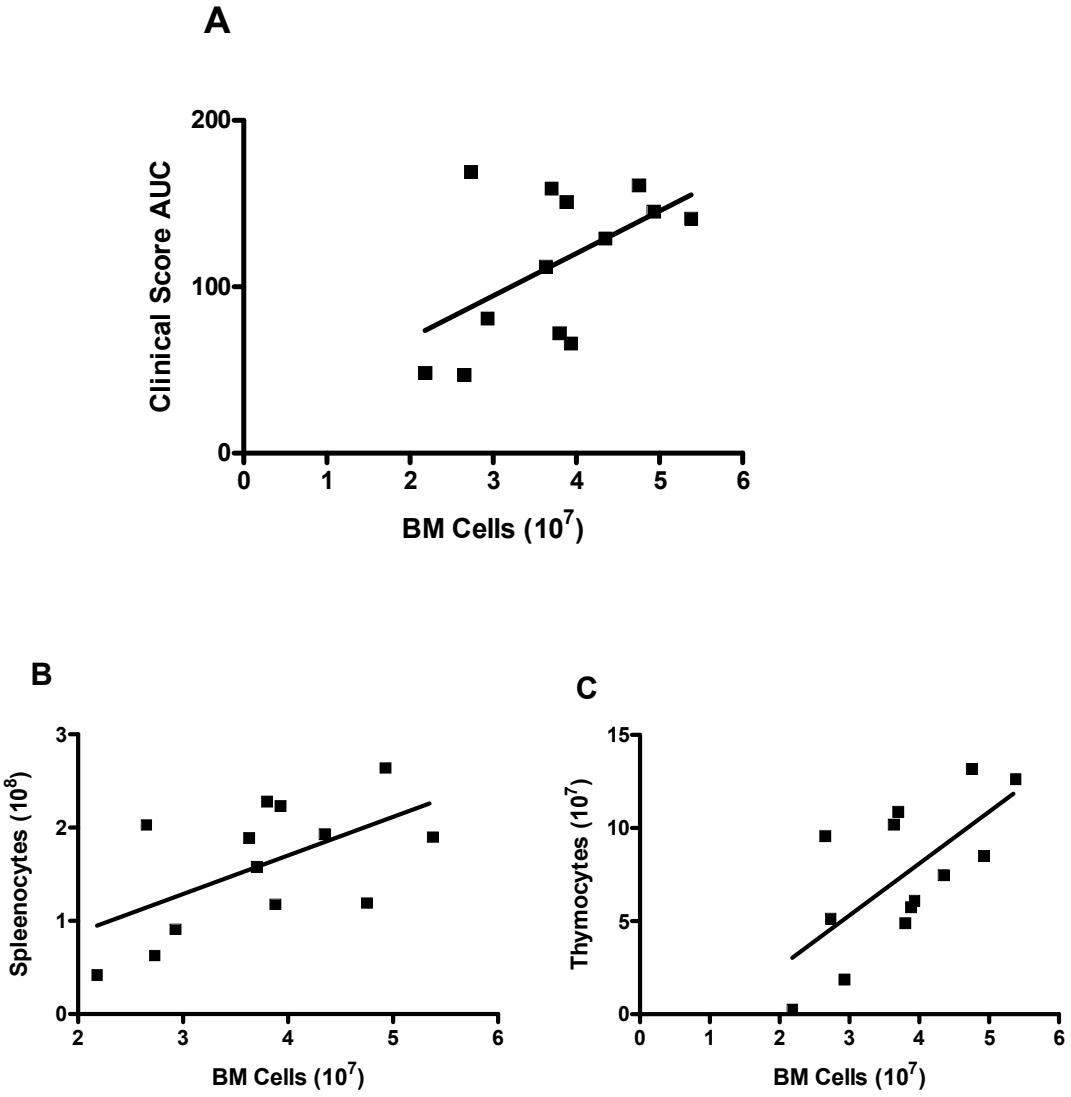

Figure 6.11 Severity of arthritis was positively associated with BM cells, irrespective of genotype.
(A) There was a positive correlation between the clinical score AUC (arbitrary units) and the number of reconstituted cells in BM (r^2=0.55, $p<0.01$). (B) There was a positive correlation between the number of BM cells (total cells collected from both femurs) and spleenocytes (r^2=0.35, $p<0.05$), as well as (C) BM cells and thymocytes (r^2=0.46, $p<0.01$). Each point corresponds to a single mouse (n=13).

6.3 Discussion

11β-HSD1 expression has been shown in immune cells, including lymphocytes and cells of the myeloid lineage, and recent work has shown that the phenotype of these cells is altered by 11β-HSD1-deficiency (reviewed in (Chapman et al., 2006)). The experiments described in this Chapter were designed to dissect the relative contributions of 'resident' immune cells (such as MC and Mϕ) and non-immune cells that form the local microenvironment (such as smooth muscle cells and fibroblasts, which also express 11β-HSD1) which are radio-resistant and the radio-sensitive 'recruited' inflammatory cells to the altered inflammatory response in *Hsd11b1*$^{-/-}$ mice. First, however, flow cytometric analysis was performed on leukocytes and their progenitors from untreated *Hsd11b1*$^{-/-}$ and control mice, to determine the consequences of 11β-HSD1-deficiency on the undisturbed immune system. Although no differences were found in total cell numbers between the genotypes, *Hsd11b1*$^{-/-}$ mice showed abnormalities in the proportions of lymphocytes and granulocytes in peritoneal and BM cells, compared to *Hsd11b1*$^{+/+}$ mice. These data warrant more experiments to fully assess the role of 11β-HSD1 in the regulation of haematopoietic differentiation programmes.

The reconstitution of immune cells in recipient mice, during the BMT-arthritis experiment, may have been sub-optimal. The high mortality rate (~50%) at ~12d following irradiation, while mice were supplemented with antibiotics, was probably a result of insufficient reconstitution of immune cells (personal communication, Ms Kay Samuel), and post mortem observations showed gastrointestinal problems. Furthermore,

upon examination of BM cell counts in surviving mice, it appeared that mice with lower cell counts (suggesting poor reconstitution) inversely correlated with severity of arthritis in both BMT groups; KO(WT) and WT(KO). The positive correlation between number of BM cells and clinical scores in the recipient mice suggested that in order to be susceptible to K/BxN arthritis, mice had to have a fairly healthy and intact immune system to begin with. Nonetheless, the preliminary BMT-arthritis experiment *hinted* at the contribution of the host (thus non-immune or resident immune cells) in worsening arthritis. Although not significant, KO(WT) mice appeared to have impaired resolution compared to WT(KO) mice.

Amendments to the experimental protocol may be used to improve the outcome of future BMT experiments aimed to determine the relative contributions of 11β-HSD1 in resident versus recruited immune cells to the inflammatory phenotype. For example, transfer of spleenocytes from donor mice to the host, in addition to i.v. injection of BM cells, will provide short term immunity and aid in post-operative recovery, ultimately reducing mortality. Importantly, it will be essential to determine the success of BM reconstitution and health of recipient mice prior to continuation of further experimental procedures. This can be achieved by using C57BL/6J mice carrying the CD45.1 marker as "WT" mice. Normal C57BL/6J mice (as well as the congenic *Hsd11b1*$^{-/-}$ mice used in all experiments) carry the antigenically distinct CD45.2 allele. Thus, flow cytometry analysis of leukocytes can be used to detect presence or absence of the CD45.1/CD45.2 antigens to confirm normal numbers and origin of leukocytes, in spleen and BM cells during the recovery period. Alternatively, the relative levels of 11β-HSD1 alleles in

circulating leukocytes, in *Hsd11b1*$^{-/-}$ and *Hsd11b1*$^{+/+}$ mice, can be determined to assess the success of reconstitution following irradiation. The BMT experiment established that *Hsd11b1*$^{+/+}$ mice can be reconstituted with BM cells from *Hsd11b1*$^{-/-}$ mice (and vice versa). However, additional control groups; *Hsd11b1*$^{-/-}$ reconstituted with BM cells from *Hsd11b1*$^{-/-}$ mice and control mice reconstituted with BM cells from control mice, should also be included.

Finally, the question of whether the inflammatory phenotype of *Hsd11b1*$^{-/-}$ mice is driven by MC, or is dependent upon the hormonal (GC) or tissue (eg. vasculature) environment can be addressed in the future using Kit$^{W\text{-}sh/W\text{-}sh}$ mice (available from Jackson labs), which are deficient in MC (Grimbaldeston et al., 2005). For example, mature MC populations can be reconstituted in non-irradiated *Kit*$^{W\text{-}sh/W\text{-}sh}$ mice by transfer of BMD-MC (cultured from *Hsd11b1*$^{-/-}$ or *Hsd11b1*$^{+/+}$ mice). Alternatively, *Kit*$^{W\text{-}sh/W\text{-}sh}$ mice can be crossed with *Hsd11b1*$^{-/-}$ mice to generate *Kit*$^{W\text{-}sh/W\text{-}sh}$ *Hsd11b1*$^{-/-}$ doubly mutant mice (achieved in F_2 mice as the *Kit* and *Hsd11b1* genes are on different chromosomes), which can then be reconstituted with BMD-MC from either *Hsd11b1*$^{-/-}$ or *Hsd11b1*$^{+/+}$ mice. Importantly, these experiments will enhance our understanding of the locus of the anti-inflammatory mechanisms of 11β-HSD1.

Chapter Seven

Summary and Discussion

7.1 Summary

Pharmacologically, GC exert powerful immunosuppressive and anti-inflammatory effects, but long term therapy is limited by the adverse metabolic side effects. The aim of this thesis was to investigate whether amplification of intracellular GC levels by 11β-HSD1 represents an important endogenous mechanism in limiting inflammation. Recent evidence (reviewed in (Chapman et al., 2006)), including work described in this thesis, suggests that 11β-HSD1 forms part of an endogenous anti-inflammatory mechanism engaged early during an inflammatory response that may program subsequent resolution. The contribution of 11β-HSD1 during an inflammatory response was examined using *Hsd11b1*$^{-/-}$ mice and *Hsd11b1*$^{+/+}$ control mice. Both the carrageenan-induced pleurisy model (described in Chapter 3), as well as the K/BxN model of self-resolving experimental arthritis (described in Chapter 4), were found to be suitable *in vivo* experimental models of inflammation, revealing worse inflammation in *Hsd11b1*$^{-/-}$ mice compared to *Hsd11b1*$^{+/+}$ mice. These data support the original findings, which suggested an anti-inflammatory function for 11β-HSD1 in a model of TG-induced peritonitis (Gilmour, 2002; Gilmour et al., 2006), and importantly, emphasize a role for 11β-HSD1 in restraining acute inflammation. Furthermore, in contrast to the TG-induced peritonitis model, where resolution occurred simultaneously in both genotypes, these data suggests that the resolution of inflammation seen both in arthritis (judged by clinical scoring of inflamed joints and supported by histology at 21d) and pleurisy (based on histological examination at 48h) was delayed in *Hsd11b1*$^{-/-}$ mice, suggesting that 11β-HSD1 may also promote resolution. It is possible however, that the altered resolution may be a consequence of the greater initial inflammatory response.

In this thesis, it was demonstrated that MC express functional 11β-HSD1 enzyme (described in Chapter 5). Crucially, 11β-HSD1-deficient mast cells show a reduced threshold for MC degranulation induced *in vitro* by K/BxN arthritogenic serum, a finding that has implications for not only inflammatory arthritis, but also infection, allergy and tolerance. This finding also provides a mechanistic insight into how 11β-HSD1 may modulate the early immune response. The studies presented in this thesis, consistently, and in more than one model, demonstrate that the phenotype of *Hsd11b1*$^{-/-}$ mice is consistent with a more rapid onset of inflammation and/or greater initial severity, with adverse downstream consequences. An altered MC phenotype is likely to underlie at least part of this phenotype. These studies have provided a basis for future experiments to tease apart the role and regulation of 11β-HSD1 in inflammation. Thus, further investigations are warranted and better understanding of the immune-regulated role of 11β-HSD1 in inflammation may lead to improved and even targeted steroid therapies.

7.2 Discussion

These findings raise intriguing questions about the importance of local modulation of GC by 11β-HSD1, with particular relevance to MC, and provide a basis for further investigation. The locus of the anti-inflammatory effect of 11β-HSD1 remains a central question. Although recently 11β-HSD1 has been identified in immune cells (reviewed in (Chapman et al., 2006)), it will be important to clearly identify which of these cells are

involved in the mechanism responsible for the acute anti-inflammatory effects of 11β-HSD1.

Previously it has been shown that 11β-HSD1 activity is rapidly induced in peritoneal cells following TG injection and the cell type responsible for this remains to be identified (Gilmour et al., 2006). Future experiments should focus on identifying and phenotyping the cell populations elicited to the peritoneum during acute TG-induced peritonitis. However, it is important to remember that the variation in 11β-HSD1 activity (measured in resident versus elicited cells) may reflect differences in the activation state of these cells rather than their source. Therefore, a direct comparison of 11β-HSD1 activity in resident and elicited peritoneal cells following their activation *ex vivo* is also necessary.

Additionally, following TG injection more cells were elicited to the peritoneum in *Hsd11b1*$^{-/-}$ than in *Hsd11b1*$^{+/+}$ mice (Coutinho et al, to be submitted). Thus, in parallel to the investigations suggested above, it will be important to establish the mechanisms responsible for the greater influx of cells seen in *Hsd11b1*$^{-/-}$ mice during an inflammatory response. The number of immune cells isolated from peritoneum, spleen, thymus, BM and peripheral circulation from untreated mice was similar between *Hsd11b1*$^{-/-}$ and *Hsd11b1*$^{+/+}$ mice (described in Chapter 6). Two possible mechanisms responsible for the greater recruitment of inflammatory cells during peritonitis are; first, cytokine and chemokine regulation of the inflammatory response involving the resident immune cells as well as non-immune cells and/or incoming inflammatory cells, and

secondly, the regulation of vascular permeability. Attempts were made (described in Chapter 5) to evaluate vascular permeability in the skin and peritoneum of *Hsd11b1*$^{-/-}$ and *Hsd11b1*$^{+/+}$ mice. However, due to technical difficulties no conclusions could be drawn and thus this question remains to be addressed.

Chapter 6 described the BMT-arthritis experiment which was designed to examine the relative contribution of recruited inflammatory cells versus host tissue to the inflammatory phenotype of the *Hsd11b1*$^{-/-}$ mice. Unfortunately, due to technical difficulties and large variability in the response of mice to the BMT, clear conclusions could not be made. However, despite its shortcomings, this preliminary experiment hinted that overall worse inflammation tracked with the host tissue. With hindsight, additional checkpoints and controls in the experimental design (described in the discussion section of Chapter 6) would have perhaps ensured a more successful reconstitution of the immune system and allowed for a more indepth interpretation of the data. To further address which type of cells are responsible for the phenotype of the *Hsd11b1*$^{-/-}$ mice, BMT should be repeated with these additional controls. It is likely that both compartments (immune/non-immune resident cells and recruited inflammatory cells) play a role and a separate set of experiments must to be designed to look individually at the contribution of specific sub-types of cells, for example MC, fibroblasts, Mϕ, vascular tissue or mesothelial cells.

The focus of Chapter 5 was to compare the phenotype of MC from *Hsd11b1*$^{-/-}$ and *Hsd11b1*$^{+/+}$ mice since 11β-HSD1 has not been characterized in MC previously. Although the number of MC was normal, the phenotype was altered in *Hsd11b1*$^{-/-}$ mice, particularly IgG-mediated degranulation, which was higher in *Hsd11b1*$^{-/-}$ than *Hsd11b1*$^{+/+}$ mice following exposure to 1/8 dilution of K/BxN serum. Therefore, future experiments should investigate the contribution of 11β-HSD1 in MC to the phenotype of *Hsd11b1*$^{-/-}$ mice to determine if it limits acute oedema and inflammation.

Since the function of 11β-HSD1 is dependent upon its substrate (inactive GC) much of the physiological function seen *in vivo* may not be apparent in an *in vitro* environment. This is an important factor to consider when planning experiments which are aimed at establishing whether 11β-HSD1 may regulate the differentiation of MC as well as the phenotype and function of mature MC, especially since these cells complete their development under influence of the local environment. Therefore, it will be of great importance to establish an appropriate MC population to use, preferably one differentiated *in vivo* (in the presence of endogenous GC). Perhaps peritoneal MC, albeit a very small cell population (3-5% of the total peritoneal population), serve as the ideal cell source in which to carry out further experiments. Recently, Malbec et al (2007) have proposed a method of culturing peritoneal MC to generate highly pure MC populations with large number of mature serosal-type mouse MC which retain most of the morphological, phenotypic, and functional features of peritoneal MC. It will be interesting to apply this culture method in further comparisons of *Hsd11b1*$^{-/-}$ and *Hsd11b1*$^{+/+}$ MC, particularly for degranulation experiments (with various stimuli, eg.

IgE mediated degranulation) and preparation of MC mRNA for microarray analysis of gene expression programmes.

A key question arising from this thesis is whether a single or separate mechanism(s) are responsible for 11β-HSD1 limiting inflammation at the acute versus the resolution stage. Evidence in the literature points to a crucial role for MC in initiating inflammation, acting prior to Mϕ and playing a major role in neutrophil recruitment (reviewed in (Nigrovic & Lee, 2005)). However, there is evidence that MC are also involved in tissue repair and remodeling processes following chronic inflammation (reviewed in (Marshall & Jawdat, 2004)). Thus, it is possible that MC may be a contributing factor, not only to the onset of arthritis, but also to the delay in resolution seen in the *Hsd11b1*$^{-/-}$ mice during arthritis. However, the mechanisms by which GC promote resolution are not well understood and MC 11β-HSD1 is only one possible mechanism in a system which is complex and more than likely to be dependent on multiple cells and pathways.

Tissue remodeling was altered in *Hsd11b1*$^{-/-}$ mice in both the pleurisy model (adhesion of lung lobes seen only in *Hsd11b1*$^{-/-}$ mice) and in arthritis (worse exostosis and ganglion cyst formation, seen only in *Hsd11b1*$^{-/-}$ mice). Additionally, data obtained from the micro-CT scanning of femur bones (described in Chapter 4) showed arthritis-induced abnormal remodeling of bone micro-architecture in *Hsd11b1*$^{-/-}$ mice, but only after 21d of arthritis and not after 2d (shown in Chapter 4) or in untreated mice (Justesen et al., 2004). To better understand the mechanism behind these skeletal changes, further

examination of histomorphometric parameters, including assessment of osteoclasts and osteoblasts, in *Hsd11b1*$^{-/-}$ mice are warranted.

Finally, in addition to the immune cells, the HPA axis plays a key role in the response to inflammatory stimuli. Plasma corticosterone levels were measured at the start and conclusion of arthritis (described in Chapter 4), with greater plasma corticosterone levels in *Hsd11b1*$^{-/-}$ mice during resolution than in *Hsd11b1*$^{+/+}$ mice. Intracellular GC concentrations can differ markedly from blood levels due to metabolism by 11β-HSD. Thus, it will be important to verify the circulating levels of both corticosterone and 11-DHC in untreated and experimental mice (at varying stages of inflammation) in order to establish the available level of substrate for 11β-HSD1. This type of experiment may explain why, despite greater activation of HPA axis during resolution, *Hsd11b1*$^{-/-}$ mice have worse inflammation than *Hsd11b1*$^{+/+}$ mice.

In this thesis, *Hsd11b1*$^{-/-}$ mice were examined during acute inflammation which resolved over days or weeks. The stimulus or irritant in each case was a sudden assault on the host immune system (eg. i.p. injection of K/BxN serum) resulting in an acute response of the immune system and recruitment of inflammatory cells. This is in contrast to the low grade inflammatory response described for obesity and the metabolic syndrome (not addressed in this thesis, but reviewed elsewhere (Hotamisligil, 2006)). Intriguingly, *Hsd11b1*$^{-/-}$ mice are protected from symptoms of the metabolic syndrome (Morton et al., 2001; Morton et al., 2004). In this context, during low grade chronic inflammation, 11β-HSD1-deficiency is protective. This paradox highlights the complexity both of GC

regulation by 11β-HSD1, but also the effect of GC on the immune system. Much more work is required to truly appreciate the differences in inflammatory response during acute, high-impact versus low-grade and chronic inflammation, and how GC mediate the immune responses in each case.

In conclusion, the experiments described in this thesis support an anti-inflammatory role for 11β-HSD1 during an inflammatory response (in at least the models described here) and begin to address the underlying mechanisms for the altered inflammatory phenotype of *Hsd11b1*$^{-/-}$ mice. Most importantly, these data provide an exciting foundation to investigate further the role of 11β-HSD1 during inflammation.

References

Abraham, S. M., Lawrence, T., Kleiman, A., Warden, P., Medghalchi, M., Tuckermann, J., Saklatvala, J. & Clark, A. R. 2006. Antiinflammatory effects of dexamethasone are partly dependent on induction of dual specificity phosphatase 1. *J Exp Med*, **203,** 1883-1889.

Adams, M., Meijer, O. C., Wang, J., Bhargava, A. & Pearce, D. 2003. Homodimerization of the glucocorticoid receptor is not essential for response element binding: activation of the phenylethanolamine N-methyltransferase gene by dimerization-defective mutants. *Mol Endocrinol*, **17,** 2583-2592.

Adcock, I. M. & Lane, S. J. 2003. Corticosteroid-insensitive asthma: molecular mechanisms. *J Endocrinol*, **178,** 347-355.

Ajuebor, M. N., Das, A. M., Virag, L., Flower, R. J., Szabo, C. & Perretti, M. 1999. Role of resident peritoneal macrophages and mast cells in chemokine production and neutrophil migration in acute inflammation: evidence for an inhibitory loop involving endogenous IL-10. *J Immunol*, **162,** 1685-1691.

Alberts, P., Nilsson, C., Selen, G., Engblom, L. O., Edling, N. H., Norling, S., Klingstrom, G., Larsson, C., Forsgren, M., Ashkzari, M., Nilsson, C. E., Fiedler, M., Bergqvist, E., Ohman, B., Bjorkstrand, E. & Abrahmsen, L. B. 2003. Selective inhibition of 11beta-hydroxysteroid dehydrogenase type 1 improves hepatic insulin sensitivity in hyperglycemic mice strains. *Endocrinology*, **144,** 4755-4762.

Albiston, A. L., Obeyesekere, V. R., Smith, R. E. & Krozowski, Z. S. 1994. Cloning and tissue distribution of the human 11beta-hydroxysteroid dehydrogenase type 2 enzyme. *Mol Cell Endocrinol*, **105,** R11-R17.

Alfaidy, N., Xiong, Z. G., Myatt, L., Lye, S. J., MacDonald, J. F. & Challis, J. R. 2001. Prostaglandin F2alpha potentiates cortisol production by stimulating 11beta-hydroxysteroid dehydrogenase 1: a novel feedback loop that may contribute to human labor. *J Clin Endocrinol Metab*, **86,** 5585-5592.

Almawi, W. Y. & Tamim, H. 2001. Posttranscriptional mechanisms of glucocorticoid antiproliferative effects: glucocorticoids inhibit IL-6-induced proliferation of B9 hybridoma cells. *Cell Transplant*, **10,** 161-164.

Andrews, R. C. & Walker, B. R. 1999. Glucocorticoids and insulin resistance: old hormones, new targets. *Clin Sci (Lond)*, **96,** 513-523.

Arcuri, F., Monder, C., Lockwood, C. J. & Schatz, F. 1996. Expression of 11 beta-hydroxysteroid dehydrogenase during decidualization of human endometrial stromal cells. *Endocrinology*, **137,** 595-600.

Asai, K., Funaki, C., Hayashi, T., Yamada, K., Naito, M., Kuzuya, M., Yoshida, F., Yoshimine, N. & Kuzuya, F. 1993. Dexamethasone-induced suppression of aortic atherosclerosis in cholesterol-fed rabbits. Possible mechanisms. *Arterioscler Thromb*, **13,** 892-899.

Ashwell, J. D., Lu, F. W. & Vacchio, M. S. 2000. Glucocorticoids in T cell development and function*. *Annu Rev Immunol*, **18,** 309-345.

Auphan, N., DiDonato, J. A., Rosette, C., Helmberg, A. & Karin, M. 1995. Immunosuppression by glucocorticoids: inhibition of NF-kappa B activity through induction of I kappa B synthesis. *Science*, **270,** 286-290.

Bahr, V., Pfeiffer, A. F. & Diederich, S. 2002. The metabolic syndrome X and peripheral cortisol synthesis. *Exp Clin Endocrinol Diabetes*, **110,** 313-8.

Bartholome, B., Spies, C. M., Gaber, T., Schuchmann, S., Berki, T., Kunkel, D., Bienert, M., Radbruch, A., Burmester, G. R., Lauster, R., Scheffold, A. & Buttgereit, F. 2004. Membrane glucocorticoid receptors (mGCR) are expressed in normal human peripheral blood mononuclear cells and up-regulated after in vitro stimulation and in patients with rheumatoid arthritis. *Faseb J*, **18,** 70-80.

Bauermeister, K., Burger, M., Almanasreh, N., Knopf, H. P., Schumann, R. R., Schollmeyer, P. & Dobos, G. J. 1998. Distinct regulation of IL-8 and MCP-1 by LPS and interferon-gamma-treated human peritoneal macrophages. *Nephrol Dial Transplant*, **13,** 1412-1419.

Berger, J., Tanen, M., Elbrecht, A., Hermanowski-Vosatka, A., Moller, D. E., Wright, S. D. & Thieringer, R. 2001. Peroxisome proliferator-activated receptor-gamma ligands inhibit adipocyte 11beta -hydroxysteroid dehydrogenase type 1 expression and activity. *J Biol Chem*, **276,** 12629-12635.

Bertini, R., Bianchi, M. & Ghezzi, P. 1988. Adrenalectomy sensitizes mice to the lethal effects of interleukin 1 and tumor necrosis factor. *J Exp Med*, **167,** 1708-1712.

Bhattacharyya, S., Brown, D. E., Brewer, J. A., Vogt, S. K. & Muglia, L. J. 2007. Macrophage glucocorticoid receptors regulate Toll-like receptor 4-mediated inflammatory responses by selective inhibition of p38 MAP kinase. *Blood*, **109,** 4313-4319.

Binstadt, B. A., Patel, P. R., Alencar, H., Nigrovic, P. A., Lee, D. M., Mahmood, U., Weissleder, R., Mathis, D. & Benoist, C. 2006. Particularities of the vasculature can promote the organ specificity of autoimmune attack. *Nat Immunol*, **7,** 284-292.

Borish, L. C. & Steinke, J. W. 2003. 2. Cytokines and chemokines. *J Allergy Clin Immunol*, **111,** S460-S475.

Brem, A. S., Bina, R. B., King, T. & Morris, D. J. 1995. Bidirectional activity of 11 beta-hydroxysteroid dehydrogenase in vascular smooth muscle cells. *Steroids*, **60,** 406-410.

Brown, R. W., Chapman, K. E., Kotelevtsev, Y., Yau, J. L., Lindsay, R. S., Brett, L., Leckie, C., Murad, P., Lyons, V., Mullins, J. J., Edwards, C. R. & Seckl, J. R. 1996. Cloning and production of antisera to human placental 11beta-hydroxysteroid dehydrogenase type 2. *Biochem J*, **313 (Pt 3),** 1007-1017.

Bruley, C., Lyons, V., Worsley, A. G., Wilde, M. D., Darlington, G. D., Morton, N. M., Seckl, J. R. & Chapman, K. E. 2006. A novel promoter for the 11beta-hydroxysteroid dehydrogenase type 1 gene is active in lung and is C/EBPalpha independent. *Endocrinology*, **147,** 2879-2885.

Bryndova, J., Zbankova, S., Kment, M. & Pacha, J. 2004. Colitis up-regulates local glucocorticoid activation and down-regulates inactivation in colonic tissue. *Scand J Gastroenterol*, **39,** 549-553.

Bujalska, I. J., Kumar, S., Hewison, M. & Stewart, P. M. 1999. Differentiation of adipose stromal cells: the roles of glucocorticoids and 11beta-hydroxysteroid dehydrogenase. *Endocrinology*, **140,** 3188-96.

Bujalska, I. J., Kumar, S. & Stewart, P. M. 1997. Does central obesity reflect "Cushing's disease of the omentum"? *Lancet*, **349,** 1210-1213.

Chapman, K. E., Coutinho, A., Gray, M., Gilmour, J. S., Savill, J. S. & Seckl, J. R. 2006. Local amplification of glucocorticoids by 11beta-hydroxysteroid dehydrogenase type 1 and its role in the inflammatory response. *Ann N Y Acad Sci*, **1088,** 265-273.

Chapman, K. E. & Seckl, J. R. 2008. 11beta-HSD1, inflammation, metabolic disease and age-related cognitive (dys)function. *Neurochem Res*, **33,** 624-636.

Chesnokova, V. & Melmed, S. 2002. Minireview: Neuro-immuno-endocrine modulation of the hypothalamic-pituitary-adrenal (HPA) axis by gp130 signaling molecules. *Endocrinology*, **143,** 1571-1574.

Clark, A. R. 2007. Anti-inflammatory functions of glucocorticoid-induced genes. *Mol Cell Endocrinol*, **275,** 79-97.

Croxtall, J. D., van Hal, P. T., Choudhury, Q., Gilroy, D. W. & Flower, R. J. 2002. Different glucocorticoids vary in their genomic and non-genomic mechanism of action in A549 cells. *Br J Pharmacol*, **135,** 511-519.

Cupps, T. R., Gerrard, T. L., Falkoff, R. J., Whalen, G. & Fauci, A. S. 1985. Effects of in vitro corticosteroids on B cell activation, proliferation, and differentiation. *J Clin Invest*, **75,** 754-761.

Cutolo, M., Foppiani, L., Prete, C., Ballarino, P., Sulli, A., Villaggio, B., Seriolo, B., Giusti, M. & Accardo, S. 1999. Hypothalamic-pituitary-adrenocortical axis function in premenopausal women with rheumatoid arthritis not treated with glucocorticoids. *J Rheumatol*, **26,** 282-288.

De Kloet, E. R., Sutanto, W., Rots, N., van Haarst, A., van den Berg, D., Oitzl, M., van Eekelen, A. & Voorhuis, D. 1991. Plasticity and function of brain corticosteroid receptors during aging. *Acta Endocrinol (Copenh)*, **125 Suppl 1,** 65-72.

Delgado, M., Pozo, D. & Ganea, D. 2004. The significance of vasoactive intestinal peptide in immunomodulation. *Pharmacol Rev*, **56,** 249-290.

Demoly, P., Basset-Seguin, N., Chanez, P., Campbell, A. M., Gauthier-Rouviere, C., Godard, P., Michel, F. B. & Bousquet, J. 1992. c-fos proto-oncogene expression in bronchial biopsies of asthmatics. *Am J Respir Cell Mol Biol*, **7,** 128-33.

Dunn, J. F., Nisula, B. C. & Rodbard, D. 1981. Transport of steroid hormones: binding of 21 endogenous steroids to both testosterone-binding globulin and corticosteroid-binding globulin in human plasma. *J Clin Endocrinol Metab*, **53,** 58-68.

Edwards, C. R., Stewart, P. M., Burt, D., Brett, L., McIntyre, M. A., Sutanto, W. S., de Kloet, E. R. & Monder, C. 1988. Localisation of 11beta-hydroxysteroid dehydrogenase--tissue specific protector of the mineralocorticoid receptor. *Lancet*, **2,** 986-989.

Eisen, L. P., Elsasser, M. S. & Harmon, J. M. 1988. Positive regulation of the glucocorticoid receptor in human T-cells sensitive to the cytolytic effects of glucocorticoids. *J Biol Chem*, **263,** 12044-12048.

Engeli, S., Bohnke, J., Feldpausch, M., Gorzelniak, K., Heintze, U., Janke, J., Luft, F. C. & Sharma, A. M. 2004. Regulation of 11beta-HSD genes in human adipose tissue: influence of central obesity and weight loss. *Obes Res*, **12,** 9-17.

Erlandsson, A. C., Bladh, L. G., Stierna, P., Yucel-Lindberg, T., Hammarsten, O., Modeer, T., Harmenberg, J. & Wikstrom, A. C. 2002. Herpes simplex virus type 1 infection and glucocorticoid treatment regulate viral yield, glucocorticoid receptor and NF-kappaB levels. *J Endocrinol*, **175,** 165-176.

Finney, R. S. & Somers, G. F. 1958. The antiinflammatory activity of glycyrrhetinic acid and derivatives. *J Pharm Pharmacol*, **10,** 613-620.

Freeman, L., Hewison, M., Hughes, S. V., Evans, K. N., Hardie, D., Means, T. K. & Chakraverty, R. 2005. Expression of 11beta-hydroxysteroid dehydrogenase type 1 permits regulation of glucocorticoid bioavailability by human dendritic cells. *Blood*, **106,** 2042-2049.

Frendl, G. 1992. Interleukin 3: from colony-stimulating factor to pluripotent immunoregulatory cytokine. *Int J Immunopharmacol*, **14,** 421-430.

Funder, J. W. 1997. Glucocorticoid and mineralocorticoid receptors: biology and clinical relevance. *Annu Rev Med*, **48,** 231-240.

Funder, J. W., Pearce, P. T., Smith, R. & Smith, A. I. 1988. Mineralocorticoid action: target tissue specificity is enzyme, not receptor, mediated. *Science*, **242,** 583-585.

Furitsu, T., Saito, H., Dvorak, A. M., Schwartz, L. B., Irani, A. M., Burdick, J. F., Ishizaka, K. & Ishizaka, T. 1989. Development of human mast cells in vitro. *Proc Natl Acad Sci U S A*, **86,** 10039-10043.

Gaillard, D., Wabitsch, M., Pipy, B. & Negrel, R. 1991. Control of terminal differentiation of adipose precursor cells by glucocorticoids. *J Lipid Res*, **32,** 569-579.

Galli, S. J., Kalesnikoff, J., Grimbaldeston, M. A., Piliponsky, A. M., Williams, C. M. & Tsai, M. 2005. Mast cells as "tunable" effector and immunoregulatory cells: recent advances. *Annu Rev Immunol*, **23,** 749-786.

Gelbmann, C. M., Mestermann, S., Gross, V., Kollinger, M., Scholmerich, J. & Falk, W. 1999. Strictures in Crohn's disease are characterised by an accumulation of mast cells colocalised with laminin but not with fibronectin or vitronectin. *Gut*, **45,** 210-217.

Gibbs, B. F., Wierecky, J., Welker, P., Henz, B. M., Wolff, H. H. & Grabbe, J. 2001. Human skin mast cells rapidly release preformed and newly generated TNF-alpha and IL-8 following stimulation with anti-IgE and other secretagogues. *Exp Dermatol*, **10,** 312-320.

Gilmour, J. S., Coutinho, A. E., Cailhier, J. F., Man, T. Y., Clay, M., Thomas, G., Harris, H. J., Mullins, J. J., Seckl, J. R., Savill, J. S. & Chapman, K. E. 2006. Local amplification of glucocorticoids by 11beta-hydroxysteroid dehydrogenase type 1 promotes macrophage phagocytosis of apoptotic leukocytes. *J Immunol*, **176,** 7605-7611.

Gordon, J. R. & Galli, S. J. 1990. Mast cells as a source of both preformed and immunologically inducible TNF-alpha/cachectin. *Nature*, **346,** 274-276.

Gout, J., Tirard, J., Thevenon, C., Riou, J. P., Begeot, M. & Naville, D. 2006. CCAAT/enhancer-binding proteins (C/EBPs) regulate the basal and cAMP-

induced transcription of the human 11beta-hydroxysteroid dehydrogenase encoding gene in adipose cells. *Biochimie*, **88,** 1115-1124.

Grad, I. & Picard, D. 2007. The glucocorticoid responses are shaped by molecular chaperones. *Mol Cell Endocrinol*, **275,** 2-12.

Greenberg, S. & Grinstein, S. 2002. Phagocytosis and innate immunity. *Curr Opin Immunol*, **14,** 136-145.

Grimbaldeston, M. A., Nakae, S., Kalesnikoff, J., Tsai, M. & Galli, S. J. 2007. Mast cell-derived interleukin 10 limits skin pathology in contact dermatitis and chronic irradiation with ultraviolet B. *Nat Immunol*, **8,** 1095-1104.

Guhl, S., Lee, H. H., Babina, M., Henz, B. M. & Zuberbier, T. 2005. Evidence for a restricted rather than generalized stimulatory response of skin-derived human mast cells to substance P. *J Neuroimmunol*, **163,** 92-101.

Hammami, M. M. & Siiteri, P. K. 1991. Regulation of 11 beta-hydroxysteroid dehydrogenase activity in human skin fibroblasts: enzymatic modulation of glucocorticoid action. *J Clin Endocrinol Metab*, **73,** 326-34.

Hammond, G. L., Smith, C. L., Paterson, N. A. & Sibbald, W. J. 1990. A role for corticosteroid-binding globulin in delivery of cortisol to activated neutrophils. *J Clin Endocrinol Metab*, **71,** 34-39.

Hanson, D., Langemo, D., Thompson, P., Anderson, J. & Hunter, S. 2005. Understanding wound fluid and the phases of healing. *Adv Skin Wound Care*, **18,** 360-362.

Hardy, R., Rabbitt, E. H., Filer, A., Emery, P., Hewison, M., Stewart, P. M., Gittoes, N. J., Buckley, C. D., Raza, K. & Cooper, M. S. 2008. Local and systemic glucocorticoid metabolism in inflammatory arthritis. *Ann Rheum Dis*, **67,** 1204-1210.

Harris, H. J., Kotelevtsev, Y., Mullins, J. J., Seckl, J. R. & Holmes, M. C. 2001. Intracellular regeneration of glucocorticoids by 11beta-hydroxysteroid dehydrogenase (11beta-HSD)-1 plays a key role in regulation of the hypothalamic-pituitary-adrenal axis: analysis of 11beta-HSD-1 deficient mice. *Endocrinology*, **142,** 114-120.

He, S. & Walls, A. F. 1998. Human mast cell chymase induces the accumulation of neutrophils, eosinophils and other inflammatory cells in vivo. *Br J Pharmacol*, **125,** 1491-1500.

Heasman, S. J., Giles, K. M., Ward, C., Rossi, A. G., Haslett, C. & Dransfield, I. 2003. Glucocorticoid-mediated regulation of granulocyte apoptosis and macrophage phagocytosis of apoptotic cells: implications for the resolution of inflammation. *J Endocrinol*, **178,** 29-36.

Hench, P. S., Kendall, E. C., Slocumb, C. H. & Polley, H. F. 1949. Adrenocortical Hormone in Arthritis : Preliminary Report. *Ann Rheum Dis*, **8,** 97-104.

Hermanowski-Vosatka, A., Balkovec, J. M., Cheng, K., Chen, H. Y., Hernandez, M., Koo, G. C., Le Grand, C. B., Li, Z., Metzger, J. M., Mundt, S. S., Noonan, H., Nunes, C. N., Olson, S. H., Pikounis, B., Ren, N., Robertson, N., Schaeffer, J. M., Shah, K., Springer, M. S., Strack, A. M., Strowski, M., Wu, K., Wu, T., Xiao, J., Zhang, B. B., Wright, S. D. & Thieringer, R. 2005. 11beta-HSD1

inhibition ameliorates metabolic syndrome and prevents progression of atherosclerosis in mice. *J Exp Med*, **202,** 517-527.

Hermanowski-Vosatka, A., Gerhold, D., Mundt, S. S., Loving, V. A., Lu, M., Chen, Y., Elbrecht, A., Wu, M., Doebber, T., Kelly, L., Milot, D., Guo, Q., Wang, P. R., Ippolito, M., Chao, Y. S., Wright, S. D. & Thieringer, R. 2000. PPARalpha agonists reduce 11beta-hydroxysteroid dehydrogenase type 1 in the liver. *Biochem Biophys Res Commun*, **279,** 330-336.

Hochberg, Z., Friedberg, M., Yaniv, L., Bader, T. & Tiosano, D. 2004. Hypothalamic regulation of adiposity: the role of 11beta-hydroxysteroid dehydrogenase type 1. *Horm Metab Res*, **36,** 365-369.

Hogaboam, C., Kunkel, S. L., Strieter, R. M., Taub, D. D., Lincoln, P., Standiford, T. J. & Lukacs, N. W. 1998. Novel role of transmembrane SCF for mast cell activation and eotaxin production in mast cell-fibroblast interactions. *J Immunol*, **160,** 6166-6171.

Holmes, M. C., Abrahamsen, C. T., French, K. L., Paterson, J. M., Mullins, J. J. & Seckl, J. R. 2006. The mother or the fetus? 11beta-hydroxysteroid dehydrogenase type 2 null mice provide evidence for direct fetal programming of behavior by endogenous glucocorticoids. *J Neurosci*, **26,** 3840-3844.

Horrocks, P. M., Jones, A. F., Ratcliffe, W. A., Holder, G., White, A., Holder, R., Ratcliffe, J. G. & London, D. R. 1990. Patterns of ACTH and cortisol pulsatility over twenty-four hours in normal males and females. *Clin Endocrinol (Oxf)*, **32,** 127-134.

Hu, Z. Q., Zhao, W. H. & Shimamura, T. 2007. Regulation of mast cell development by inflammatory factors. *Curr Med Chem*, **14,** 3044-3050.

Iemura, A., Tsai, M., Ando, A., Wershil, B. K. & Galli, S. J. 1994. The c-kit ligand, stem cell factor, promotes mast cell survival by suppressing apoptosis. *Am J Pathol*, **144,** 321-328.

Ito, K., Barnes, P. J. & Adcock, I. M. 2000. Glucocorticoid receptor recruitment of histone deacetylase 2 inhibits interleukin-1beta-induced histone H4 acetylation on lysines 8 and 12. *Mol Cell Biol*, **20,** 6891-6903.

Jamieson, P. M., Chapman, K. E., Edwards, C. R. & Seckl, J. R. 1995. 11beta-hydroxysteroid dehydrogenase is an exclusive 11beta-reductase in primary cultures of rat hepatocytes: effect of physicochemical and hormonal manipulations. *Endocrinology*, **136,** 4754-4761.

Jamieson, P. M., Chapman, K. E. & Seckl, J. R. 1999. Tissue- and temporal-specific regulation of 11beta-hydroxysteroid dehydrogenase type 1 by glucocorticoids in vivo. *J Steroid Biochem Mol Biol*, **68,** 245-250.

Jamieson, P. M., Walker, B. R., Chapman, K. E., Andrew, R., Rossiter, S. & Seckl, J. R. 2000. 11 beta-hydroxysteroid dehydrogenase type 1 is a predominant 11beta-reductase in the intact perfused rat liver. *J Endocrinol*, **165,** 685-692.

Jellinck, P. H., Dhabhar, F. S., Sakai, R. R. & McEwen, B. S. 1997. Long-term corticosteroid treatment but not chronic stress affects 11beta-hydroxysteroid dehydrogenase type I activity in rat brain and peripheral tissues. *J Steroid Biochem Mol Biol*, **60,** 319-323.

Jonsson, H., Allen, P. & Peng, S. L. 2005. Inflammatory arthritis requires Foxo3a to prevent Fas ligand-induced neutrophil apoptosis. *Nat Med*, **11,** 666-671.

Kanwar, S. & Kubes, P. 1994. Ischemia/reperfusion-induced granulocyte influx is a multistep process mediated by mast cells. *Microcirculation*, **1,** 175-182.

Kassel, O. & Cato, A. C. 2002. Mast cells as targets for glucocorticoids in the treatment of allergic disorders. *Ernst Schering Res Found Workshop***,** 153-176.

Kiener, H. P., Baghestanian, M., Dominkus, M., Walchshofer, S., Ghannadan, M., Willheim, M., Sillaber, C., Graninger, W. B., Smolen, J. S. & Valent, P. 1998. Expression of the C5a receptor (CD88) on synovial mast cells in patients with rheumatoid arthritis. *Arthritis Rheum*, **41,** 233-45.

Kolaczkowska, E., Seljelid, R. & Plytycz, B. 2001. Critical role of mast cells in morphine-mediated impairment of zymosan-induced peritonitis in mice. *Inflamm Res*, **50,** 415-421.

Kolaczkowska, E., Shahzidi, S., Seljelid, R., van Rooijen, N. & Plytycz, B. 2002. Early vascular permeability in murine experimental peritonitis is co-mediated by resident peritoneal macrophages and mast cells: crucial involvement of macrophage-derived cysteinyl-leukotrienes. *Inflammation*, **26,** 61-71.

Kotelevtsev, Y., Brown, R. W., Fleming, S., Kenyon, C., Edwards, C. R., Seckl, J. R. & Mullins, J. J. 1999. Hypertension in mice lacking 11beta-hydroxysteroid dehydrogenase type 2. *J Clin Invest*, **103,** 683-689.

Kotelevtsev, Y., Holmes, M. C., Burchell, A., Houston, P. M., Schmoll, D., Jamieson, P., Best, R., Brown, R., Edwards, C. R., Seckl, J. R. & Mullins, J. J. 1997. 11beta-hydroxysteroid dehydrogenase type 1 knockout mice show attenuated glucocorticoid-inducible responses and resist hyperglycemia on obesity or stress. *Proc Natl Acad Sci U S A*, **94,** 14924-14929.

Lakshmi, V. & Monder, C. 1988. Purification and characterization of the corticosteroid 11beta-dehydrogenase component of the rat liver 11beta-hydroxysteroid dehydrogenase complex. *Endocrinology*, **123,** 2390-2398.

Lechner, O., Hu, Y., Jafarian-Tehrani, M., Dietrich, H., Schwarz, S., Herold, M., Haour, F. & Wick, G. 1996. Disturbed immunoendocrine communication via the hypothalamo-pituitary-adrenal axis in murine lupus. *Brain Behav Immun*, **10,** 337-350.

Lee, D. M., Friend, D. S., Gurish, M. F., Benoist, C., Mathis, D. & Brenner, M. B. 2002. Mast cells: a cellular link between autoantibodies and inflammatory arthritis. *Science*, **297,** 1689-1692.

Lewis, S. & Holmes, C. 1991. Host defense mechanisms in the peritoneal cavity of continuous ambulatory peritoneal dialysis patients. 1. *Perit Dial Int*, **11,** 14-21.

Lindholm, J. 2000. Cushing's syndrome: historical aspects. *Pituitary*, **3,** 97-104.

Liu, Y. Q., Cousin, J. M., Hughes, J., VanDamme, J., Seckl, J. R., Haslett, C., Dransfield, I., Savill, J. & Rossi, A. G. 1999. Glucocorticoids promote nonphlogistic phagocytosis of apoptotic leukocytes. *J Immunol*, **162,** 3639-3646.

Livingstone, D. E., Jones, G. C., Smith, K., Jamieson, P. M., Andrew, R., Kenyon, C. J. & Walker, B. R. 2000. Understanding the role of glucocorticoids in obesity: tissue-specific alterations of corticosterone metabolism in obese Zucker rats. *Endocrinology*, **141,** 560-563.

Loghmani, F., Mohammed, K. A., Nasreen, N., Van Horn, R. D., Hardwick, J. A., Sanders, K. L. & Antony, V. B. 2002. Inflammatory cytokines mediate C-C (monocyte chemotactic protein 1) and C-X-C (interleukin 8) chemokine expression in human pleural fibroblasts. *Inflammation*, **26,** 73-82.

Low, S. C., Chapman, K. E., Edwards, C. R. & Seckl, J. R. 1994a. 'Liver-type' 11beta-hydroxysteroid dehydrogenase cDNA encodes reductase but not dehydrogenase activity in intact mammalian COS-7 cells. *J Mol Endocrinol*, **13,** 167-174.

Low, S. C., Chapman, K. E., Edwards, C. R., Wells, T., Robinson, I. C. & Seckl, J. R. 1994b. Sexual dimorphism of hepatic 11 beta-hydroxysteroid dehydrogenase in the rat: the role of growth hormone patterns. *J Endocrinol*, **143,** 541-548.

Marshall, J. S. & Jawdat, D. M. 2004. Mast cells in innate immunity. *J Allergy Clin Immunol*, **114,** 21-27.

Masuzaki, H., Paterson, J., Shinyama, H., Morton, N. M., Mullins, J. J., Seckl, J. R. & Flier, J. S. 2001. A transgenic model of visceral obesity and the metabolic syndrome. *Science*, **294,** 2166-2170.

Masuzaki, H., Yamamoto, H., Kenyon, C. J., Elmquist, J. K., Morton, N. M., Paterson, J. M., Shinyama, H., Sharp, M. G., Fleming, S., Mullins, J. J., Seckl, J. R. & Flier, J. S. 2003. Transgenic amplification of glucocorticoid action in adipose tissue causes high blood pressure in mice. *J Clin Invest*, **112,** 83-90.

Matyszak, M. K., Citterio, S., Rescigno, M. & Ricciardi-Castagnoli, P. 2000. Differential effects of corticosteroids during different stages of dendritic cell maturation. *Eur J Immunol*, **30,** 1233-1242.

McEwen, B. S., Biron, C. A., Brunson, K. W., Bulloch, K., Chambers, W. H., Dhabhar, F. S., Goldfarb, R. H., Kitson, R. P., Miller, A. H., Spencer, R. L. & Weiss, J. M. 1997. The role of adrenocorticoids as modulators of immune function in health and disease: neural, endocrine and immune interactions. *Brain Res Rev*, **23,** 79-133.

Meagher, L. C., Savill, J. S., Baker, A., Fuller, R. W. & Haslett, C. 1992. Phagocytosis of apoptotic neutrophils does not induce macrophage release of thromboxane B2. *J Leukoc Biol*, **52,** 269-273.

Mekori, Y. A., Oh, C. K. & Metcalfe, D. D. 1993. IL-3-dependent murine mast cells undergo apoptosis on removal of IL-3. Prevention of apoptosis by c-kit ligand. *J Immunol*, **151,** 3775-3784.

Metcalfe, D. D., Baram, D. & Mekori, Y. A. 1997. Mast cells. *Physiol Rev*, **77,** 1033-79.

Miller, A. H., Spencer, R. L., Pearce, B. D., Pisell, T. L., Azrieli, Y., Tanapat, P., Moday, H., Rhee, R. & McEwen, B. S. 1998. Glucocorticoid receptors are differentially expressed in the cells and tissues of the immune system. *Cell Immunol*, **186,** 45-54.

Moisan, M. P., Edwards, C. R. & Seckl, J. R. 1992. Differential promoter usage by the rat 11beta-hydroxysteroid dehydrogenase gene. *Mol Endocrinol*, **6,** 1082-1087.

Moisan, M. P., Seckl, J. R. & Edwards, C. R. 1990. 11beta-hydroxysteroid dehydrogenase bioactivity and messenger RNA expression in rat forebrain: localization in hypothalamus, hippocampus, and cortex. *Endocrinology*, **127,** 1450-1455.

Morton, N. M., Holmes, M. C., Fievet, C., Staels, B., Tailleux, A., Mullins, J. J. & Seckl, J. R. 2001. Improved lipid and lipoprotein profile, hepatic insulin sensitivity, and glucose tolerance in 11beta-hydroxysteroid dehydrogenase type 1 null mice. *J Biol Chem*, **276,** 41293-41300.

Morton, N. M., Ramage, L. & Seckl, J. R. 2004. Down-regulation of adipose 11beta-hydroxysteroid dehydrogenase type 1 by high-fat feeding in mice: a potential adaptive mechanism counteracting metabolic disease. *Endocrinology*, **145,** 2707-2712.

Mountjoy, K. G. & Wong, J. 1997. Obesity, diabetes and functions for proopiomelanocortin-derived peptides. *Mol Cell Endocrinol*, **128,** 171-177.

Munck, A., Guyre, P. M. & Holbrook, N. J. 1984. Physiological functions of glucocorticoids in stress and their relation to pharmacological actions. *Endocr Rev*, **5,** 25-44.

Mune, T., Rogerson, F. M., Nikkila, H., Agarwal, A. K. & White, P. C. 1995. Human hypertension caused by mutations in the kidney isozyme of 11 beta-hydroxysteroid dehydrogenase. *Nat Genet*, **10,** 394-399.

Nagle, D. L., Kozak, C. A., Mano, H., Chapman, V. M. & Bucan, M. 1995. Physical mapping of the Tec and Gabrb1 loci reveals that the Wsh mutation on mouse chromosome 5 is associated with an inversion. *Hum Mol Genet*, **4,** 2073-2079.

Nakagawa, M., Terashima, T., D'Yachkova, Y., Bondy, G. P., Hogg, J. C. & van Eeden, S. F. 1998. Glucocorticoid-induced granulocytosis: contribution of marrow release and demargination of intravascular granulocytes. *Circulation*, **98,** 2307-2313.

Necela, B. M. & Cidlowski, J. A. 2004. Mechanisms of glucocorticoid receptor action in noninflammatory and inflammatory cells. *Proc Am Thorac Soc*, **1,** 239-246.

Neeck, G., Federlin, K., Graef, V., Rusch, D. & Schmidt, K. L. 1990. Adrenal secretion of cortisol in patients with rheumatoid arthritis. *J Rheumatol*, **17,** 24-29.

Odermatt, A. & Atanasov, A. G. 2009. Mineralocorticoid receptors: Emerging complexity and functional diversity. *Steroids*, **74,** 163-171.

Olsson, N., Ulfgren, A. K. & Nilsson, G. 2001. Demonstration of mast cell chemotactic activity in synovial fluid from rheumatoid patients. *Ann Rheum Dis*, **60,** 187-93.

Payne, V. A., Au, W. S., Gray, S. L., Nora, E. D., Rahman, S. M., Sanders, R., Hadaschik, D., Friedman, J. E., O'Rahilly, S. & Rochford, J. J. 2007. Sequential regulation of diacylglycerol acyltransferase 2 expression by CAAT/enhancer-binding protein beta (C/EBPbeta) and C/EBPalpha during adipogenesis. *J Biol Chem*, **282,** 21005-21014.

Poli, V. 1998. The role of C/EBP isoforms in the control of inflammatory and native immunity functions. *J Biol Chem*, **273,** 29279-29282.

Pompei, R., Flore, O., Marccialis, M. A., Pani, A. & Loddo, B. 1979. Glycyrrhizic acid inhibits virus growth and inactivates virus particles. *Nature*, **281,** 689-690.

Poon, M., Gertz, S. D., Fallon, J. T., Wiegman, P., Berman, J. W., Sarembock, I. J. & Taubman, M. B. 2001. Dexamethasone inhibits macrophage accumulation after balloon arterial injury in cholesterol fed rabbits. *Atherosclerosis*, **155,** 371-380.

Pratt, W. B. & Toft, D. O. 1997. Steroid receptor interactions with heat shock protein and immunophilin chaperones. *Endocr Rev*, **18,** 306-360.

Qureshi, R. & Jakschik, B. A. 1988. The role of mast cells in thioglycollate-induced inflammation. *J Immunol*, **141,** 2090-2096.

Rajan, V., Edwards, C. R. & Seckl, J. R. 1996. 11beta-Hydroxysteroid dehydrogenase in cultured hippocampal cells reactivates inert 11-dehydrocorticosterone, potentiating neurotoxicity. *J Neurosci*, **16,** 65-70.

Rask, E., Olsson, T., Soderberg, S., Andrew, R., Livingstone, D. E., Johnson, O. & Walker, B. R. 2001. Tissue-specific dysregulation of cortisol metabolism in human obesity. *J Clin Endocrinol Metab*, **86,** 1418-1421.

Razin, E., Ihle, J. N., Seldin, D., Mencia-Huerta, J. M., Katz, H. R., LeBlanc, P. A., Hein, A., Caulfield, J. P., Austen, K. F. & Stevens, R. L. 1984. Interleukin 3: A differentiation and growth factor for the mouse mast cell that contains chondroitin sulfate E proteoglycan. *J Immunol*, **132,** 1479-1486.

Reichardt, H. M., Umland, T., Bauer, A., Kretz, O. & Schutz, G. 2000. Mice with an increased glucocorticoid receptor gene dosage show enhanced resistance to stress and endotoxic shock. *Mol Cell Biol*, **20,** 9009-9017.

Reul, J. M. & de Kloet, E. R. 1985. Two receptor systems for corticosterone in rat brain: microdistribution and differential occupation. *Endocrinology*, **117,** 2505-2511.

Reul, J. M., Pearce, P. T., Funder, J. W. & Krozowski, Z. S. 1989. Type I and type II corticosteroid receptor gene expression in the rat: effect of adrenalectomy and dexamethasone administration. *Mol Endocrinol*, **3,** 1674-1680.

Reynolds, D. S., Stevens, R. L., Lane, W. S., Carr, M. H., Austen, K. F. & Serafin, W. E. 1990. Different mouse mast cell populations express various combinations of at least six distinct mast cell serine proteases. *Proc Natl Acad Sci U S A*, **87,** 3230-3234.

Robson, A. C., Leckie, C. M., Seckl, J. R. & Holmes, M. C. 1998. 11Beta-hydroxysteroid dehydrogenase type 2 in the postnatal and adult rat brain. *Brain Res Mol Brain Res*, **61,** 1-10.

Roland, B. L., Li, K. X. & Funder, J. W. 1995. Hybridization histochemical localization of 11beta-hydroxysteroid dehydrogenase type 2 in rat brain. *Endocrinology*, **136,** 4697-4700.

Sai, S., Esteves, C. L., Kelly, V., Michailidou, Z., Anderson, K., Coll, A. P., Nakagawa, Y., Ohzeki, T., Seckl, J. R. & Chapman, K. E. 2008. Glucocorticoid regulation of the promoter of 11beta-hydroxysteroid dehydrogenase type 1 is indirect and requires CCAAT/enhancer-binding protein-beta. *Mol Endocrinol*, **22,** 2049-2060.

Salata, R. A., Jarrett, D. B., Verbalis, J. G. & Robinson, A. G. 1988. Vasopressin stimulation of adrenocorticotropin hormone (ACTH) in humans. In vivo bioassay of corticotropin-releasing factor (CRF) which provides evidence for CRF mediation of the diurnal rhythm of ACTH. *J Clin Invest*, **81,** 766-774.

Sapolsky, R. M., Romero, L. M. & Munck, A. U. 2000. How do glucocorticoids influence stress responses? Integrating permissive, suppressive, stimulatory, and preparative actions. *Endocr Rev*, **21,** 55-89.

Savill, J., Dransfield, I., Gregory, C. & Haslett, C. 2002. A blast from the past: clearance of apoptotic cells regulates immune responses. *Nat Rev Immunol*, **2,** 965-975.

Savill, J. S., Wyllie, A. H., Henson, J. E., Walport, M. J., Henson, P. M. & Haslett, C. 1989. Macrophage phagocytosis of aging neutrophils in inflammation. Programmed cell death in the neutrophil leads to its recognition by macrophages. *J Clin Invest*, **83,** 865-875.

Scheinman, R. I., Cogswell, P. C., Lofquist, A. K. & Baldwin, A. S., Jr. 1995. Role of transcriptional activation of I kappa B alpha in mediation of immunosuppression by glucocorticoids. *Science*, **270,** 283-286.

Schmidt, M., Weidler, C., Naumann, H., Anders, S., Scholmerich, J. & Straub, R. H. 2005. Reduced capacity for the reactivation of glucocorticoids in rheumatoid arthritis synovial cells: possible role of the sympathetic nervous system? *Arthritis Rheum*, **52,** 1711-1720.

Schneider, J., Bruckmann, W. & Zwingenberger, K. 1997. Extravasation of leukocytes assessed by intravital microscopy: effect of thalidomide. *Inflamm Res*, **46,** 392-397.

Schobitz, B., Van Den Dobbelsteen, M., Holsboer, F., Sutanto, W. & De Kloet, E. R. 1993. Regulation of interleukin 6 gene expression in rat. *Endocrinology*, **132,** 1569-1576.

Schramm, R., Schaefer, T., Menger, M. D. & Thorlacius, H. 2002. Acute mast cell-dependent neutrophil recruitment in the skin is mediated by KC and LFA-1: inhibitory mechanisms of dexamethasone. *J Leukoc Biol*, **72,** 1122-1132.

Seckl, J. R. 2004. 11®-hydroxysteroid dehydrogenases: changing glucocorticoid action. *Curr Opin Pharmacol*, **4,** 597-602.

Seckl, J. R., Morton, N. M., Chapman, K. E. & Walker, B. R. 2004. Glucocorticoids and 11beta-hydroxysteroid dehydrogenase in adipose tissue. *Recent Prog Horm Res*, **59,** 359-393.

Serhan, C. N. & Savill, J. 2005. Resolution of inflammation: the beginning programs the end. *Nat Immunol*, **6,** 1191-1197.

Stern, M., Meagher, L., Savill, J. & Haslett, C. 1992. Apoptosis in human eosinophils. Programmed cell death in the eosinophil leads to phagocytosis by macrophages and is modulated by IL-5. *J Immunol*, **148,** 3543-3549.

Sternberg, E. M. 2006. Neural regulation of innate immunity: a coordinated nonspecific host response to pathogens. *Nat Rev Immunol*, **6,** 318-328.

Stevens, R. L., Friend, D. S., McNeil, H. P., Schiller, V., Ghildyal, N. & Austen, K. F. 1994. Strain-specific and tissue-specific expression of mouse mast cell secretory granule proteases. *Proc Natl Acad Sci U S A*, **91,** 128-132.

Stewart, P. M. & Krozowski, Z. S. 1999. 11beta-Hydroxysteroid dehydrogenase. *Vitam Horm*, **57,** 249-324.

Stewart, P. M. & Tomlinson, J. W. 2002. Cortisol, 11 beta-hydroxysteroid dehydrogenase type 1 and central obesity. *Trends Endocrinol Metab*, **13,** 94-96.

Sun, K., Yang, K. & Challis, J. R. 1997. Differential regulation of 11beta-hydroxysteroid dehydrogenase type 1 and 2 by nitric oxide in cultured human placental trophoblast and chorionic cell preparation. *Endocrinology*, **138,** 4912-4920.

Sylvestre, D. L. & Ravetch, J. V. 1996. A dominant role for mast cell Fc receptors in the Arthus reaction. *Immunity*, **5,** 387-390.

Tailor, A., Tomlinson, A., Salas, A., Panes, J., Granger, D. N., Flower, R. J. & Perretti, M. 1999. Dexamethasone inhibition of leucocyte adhesion to rat mesenteric postcapillary venules: role of intercellular adhesion molecule 1 and KC. *Gut*, **45,** 705-712.

Teelucksingh, S., Mackie, A. D., Burt, D., McIntyre, M. A., Brett, L. & Edwards, C. R. 1990. Potentiation of hydrocortisone activity in skin by glycyrrhetinic acid. *Lancet*, **335,** 1060-1063.

Thieringer, R., Le Grand, C. B., Carbin, L., Cai, T. Q., Wong, B., Wright, S. D. & Hermanowski-Vosatka, A. 2001. 11 Beta-hydroxysteroid dehydrogenase type 1 is induced in human monocytes upon differentiation to macrophages. *J Immunol*, **167,** 30-35.

Tonko, M., Ausserlechner, M. J., Bernhard, D., Helmberg, A. & Kofler, R. 2001. Gene expression profiles of proliferating vs. G1/G0 arrested human leukemia cells suggest a mechanism for glucocorticoid-induced apoptosis. *Faseb J*, **15,** 693-699.

Topley, N., Mackenzie, R., Jorres, A., Coles, G. A., Davies, M. & Williams, J. D. 1993. Cytokine networks in continuous ambulatory peritoneal dialysis: interactions of resident cells during inflammation in the peritoneal cavity. *Perit Dial Int*, **13 Suppl 2,** S282-S285.

Topley, N., Petersen, M. M., Mackenzie, R., Neubauer, A., Stylianou, E., Kaever, V., Davies, M., Coles, G. A., Jorres, A. & Williams, J. D. 1994. Human peritoneal mesothelial cell prostaglandin synthesis: induction of cyclooxygenase mRNA by peritoneal macrophage-derived cytokines. *Kidney Int*, **46,** 900-909.

Turner, H. & Kinet, J. P. 1999. Signalling through the high-affinity IgE receptor Fc epsilonRI. *Nature*, **402,** B24-B30.

Vagnerova, K., Kverka, M., Klusonova, P., Ergang, P., Miksik, I., Tlaskalova-Hogenova, H. & Pacha, J. 2006. Intestinal inflammation modulates expression of 11beta-hydroxysteroid dehydrogenase in murine gut. *J Endocrinol*, **191,** 497-503.

Vale, W., Spiess, J., Rivier, C. & Rivier, J. 1981. Characterization of a 41-residue ovine hypothalamic peptide that stimulates secretion of corticotropin and beta-endorphin. *Science*, **213,** 1394-1397.

Voice, M. W., Seckl, J. R., Edwards, C. R. & Chapman, K. E. 1996. 11 beta-hydroxysteroid dehydrogenase type 1 expression in 2S FAZA hepatoma cells is hormonally regulated: a model system for the study of hepatic glucocorticoid metabolism. *Biochem J*, **317 (Pt 2),** 621-5.

Wang, S. J., Birtles, S., de Schoolmeester, J., Swales, J., Moody, G., Hislop, D., O'Dowd, J., Smith, D. M., Turnbull, A. V. & Arch, J. R. 2006. Inhibition of 11beta-hydroxysteroid dehydrogenase type 1 reduces food intake and weight gain but maintains energy expenditure in diet-induced obese mice. *Diabetologia*, **49,** 1333-1337.

Whorwood, C. B., Donovan, S. J., Wood, P. J. & Phillips, D. I. 2001. Regulation of glucocorticoid receptor alpha and beta isoforms and type I 11beta-hydroxysteroid

dehydrogenase expression in human skeletal muscle cells: a key role in the pathogenesis of insulin resistance? *J Clin Endocrinol Metab*, **86,** 2296-308.

Whorwood, C. B., Sheppard, M. C. & Stewart, P. M. 1993. Tissue specific effects of thyroid hormone on 11 beta-hydroxysteroid dehydrogenase gene expression. *J Steroid Biochem Mol Biol*, **46,** 539-547.

Williams, L. J., Lyons, V., MacLeod, I., Rajan, V., Darlington, G. J., Poli, V., Seckl, J. R. & Chapman, K. E. 2000. C/EBP regulates hepatic transcription of 11beta - hydroxysteroid dehydrogenase type 1. A novel mechanism for cross-talk between the C/EBP and glucocorticoid signaling pathways. *J Biol Chem*, **275,** 30232-30239.

Witowski, J., Thiel, A., Dechend, R., Dunkel, K., Fouquet, N., Bender, T. O., Langrehr, J. M., Gahl, G. M., Frei, U. & Jorres, A. 2001. Synthesis of C-X-C and C-C chemokines by human peritoneal fibroblasts: induction by macrophage-derived cytokines. *Am J Pathol*, **158,** 1441-1450.

Woolley, D. E. 2003. The mast cell in inflammatory arthritis. *N Engl J Med*, **348,** 1709-1711.

Wu, Z., Rosen, E. D., Brun, R., Hauser, S., Adelmant, G., Troy, A. E., McKeon, C., Darlington, G. J. & Spiegelman, B. M. 1999. Cross-regulation of C/EBP alpha and PPAR gamma controls the transcriptional pathway of adipogenesis and insulin sensitivity. *Mol Cell*, **3,** 151-158.

Yang, Z., Guo, C., Zhu, P., Li, W., Myatt, L. & Sun, K. 2007. Role of glucocorticoid receptor and CCAAT/enhancer-binding protein alpha in the feed-forward induction of 11beta-hydroxysteroid dehydrogenase type 1 expression by cortisol in human amnion fibroblasts. *J Endocrinol*, **195,** 241-253.

Yau, J. L., McNair, K. M., Noble, J., Brownstein, D., Hibberd, C., Morton, N., Mullins, J. J., Morris, R. G., Cobb, S. & Seckl, J. R. 2007. Enhanced hippocampal long-term potentiation and spatial learning in aged 11beta-hydroxysteroid dehydrogenase type 1 knock-out mice. *J Neurosci*, **27,** 10487-10496.

Yau, J. L., Noble, J., Kenyon, C. J., Hibberd, C., Kotelevtsev, Y., Mullins, J. J. & Seckl, J. R. 2001. Lack of tissue glucocorticoid reactivation in 11®-hydroxysteroid dehydrogenase type 1 knockout mice ameliorates age-related learning impairments. *Proc Natl Acad Sci U S A*, **98,** 4716-4721.

Yeager, M. P., Guyre, P. M. & Munck, A. U. 2004. Glucocorticoid regulation of the inflammatory response to injury. *Acta Anaesthesiol Scand*, **48,** 799-813.

Zbankova, S., Bryndova, J., Leden, P., Kment, M., Svec, A. & Pacha, J. 2007. 11beta-hydroxysteroid dehydrogenase 1 and 2 expression in colon from patients with ulcerative colitis. *J Gastroenterol Hepatol*, **22,** 1019-1023.

Zhang, N., Truong-Tran, Q. A., Tancowny, B., Harris, K. E. & Schleimer, R. P. 2007. Glucocorticoids enhance or spare innate immunity: effects in airway epithelium are mediated by CCAAT/enhancer binding proteins. *J Immunol*, **179,** 578-589.

Zhang, T. Y. & Daynes, R. A. 2007. Macrophages from 11beta-hydroxysteroid dehydrogenase type 1-deficient mice exhibit an increased sensitivity to lipopolysaccharide stimulation due to TGF-beta-mediated up-regulation of SHIP1 expression. *J Immunol*, **179,** 6325-6335.

Zhang, T. Y., Ding, X. & Daynes, R. A. 2005. The expression of 11beta-hydroxysteroid dehydrogenase type I by lymphocytes provides a novel means for intracrine regulation of glucocorticoid activities. *J Immunol*, **174,** 879-889.

Zhang, X., Moilanen, E. & Kankaanranta, H. 2001. Beclomethasone, budesonide and fluticasone propionate inhibit human neutrophil apoptosis. *Eur J Pharmacol*, **431,** 365-371.

Appendix I

Summary of flow cytometric assessment of immune cells from BMT/arthritis experiment

Appendix I 1.1 Flow cytometric analysis of immune cells following BMT and K/BxN arthritis

At the end of the BMT-arthritis experiment, cells recovered from the thymus, peritoneum, spleen and BM were assessed by flow cytometry (described for untreated mice in Chapter 6, Section 6.2.3), using similar antibody panel (listed in Chapter 6, Section 6.2.2.). In the thymus, there was no difference in the ratio of $CD4^+$ and $CD8^+$ cells in any of the groups (Appendix I, Table 1). Flow cytometric analysis did reveal some differences in cell staining between various groups as described bellow:

In normal *Hsd11b1*$^{-/-}$ and *Hsd11b1*$^{+/+}$ mice, subjected to arthritis, differences were noted in spleen (particularly severe deficiency in $CD45^+$ cells in *Hsd11b1*$^{-/-}$ in comparison to *Hsd11b1*$^{+/+}$ mice) and BM cell distribution (Appendix I, Table 2). However, due to small group sizes (n=3/genotype) definite conclusions cannot be made. No differences were found in peritoneal cells (data not shown) between *Hsd11b1*$^{-/-}$ and *Hsd11b1*$^{+/+}$ mice following arthritis, although, large within-group variability and small group size prevented conclusive results.

In mice subjected to BMT but not arthritis, flow cytometric analysis did not reveal significant differences between WT(KO) and KO(WT) groups in any of the tissues (data not shown), although there appeared to be a higher percent of c-kit^+ BM cells in KO(WT) (3.6%±0.1) than in WT(KO) mice (2.6%±0.2) ($p=0.05$), with very small variability within-groups. However, as there were only two mice per group, definite conclusions cannot be made.

Flow cytometry assessment of cells from mice in the BMT-arthritis groups showed most differences in staining between mice in WT(KO) and KO(WT) groups in cells from BM; WT(KO) mice had a lower percent of $CD45^+$ cells, and a higher percent of Lin^+ and c-kit^+ cells in the BM than KO(WT) mice (Appendix I, Figure 1.1). No differences between the two groups were seen in cells isolated from the peritoneum or spleen (Appendix I, Table 3).

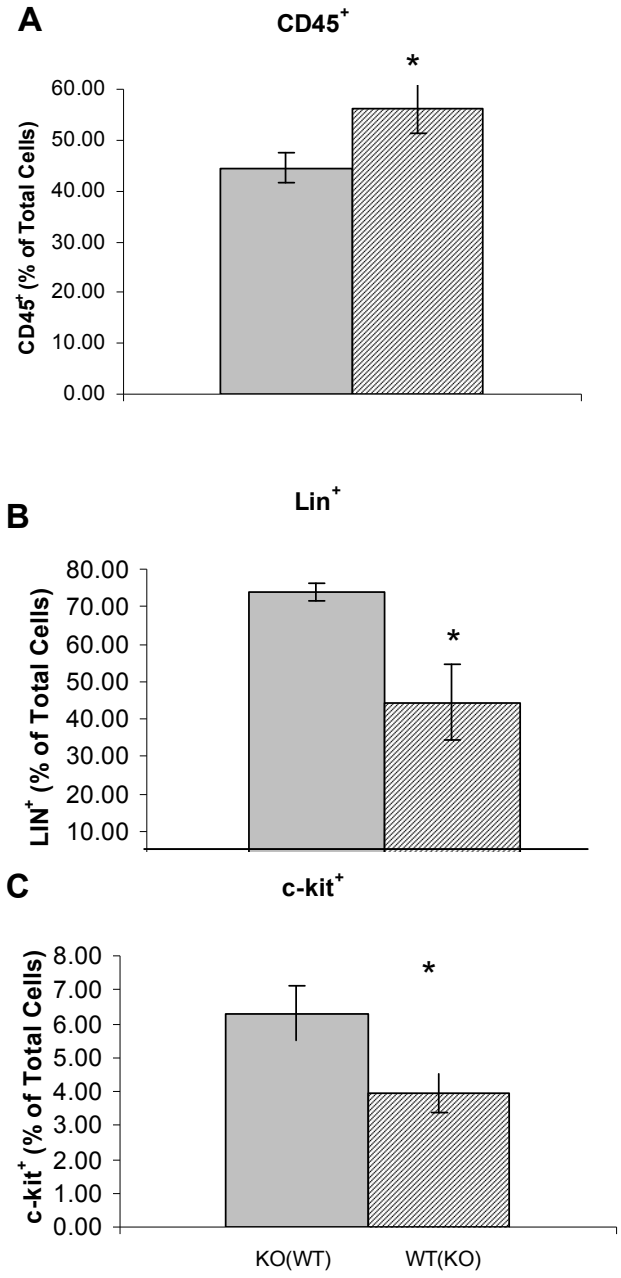

Appendix I, Figure 1.1 Altered cell markers in cells from BM in BMT-arthritis mice.

Flow cytometry analysis showed less $CD45^+$ cells (A) and more Lin^+ cells (B) and c-kit^+ (C) cells in BM of KO(WT) (grey bars; n=5) than WT(KO) (hatched lines; n=7) mice. Values shown are mean ± SEM. * $p<0.05$ when compared by unpaired Student's t-test.

Appendix I, Table 1. Flow cytometry analysis of $CD4^+$ and $CD8^+$ cells in the thymus from all BMT/arthritis experimental groups.

Thymocytes	Group	Mean			T-test
$CD8^+/CD4^-$	WT(KO) + arthritis, n=7	2.8	±	0.6	*p>0.05*
	KO(WT) + arthritis, n=5	3.3	±	1.1	
$CD8^+/CD4^+$	WT(KO) + arthritis, n=7	86.2	±	1.3	*p>0.05*
	KO(WT) + arthritis, n=5	76.8	±	13.3	
$CD8^-/CD4^-$	WT(KO) + arthritis, n=7	2.0	±	0.5	*p>0.05*
	KO(WT) + arthritis, n=5	5.0	±	3.4	
$CD8^-/CD4^+$	WT(KO) + arthritis, n=7	9.0	±	0.4	*p>0.05*
	KO(WT) + arthritis, n=5	14.9	±	9.1	

Thymocytes	Group	Mean			T-test
$CD8^+/CD4^-$	*$Hsd11b1^{-/-}$* + arthritis, n=3	5.4	±	0.8	*p>0.05*
	$Hsd11b1^{+/+}$ + arthritis, n=3	5.7	±	0.8	
$CD8^+/CD4^+$	*$Hsd11b1^{-/-}$* + arthritis, n=3	71.3	±	1.5	*p>0.05*
	$Hsd11b1^{+/+}$ + arthritis, n=3	72.8	±	4.7	
$CD8^-/CD4^-$	*$Hsd11b1^{-/-}$* + arthritis, n=3	11.9	±	0.9	*p>0.05*
	$Hsd11b1^{+/+}$ + arthritis, n=3	10.6	±	4.1	
$CD8^-/CD4^+$	*$Hsd11b1^{-/-}$* + arthritis, n=3	11.4	±	0.5	*p>0.05*
	$Hsd11b1^{+/+}$ + arthritis, n=3	10.9	±	0.5	

Thymocytes	Group	Mean			T-test
$CD8^+/CD4^-$	WT(KO), n=2	9.78	±	5.91	*p>0.05*
	KO(WT), n=2	2.07	±	0.83	
$CD8^+/CD4^+$	WT(KO), n=2	46.40	±	33.28	*p>0.05*
	KO(WT), n=2	83.25	±	2.75	
$CD8^-/CD4^-$	WT(KO), n=2	8.80	±	5.86	*p>0.05*
	KO(WT), n=2	2.72	±	1.46	
$CD8^-/CD4^+$	WT(KO), n=2	35.03	±	21.53	*p>0.05*
	KO(WT), n=2	11.97	±	2.10	

Appendix I, Table 2. Flow cytometry analysis of spleenocytes and BM cells from *Hsd11b1*$^{-/-}$ and *Hsd11b*$^{+/+}$ mice subjected to 21d of K/BxN arthritis.

Spleenocytes	Group	Mean			T-test
Lin^{+}	*Hsd11b1*$^{+/+}$ + arthritis, n=3	42.20	±	1.99	***p<0.05***
	Hsd11b1$^{-/-}$ + arthritis, n=3	36.20	±	1.21	
CD45^{+}	*Hsd11b1*$^{+/+}$ + arthritis, n=3	65.19	±	9.39	***p<0.01***
	Hsd11b1$^{-/-}$ + arthritis, n=3	2.61	±	1.44	
CD45^{+}*/c-kit*$^{+}$	*Hsd11b1*$^{+/+}$ + arthritis, n=3	1.40	±	0.20	***p<0.01***
	Hsd11b1$^{-/-}$ + arthritis, n=3	0.61	±	0.14	
CD45^{+}*/c-kit*$^{+}$ *excluding Lin*$^{+}$	*Hsd11b1*$^{+/+}$ + arthritis, n=3	59.94	±	18.47	***p<0.01***
	Hsd11b1$^{-/-}$ + arthritis, n=3	2.12	±	0.68	
c-kit^{+}	*Hsd11b1*$^{+/+}$ + arthritis, n=3	*2.23*	±	*0.29*	*p>0.05*
	Hsd11b1$^{-/-}$ + arthritis, n=3	*2.28*	±	*0.79*	
B220^{+}*/Thy-1*$^{-}$	*Hsd11b1*$^{+/+}$ + arthritis, n=3	58.65	±	0.59	***p<0.01***
	Hsd11b1$^{-/-}$ + arthritis, n=3	53.70	±	0.86	
B220^{-}*/Thy-1*$^{+}$	*Hsd11b1*$^{+/+}$ + arthritis, n=3	24.73	±	0.10	*p>0.05*
	Hsd11b1$^{-/-}$ + arthritis, n=3	22.43	±	2.15	
CD11b^{-}*/Gr-1*$^{+}$	*Hsd11b1*$^{+/+}$ + arthritis, n=3	*1.12*	±	*0.69*	*p>0.05*
	Hsd11b1$^{-/-}$ + arthritis, n=3	*0.45*	±	*0.09*	
CD11b^{+}*/Gr-1*$^{+}$	*Hsd11b1*$^{+/+}$ + arthritis, n=3	*2.71*	±	*0.14*	***p<0.01***
	Hsd11b1$^{-/-}$ + arthritis, n=3	*3.76*	±	*0.15*	
CD11b^{+}*/Gr-1*$^{-}$	*Hsd11b1*$^{+/+}$ + arthritis, n=3	*5.97*	±	*1.74*	*p>0.05*
	Hsd11b1$^{-/-}$ + arthritis, n=3	*3.56*	±	*1.45*	

BM Cells	Group	Mean			T-test
Lin^{+}	*Hsd11b1*$^{+/+}$ + arthritis, n=3	21.55	±	1.68	*p>0.05*
	Hsd11b1$^{-/-}$ + arthritis, n=3	18.24	±	1.15	
c-kit^{+}	*Hsd11b1*$^{+/+}$ + arthritis, n=3	2.00	±	0.07	***p<0.01***
	Hsd11b1$^{-/-}$ + arthritis, n=3	3.07	±	0.10	
B220^{+}*/Thy-1*$^{-}$	*Hsd11b1*$^{+/+}$ + arthritis, n=3	17.35	±	2.27	***p<0.01***
	Hsd11b1$^{-/-}$ + arthritis, n=3	26.50	±	2.86	
B220^{-}*/Thy-1*$^{+}$	*Hsd11b1*$^{+/+}$ + arthritis, n=3	2.83	±	0.13	***p<0.01***
	Hsd11b1$^{-/-}$ + arthritis, n=3	2.07	±	0.15	
CD11b^{-}*/Gr-1*$^{+}$	*Hsd11b1*$^{+/+}$ + arthritis, n=3	8.24	±	1.01	*p>0.05*
	Hsd11b1$^{-/-}$ + arthritis, n=3	5.87	±	0.97	
CD11b^{+}*/Gr-1*$^{+}$	*Hsd11b1*$^{+/+}$ + arthritis, n=3	20.53	±	1.58	*p>0.05*
	Hsd11b1$^{-/-}$ + arthritis, n=3	25.42	±	6.27	
CD11b^{+}*/Gr-1*$^{-}$	*Hsd11b1*$^{+/+}$ + arthritis, n=3	4.89	±	0.42	***p<0.05***
	Hsd11b1$^{-/-}$ + arthritis, n=3	7.69	±	1.01	

Appendix I, Table 3. Flow cytometry comparison of BM cells, peritoneal cells and spleenocytes from WT(KO) and KO(WT) mice following BMT-arthritis.

BM Cells	Group	Mean			T-test
$B220^{+}/Thy\text{-}1^{-}$	WT(KO)	14.1	±	2.8	*p>0.05*
	KO(WT)	11.0	±	1.8	
$B220^{-}/Thy\text{-}1^{+}$	WT(KO)	3.9	±	0.8	*p>0.05*
	KO(WT)	3.7	±	0.9	
$CD11b^{-}/Gr\text{-}1^{+}$	WT(KO)	5.4	±	1.6	*p>0.05*
	KO(WT)	5.7	±	1.1	
$CD11b^{+}/Gr\text{-}1^{+}$	WT(KO)	62.5	±	2.6	*p>0.05*
	KO(WT)	65.4	±	2.2	
$CD11b^{+}/Gr\text{-}1^{-}$	WT(KO)	3.3	±	0.6	*p>0.05*
	KO(WT)	2.9	±	0.4	

Peritoneal Cells	Group	Mean			T-test
Lin^{+}	WT(KO)	27.5	±	7.3	*p>0.05*
	KO(WT)	25.0	±	2.2	
$CD45^{+}$	WT(KO)	30.2	±	4.1	*p>0.05*
	KO(WT)	36.5	±	7.0	
$c\text{-}kit^{+}$	WT(KO)	17.2	±	4.3	*p>0.05*
	KO(WT)	14.1	±	3.3	
$B220^{+}/Thy\text{-}1^{-}$	WT(KO)	48.5	±	7.5	*p>0.05*
	KO(WT)	46.5	±	6.0	
$B220^{-}/Thy\text{-}1^{+}$	WT(KO)	20.8	±	7.2	*p>0.05*
	KO(WT)	21.0	±	6.8	
$CD11b^{-}/Gr\text{-}1^{+}$	WT(KO)	2.0	±	0.7	*p>0.05*
	KO(WT)	1.8	±	0.4	
$CD11b^{+}/Gr\text{-}1^{+}$	WT(KO)	66.4	±	4.6	*p>0.05*
	KO(WT)	60.8	±	7.0	
$CD11b^{+}/Gr\text{-}1^{-}$	WT(KO)	30.2	±	4.1	*p>0.05*
	KO(WT)	36.5	±	7.0	

Spleenocytes	Group	Mean			T-test
Lin^{+}	WT(KO)	14.2	±	2.6	*p>0.05*
	KO(WT)	15.5	±	4.9	
CD45^{+}	WT(KO)	65.2	±	27.1	*p>0.05*
	KO(WT)	57.3	±	18.7	
c-kit^{+}	WT(KO)	0.8	±	0.1	*p>0.05*
	KO(WT)	0.8	±	0.1	
B220^{+}*/Thy-1*$^{-}$	WT(KO)	63.1	±	4.5	*p>0.05*
	KO(WT)	56.0	±	5.2	
B220^{-}*/Thy-1*$^{+}$	WT(KO)	21.7	±	2.9	*p>0.05*
	KO(WT)	24.5	±	5.2	
CD11b^{-}*/Gr-1*$^{+}$	WT(KO)	1.1	±	0.3	*p>0.05*
	KO(WT)	0.9	±	0.2	
CD11b^{+}*/Gr-1*$^{+}$	WT(KO)	2.3	±	0.5	*p>0.05*
	KO(WT)	3.3	±	0.7	
CD11b^{+}*/Gr-1*$^{-}$	WT(KO)	5.8	±	1.5	*p>0.05*
	KO(WT)	5.4	±	0.6	

Appendix II

Awards, Presentations and Publications

AWARDS:

Feb 2008	Moray Endowment Fund, College of Medicine and Veterinary Medicine, University of Edinburgh
June 2006	The Endocrine Society Travel Grant
2004-2007	College of Medicine and Veterinary Medicine PhD Scholarship, University of Edinburgh
2004-2007	Overseas Research Student Award (ORS), United Kingdom

MANUSCRIPTS

Coutinho AE, Gray M, Brown JK, Yang F, Salter DM, Brownstein DG, Gilmour JS, Seckl JR, Savill JS, Chapman KE. 11β-Hydroxysteroid dehydrogenase Type 1 deficiency lowers threshold for mast cell degranulation and accelerates acute inflammation. 2009 *Manuscript in preparation.*

Chapman KE, **Coutinho AE**, Gray M, Gilmour JS, Savill JS, Seckl JR. The role and regulation of 11beta-hydroxysteroid dehydrogenase type 1 in the inflammatory response. Mol Cell Endocrinol 2008 Oct. *ahead of print*

Chapman KE, **Coutinho A**, Gray M, Gilmour JS, Savill JS, Seckl JR. Local amplification of glucocorticoids by 11beta-hydroxysteroid dehydrogenase type 1 and its role in the inflammatory response. Ann N Y Acad Sci. 2006 Nov;1088:265-73.

Gilmour JS, **Coutinho AE**, Cailhier JF, Man TY, Clay M, Thomas G, Harris HJ, Mullins JJ, Seckl JR, Savill JS, Chapman KE. Local amplification of glucocorticoids by 11 beta-hydroxysteroid dehydrogenase type 1 promotes macrophage phagocytosis of apoptotic leukocytes. J Immunol. 2006 Jun 15;176(12):7605-11.

Chapman KE, Gilmour JS, **Coutinho AE**, Savill JS, Seckl JR. 11Beta-hydroxysteroid dehydrogenase type 1--a role in inflammation? Mol Cell Endocrinol. 2006 Mar 27;248(1-2):3-8.

ABSTRACTS

Coutinho AE, Gray M, Salter D, Brownstein D, Seckl JR, Savill JS, Chapman KE Arthritis severity is modulated by 11β-Hydroxysteroid Dehydrogenase Type 1. *The Endocrine Society 89th Meeting* (June 2007, Toronto, Canada). **Oral Presentation**

Coutinho AE, Gray M, Sawatzky DA, Brownstein D, Gilmour J, Mullins J, Seckl JR, Savill JS, Chapman KE Deficiency in 11β-Hydroxysteroid dehydrogenase Type 1 results in a more rapid and severe inflammation. *The Endocrine Society 88th Meeting* (June 2006, Boston, USA). Poster Presentation

Coutinho AE, Gray M, Sawatzky DA, Brownstein D, Mullins J, Seckl JR, Savill JS, Chapman KE. 11β-HSD1: Anti-inflammatory Mechanism in Acute and Chronic Inflammation? *British Endocrine Society Meeting* (April 2006, Glasgow, Scotland, UK) **Oral Presentation**